Invisible to the naked eye, planktonic prokaryotes—comprising both bacteria and archaea—represent a large fraction of marine biomass, with abundances typically ranging from thousands to millions of cells per millilitre. From primary producers (photo- and chemoautotrophic) to heterotrophs, they display extremely diverse metabolisms and are of the utmost importance for the biogeochemical cycles in the ocean. During their involvement in elemental cycling, prokaryotes interact with the organic matter continuum (particulate and dissolved), utilising it as source of energy and carbon. In doing so, they transform the organic matter pool, diversifying it and remineralising compounds into their inorganic constituents. Moreover, by converting organic matter into biomass, prokaryotes return carbon into the marine trophic webs, a process known as the *microbial loop*. Hence, the activity of prokaryotes is crucial for organic matter cycling in the oceans. Upwelling regions represent some of the most productive marine systems, with large pools of organic matter subject to dynamic interactions with prokaryotic communities. Such environments thus have major importance for carbon cycling at the global scale, making very relevant the study of the prokaryotes that inhabit them. Combining mesocosm experiments and synoptic field samplings, this thesis aims to study prokaryotic communities in upwelling environments, with special attention to how they relate to organic matter cycling in such systems. Rather than limiting its scope to the direct effect of upwelling on surface prokaryotes, the present work explores how the influence of upwelling propagates down in the water column, addressing the vertical connectivity between highly productive surface waters and the prokaryotic communities of the dark realm of the ocean.

ULPGC
Universidad de Las Palmas de Gran Canaria
Instituto Universitario de Oceanografía y Cambio Global
IOCAG
GOB OCEANOGRAFÍA BIOLÓGICA
GOBIERNO DE ESPAÑA
MINISTERIO DE UNIVERSIDADES

RESPONSE OF PROKARYOTIC COMMUNITIES TO DEEP WATER UPWELLING

Response of Prokaryotic Communities to Deep Water Upwelling

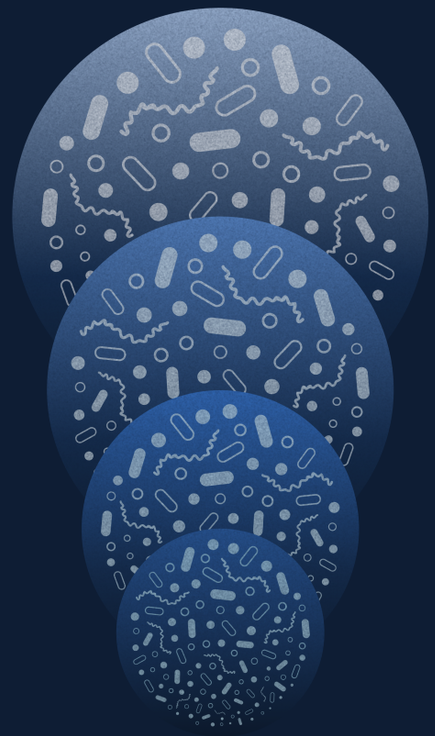

Markel Gómez Letona

PhD thesis

Doctorado en Oceanografía y Cambio Global

ULPGC

Las Palmas de Gran Canaria
Febrero 2023

ULPGC • UNIVERSIDAD DE LAS PALMAS DE GRAN CANARIA

Dª Juana Magdalena Santana Casiano coordinadora del programa de doctorado en Oceanografía y Cambio Global de la Universidad de Las Palmas de Gran Canaria

INFORMA,

De que la Comisión Académica del Programa de Doctorado, en su sesión de fecha tomó el acuerdo de dar el consentimiento para su tramitación, a la tesis doctoral titulada "*Response of prokaryotic communities to deep water upwelling*" presentada por el/la doctorando/a **Markel Gómez Letona** y dirigida por el/la Doctor/a **Javier Arístegui Ruiz y Marta Sebatián Caumel.**

Y para que así conste, y a efectos de lo previsto en el Artº 11 del Reglamento de Estudios de Doctorado (BOULPGC 04/03/2019) de la Universidad de Las Palmas de Gran Canaria, firmo la presente en Las Palmas de Gran Canaria, a de de dos mil veintitrés.

UNIVERSIDAD DE LAS PALMAS DE GRAN CANARIA

ESCUELA DE DOCTORADO

Programa de doctorado en Oceanografía y Cambio Global.

Título de la Tesis "*Response of prokaryotic communities to deep water upwelling*" ("*Respuesta de las comunidades procariotas al afloramiento de aguas profundas*").

Tesis Doctoral presentada por Markel Gómez Letona.

Dirigida por el Dr. D. Javier Arístegui Ruiz.

Dirigida por la Dra. Dª. Marta Sebastián Caumel.

Las Palmas de Gran Canaria, a 08 de febrero de 2023

El Director, La Directora, Doctorando,

(firma) (firma) (firma)

Response of Prokaryotic Communities to Deep Water Upwelling

Respuesta de las Comunidades Procariotas al Afloramiento de Aguas Profundas

Tesis doctoral realizada por Markel Gómez Letona dentro del Programa de Doctorado en Oceanografía y Cambio Global de la Universidad de Las Palmas de Gran Canaria con la financiación del Ministerio de Universidades (ayuda FPU17/01435)

Dirigida por la Dra. Marta Sebastián Caumel y el Dr. Javier Arístegui Ruiz

Las Palmas de Gran Canaria

2023

During their thesis Markel Gómez Letona has been supported by an FPU PhD fellowship funded by the Spanish Ministry of Universities (FPU17/01435). This thesis is a contribution to the Ocean artUp (ERC Advanced Grant, no. 695094), TRIATLAS (AMD-817578-5), MAFIA (CTM2012-39587-C04-01), FLUXES (CTM2015-69392-C3), e-IMPACT (PID2019-109084RB-C21), INTERES (CTM2017-83362-R) and SUMMER (AMD-817806-5) projects.

Nire gurasoei,
bidean zehar eskainitako babes guztiagatik

MONJE. *¿Y usted no cree que la verdad, si es tal, se impone también sin nosotros?*

GALILEI. *No, no y no. Se impone tanta verdad en la medida en que nosotros la impongamos. La victoria de la razón sólo puede ser la victoria de los que razonan.*

— Bertolt Brecht, La Vida de Galileo, acto VIII.

Acknowledgements

2017. urtea amaitzeko asko falta ez zela doktoretza tesia hasteko erabakia hartu nuen. Bost urte eta aste gutxi batzuk geroago idazten ditut hitz hauek, orduan hasi nuen bide hura amaitzear nagoenaren seinale. Aitortu beharra dut bide hura hasi banuen hasi, hein handi batean inertziagatik hasi nuela. Ez nuke esango horrelako erabaki bat hartzeko modu egokiena denik baina, tira, horrela izan zen. Kasu hauetan iraganeko kontuez kexatzeak ezer gutxi konpontzen duenez, hobe nuke ur harro hauek nolabaiteko arrakastaz nabigatzera lagundu didaten pertsonei nire esker ona erakustea. Izan daitezela ba hurrengo lerroak horren adierazle.

No podría empezar estos agradecimientos por otras personas que no fuesen las dos que han dirigido mi camino durante el doctorado. Muchas gracias, Marta, por todo lo que me has enseñado durante estos años, que es mucho. Llegué al ICM sin apenas saber nada sobre procariotas y ahora estoy cerca de acabar una tesis doctoral sobre ellos. Y, aunque en el fondo sigo sabiendo muy poco de todo esto, mirando atrás tengo que repetirme a mí mismo que algo sí que he avanzando, y en ello has contribuido mucho tú. Gracias por aguantar mis mensajes diarios por Slack—que, de alguna forma, han acortado la distancia entre Las Palmas y Barcelona. Por hacerme ver que, por mucho que el algunos de los gráficos que hiciera fueran muy elaborados y vistosos, igual no eran la forma adecuada de comunicar la información. Por acogerme en el ICM durante las dos estancias que hice allá, en las cuales aprendí mucho, desde bioinformática hasta a pelearme con el microscopio. Por la atención y detalle que has puesto corrigiendo cada una de las versiones de cada uno de los capítulos—vamos, un montón de correcciones. Siempre has tenido algo que comentar, sugerir y aportar a todo lo que hacía y—aunque a veces pensase, 'jo, no voy a conseguir hacer algo que le parezca del todo bien'—eso me ha ayudado de forma incalculable. A ver qué hago ahora que no pueda recurrir a ti de la misma forma. Javier, gracias a ti por acogerme en el grupo hace 7 años (que se dice pronto) cuando hice el trabajo de fin de grado. En cierto modo el camino hasta finalizar esta tesis empezó por aquel entonces. Empecé trabajando con datos de teledetección y he acabado filtrando agua y mirando por un microscopio. Desde luego es difícil hacer una cambio de escalas mayor (aunque, como con casi todo, las cosas acaban estando interconectadas). Contigo empecé a aprender cómo abordar una investigación. También a escribir de forma adecuada, dejándome de florituras. Además, he aprendido a ser independiente. En definitiva, mi iniciación en la investigación ha sido a través de ti. Gracias por ello.

El Grupo de Oceanografía Biológica. No somos muchas pero nos hacemos valer. Aja, Bea, Claudia, Cory, Isa, Laura, Lucía, Mine, Nandi, Nau. Son ustedes quienes mantienen en marcha el laboratorio en el día a día. Sirvan estas palabras para agradecer y reconocer su trabajo. Siempre han estado dispuestas a ayudar cuando he necesitado algo. También he aprendido con ustedes, claro. De ciencia *sensu stricto*, pero también de organización, de arreglar cosas, de gestiones, papeleo y trámites. Que es el reverso tedioso de todo esto, pero fundamental para que nuestro grupo funcione. Que no luce, pero que creo es importante visibilizar. Gracias.

Gracias también a Nandi y Juan Luís por aceptar que impartiese las prácticas docentes junto a ustedes. Tan importante como generar conocimiento es transmitirlo y tras estos cursos ahora sé qué es estar al otro lado. Pepe y Eva, dos de los capítulos de esta tesis tienen importantes contribuciones vuestras y por tanto una parte de esto también es vuestro.

En total, durante la tesis he pasado varios meses en el ICM de Barcelona, donde he conocido a personas geniales que me ha aportado tanto en lo científico como en lo personal. Irene, gracias en especial a ti por tu ayuda con el procesamiento de las muestras de BONCAT y el análisis con el microscopio. Sobretodo cuando empezó a fallar y aparecía cada dos por tres en tus despacho—gracias por tu paciencia, especialmente cuando intentaba enseñarte cómo fallaba y el microscopio decidía entonces funcionar bien. A Ona y María debo agradecerles el que me acogieran en su casa durante la segunda estancia que hice en Barcelona. A pesar de que suene a cliché prometo estar siendo totalmente sincero al decir que me sentí como en casa desde el primer día. Que esos tres meses fueran un tiempo realmente agradable es debido, en gran medida, a vosotras. Moltes gràcies.

I would like to thank the whole KOSMOS team from GEOMAR for allowing us to participate on their experiments within the Ocean artUp project. It was a pleasure meeting you and sharing such an experience. The relentless effort of the whole team organizing and carrying out all the logistic and technical work necessary for such big experiments meant that, despite the difficulties, they were a success. Dankeschön. A Clàudia debo agradecerle también su ayuda con todo el procesamiento de las muestras durante las largas tardes de laboratorio a lo largo del experimento. Te mando un abrazo desde la isla vecina.

To all the members of the TRATLEQ cruises (mostly from GEOMAR too, but also from elsewhere), thank you for your company during our crossings of the Atlantic, it was a great experience—despite all the problems that I encountered, particularly in

the first cruise. It would take me too long to name each one of you here, but I do not want to leave anyone out. So let this be an expression of collective gratitude. Even if the work I did onboard the Meteor has finally not been included in this thesis, those two cruises have been incredibly valuable lessons. Sí debo agradecer en especial a Alba y Ona, por su inestimable ayuda y compañía en cada una de las campañas. Si pude hacer todos esos CTDs a las 2, 3 o 4 de la madrugada fue gracias a vosotras. Al final con tanto CTD acabamos cogiendo literalmente varios miles de muestras, lo cual puesto en perspectiva es bastante alucinante. Y a Airam, que tuvo que aguantarme en la litera de arriba durante ¿11? semanas en las que todo lo que se asemejase a un horario de sueño mínimamente regular era un espejismo. Los amaneceres, los atardeceres, el sol de mediodía, los ratos muertos de noche sentados en la cubierta—algo compensaban.

Antes de acabar quiero recordar a las personas con las que, durante este tiempo, he compartido mi vida más allá del doctorado. En especial a dos Sandras. Sandra R., aunque estés desde hace un tiempo lejos me alegra cada vez que nos escribimos. A Sandra N. por suerte la sigo teniendo bien cerca, y menos mal. Gracias a ambas de corazón por ser mi apoyo.

Azkenik, nire gurasoei eskertu nahi diet bide osoan zehar eskaini didaten babesa. Ez soilik doktoretzan zehar, baizik eta itsas zientziak ikastera Kanariar Uharteetara joatea ahalbidetu zidaten egunetik. Honaino heldu banaiz ein ez txiki batean beraie esker izanda da. Pozak eta atsekabeak, biak izan dira nire bidelagun—sarritan bigarrenak gehiago—eta bietan egon dira nirekin. Ziur nahiz beraiei galdetuta esango dutela, laguntzak laguntza, meritua nirea dela. Baina, irakurle, ez zaitzatela engainatu: ezibestekoa izan da beraien ekarpena. Hitz xume hauek dira erakutsi nahi diedan eskerraren islada. Berriz ere, ama, aita, mila esker bihotzez.

Contents

Summary

Invisible to the naked eye, planktonic prokaryotes—comprising both bacteria and archaea—represent a large fraction of marine biomass, with abundances typically ranging from thousands to millions of cells per millilitre. From primary producers (photo- and chemoautotrophic) to heterotrophs, they display extremely diverse metabolisms and are of the utmost importance for the biogeochemical cycles in the ocean. During their involvement in elemental cycling, prokaryotes interact with the organic matter continuum (particulate and dissolved), utilising it as source of energy and carbon. In doing so, they transform the organic matter pool, diversifying it and remineralising compounds into their inorganic constituents. Moreover, by converting organic matter into biomass, prokaryotes return carbon into the marine trophic webs, a process known as the microbial loop. Hence, this pathway is crucial for organic matter cycling in the oceans. Upwelling regions represent some of the most productive marine systems, with large pools of organic matter subject to dynamic interactions with prokaryotic communities. Such environments thus have major importance for carbon cycling at the global scale, making very relevant the study of the prokaryotes that inhabit them. In this thesis we combine mesocosm experiments and synoptic field samplings to study prokaryotic communities in upwelling environments, with special attention to how they relate to organic matter cycling. The first half of the thesis is devoted to an upwelling simulation experiment carried out in the oligotrophic waters of the subtropical Eastern North Atlantic. By simulating different upwelling intensities and frequencies (singular pulse versus recurring upwelling), we studied how the dissolved organic matter pool and the prokaryotic communities respond to variable upwelling scenarios. First, we measured the dissolved organic matter concentrations and optical properties, observing that upwelling intensity was positively related to dissolved organic matter accumulations. Singular and recurring upwellings yielded mostly similar changes in concentrations and optical properties despite the markedly contrasting outcome of their phytoplankton blooms (a single large bloom in the singular mode versus sustained smaller blooms in the recurring one). Although optical properties suggested ongoing transformation of organic matter, the accumulated dissolved organic matter did not decrease, indicating that during the experiment production and consumption tended to be balanced. In parallel, prokaryotic successional patterns also displayed remarkable similarities in singular and recurring upwelling treatments. The dominant taxa within the successional assemblages differed mostly between the particle-associated and the free-living fractions, but upwelling modes also displayed some

differences in composition. Thus, it is striking that prokaryotic communities shared common successional patterns even across size fractions under the different blooming scenarios. The second half of the thesis in turn explores how the influence of upwelling propagates down in the water column, addressing the vertical connectivity between highly productive surface waters and the prokaryotic communities inhabiting the water masses of the dark ocean. We studied natural communities along an oceanographic transect in the tropical and subtropical Atlantic (which included areas under the influence of the Northwest African upwelling system), showing how the standing stocks and physiological status of meso- and bathypelagic prokaryotes are coupled with surface productivity. We showed that the cell-viability of deep ocean prokaryotes increased under the productive waters of the upwelling, evidencing that its effect reaches the deep layers. The analysis of the water masses also showed that the distribution of prokaryotic taxa and the optical properties of dissolved organic matter were explained in varying degrees by i) the mixing and ageing history of water masses, and ii) intraregional biogeochemical processes (including links to surface productivity). Thus, we conclude that upwelling markedly influences the dissolved organic matter and prokaryotic communities of surface and deep waters.

Introduction

Prokaryotes and dissolved organic matter cycling in the ocean

Marine dissolved organic matter (DOM) is estimated to represent close to 660 Pg C (1 Pg = 10^{15} g), making it the largest pool of reduced carbon in the oceans and one of the largest on Earth (Hansell et al. 2009). Its spatial distribution is, however, not homogeneous, neither horizontally nor vertically. Dissolved organic carbon (DOC) concentrations in surface waters range from 70-80 μmol · kg^{-1} in stratified low latitude waters (30°S–30°N) to 40-50 μmol · kg^{-1} in the Southern Ocean (Fig. 1a). Conversely, deep waters display lower concentrations that vary following the thermohaline circulation, from 50 μm · kg^{-1} in the North Atlantic to 34 μm · kg^{-1} in the North Pacific (Fig. 1b). This distribution of DOM across the global ocean is largely controlled by microbes, unicellular organisms that are major drivers of the biogeochemical cycles. Among them, prokaryotes—a widely diverse group encompassing bacteria and archaea—play a role of paramount importance as they both produce and consume DOM, remineralising a fraction of it back to its inorganic constituents.

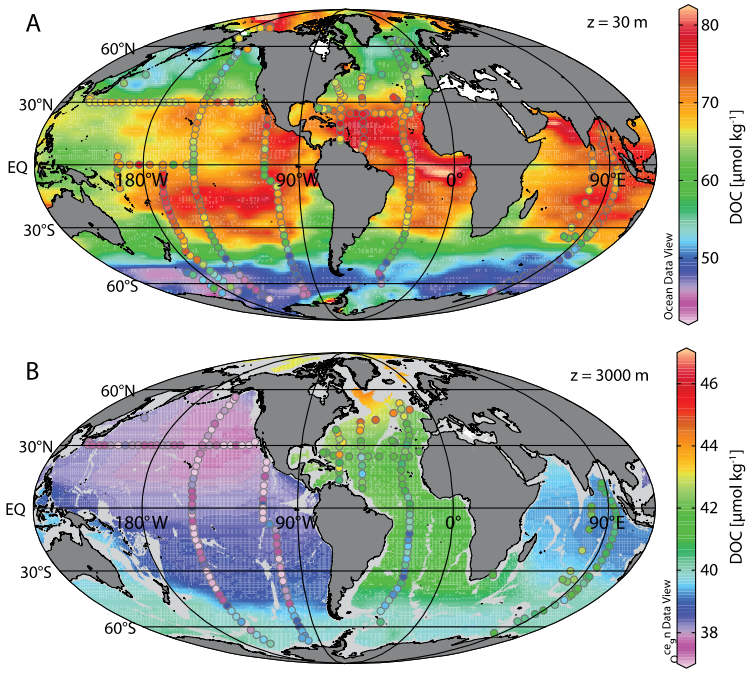

Figure 1. Global distribution of dissolved organic carbon (DOC). Concentrations (in μmol · kg^{-1}) are shown at depths of 30 m (a) and 3000 m (b). Points represent observations and the background field corresponds to modelled estimates. From Hansell et al. (2009).

Dissolved organic matter within the microbial web of life

The main source of organic matter in the ocean is primary production by unicellular photoautotrophs known as phytoplankton, which, through photosynthesis, fix CO_2 into organic carbon at an approximate rate of 100 Pg C · year^{-1} (around half of which is lost through respiration), a figure roughly equivalent to that of terrestrial primary producers (Chavez et al. 2011). Phytoplankton inhabit the euphotic layer of the oceans, i.e., its sunlit waters, and while their primary production occurs in the form of particulate organic matter (POM)—and is partly transferred to higher trophic levels—an important fraction is channelled to the dissolved organic matter pool through a series of processes involving an intricate web of microbial interactions (Fig. 2).

Phytoplankton can experience uncoupling between photosynthesis and cell growth, resulting in the extracellular release of photosynthetic products (Carlson and Hansell 2015). When cell growth is limited by factors such as nutrient availability,

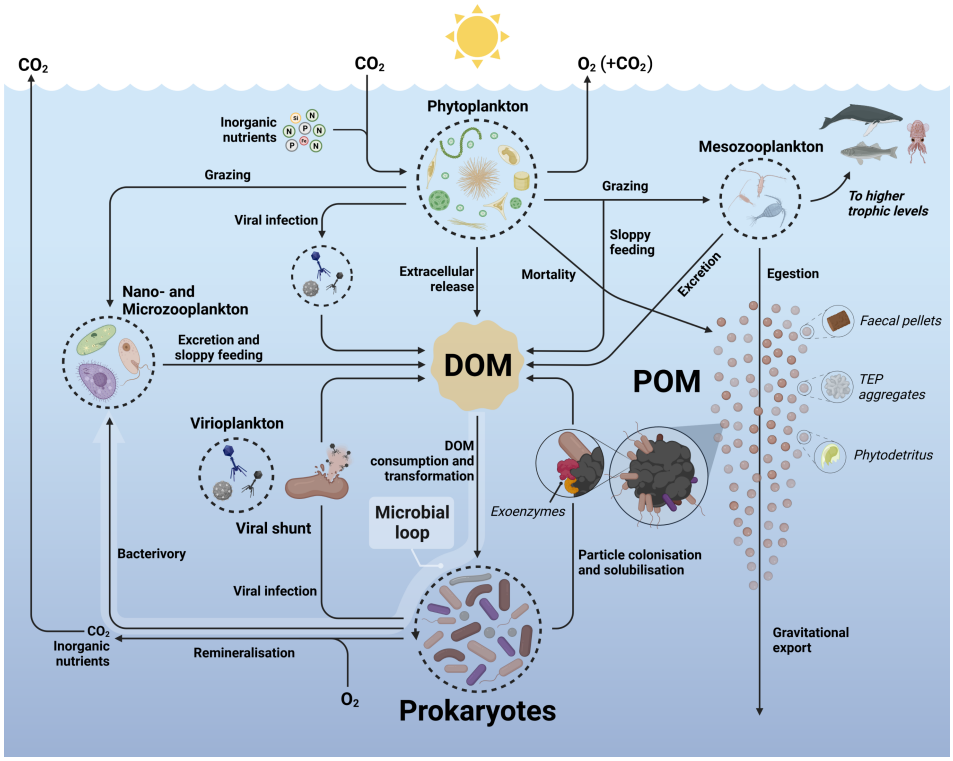

Figure 2. The microbial trophic web and dissolved organic matter cycling. Shown are the most important pathways for dissolved organic matter production and consumption as presented in the text. Created with BioRender.com.

phytoplankton actively release organic molecules as a means to balance cellular carbon demand and photosynthetic assimilation (Thornton 2014). Carbohydrates, particularly polysaccharides, make up much of the released DOM, and act as precursors for the formation of transparent exopolymer particles (TEPs) (Mühlenbruch et al. 2018). Passive leakage of low molecular weight compounds through the cell membrane also contributes to the extracellular release of DOM by phytoplankton (Thornton 2014).

Predation by zooplankton over phytoplankton (termed *grazing*) and other planktonic organisms also releases DOM to the environment. During prey ingestion, part of its contents are lost to the surroundings, a process known as *sloppy feeding* (Steinberg and Landry 2017). Mesozooplankton (e.g., copepods) prey on nano- and microphytoplankton, while nano- and microzooplankton (e.g. ciliates, nanoflagellates) do so on picophytoplankton and prokaryotes (Jürgens and Massana 2008). Many of the unicellular predators are mixotrophs able to perform photosynthesis (Worden et al. 2015; Stoecker et al. 2017). Zooplankton release organic compounds through excretion too, notably liberating significant amounts of amino acids, ammonia and urea, representing important sources of dissolved organic nitrogen (DON) (Urban-Rich et al. 2006; Saba et al. 2011). Egestion of unassimilated materials, including within faecal pellets of mesozooplankton, is another major form by which zooplankton introduce DOM to seawater (Saba et al. 2011).

Viruses play a prominent role in organic matter cycling as well (Suttle 2007). They are the most abundant members of planktonic communities, with over 10^{30} viruses in the ocean and 10^{23} infections per second (mainly of phytoplankton and, specially, prokaryotes). Viral infections are an important cause of mortality among planktonic organisms, resulting in releases of DOM as infected cells are lysed. This pathway is known as the *viral shunt*, through which viruses channel POM into DOM, effectively subtracting that organic matter from the marine trophic web (Breitbart et al. 2018). Similarly, prokaryotes may contribute to the cell lysis of phytoplankton through antagonistic relationships involving the release of secondary metabolites such as extracellular proteases (Seymour et al. 2017).

Prokaryotes are also involved in the solubilisation of organic matter from sinking and suspended particles, which represent resource hot spots in the highly heterogeneous marine environment (Carlson and Hansell 2015). Organic particles range from colloids (at or below the micrometre scale) to large macroscopic aggregates (in the order of millimetres) and are rich in biopolymers such as carbohydrates, proteins and lipids. They are colonised by specialised prokaryotes, in a process in which

chemotaxis and motility play vital roles (Stocker and Seymour 2012). As obligate osmotrophs, these prokaryotes hydrolyse POM by means of extracellular enzymes (both exo- and ectoenzymes) releasing dissolved molecules (Arnosti 2011). The solubilised DOM creates highly enriched microenvironments that support active communities of particle-attached prokaryotes (Ivančić et al. 2018). Diffusion of the solubilised molecules creates gradients around particles which, if sinking down in the water column, leave behind a plume of DOM (Kiørboe and Thygesen 2001). This source of nutrients may be used by free-living prokaryotes, thus benefiting from the activity of their particle-attached counterparts (Kiørboe and Jackson 2001; Stocker et al. 2008).

The microbial loop

Prokaryotes use DOM from all these sources as a carbon and energy supply (Azam and Malfatti 2007). In doing so, they consume O_2 and ultimately remineralise organic matter into its inorganic constituents, including carbon, nitrogen and phosphorus (Fig. 2). This results in the recycling of essential nutrients for primary producers in surface waters, while in deep waters those nutrients are accumulated as they are not consumed quickly enough (Levitus et al. 1993). Moreover, as prokaryotes turn DOM into biomass, that carbon re-enters marine trophic webs and, hence, becomes available to higher trophic levels through bacterivory by nano- and microzooplanktonic grazers (Jürgens and Massana 2008; Stoecker et al. 2017), a pathway termed the *microbial loop* (Azam et al. 1983; Fenchel 2008). The activity of prokaryotes is thus crucial for organic matter cycling in the oceans.

While primary production and DOM cycling disproportionately occur in the epipelagic ocean (0-200 m), prokaryotes inhabit and are active throughout the entire water column. Indeed, mesopelagic (200-1000 m) and bathypelagic (1000-4000 m) prokaryotes together represent close to 75% and 50% of the biomass and production of marine prokaryotes, respectively (Arístegui et al. 2009b). Despite chemoautotrophs may contribute with approximately 0.1 Pg C · year^{-1} (Middelburg 2011) to the dark ocean organic carbon budget, carbon is primarily introduced to the dark ocean through the downward transport of organic matter from the euphotic layer, estimated at 5-10 Pg C · year^{-1} (Henson et al. 2011; Siegel et al. 2014; Nowicki et al. 2022). This vertical export occurs by means of a series of processes collectively known as the *biological carbon pump* (BCP) (Boyd et al. 2019). They can be grouped into three main pathways: the gravitational flux, the mixing flux and the active migration flux (Le Moigne 2019). The gravitational flux refers to the sinking of

particles, which vary in carbon content and sinking rates depending on their properties and origin: either tightly packed faecal pellets, dead phytoplankton cells or loose aggregates formed by TEPs (Turner 2015; Mari et al. 2017). Moreover, the sinking of those particles is a dynamic process, where the carbon flux is attenuated by coloniser prokaryotes and zooplankton feeding (Iversen 2023). The mixing flux encompasses the downward transport of both DOM and suspended, non-sinking particles. Seasonal convective mixing, water mass formation and eddy-driven subduction all contribute to organic matter export (Fontela et al. 2016; Boyd et al. 2019; Baetge et al. 2020). Lastly, the active flux is mediated by the zooplankton and fish that perform diel vertical migrations, feeding in surface waters at night and excreting in mesopelagic waters during the day (Steinberg and Landry 2017; Saba et al. 2021). Modelling results suggest that the gravitational and mixing fluxes are the most important ones at the global scale, albeit the active flux by migrants can also represent relevant contributions regionally (Stukel et al. 2022). The combined transport of organic matter to the subsurface ocean yields remineralisation processes at depth by prokaryotes, resulting in high inorganic nutrient concentrations which, if returned to euphotic waters, can fuel new primary production. If sufficiently intense and devoid of proper ventilation by currents, the deep remineralisation by heterotrophic prokaryotes creates oxygen minimum zones, environments that have a peculiar set of conditions (most importantly, redox conditions different to the oxygenated ocean) that fundamentally affect microbial communities (Bertagnolli and Stewart 2018; Engel et al. 2022).

The activity of the prokaryotes that drive the DOM consumption and remineralisation is, however, limited by a variety of factors. This limitation results in DOM accumulations in very different oceanic environments, from surface waters in oligotrophic areas to the nutrient replete ocean interior (Fig. 1). While in surface waters scarcity of essential nutrients could explain the inability of prokaryotes to degrade DOM, deep waters do not apparently lack any resource that could hinder their metabolic capacity (Arístegui et al. 2009b). Two main hypotheses aim to explain this (Fig. 3). Historically, the preponderant explanation for DOM persistence has been that the different compounds forming the DOM pool have varying levels of intrinsic lability/recalcitrance—i.e., how easily they can be degraded—depending on their molecular structure (Jiao et al. 2010). In opposition to this, a more recent hypothesis holds that DOM is continuously transformed within complex networks and that recalcitrance is only an emergent property consequence of ecological interactions (Mentges et al. 2019). Under the intrinsic recalcitrance hypothesis, prokaryotes consume fresh, labile DOM and produce recalcitrant by-products,

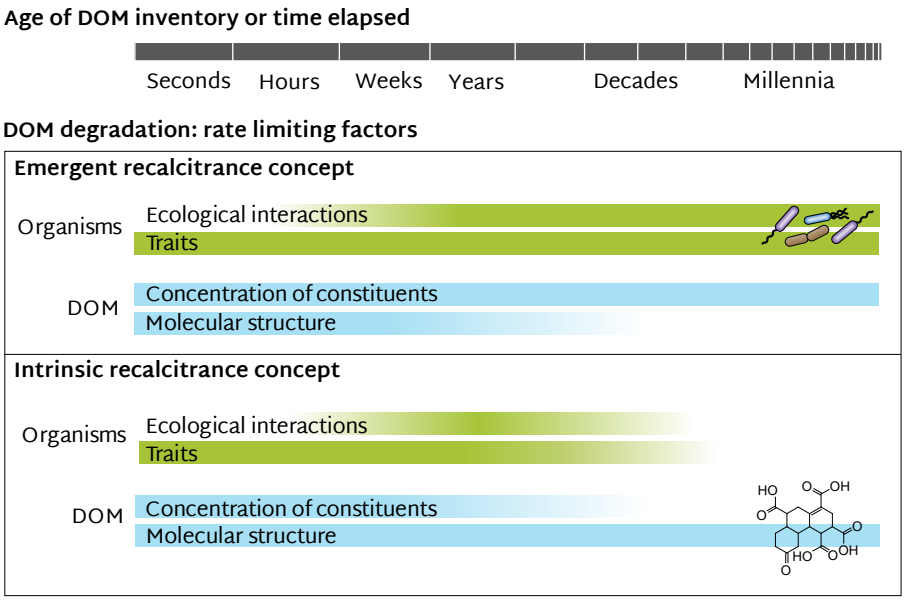

Figure 3. The two main hypotheses of dissolved organic matter persistence. Rate limiting factors for DOM degradation on different time scales. Bar transparency shows which factors control DOM turnover at different time scales according to each hypothesis. Adapted from Dittmar et al. (2021).

which they are incapable of degrading and thus accumulate in seawater. As set out in the comprehensive review by Dittmar et al. (2021), intrinsic recalcitrance rests on three main lines of evidence: 1) during water mass ageing, accumulation of some compounds is greater than for others, suggesting that they are more stable (Hertkorn et al. 2006; Flerus et al. 2012), 2) radiocarbon ages indicate that the DOM pool is formed by molecules of different ages, the older ones being those that are cycled slower (Loh et al. 2004; Follett et al. 2014), 3) prokaryotes seem to engage in preferential consumption of certain compounds over others (Teeling et al. 2012; Hach et al. 2020). The formation of such recalcitrant DOM would have a long-term carbon sequestration potential of 0.2 Pg C · year^{-1}, not far from the 0.4 Pg C · year^{-1} estimated for the sinking of organic matter below 2000 m (Legendre et al. 2015). The emergent recalcitrance hypothesis itself is also supported by different observations (Dittmar et al. 2021): 1) numerical modelling has shown that longevity of DOM can be reproduced by networks of microorganism-substrate interactions (Mentges et al. 2019), 2) prokaryotes are known to degrade deep sea DOM when it is found at sufficient concentrations (when too low, the required cellular machinery for degradation is not cost-efficient) (Arrieta et al. 2015), and 3) molecules with higher concentrations (e.g., because of higher production) have higher encounter rates with

microbes and, thus, increased uptake (and vice versa), influencing their radiocarbon ages and reactivity (Loh et al. 2004; Follett et al. 2014). Ultimately, the long-term stabilisation of the DOM pool would occur by an equilibrium between the consumption rates of molecules and their concentrations: as individual molecules within widely diverse DOM are consumed, their concentrations decrease, thereby reducing the consumption rates by microbes—the abundances and growth rates of which are accordingly affected. This tendency towards equilibrium, however, would be altered by short-term events (blooms, sinking particles), resulting in a microbial-molecular web of interactions in continuous change.

Tracking microbial transformation of DOM through its optical properties

With possibly millions of individual compounds, the continuously changing DOM pool is one of the most complex and diverse mixtures in nature (Zark et al. 2017b; Dittmar et al. 2021). Nonetheless, identification of the molecular structure and quantification of individual organic compounds remains highly challenging, and only a small fraction of DOM has been characterised in such a manner (Dittmar and Stubbins 2014). Advanced techniques such as Fourier Transform Ion Cyclotron Resonance Mass Spectra (FT-ICR-MS) and high-field nuclear magnetic resonance spectroscopy (NMR) enable the identification of organic molecule formulae in seawater (Hertkorn et al. 2013) and have been used to study the microbial transformation of DOM (Lechtenfeld et al. 2015; Zark et al. 2017a). These approaches, however, pose technical challenges and have limited availability, curbing

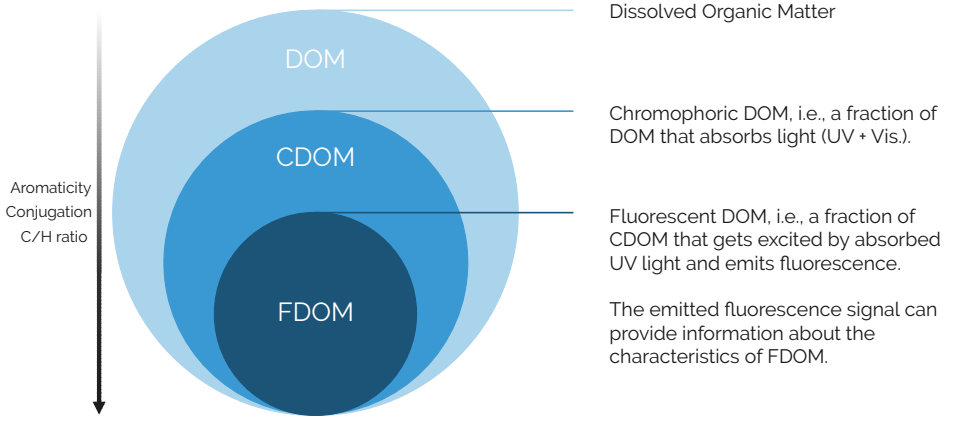

Figure 4. Major pools of dissolved organic matter (DOM) according to their optical properties. The arrow depicts increasing levels of aromaticity, conjugation, and carbon-to-hydrogen ratio (C/H) from the overall pool of DOM to chromophoric DOM (CDOM), to fluorescent DOM (FDOM). Based on Stedmon and Álvarez-Salgado (2011).

their application for regular measurements of environmental samples. While more reduced in scope, spectroscopic techniques offer an accessible alternative to gain insights into the broad composition of DOM and have been proven to be a useful tool to track DOM transformation processes in the ocean (Nelson and Siegel 2013).

Two nested subsets of DOM exist based on the optical properties they display (Fig. 4). Chromophoric DOM (CDOM) is the fraction of DOM that absorbs solar radiation in the ultraviolet and visible bands. It is ubiquitous in the marine environment and represents the most important factor controlling light penetration in seawater (Nelson and Siegel 2013). Its absorption spectrum is typically smooth and decreases with wavelength in approximately an exponential way (Fig. 5). CDOM characterisation usually involves estimating the absorption coefficients at wavelengths

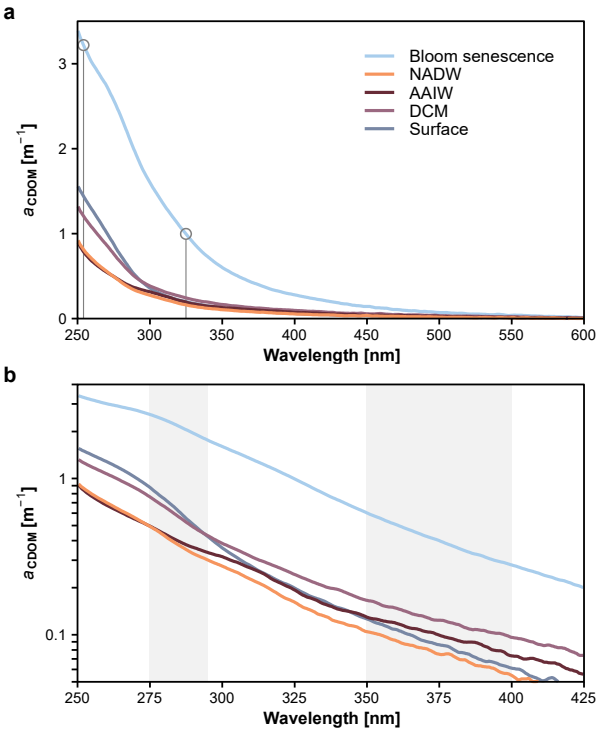

Figure 5. CDOM characterisation in seawater. Examples of absorption spectra of chromophoric DOM in a set of contrasting seawater samples (a). In (b), the same spectra are shown natural log-transformed. Samples correspond to the senescence phase of a diatom bloom in the eastern subtropical North Atlantic and the water column in the Equatorial Atlantic (0°N, 2°W; North Atlantic Deep Water, NADW, 2000 m; Antarctic Intermediate Water, AAIW, 815 m; Deep Chlorophyll Maximum, DCM, 55 m; surface layer, 5 m). Circles in (a) indicate wavelengths of interest (254 and 325 nm). Shaded areas in (b) depict the wavelength ranges for which common spectral slopes are estimated (275-295 and 350-400 nm). Based on data from **Chapter 1** and Gomez-Letona et al. (2022).

of interest (254 and 325 nm are of widespread use; Fig. 5a) and the spectral slopes at certain wavelength ranges (e.g., 275-295 and 350-400 nm; Fig. 5b). Absorption coefficients provide quantitative information on different CDOM fractions, while spectral slopes have been shown to be related to its average molecular weight (Helms et al. 2008). CDOM displays more intense signals in highly productive and coastal areas and, while it has been positively correlated to DOC concentrations in diverse marine environments (Mannino et al. 2008; Lønborg and Álvarez-Salgado 2014; Catalá et al. 2018), this relationship does not seem to be universal (Nelson et al. 2010). Subtle changes in the quantity and properties of CDOM have also been observed, tracing both abiotic and biotic processes. For instance, in surface waters photobleaching by ultraviolet radiation is a major driver of CDOM loss, shifting spectra to shorter wavelengths (Helms et al. 2013). Microbial transformation of DOM has also been shown to modify CDOM quantities and spectral slopes during water mass ageing, a process relevant for global biogeochemical cycles (Catalá et al. 2015a, 2018).

Part of CDOM is excited by the ultraviolet radiation it absorbs and in turn emits fluorescence (Fig. 4). This fluorescent DOM (FDOM) is usually measured by exciting seawater along a series of wavelengths, registering the emitted fluorescence along a second range of wavelengths, which are slightly longer than the excitation ones, as photons lose energy during the process (a phenomenon known as the Stokes shift).

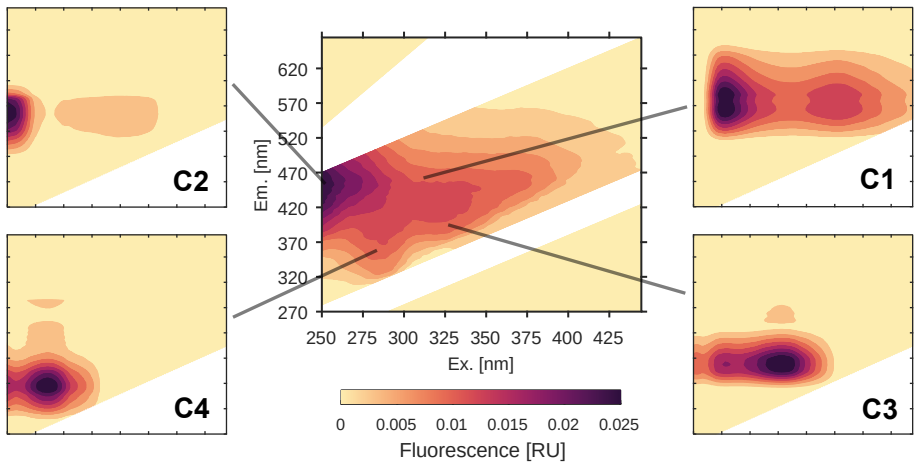

Figure 6. Measuring FDOM in seawater. Example of an excitation-emission matrix (centre) and corresponding fluorescence components (sides) derived from a parallel factor analysis (Stedmon et al. 2003) for a seawater sample set from the tropical and subtropical Atlantic. Components C1-C3 correspond to different kinds of humic-like fluorescence, while C4 is an amino acid-like component. Based on data from **Chapter 4**.

The results are typically arranged into an excitation-emission matrix (Fig. 6). From such matrices, fluorescence values at wavelength pairs of interest can be extracted based on typical FDOM signals observed in marine environments (Coble 1996). A more nuanced approach involves determining the specific fluorescence components for each set of environmental samples, which can be obtained through parallel factor analysis (Stedmon et al. 2003). In marine environments, these fluorescence components, also known as fluorophores, usually fall into two broad categories: amino acid-like and humic-like fluorescence components (Fig. 6). The former have been associated with primary production and are deemed to be at least partly bioavailable for consumption (Coble et al. 1998; Lønborg et al. 2010). Production of humic-like FDOM, on the other hand, has been associated with the microbial reworking of DOM, as increasing intensities of humic-like fluorescence tend to correlate with oxygen utilisation (Jørgensen et al. 2011; Martínez–Pérez et al. 2019). Moreover, humic-like FDOM itself seems to be resistant to degradation, leaving particular imprints in the water masses (Jørgensen et al. 2014; Catalá et al. 2015b). In conjunction, CDOM and FDOM have been shown to provide valuable information to track microbial transformation of DOM in the ocean.

Prokaryotic diversity

Marine prokaryotes, while traditionally have been referred to as *bacterioplankton*, comprise both bacteria *and* archaea. The estimated ~10^{29} prokaryotic cells that live in the ocean (Whitman et al. 1998) form an extremely diverse assemblage of microorganisms in terms of taxonomy, metabolic capabilities and activities (Sunagawa et al. 2015; Louca et al. 2016; Acinas et al. 2021; Munson-McGee et al. 2022). Although the role of bacteria in marine environments started to be acknowledged in the 1970s and was fully recognised in the 1980s (Azam et al. 1983; Fenchel 2008), archaea were not even known to be part of planktonic communities until more recently. Originally thought to be extremophiles, the presence of archaea among marine plankton was first recognised in the early 1990s (Fuhrman et al. 1992) and have since been observed to be ubiquitous in the ocean, fulfilling key biogeochemical processes (Santoro et al. 2019). Together, bacteria and archaea inhabit every single marine environment, from sunlit eutrophic waters to the deepest reaches of the ocean, where they are subject to perpetual darkness, extreme pressures, low temperature and limited organic carbon availability.

Distribution of prokaryotic lineages in the global ocean

The advent of high throughput sequencing techniques (Sogin et al. 2006; Reuter et al. 2015; Slatko et al. 2018) revolutionised the scope of studies looking at non-cultured prokaryotes in environmental samples. Currently it is relatively straightforward and affordable to study the distribution of different prokaryotic taxa in any environment by means of the sequencing of the 16S subunit ribosomal gene (Parada et al. 2016), obtaining thousands of reads per sample. This, combined with regional and global sampling efforts such as the Tara Oceans and Malaspina circumnavigation expeditions (Sunagawa et al. 2015; Villarino et al. 2022), has provided unprecedented knowledge on prokaryotic biogeography.

The vast oligotrophic regions of the oceans are dominated by taxa highly efficient under low nutrient conditions. The SAR11 clade (also known as *Pelagibacterales* and ubiquitous in the ocean) stands out among oligotrophic specialists as the numerically dominant bacteria in the subtropical gyres. This bacteria are aerobic, free-living heterotrophs that have streamlined genomes and are specialised in the expression of transporter proteins for the uptake of low molecular weight DOM and nutrients at very low concentrations, enabling them to succeed in oligotrophic environments to the point that they represent roughly 1-in-4 planktonic cells (Giovannoni 2017). Opposed to them are the copiotrophic taxa, feeding on the high organic matter concentrations found in the most productive marine waters, including during phytoplankton blooms, or in nutrient-rich microenvironments, such as sinking-particles (Buchan et al. 2014). These prokaryotes typically include, among others, bacteria from the Flavobacteriales, Rhodobacterales and Enterobacterales (*Alteromonas*, *Vibrio*) orders (Teeling et al. 2016; Pontiller et al. 2022). They present high expression of genes for glycoside hydrolases and peptidases, enabling them to breakdown the DOM released by the blooming communities (Teeling et al. 2012; Pontiller et al. 2022) and, in doing so, they function as key players in global carbon cycling.

Down in the water column the abundance and activity of prokaryotes decrease due to more adverse conditions (Arístegui et al. 2009b). The physiological state of cells also becomes deteriorated, as indicated by the increasing fraction of dead or injured cells (Gasol et al. 2009; Baltar et al. 2012). These changes are accompanied by depth-dependent shifts in the composition of the communities (DeLong et al. 2006), tending to higher contributions by chemolithoautotrophic archaea (e.g., Nitrosopumilales) and by heterotrophic bacteria able to degrade DOM with low reactivity (e.g., the SAR202 clade) (Herndl et al. 2023). Differences have been

identified, however, between water masses, meaning that deep ocean circulation patterns have an imprint on prokaryotic diversity (Galand et al. 2010; Agogué et al. 2011; Frank et al. 2016). This suggests that water masses act as physical barriers (e.g., as density boundaries) that limit dispersion and/or that the specific environmental characteristics (temperature, oxygen, DOM, etc.) of each water mass (Álvarez-Salgado et al. 2013; Álvarez et al. 2014) limit the prokaryotic taxa that can maintain significant populations in them. Since these properties vary during water mass mixing and ageing as they circulate from their source region around the globe, changes in the prokaryotic assemblages would be expected. This is known to occur in prokaryotic communities living in water masses with suboxic or even anoxic conditions (Karstensen et al. 2008). The scarcity or even lack of O_2 favours the use of alternative electron acceptors, like NO_3^-, Mn(IV), Fe(III), SO_4^{2-} and CO_2, changing the microbial metabolic landscape of these environments (Wright et al. 2012).

Vertical connectivity of prokaryotic communities

Particles have been shown to harbour prokaryotic communities with distinct taxonomic compositions and higher activities than non-attached, i.e., free-living prokaryotes (Turley 1993; Baltar et al. 2010; Salazar et al. 2015). Among particles, increasing size has been observed to be positively related to diversity, pointing to a larger variety of microenvironments in larger particles (Mestre et al. 2017). Prokaryotic groups typically found associated with particles include Planctomycetes, Bacteroidetes, Firmicutes, and several Alpha- and Gammaproteobacteria, while the likes of SAR11, SAR86, SAR324, and SAR406 clades, and many archaea tend to have a free-living lifestyle (Salazar et al. 2015; Mestre et al. 2017; Bachmann et al. 2018).

Even if communities display marked vertical differences in composition, they are not isolated. Beyond the effect that vertical mixing can have mostly in the upper layers, the gravitational flux of particles acts as a vector connecting otherwise distant realms of the water column. Besides the flux of organic matter they provide to deep layers as part of the biological carbon pump, particles also transport the very same prokaryotes that colonise them. Sinking particles are known to be positively correlated with prokaryotic abundances in meso- and bathypelagic layers (Arístegui et al. 2009b), indicating that they help communities to sustain higher numbers through the introduction of carbon and energy, although relationships between sinking organic matter and activity are inconsistent (Hansell and Ducklow 2003; Yokokawa et al. 2013). Moreover, the input of DOM by sinking particles has also been shown to

influence the composition and activity of deep ocean communities (Ruiz-González et al. 2020), acting as resource hotspots for copiotrophic taxa that live in *boom-and-bust* dynamics (Reintjes et al. 2020). These patterns have been posited to relate to surface conditions, as highly productive areas display larger particle fluxes. Indeed, in regions with high surface productivity, surface and deep ocean communities are more similar to each other than in oligotrophic areas, showcasing how particles deliver prokaryotes from upper layers into the interior of the ocean and thus pointing to their role as vectors of vertical connectivity (Mestre et al. 2018; Ruiz-González et al. 2020).

Upwelling systems: hotspots of primary productivity

Broadly speaking, upwelling is defined as the upward transport of a water volume that needs to 1) be maintained over a sufficiently long period (at least several days) and 2) lift the water volume across a considerable vertical distance (approximately over 100 m) (Kämpf and Chapman 2016). In the ocean, multiple physical processes result in upwelling (eddy pumping, equatorial divergence, topographic upwelling), but wind-driven upwelling in the eastern limits of oceanic basins is probably the most prominent one in terms of global relevance, as it generates the highly productive eastern boundary upwelling ecosystems. Indeed, such systems have a disproportionate importance for marine production: even though the four most important eastern boundary upwelling ecosystems—Canary, Benguela, Humboldt and California current systems—represent approximately only 0.3% of the ocean, they contribute 2% to global primary production and are key for marine animals (Carr 2002; Kämpf and Chapman 2016).

Fundamental to understand coastal upwelling is knowing how water responds to the friction generated by wind stress in the ocean-atmosphere boundary (Kämpf and Chapman 2016). Briefly, the combined effect of the wind and the Coriolis force (created by Earth's rotation), results in an offshore transport of surface waters, which are replaced by the deeper waters laying below them (see details in Fig. 7). These upwelled waters are cold and have high concentrations of inorganic nutrients due to the remineralisation processes at depth (see section *The microbial loop*). The introduction of these nutrients nourishes the microbial communities found in these environments, greatly enhancing primary production (Carr and Kearns 2003). Even if upwelling dynamics in these systems are controlled by large-scale atmospheric circulation patterns, marked spatial and temporal variability exists, with clear subregional and seasonal changes (Arístegui et al. 2009a; Chavez and Messié 2009).

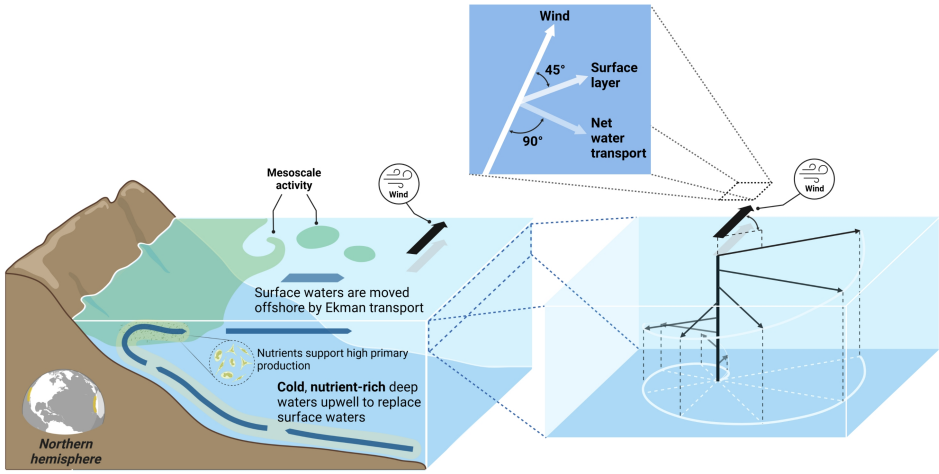

Figure 7. Ekman transport and eastern boundary upwelling ecosystems. Due to the effect of the Coriolis force, at times scales of over a day the response of the water to the wind stress occurs at an angle (clockwise in the northern hemisphere, counterclockwise in the southern) relative to the wind direction. In the absence of other processes, in the sea surface the resulting water movement occurs at an angle of 45°, but as momentum is transferred down in the water column due to drag, the displacement angle relative to the wind direction increases with depth (until all energy is transferred/dissipated and the process ceases), a structure known as *Ekman spiral* (right panel). The water column portion encompassed by this phenomenon is the *Ekman layer*. Most importantly, the resulting net transport (Ekman transport) for the Ekman layer occurs at 90° relative to wind direction. If wind blows parallel to a coast at its left (in the Northern hemisphere, right in the Southern), the Ekman layer that is generated will exert a net transport of surface waters in the offshore direction (left panel). This induces the upwelling of deep waters by two ways (Kämpf and Chapman, 2016): 1) to ensure mass conservation, deep waters replace the displaced surface waters, as the coastline avoids replacement by adjacent surface waters; and 2) the offshore water movement results in a 5-10 cm lowering of the coastal sea level, creating a shoreward pressure gradient force that drives a fast geostrophic current along the coast. This current creates a second Ekman layer at the bottom boundary, generating a shoreward net transport which contributes to the upward movement of deep waters as it approaches the coast. Created with BioRender.com. Partly adapted from NASA (http://oceanmotion.org/html/background/ocean-in-motion.htm).

Mesoscale and submesoscale processes bear significant importance in upwelling areas. For instance, horizontal export through filaments can extend the influence of upwelling more than 100 km offshore (Arístegui et al. 2004; Santana-Falcón et al. 2016). Mesoscale processes in eastern boundary upwelling systems also favour the formation of eddies, adding to their complexity (Pegliasco et al. 2015; Amos et al. 2019). The concomitant variability in the introduction of macronutrients, however,

is not sufficient to explain the variation in primary production. Other factors such as iron limitation, physical export and light limitation have been found to modulate the productivity of eastern boundary upwelling ecosystems (Messié and Chavez 2015). On top of this, climate change poses potential long-term changes, as modifications in the atmospheric circulation will have effects on upwelling. The deepening and/or displacement of the pressure gradients governing atmospheric circulation have been predicted to modify upwelling in some systems, with potential intensifications in some areas (Sydeman et al. 2014; García-Reyes et al. 2015; Rykaczewski et al. 2015), although the impact on productivity is more uncertain (Bograd et al. 2023).

Upwelling systems bear great biogeochemical significance. The phytoplankton community, typically dominated by diatoms, drives large drawdowns of CO_2—found oversaturated in upwelled waters with respect to atmospheric values—and nutrients (Loucaides et al. 2012). The associated production of organic matter is exported both horizontally offshore and vertically to subsurface layers. Areas under the influence of upwelling systems are in fact subject to high vertical particle fluxes (Hebbeln et al. 2000; Fischer et al. 2020), meaning that this gravitational export of carbon provides large amounts of organic matter to the prokaryotic communities inhabiting deep waters below these environments. Indeed, high export fluxes result in intense organic matter remineralisation and O_2 consumption which, combined with poor ventilation of subsurface waters by currents, create oxygen minimum zones at depths of 100-900 m (Engel et al. 2022). Such zones are present in all eastern boundary upwelling ecosystems, but are more intense and widespread in the Pacific, even reaching anoxic levels in large areas (Engel et al. 2022). Notably, oxygen minimum zones themselves can influence the attenuation of the vertical particle flux, as particle remineralisation processes for different size fractions can vary in low O_2 environments (Rasse and Dall'Olmo 2019). Thus, prokaryotes play a major role in the biogeochemistry of upwelling systems as they are fundamental to the remineralisation and recycling of the organic matter that 1) is generated in the surface by the blooming phytoplankton communities, and 2) is exported down in the water column. Detailed characterisation of how these processes unfold is, however, not complete. Experimental approaches usually rely on additions of nutrients to simulate different fertilisation settings (Allers et al. 2007; Zark et al. 2017a; Taucher et al. 2018), which do not involve the translocation of deep waters along with their DOM pools and prokaryotic communities, key to properly understand the potential influence of upwelling on surface waters. Field samplings of upwelling events under natural conditions on the other hand (Needham and Fuhrman 2016; Pontiller et al. 2022) are spatiotemporally constrained and hence hinder comparison of variable

scenarios. Regarding vertical connectivity, recognition of its importance for deep ocean prokaryotes and DOM has significantly increased in recent years (Arístegui et al. 2009b; Frank et al. 2016; Mestre et al. 2018; Ruiz-González et al. 2020), but little is known about how it may affect the physiology and composition of communities inhabiting the water masses under areas influenced by upwelling systems, as well as the DOM pool they interact with. We will need to address these open questions if we are to inch closer to a comprehensive understanding of prokaryotes and DOM in upwelling environments.

Aim of the thesis

The overarching aim of this thesis is to study the link between the distribution and dynamics of organic matter and prokaryotic communities during upwelling events. Given the large influence of upwelling on biogeochemical processes, we want to address not only its immediate effects, but whether these propagate in the water column and affect the microbial communities in the dark ocean. For this purpose, we assessed three main questions:

1. How is the dissolved organic matter of the surface ocean influenced by upwelling of nutrient-rich deep waters?
2. Which are the changes observed in prokaryotic communities following phytoplankton blooms induced by different upwelling intensity and frequency scenarios, and how are they related to the dissolved organic matter pool?
3. Does the surface productivity enhancement caused by upwelling events influence prokaryotic communities and dissolved organic matter beyond the epipelagic layer?

These questions have been addressed in four chapters, which combine both experimental approaches and the analysis of field samplings. The first question is tackled in **Chapter 1**, where we describe the response of the dissolved organic matter pool observed during a simulated upwelling experiment carried out in the oligotrophic waters of the Canary Islands, in the subtropical Eastern North Atlantic. By simulating different combinations of upwelling intensity and frequency (single pulse vs sustained upwelling), we evaluated how the concentrations and characteristics of the dissolved organic matter are altered under variable upwelling conditions. **Chapter 2** addresses the second question, focusing on how prokaryotic communities behave under that variable set of upwelling scenarios. It assesses the prokaryotic successions that occur and their relationship with the evolving organic matter pool.

The other two chapters are devoted to the final question, studying how upwelling regions affect prokaryotic communities and organic matter distributions beyond the photic layer. As vertical connectivity between surface waters and the dark ocean is mediated by the flux of organic matter in the water column, areas with enhanced productivity regimes such as upwelling systems are expected to exert a greater influence on prokaryotes living below them than oligotrophic surface waters. To

address this, we analysed samples collected during an oceanographic cruise that crossed the tropical and subtropical Atlantic Ocean along a surface productivity gradient, from Brazil to the Canary Islands, including an area under the influence of the Northwest African upwelling system. In **Chapter 3**, we analyse the standing stocks, metabolic rates and the physiological status of prokaryotes over the entire water column, and how these are related to surface productivity along the described oceanographic section. Lastly, as water masses have been shown to harbour distinct prokaryotic communities in the dark ocean, in **Chapter 4** we aim to determine the contribution of water mass mixing and ageing versus local biogeochemical processes (including vertical connectivity) to the distribution of prokaryotes and dissolved organic matter characteristics in the same oceanographic section.

References

Acinas, S. G., P. Sánchez, G. Salazar, and others. 2021. Deep ocean metagenomes provide insight into the metabolic architecture of bathypelagic microbial communities. Commun. Biol. **4**: 604. doi:10.1038/s42003-021-02112-2

Agogué, H., D. Lamy, P. R. Neal, M. L. Sogin, and G. J. Herndl. 2011. Water mass-specificity of bacterial communities in the North Atlantic revealed by massively parallel sequencing. Mol. Ecol. **20**: 258–274. doi:10.1111/j.1365-294X.2010.04932.x

Allers, E., L. Gómez-Consarnau, J. Pinhassi, J. M. Gasol, K. Šimek, and J. Pernthaler. 2007. Response of Alteromonadaceae and Rhodobacteriaceae to glucose and phosphorus manipulation in marine mesocosms. Environ. Microbiol. **9**: 2417–2429. doi:10.1111/j.1462-2920.2007.01360.x

Álvarez-Salgado, X. A., M. Nieto-Cid, M. Álvarez, F. F. Pérez, P. Morin, and H. Mercier. 2013. New insights on the mineralization of dissolved organic matter in central, intermediate, and deep water masses of the northeast North Atlantic. Limnol. Oceanogr. **58**: 681–696. doi:10.4319/lo.2013.58.2.0681

Álvarez, M., S. Brea, H. Mercier, and X. A. Álvarez-Salgado. 2014. Mineralization of biogenic materials in the water masses of the South Atlantic Ocean. I: Assessment and results of an optimum multiparameter analysis. Prog. Oceanogr. **123**: 1–23. doi:10.1016/j.pocean.2013.12.007

Amos, C. M., R. M. Castelao, and P. M. Medeiros. 2019. Offshore transport of particulate organic carbon in the California Current System by mesoscale eddies. Nat. Commun. **10**: 4940. doi:10.1038/s41467-019-12783-5

Arístegui, J., E. D. Barton, X. A. Álvarez-Salgado, and others. 2009a. Sub-regional ecosystem variability in the Canary Current upwelling. Prog. Oceanogr. **83**: 33–48. doi:10.1016/j.pocean.2009.07.031

Arístegui, J., E. D. Barton, P. Tett, and others. 2004. Variability in plankton community structure, metabolism, and vertical carbon fluxes along an upwelling filament (Cape Juby, NW Africa). Prog. Oceanogr. **62**: 95–113. doi:10.1016/j.pocean.2004.07.004

Arístegui, J., J. M. Gasol, C. M. Duarte, and G. J. Herndl. 2009b. Microbial oceanography of the dark ocean's pelagic realm. Limnol. Oceanogr. **54**: 1501–1529. doi:10.4319/lo.2009.54.5.1501

Arnosti, C. 2011. Microbial Extracellular Enzymes and the Marine Carbon Cycle. Ann. Rev. Mar. Sci. **3**: 401–425. doi:10.1146/annurev-marine-120709-142731

Arrieta, J. M., E. Mayol, R. L. Hansman, G. J. Herndl, T. Dittmar, and C. M. Duarte. 2015. Dilution limits dissolved organic carbon utilization in the deep ocean. Science (80-.). **348**: 331–333. doi:10.1126/science.1258955

Azam, F., T. Fenchel, J. Field, J. Gray, L. Meyer-Reil, and F. Thingstad. 1983. The Ecological Role of Water-Column Microbes in the Sea. Mar. Ecol. Prog. Ser. **10**: 257–263. doi:10.3354/meps010257

Azam, F., and F. Malfatti. 2007. Microbial structuring of marine ecosystems. Nat. Rev. Microbiol. **5**: 782–791. doi:10.1038/nrmicro1747

Bachmann, J., T. Heimbach, C. Hassenrück, G. A. Kopprio, M. H. Iversen, H. P. Grossart, and A. Gärdes. 2018. Environmental Drivers of Free-Living vs. Particle-Attached Bacterial Community Composition in the Mauritania Upwelling System. Front. Microbiol. **9**: 2836. doi:10.3389/fmicb.2018.02836

Baetge, N., J. R. Graff, M. J. Behrenfeld, and C. A. Carlson. 2020. Net Community Production, Dissolved Organic Carbon Accumulation, and Vertical Export in the Western North Atlantic. Front. Mar. Sci. **7**: 227. doi:10.3389/fmars.2020.00227

Baltar, F., J. Arístegui, J. M. Gasol, and G. J. Herndl. 2012. Microbial functioning and community structure variability in the mesopelagic and epipelagic waters of the subtropical northeast Atlantic Ocean. Appl. Environ. Microbiol. **78**: 3309–3316. doi:10.1128/AEM.07962-11

Baltar, F., J. Arístegui, J. M. Gasol, E. Sintes, H. M. Van Aken, and G. J. Herndl. 2010. High dissolved extracellular enzymatic activity in the deep central Atlantic ocean. Aquat. Microb. Ecol. **11**: 1998–2014. doi:10.3354/ame01377

Bertagnolli, A. D., and F. J. Stewart. 2018. Microbial niches in marine oxygen minimum zones. Nat. Rev. Microbiol. **16**: 723–729. doi:10.1038/s41579-018-0087-z

Bograd, S. J., M. G. Jacox, E. L. Hazen, and others. 2023. Climate Change Impacts on Eastern Boundary Upwelling Systems. Ann. Rev. Mar. Sci. **15**. doi:10.1146/annurev-marine-032122-021945

Boyd, P. W., H. Claustre, M. Levy, D. A. Siegel, and T. Weber. 2019. Multi-faceted particle pumps drive carbon sequestration in the ocean. Nature **568**: 327–335. doi:10.1038/s41586-019-1098-2

Breitbart, M., C. Bonnain, K. Malki, and N. A. Sawaya. 2018. Phage puppet masters of the marine microbial realm. Nat. Microbiol. **3**: 754–766. doi:10.1038/s41564-018-0166-y

Buchan, A., G. R. LeCleir, C. A. Gulvik, and J. M. González. 2014. Master recyclers: features and functions of bacteria associated with phytoplankton blooms. Nat. Rev. Microbiol. **12**: 686–698. doi:10.1038/nrmicro3326

Carlson, C. A., and D. A. Hansell. 2015. DOM Sources, Sinks, Reactivity, and Budgets, p. 65–126. *In* D.A. Hansell and C.A. Carlson [eds.], Biogeochemistry of Marine Dissolved Organic Matter: Second Edition. Academic Press.

Carr, M.-E. 2002. Estimation of potential productivity in Eastern Boundary Currents using remote sensing. Deep Sea Res. Part II Top. Stud. Oceanogr. **49**: 59–80. doi:10.1016/S0967-0645(01)00094-7

Carr, M. E., and E. J. Kearns. 2003. Production regimes in four Eastern Boundary Current systems. Deep-Sea Res. Part II Top. Stud. Oceanogr. **50**: 3199–3221. doi:10.1016/j.dsr2.2003.07.015

Catalá, T. S., A. M. Martínez-Pérez, M. Nieto-Cid, and others. 2018. Dissolved Organic Matter (DOM) in the open Mediterranean Sea. I. Basin–wide distribution and drivers of chromophoric DOM. Prog. Oceanogr. **165**: 35–51. doi:10.1016/j.pocean.2018.05.002

Catalá, T. S., I. Reche, M. Álvarez, and others. 2015a. Water mass age and aging driving chromophoric dissolved organic matter in the dark global ocean. Global Biogeochem. Cycles **29**: 917–934. doi:10.1002/2014GB005048

Catalá, T. S., I. Reche, A. Fuentes-Lema, and others. 2015b. Turnover time of fluorescent dissolved organic matter in the dark global ocean. Nat. Commun. **6:5986**. doi:10.1038/ncomms6986

Chavez, F. P., and M. Messié. 2009. A comparison of Eastern Boundary Upwelling Ecosystems. Prog. Oceanogr. **83**: 80–96. doi:10.1016/j.pocean.2009.07.032

Chavez, F. P., M. Messié, and J. T. Pennington. 2011. Marine Primary Production in Relation to Climate Variability and Change. Ann. Rev. Mar. Sci. **3**: 227–260. doi:10.1146/annurev.marine.010908.163917

Coble, P. G. 1996. Characterization of marine and terrestrial DOM in seawater using excitation-

emission matrix spectroscopy. Mar. Chem. **51**: 325–346. doi:10.1016/0304-4203(95)00062-3

Coble, P. G., C. E. Del Castillo, and B. Avril. 1998. Distribution and optical properties of CDOM in the Arabian Sea during the 1995 Southwest Monsoon. Deep Sea Res. Part II Top. Stud. Oceanogr. **45**: 2195–2223. doi:10.1016/S0967-0645(98)00068-X

DeLong, E. F., C. M. Preston, T. Mincer, and others. 2006. Community genomics among stratified microbial assemblages in the ocean's interior. Science (80-.). **311**: 496–503. doi:10.1126/science.1120250

Dittmar, T., S. T. Lennartz, H. Buck-Wiese, D. A. Hansell, C. Santinelli, C. Vanni, B. Blasius, and J.-H. Hehemann. 2021. Enigmatic persistence of dissolved organic matter in the ocean. Nat. Rev. Earth Environ. **2**: 570–583. doi:10.1038/s43017-021-00183-7

Dittmar, T., and A. Stubbins. 2014. 12.6 - Dissolved Organic Matter in Aquatic Systems, p. 125–156. *In* H.D. Holland and K.K.B.T.-T. on G. (Second E. Turekian [eds.], Treatise on Geochemistry. Elsevier.

Engel, A., R. Kiko, and M. Dengler. 2022. Organic Matter Supply and Utilization in Oxygen Minimum Zones. Ann. Rev. Mar. Sci. **14**: 355–378. doi:10.1146/annurev-marine-041921-090849

Fenchel, T. 2008. The microbial loop – 25 years later. J. Exp. Mar. Bio. Ecol. **366**: 99–103. doi:10.1016/j.jembe.2008.07.013

Fischer, G., S. Neuer, S. Ramondenc, and others. 2020. Long-Term Changes of Particle Flux in the Canary Basin Between 1991 and 2009 and Comparison to Sediment Trap Records Off Mauritania. Front. Earth Sci. **8**: 280. doi:10.3389/feart.2020.00280

Flerus, R., O. J. Lechtenfeld, B. P. Koch, S. L. McCallister, P. Schmitt-Kopplin, R. Benner, K. Kaiser, and G. Kattner. 2012. A molecular perspective on the ageing of marine dissolved organic matter. Biogeosciences **9**: 1935–1955. doi:10.5194/bg-9-1935-2012

Follett, C. L., D. J. Repeta, D. H. Rothman, L. Xu, and C. Santinelli. 2014. Hidden cycle of dissolved organic carbon in the deep ocean. Proc. Natl. Acad. Sci. **111**: 16706–16711. doi:10.1073/pnas.1407445111

Fontela, M., M. I. García-Ibáñez, D. A. Hansell, H. Mercier, and F. F. Pérez. 2016. Dissolved Organic Carbon in the North Atlantic Meridional Overturning Circulation. Sci. Rep. **6**: 26931. doi:10.1038/srep26931

Frank, A. H., J. A. L. Garcia, G. J. Herndl, and T. Reinthaler. 2016. Connectivity between surface and deep waters determines prokaryotic diversity in the North Atlantic Deep Water. Environ. Microbiol. **18**: 2052–2063. doi:10.1111/1462-2920.13237

Fuhrman, J. A., K. McCallum, and A. A. Davis. 1992. Novel major archaebacterial group from marine plankton. Nature **356**: 148–149. doi:10.1038/356148a0

Galand, P. E., M. Potvin, E. O. Casamayor, and C. Lovejoy. 2010. Hydrography shapes bacterial biogeography of the deep Arctic Ocean. ISME J. **4**: 564–576. doi:10.1038/ismej.2009.134

García-Reyes, M., W. J. Sydeman, D. S. Schoeman, R. R. Rykaczewski, B. A. Black, A. J. Smit, and S. J. Bograd. 2015. Under Pressure: Climate Change, Upwelling, and Eastern Boundary Upwelling Ecosystems. Front. Mar. Sci. **2**: 109. doi:10.3389/fmars.2015.00109

Gasol, J. M., L. Alonso-Sáez, D. Vaqué, F. Baltar, M. L. Calleja, C. M. Duarte, and J. Arístegui. 2009. Mesopelagic prokaryotic bulk and single-cell heterotrophic activity and community composition in the NW Africa-Canary Islands coastal-transition zone. Prog. Oceanogr. **83**: 189–196.

doi:10.1016/j.pocean.2009.07.014

Giovannoni, S. J. 2017. SAR11 Bacteria: The Most Abundant Plankton in the Oceans. Ann. Rev. Mar. Sci. **9**: 231–255. doi:10.1146/annurev-marine-010814-015934

Gomez-Letona, M., M. Sebastián, X. A. Álvarez-Salgado, R. Kiko, P. Brandt, and J. Arístegui. 2022. Zonal variability in organic matter distribution along the equatorial Atlantic Ocean: insigths for vertical carbon export. Ocean Sciences Meeting. http://hdl.handle.net/10261/264550.

Hach, P. F., H. K. Marchant, A. Krupke, and others. 2020. Rapid microbial diversification of dissolved organic matter in oceanic surface waters leads to carbon sequestration. Sci. Rep. **10**: 13025. doi:10.1038/s41598-020-69930-y

Hansell, D. A., C. A. Carlson, D. J. Repeta, and R. Schlitzer. 2009. Dissolved organic matter in the ocean: A controversy stimulates new insights. Oceanography **22**: 202–211.

Hansell, D. A., and H. W. Ducklow. 2003. Bacterioplankton distribution and production in the bathypelagic ocean: Directly coupled to particulate organic carbon export?,. Limnol. Oceanogr. **48**: 150–156. doi:10.4319/lo.2003.48.1.0150

Hebbeln, D., M. Marchant, and G. Wefer. 2000. Seasonal variations of the particle flux in the Peru-Chile current at 30 °S under "normal" and El Nino conditions. Deep-Sea Res. Part II Top. Stud. Oceanogr. **47**: 2101–2128. doi:10.1016/S0967-0645(00)00018-7

Helms, J. R., A. Stubbins, E. M. Perdue, N. W. Green, H. Chen, and K. Mopper. 2013. Photochemical bleaching of oceanic dissolved organic matter and its effect on absorption spectral slope and fluorescence. Mar. Chem. **155**: 81–91. doi:10.1016/j.marchem.2013.05.015

Helms, J. R., A. Stubbins, J. D. Ritchie, E. C. Minor, D. J. Kieber, and K. Mopper. 2008. Absorption spectral slopes and slope ratios as indicators of molecular weight, source, and photobleaching of chromophoric dissolved organic matter. Limnol. Oceanogr. **53**: 955–969. doi:10.4319/lo.2008.53.3.0955

Henson, S. A., R. Sanders, E. Madsen, P. J. Morris, F. Le Moigne, and G. D. Quartly. 2011. A reduced estimate of the strength of the ocean's biological carbon pump. Geophys. Res. Lett. **38**. doi:10.1029/2011GL046735

Herndl, G. J., B. Bayer, F. Baltar, and T. Reinthaler. 2023. Prokaryotic Life in the Deep Ocean's Water Column. Ann. Rev. Mar. Sci. **15**. doi:10.1146/annurev-marine-032122-115655

Hertkorn, N., R. Benner, M. Frommberger, P. Schmitt-Kopplin, M. Witt, K. Kaiser, A. Kettrup, and J. I. Hedges. 2006. Characterization of a major refractory component of marine dissolved organic matter. Geochim. Cosmochim. Acta **70**: 2990–3010. doi:10.1016/j.gca.2006.03.021

Hertkorn, N., M. Harir, B. P. Koch, B. Michalke, and P. Schmitt-Kopplin. 2013. High-field NMR spectroscopy and FTICR mass spectrometry: powerful discovery tools for the molecular level characterization of marine dissolved organic matter. Biogeosciences **10**: 1583–1624. doi:10.5194/bg-10-1583-2013

Ivančić, I., P. Paliaga, M. Pfannkuchen, and others. 2018. Seasonal variations in extracellular enzymatic activity in marine snow-associated microbial communities and their impact on the surrounding water. FEMS Microbiol. Ecol. **94**: fiy198. doi:10.1093/femsec/fiy198

Iversen, M. H. 2023. Carbon Export in the Ocean: A Biologist's Perspective. Ann. Rev. Mar. Sci. **15**. doi:10.1146/annurev-marine-032122-035153

Jiao, N., G. J. Herndl, D. A. Hansell, and others. 2010. Microbial production of recalcitrant dissolved

organic matter: long-term carbon storage in the global ocean. Nat. Rev. Microbiol. **8**: 593–599. doi:10.1038/nrmicro2386

Jørgensen, L., C. A. Stedmon, M. A. Granskog, and M. Middelboe. 2014. Tracing the long-term microbial production of recalcitrant fluorescent dissolved organic matter in seawater. Geophys. Res. Lett. **41**: 2481–2488. doi:10.1002/2014GL059428

Jørgensen, L., C. A. Stedmon, T. Kragh, S. Markager, M. Middelboe, and M. Søndergaard. 2011. Global trends in the fluorescence characteristics and distribution of marine dissolved organic matter. Mar. Chem. **126**: 139–148. doi:10.1016/j.marchem.2011.05.002

Jürgens, K., and R. Massana. 2008. Protistan Grazing on Marine Bacterioplankton, p. 383–441. *In* Microbial Ecology of the Oceans.

Kämpf, J., and P. Chapman. 2016. Upwelling Systems of the World, 1st ed. Springer Cham.

Karstensen, J., L. Stramma, and M. Visbeck. 2008. Oxygen minimum zones in the eastern tropical Atlantic and Pacific oceans. Prog. Oceanogr. **77**: 331–350. doi:10.1016/j.pocean.2007.05.009

Kiørboe, T., and G. A. Jackson. 2001. Marine snow, organic solute plumes, and optimal chemosensory behavior of bacteria. Limnol. Oceanogr. **46**: 1309–1318. doi:10.4319/lo.2001.46.6.1309

Kiørboe, T., and U. H. Thygesen. 2001. Fluid motion and solute distribution around sinking aggregates. Mar. Ecol. Prog. Ser. **211**: 15–25.

Lechtenfeld, O. J., N. Hertkorn, Y. Shen, M. Witt, and R. Benner. 2015. Marine sequestration of carbon in bacterial metabolites. Nat. Commun. **6**: 6711. doi:10.1038/ncomms7711

Legendre, L., R. B. Rivkin, M. G. Weinbauer, L. Guidi, and J. Uitz. 2015. The microbial carbon pump concept: Potential biogeochemical significance in the globally changing ocean. Prog. Oceanogr. **134**: 432–450. doi:10.1016/j.pocean.2015.01.008

Levitus, S., M. E. Conkright, J. L. Reid, R. G. Najjar, and A. Mantyla. 1993. Distribution of nitrate, phosphate and silicate in the world oceans. Prog. Oceanogr. **31**: 245–273. doi:10.1016/0079-6611(93)90003-V

Loh, A. N., J. E. Bauer, and E. R. M. Druffel. 2004. Variable ageing and storage of dissolved organic components in the open ocean. Nature **430**: 877–881. doi:10.1038/nature02780

Lønborg, C., and X. A. Álvarez-Salgado. 2014. Tracing dissolved organic matter cycling in the eastern boundary of the temperate North Atlantic using absorption and fluorescence spectroscopy. Deep Sea Res. Part I Oceanogr. Res. Pap. **85**: 35–46. doi:10.1016/j.dsr.2013.11.002

Lønborg, C., X. A. Álvarez-Salgado, K. Davidson, S. Martínez-García, and E. Teira. 2010. Assessing the microbial bioavailability and degradation rate constants of dissolved organic matter by fluorescence spectroscopy in the coastal upwelling system of the Ría de Vigo. Mar. Chem. **119**: 121–129. doi:10.1016/j.marchem.2010.02.001

Louca, S., L. W. Parfrey, and M. Doebeli. 2016. Decoupling function and taxonomy in the global ocean microbiome. Science (80-.). **353**: 1272–1277. doi:10.1126/science.aaf4507

Loucaides, S., T. Tyrrell, E. P. Achterberg, and others. 2012. Biological and physical forcing of carbonate chemistry in an upwelling filament off northwest Africa: Results from a Lagrangian study. Global Biogeochem. Cycles **26**. doi:10.1029/2011GB004216

Mannino, A., M. E. Russ, and S. B. Hooker. 2008. Algorithm development and validation for satellite-derived distributions of DOC and CDOM in the U.S. Middle Atlantic Bight. J. Geophys. Res. Ocean. **113**: C07051. doi:10.1029/2007JC004493

Mari, X., U. Passow, C. Migon, A. B. Burd, and L. Legendre. 2017. Transparent exopolymer particles: Effects on carbon cycling in the ocean. Prog. Oceanogr. **151**: 13–37. doi:10.1016/j.pocean.2016.11.002

Martínez–Pérez, A. M., T. S. Catalá, M. Nieto–Cid, and others. 2019. Dissolved organic matter (DOM) in the open Mediterranean Sea. II: Basin–wide distribution and drivers of fluorescent DOM. Prog. Oceanogr. **170**: 93–106. doi:10.1016/j.pocean.2018.10.019

Mentges, A., C. Feenders, C. Deutsch, B. Blasius, and T. Dittmar. 2019. Long-term stability of marine dissolved organic carbon emerges from a neutral network of compounds and microbes. Sci. Rep. **9**: 17780. doi:10.1038/s41598-019-54290-z

Messié, M., and F. P. Chavez. 2015. Seasonal regulation of primary production in eastern boundary upwelling systems. Prog. Oceanogr. **134**: 1–18. doi:10.1016/j.pocean.2014.10.011

Mestre, M., E. Borrull, M. M. Sala, and J. M. Gasol. 2017. Patterns of bacterial diversity in the marine planktonic particulate matter continuum. ISME J. **11**: 999–1010. doi:10.1038/ismej.2016.166

Mestre, M., C. Ruiz-González, R. Logares, C. M. Duarte, J. M. Gasol, and M. M. Sala. 2018. Sinking particles promote vertical connectivity in the ocean microbiome. Proc. Natl. Acad. Sci. U. S. A. **115**: E6799–E6807. doi:10.1073/pnas.1802470115

Middelburg, J. J. 2011. Chemoautotrophy in the ocean. Geophys. Res. Lett. **38**: L24604. doi:10.1029/2011GL049725

Le Moigne, F. A. C. 2019. Pathways of Organic Carbon Downward Transport by the Oceanic Biological Carbon Pump. Front. Mar. Sci. **6**: 634. doi:10.3389/fmars.2019.00634

Mühlenbruch, M., H.-P. Grossart, F. Eigemann, and M. Voss. 2018. Mini-review: Phytoplankton-derived polysaccharides in the marine environment and their interactions with heterotrophic bacteria. Environ. Microbiol. **20**: 2671–2685. doi:10.1111/1462-2920.14302

Munson-McGee, J. H., M. R. Lindsay, E. Sintes, and others. 2022. Decoupling of respiration rates and abundance in marine prokaryoplankton. Nature. doi:10.1038/s41586-022-05505-3

Needham, D. M., and J. A. Fuhrman. 2016. Pronounced daily succession of phytoplankton, archaea and bacteria following a spring bloom. Nat. Microbiol. **1**: 16005. doi:10.1038/nmicrobiol.2016.5

Nelson, N. B., and D. A. Siegel. 2013. The Global Distribution and Dynamics of Chromophoric Dissolved Organic Matter. Ann. Rev. Mar. Sci. **5**: 447–476. doi:10.1146/annurev-marine-120710-100751

Nelson, N. B., D. A. Siegel, C. A. Carlson, and C. M. Swan. 2010. Tracing global biogeochemical cycles and meridional overturning circulation using chromophoric dissolved organic matter. Geophys. Res. Lett. **37**: L03610. doi:10.1029/2009GL042325

Nowicki, M., T. DeVries, and D. A. Siegel. 2022. Quantifying the Carbon Export and Sequestration Pathways of the Ocean's Biological Carbon Pump. Global Biogeochem. Cycles **36**: e2021GB007083. doi:10.1029/2021GB007083

Parada, A. E., D. M. Needham, and J. A. Fuhrman. 2016. Every base matters: Assessing small subunit rRNA primers for marine microbiomes with mock communities, time series and global field samples. Environ. Microbiol. **18**: 1403–1414. doi:10.1111/1462-2920.13023

Pegliasco, C., A. Chaigneau, and R. Morrow. 2015. Main eddy vertical structures observed in the four major Eastern Boundary Upwelling Systems. J. Geophys. Res. Ocean. **120**: 6008–6033.

doi:10.1002/2015JC010950

Pontiller, B., S. Martínez-García, V. Joglar, and others. 2022. Rapid bacterioplankton transcription cascades regulate organic matter utilization during phytoplankton bloom progression in a coastal upwelling system. ISME J. **16**: 2360–2372. doi:10.1038/s41396-022-01273-0

Rasse, R., and G. Dall'Olmo. 2019. Do Oceanic Hypoxic Regions Act as Barriers for Sinking Particles? A Case Study in the Eastern Tropical North Atlantic. Global Biogeochem. Cycles **33**: 1611–1630. doi:10.1029/2019GB006305

Reintjes, G., B. M. Fuchs, R. Amann, and C. Arnosti. 2020. Extensive Microbial Processing of Polysaccharides in the South Pacific Gyre via Selfish Uptake and Extracellular Hydrolysis. Front. Microbiol. **11**: 583158. doi:10.3389/fmicb.2020.583158

Reuter, J. A., D. V Spacek, and M. P. Snyder. 2015. High-Throughput Sequencing Technologies. Mol. Cell **58**: 586–597. doi:10.1016/j.molcel.2015.05.004

Ruiz-González, C., M. Mestre, M. Estrada, and others. 2020. Major imprint of surface plankton on deep ocean prokaryotic structure and activity. Mol. Ecol. **29**: 1820–1838. doi:10.1111/mec.15454

Rykaczewski, R. R., J. P. Dunne, W. J. Sydeman, M. García-Reyes, B. A. Black, and S. J. Bograd. 2015. Poleward displacement of coastal upwelling-favorable winds in the ocean's eastern boundary currents through the 21st century. Geophys. Res. Lett. **42**: 6424–6431. doi:10.1002/2015GL064694

Saba, G. K., A. B. Burd, J. P. Dunne, and others. 2021. Toward a better understanding of fish-based contribution to ocean carbon flux. Limnol. Oceanogr. **66**: 1639–1664. doi:10.1002/lno.11709

Saba, G. K., D. K. Steinberg, and D. A. Bronk. 2011. The relative importance of sloppy feeding, excretion, and fecal pellet leaching in the release of dissolved carbon and nitrogen by Acartia tonsa copepods. J. Exp. Mar. Bio. Ecol. **404**: 47–56. doi:10.1016/j.jembe.2011.04.013

Salazar, G., F. M. Cornejo-Castillo, E. Borrull, and others. 2015. Particle-association lifestyle is a phylogenetically conserved trait in bathypelagic prokaryotes. Mol. Ecol. **24**: 5692–5706. doi:10.1111/mec.13419

Santana-Falcón, Y., M. Benavides, P. Sangrà, E. Mason, E. D. Barton, A. Orbi, and J. Arístegui. 2016. Coastal–offshore exchange of organic matter across the Cape Ghir filament (NW Africa) during moderate upwelling. J. Mar. Syst. **154**: 233–242. doi:10.1016/j.jmarsys.2015.10.008

Santoro, A. E., R. A. Richter, and C. L. Dupont. 2019. Planktonic Marine Archaea. Ann. Rev. Mar. Sci. **11**: 131–158. doi:10.1146/annurev-marine-121916-063141

Seymour, J. R., S. A. Amin, J. B. Raina, and R. Stocker. 2017. Zooming in on the phycosphere: The ecological interface for phytoplankton-bacteria relationships. Nat. Microbiol. **2**. doi:10.1038/nmicrobiol.2017.65

Siegel, D. A., K. O. Buesseler, S. C. Doney, S. F. Sailley, M. J. Behrenfeld, and P. W. Boyd. 2014. Global assessment of ocean carbon export by combining satellite observations and food-web models. Global Biogeochem. Cycles **28**: 181–196. doi:10.1002/2013GB004743

Slatko, B. E., A. F. Gardner, and F. M. Ausubel. 2018. Overview of Next-Generation Sequencing Technologies. Curr. Protoc. Mol. Biol. **122**: e59. doi:10.1002/cpmb.59

Sogin, M. L., H. G. Morrison, J. A. Huber, D. M. Welch, S. M. Huse, P. R. Neal, J. M. Arrieta, and G. J. Herndl. 2006. Microbial diversity in the deep sea and the underexplored "rare biosphere." Proc. Natl. Acad. Sci. U. S. A. **103**: 12115–12120. doi:10.1073/pnas.0605127103

Stedmon, C. A., S. Markager, and R. Bro. 2003. Tracing dissolved organic matter in aquatic environments using a new approach to fluorescence spectroscopy. Mar. Chem. **82**: 239–254. doi:10.1016/S0304-4203(03)00072-0

Stedmon, C., and X. A. Álvarez-Salgado. 2011. Shedding light on a black box: UV–Visible spectroscopic characterization of marine dissolved organic matter, p. 62–63. *In* N. Jiao, F. Azam, and S. Sanders [eds.], Microbial Carbon Pump in the Ocean. American Association for the Advancement of Science.

Steinberg, D. K., and M. R. Landry. 2017. Zooplankton and the Ocean Carbon Cycle. Ann. Rev. Mar. Sci. **9**: 413–444. doi:10.1146/annurev-marine-010814-015924

Stocker, R., and J. R. Seymour. 2012. Ecology and physics of bacterial chemotaxis in the ocean. Microbiol. Mol. Biol. Rev. **76**: 792–812. doi:10.1128/MMBR.00029-12

Stocker, R., J. R. Seymour, A. Samadani, D. E. Hunt, and M. F. Polz. 2008. Rapid chemotactic response enables marine bacteria to exploit ephemeral microscale nutrient patches. Proc. Natl. Acad. Sci. **105**: 4209–4214. doi:10.1073/pnas.0709765105

Stoecker, D. K., P. J. Hansen, D. A. Caron, and A. Mitra. 2017. Mixotrophy in the Marine Plankton. Ann. Rev. Mar. Sci. **9**: 311–335. doi:10.1146/annurev-marine-010816-060617

Stukel, M. R., M. Décima, and M. R. Landry. 2022. Quantifying biological carbon pump pathways with a data-constrained mechanistic model ensemble approach. Biogeosciences **19**: 3595–3624. doi:10.5194/bg-19-3595-2022

Sunagawa, S., L. P. Coelho, S. Chaffron, and others. 2015. Structure and function of the global ocean microbiome. Science (80-.). **348**: 1261359. doi:10.1126/science.1261359

Suttle, C. A. 2007. Marine viruses - Major players in the global ecosystem. Nat. Rev. Microbiol. **5**: 801–812. doi:10.1038/nrmicro1750

Sydeman, W. J., M. García-Reyes, D. S. Schoeman, R. R. Rykaczewski, S. A. Thompson, B. . A. Black, and S. J. Bograd. 2014. Climate change and wind intensification in coastal upwelling ecosystems. Science (80-.). **345**: 77–80. doi:10.1126/science.1251635

Taucher, J., J. Arístegui, L. T. Bach, W. Guan, M. F. Montero, A. Nauendorf, E. P. Achterberg, and U. Riebesell. 2018. Response of Subtropical Phytoplankton Communities to Ocean Acidification Under Oligotrophic Conditions and During Nutrient Fertilization. Front. Mar. Sci. **5**: 330. doi:10.3389/fmars.2018.00330

Teeling, H., B. M. Fuchs, D. Becher, and others. 2012. Substrate-Controlled Succession of Marine Bacterioplankton Populations Induced by a Phytoplankton Bloom. Science, **336**: 608–611. doi:10.1126/science.1218344

Teeling, H., B. M. Fuchs, C. M. Bennke, and others. 2016. Recurring patterns in bacterioplankton dynamics during coastal spring algae blooms A.A. Brakhage [ed.]. Elife **5**: e11888. doi:10.7554/eLife.11888

Thornton, D. C. O. 2014. Dissolved organic matter (DOM) release by phytoplankton in the contemporary and future ocean. Eur. J. Phycol. **49**: 20–46. doi:10.1080/09670262.2013.875596

Turley, C. M. 1993. The effect of pressure on leucine and thymidine incorporation by free-living bacteria and by bacteria attached to sinking oceanic particles. Deep Sea Res. Part I Oceanogr. Res. Pap. **40**: 2193–2206. doi:10.1016/0967-0637(93)90098-N

Turner, J. T. 2015. Zooplankton fecal pellets, marine snow, phytodetritus and the ocean's biological

pump. Prog. Oceanogr. **130**: 205–248. doi:10.1016/j.pocean.2014.08.005

Urban-Rich, J., J. T. McCarty, D. Fernández, and J. L. Acuña. 2006. Larvaceans and copepods excrete fluorescent dissolved organic matter (FDOM). J. Exp. Mar. Bio. Ecol. **332**: 96–105. doi:10.1016/j.jembe.2005.11.023

Villarino, E., J. R. Watson, G. Chust, and others. 2022. Global beta diversity patterns of microbial communities in the surface and deep ocean. Glob. Ecol. Biogeogr. **31**: 2323–2336. doi:10.1111/geb.13572

Whitman, W. B., D. C. Coleman, and W. J. Wiebe. 1998. Prokaryotes: The unseen majority. Proc. Natl. Acad. Sci. **95**: 6578 LP – 6583. doi:10.1073/pnas.95.12.6578

Worden, A. Z., M. J. Follows, S. J. Giovannoni, S. Wilken, A. E. Zimmerman, and P. J. Keeling. 2015. Rethinking the marine carbon cycle: Factoring in the multifarious lifestyles of microbes. Science (80-.). **347**: 1257594. doi:10.1126/science.1257594

Wright, J. J., K. M. Konwar, and S. J. Hallam. 2012. Microbial ecology of expanding oxygen minimum zones. Nat. Rev. Microbiol. **10**: 381–394. doi:10.1038/nrmicro2778

Yokokawa, T., Y. Yang, C. Motegi, and T. Nagata. 2013. Large-scale geographical variation in prokaryotic abundance and production in meso- and bathypelagic zones of the central Pacific and Southern Ocean. Limnol. Oceanogr. **58**: 61–73. doi:10.4319/lo.2013.58.1.0061

Zark, M., N. K. Broda, T. Hornick, H.-P. Grossart, U. Riebesell, and T. Dittmar. 2017a. Ocean Acidification Experiments in Large-Scale Mesocosms Reveal Similar Dynamics of Dissolved Organic Matter Production and Biotransformation. Front. Mar. Sci. **4**: 271. doi:10.3389/fmars.2017.00271

Zark, M., J. Christoffers, and T. Dittmar. 2017b. Molecular properties of deep-sea dissolved organic matter are predictable by the central limit theorem: Evidence from tandem FT-ICR-MS. Mar. Chem. **191**: 9–15. doi:10.1016/j.marchem.2017.02.005

Chapter 1

Dissolved organic matter under simulated upwelling

The importance of the dissolved organic matter pool for the carbon sequestration potential of artificial upwelling

Markel Gómez-Letona, Marta Sebastián, Isabel Baños, María F. Montero, Clàudia Pérez Barrancos, Moritz Baumann, Ulf Riebesell and Javier Arístegui

Frontiers in Marine Science, 2022. doi: 10.3389/fmars.2022.969714

In the face of climate change there is a need to reduce atmospheric CO_2 concentrations. Artificial upwelling of nutrient-rich deep waters has been proposed as a method to enhance the biological carbon pump in oligotrophic oceanic regions in order to increase carbon sequestration. Here we examine the effect of different artificial upwelling intensities and modes (single pulse versus recurring pulses) on the dynamics of the dissolved organic matter pool (DOM). We introduced nutrient-rich deep water to large scale mesocosms (~44 m^3) in the oligotrophic subtropical North Atlantic and found that artificial upwelling strongly increased DOM concentrations and changed its characteristics. The magnitude of the observed changes was related to the upwelling intensity: more intense treatments led to higher accumulation of dissolved organic carbon (>70 μM of excess DOC over ambient waters for the most intense) and to comparatively stronger changes in DOM characteristics (increased proportions of chromophoric DOM (CDOM) and humic-like fluorescent DOM), suggesting a transformation of the DOM pool at the molecular level. Moreover, the single upwelling pulse resulted in higher CDOM quantities with higher molecular weight than the recurring upwelling mode. Together, our results indicate that under artificial upwelling, large DOM pools may accumulate in the surface ocean without being remineralised in the short-term. Possible reasons for this persistence could be a combination of the molecular diversification of DOM due to microbial reworking, nutrient limitation and reduced metabolic capabilities of the prokaryotic communities within the mesocosms. Our study demonstrates the importance of the DOC pool when assessing the carbon sequestration potential of artificial upwelling.

Introduction

Primary producers and bacterioplankton require the uptake of inorganic nutrients from their surrounding waters to grow and keep their metabolism functioning (Azam and Malfatti 2007). Inorganic nutrients are found in high concentrations below the photic layer (Levitus et al. 1993; Johnson et al. 1997), due to the absence of nutrient-consuming, light-driven primary production and the predominance of nutrient-releasing remineralization of organic matter. These nutrient-rich waters can reach the surface by a range of physical processes, such as winter convection (Severin et al. 2017), wind-driven coastal upwelling (Jacox et al. 2018), mesoscale eddies (McGillicuddy et al. 2007) or diapycnal diffusion (Arcos-Pulido et al. 2014), and play a key role in driving primary production and, consequently, CO_2 fixation in the surface ocean (Field et al. 1998). A fraction of this newly produced organic matter is in turn exported, via multiple pathways, out of the photic layer into the deep ocean, where it is ultimately remineralised, releasing inorganic nutrients and carbon back to seawater. This process is known as the biological carbon pump (Le Moigne 2019).

The biological carbon pump plays a major role in the atmosphere-ocean CO_2 dynamics and acts as a key mechanism in the sequestration of CO_2 in the deep ocean (Le Moigne 2019). Nonetheless, there are great extents of the global oceans, such as the subtropical gyres that make up ~40% of Earth's surface (Polovina et al. 2008), where the vertical input of nutrients is limited and, thus, phytoplankton rely on nutrients recycled within the photic layer, resulting in low primary production and CO_2 fixation (Field et al. 1998). In the context of climate change and increasing CO_2 emissions, the possibility of fertilizing these nutrient-poor waters to fuel primary production has been put forward as a climate intervention approach to enhance CO_2 sequestration in the ocean and help reduce its atmospheric concentration (Williamson et al. 2012; Fawzy et al. 2020). One of the proposed fertilization methods consists in bringing nutrient-rich deep waters into the surface, an approach known as artificial upwelling (Pan et al. 2016). Artificial upwelling is envisioned to enhance the biological carbon pump by increasing primary production in nutrient-limited oceanic regions, amplifying carbon export and ideally yielding a net increase in carbon sequestration (if the C:N and C:P ratios of the exported organic matter are higher than the Redfield ratio). However, the efficiency of artificial upwelling to sequester atmospheric CO_2 has been questioned (Shepherd et al. 2007; Yool et al. 2009), evidencing the need of further research.

Dissolved organic carbon (DOC) represents the largest pool of reduced carbon in the ocean and its downward flux is an important contributor to the biological carbon pump (Hansell et al. 2009; Le Moigne 2019). The efficiency of the DOC pathway of carbon export will depend on the extent of its remineralization by prokaryotes and the depth at which it occurs in the water column. Some DOM is readily consumed by prokaryotes, and this process influences the absorption spectrum and fluorescence characteristics of DOM (Catalá et al. 2015b, 2018). A fraction of it, however, seems to escape remineralization and is accumulated. Two main hypotheses seek to explain this persistence (Dittmar et al. 2021): on the one hand, the intrinsic inability (or very reduced ability) of prokaryotes to consume some classes of organic molecules would lead to their accumulation and the long-term persistence of a fraction of DOM. On the contrary, the accumulated DOM might not be inherently resistant to degradation, its persistence being instead a consequence of complex ecological interactions between the vast molecular diversity of DOM (Zark et al. 2017b) and the wide metabolic capabilities of prokaryotes (Sunagawa et al. 2015; Acinas et al. 2021). In this scenario, all compounds would be continuously produced and degraded, stabilization occurring as a consequence of parallel decreases in the concentration of specific compounds and the abundance of prokaryotes able to degrade them (Dittmar et al. 2021). For instance, in the subtropical North Atlantic, seasonally accumulated DOC has been shown to resist remineralization by surface prokaryotic communities, but it is remineralized when exported into the mesopelagic layer (Carlson et al. 2004). In summary, the balance between the transport of DOM to the ocean's interior and how rapidly remineralization occurs above the permanent pycnocline (which depends on both physical dynamics and the ability of prokaryotes to consume DOM) will determine the net contribution of DOC to carbon sequestration. This balance will consequently influence the efficiency of artificial upwelling, making DOM a major factor to consider when addressing carbon sequestration by this approach.

In the present work we studied the effect of the intensity and mode of artificial upwelling on the DOM pool in an oligotrophic marine environment. Using mesocosms that simulate ecological systems in close-to-natural conditions, we introduced nutrient-rich deep water into nutrient-depleted surface waters, aiming to investigate how the quantity, stoichiometry and composition of DOM is affected by upwelling and the subsequent enhancement of primary production. Deep-water addition was done simulating two modes of artificial upwelling: a singular addition, representing a moored system that upwells water into passing water patches,

fertilizing them once (e.g., Zhang et al. 2016), and recurring deep water additions, simulating a system that drifts within a water parcel, repeatedly upwelling water into it (e.g., Maruyama et al. 2011). We aimed to study DOM dynamics under the different artificial upwelling scenarios to gain insights into the short-term fate of DOM and the potential long-term implications for the efficiency of carbon sequestration.

Materials and methods

Experimental setup and sampling

Our experiment was conducted in Gando Bay (27° 55′ 41″ N, 15° 21′ 55″ W, Gran Canaria, Canary Islands) during the autumn of 2018 as a part of the Ocean artUp project. Nine KOSMOS (Kiel Off-Shore Mesocosms for Ocean Simulations; Riebesell et al. 2013) were deployed (M1-M9) and filled with *in situ* oligotrophic water (mean volume 43.775 ± 1.352 m^3). To simulate artificial upwelling, nutrient-rich deep water was collected off Gran Canaria from 330 m (on day -10) and 280 m

Table 1. Information of the treatments applied to each mesocosm. Total additions of deep water (as absolute values and % relative to the volume of the mesocosms), nitrogen (N), phosphorus (P) and silica (Si). N, P and Si values include both inorganic and organic forms.

Mesocosm	Upwelling mode	Upwelling intensity	Added deep water volume [m^3]	Added deep water volume [%]*	Added N [$\mu mol \cdot L^{-1}$]	Added P [$\mu mol \cdot L^{-1}$]	Added Si [$\mu mol \cdot L^{-1}$]
M5	Control		0.0	0.0	0.00	0.000	0.00
M3	Singular	Low	2.8	6.4	1.62	0.094	0.74
M7		Medium	5.3	12.0	3.07	0.177	1.41
M9		High	9.8	22.4	5.56	0.325	2.63
M1		Extreme	17.2	39.2	9.80	0.567	4.58
M2	Recurring	Low	2.8	6.3	1.61	0.094	0.69
M4		Medium	5.6	12.7	3.15	0.187	1.35
M6		High	11.2	25.6	6.16	0.363	2.64
M8		Extreme	22.4	51.1	10.97	0.682	4.96

** Considering average mesocosm volume of 43.775 m^3*

depth (on day 23), and added to the mesocosms in two different treatment modes (Table 1): a *singular* mode (M3, M7, M9, M1), in which a single deep-water (DW) addition was performed (on day 4), and a *recurring* mode (M2, M4, M6, M8), in which consecutive deep-water additions were performed (on days 4, 8, 12, 16, 21, 24, 28 and 32). For each artificial upwelling mode, four levels of intensity were simulated, with increasing quantities of DW added to them: *low* (M2, M3), *medium* (M7, M4), *high* (M6, M9) and *extreme* (M8, M1). For the same intensity level, the singular and recurring modes had overall similar amounts of nutrients added during the entire course of the experiment, yielding comparable treatments (Table 1). A characterisation of the DOM found in the deep water can be found in Table S1. No deep water was added to M5 (*Control*) and ambient waters outside of the mesocosms were monitored during regular sampling (*Atlantic*). A detailed description of the experimental set up and sampling procedures can be found in Baumann et al. (2021b).

Integrated samples of the water column within the mesocosms were collected using depth-integrated water samplers (IWS, HYDRO-BIOS, Kiel) and stored in acid-cleaned shaded glass bottles. To minimize photobleaching and degradation, samples were kept in dark, cool conditions until freezing/analysis (see below) on the same day. Prior to analysis/freezing, samples for dissolved organic matter quantification and characterisation were filtered through precombusted (450ºC, 6h) glass fibre filters (GF/F, 0.7 μm nominal pore size) using acid-cleaned syringes and filter holders.

Dissolved Organic Carbon (DOC), Nitrogen (DON) and Phosphorus (DOP)

For DOC measurements, 10 mL of filtered samples were stored in high density polyethylene bottles and frozen (-20°C) until analysis. Samples were analysed with a Shimadzu TOC-5000 analyser (Sharp et al. 1993). Prior to the analysis, samples were thawed, acidified with 50 μL of H_3PO_4 (50%) and sparged with CO_2-free air for several minutes to remove inorganic carbon. DOC concentrations were estimated based on standard curves (30–200 μM) of potassium hydrogen phthalate produced every day (Thomas et al. 1995). Reference material of deep-sea water (DSW, 42–45 μM C) provided by D. A. Hansell laboratory (University of Miami) was analysed daily.

DON and DOP samples were collected in acid-rinsed, high-density polyethylene (HDPE) bottles and analysed according to Hansen and Koroleff (1999). Upon arrival in the laboratory, 40 mL of the samples were filtered (0.45 μm cellulose acetate filters,

Whatman) under sterile conditions. Total dissolved nitrogen and phosphorus were decomposed to phosphate and nitrate by adding one spoon of the oxidizing reagent Oxisolv (Merck) and cooking the solution for approximately one hour (90-100ºC). The samples were left to cool overnight, and the next day total dissolved nitrogen and phosphorus concentrations were measured spectrophotometrically on a continuous flow analyser (QuAAtro AutoAnalyzer, SEAL Analytical). Triplicates of artificial seawater were treated and measured similarly on each measurement day. They acted as blanks and were averaged and subtracted from the samples. DON and DOP concentrations were calculated from the total dissolved nitrogen and phosphorus by subtracting the dissolved inorganic nitrogen and phosphate concentrations.

Chromophoric Dissolved Organic Matter (CDOM) characterisation

Absorbance spectra were determined using an Ocean Optics USB2000+UV-VIS-ES Spectrometer alongside a World Precision Instruments liquid waveguide capillary cell (LWCC) with a path length of 0.9982 m. For each sample, absorbance was measured across a wavelength spectrum between 178 nm and 878 nm, performing a blank measurement prior to each sample using ultrapure Milli-Q water. Data processing was done in R (v. 4.1.2; R Core Team, 2021): raw spectra (samples and blanks) were cropped between 250 and 700 nm, blank spectra were subtracted from sample spectra and a baseline correction was performed by subtracting the average absorbance of each sample between 600 and 700 nm to the whole spectrum. The effect of refractive index changes due to salinity on the absorbance measurements of our equipment was negligible (as reported in Catalá et al. 2018) and, thus, no corrections were applied.

After processing, absorbance was transformed into absorption following the definition of the Napierian absorption coefficient:

$$a_\lambda = 2.303 \cdot \frac{\mathrm{Abs}_\lambda}{L}$$

Where, for each wavelength λ, the absorption coefficient a_λ is given by the absorbance at wavelength λ (Abs_λ), the path length of the cuvette (L, in meters; here 0.9982) and 2.303 (the factor that converts from decadic to natural logarithms).

From a_λ spectra values at 254 and 325 nm were considered. Both are proxies of CDOM concentration, although for different fractions of it: while a_{254} represents conjugated double bonds a_{325} is related to the aromatic fraction (Lønborg and

Álvarez-Salgado 2014; Catalá et al. 2016, 2018). Furthermore, spectral slopes between 275-295 nm and 350-400 nm were estimated from the natural log transformed absorption spectra following Helms et al. (2008). These regions of the spectra (as well as their ratio, S_R) have been shown to be especially sensitive to changes in the molecular weight of CDOM, with higher slopes denoting lower average molecular weight (Helms et al. 2008, 2013). Moreover, these spectral slope parameters have been related to the microbial reworking of organic matter in the ocean, decreasing values being associated to increased transformation of DOM by prokaryotes (Catalá et al. 2015a, 2018).

Fluorescent Dissolved Organic Matter (FDOM) characterisation

Fluorescence measurements were performed with a Jobin Yvon Horiba Fluoromax-4 spectrofluorometer, exciting the water samples in a wavelength range of 240-450 nm (10 nm increments), and measuring the fluorescence emission in a range of 300-560 nm (2 nm increments), with excitation and emission slit widths of 5 nm, and an integration time of 0.25 s. Fluorescence measurements were collected into excitation-emission matrices. To correct for lamp spectral properties and be able to compare results with other studies, excitation-emission matrices were measured in signal-to-reference mode with instrument-specific excitation and emission corrections applied during collection (Sc:Rc).

Excitation-emission matrices were processed using the DOMFluor toolbox (v. 1.7; Stedmon and Bro, 2008) for Matlab (R2017a). Alongside seawater samples, each sampling day three blank samples were measured using ultrapure Milli-Q water (at the beginning, middle and end of the measurement process). A weighted mean of the blanks was subtracted from each sample. Furthermore, excitation-emission matrices were normalized to the Raman area using the emission scan at 350 nm of ultrapure water blanks, calculating the area following the trapezoidal integration method (Lawaetz and Stedmon 2009). Inner-filter correction was not performed as the average absorption coefficient of CDOM at 250 nm in all samples was 2.120 ± 0.544 m^{-1} (mean ± sd, n = 208; max. = 3.4 m^{-1}), which was lower than the threshold of 10 m^{-1} above which this correction is considered to be necessary (Stedmon and Bro 2008). Rayleigh scatter bands of 1st (*Em = Ex ± bandwidth*) and 2nd (*Em = 2·Ex ± 2·bandwith*) orders were cut at each wavelength pair.

Parallel factor analysis of fluorescence data

The processed excitation-emission matrices (n = 175, samples with measurement errors were removed) were analysed applying a parallel factor (PARAFAC) analysis (Stedmon et al. 2003; Stedmon and Bro 2008) using the DOMFluor toolbox. A model consisting of five components (Table S2, Fig. S1) was validated by split-half validation and random initialization. For each sample, the fluorescence maximum (F_{max}) of the components was recorded.

The optical characteristics of the five fluorescent DOM (FDOM) components are summarized in Table S2, along with similar fluorophores found in the literature. The identification of previously described fluorophores was performed using the OpenFluor database (openfluor.lablicate.com, Murphy et al. 2014), based on the combined Tucker Congruence Coefficient of the excitation and emission spectra ($TCC_{ex\text{-}em}$). C1, C2, C4 and C5 had 17, 28, 11 and 6 matches with high congruence ($TCC_{ex\text{-}em}$ >0.95), respectively. C1 presented characteristics similar to fluorophores identified as amino acid-/tryptophan-like, with primary and secondary excitation maxima at 300 and 240 nm, respectively, and an emission maximum at 354 nm (Table S2). Such amino acid-like compounds have been previously described as partially bioavailable for prokaryotic consumption (Lønborg et al. 2010). C2 (excitation maxima at 250 and 330 nm, emission maximum at 410 nm) displayed high similarities with humic-like fluorophores (peak M, Table S2) that have been observed to be positively correlated to apparent oxygen utilization in the ocean (Catalá et al. 2015b). C4 was also similar to previously identified humic-like components but, unlike C2, its signal presented peaks at higher wavelengths (excitation maxima at 260 and 370 nm, emission maximum at 466 nm). It resembled a mixture of peaks A and C, formed by compounds with high aromaticity (Table S2). Similarly to C1, C5 also presented excitation and emission spectra highly congruent with amino acid-/tryptophan-like fluorophores, but had lower maxima than C1 (excitation and emission maxima at 270 and 342 nm, respectively; Table S2). Notably, the spectrum of this component was highly similar to that of indole (Wünsch et al. 2015). As opposed to the other components, C3 presented matches with congruence lower than 0.95. With excitation maximum below 240 nm and a broad emission spectrum (maximum at 330 – 472 nm), it was identified as similar to fluorophores potentially related to fluorometer artifacts (Table S2). Thus, the C3 component was not further considered in the analyses.

Prokaryotic heterotrophic production and cell abundance

Prokaryotic heterotrophic production (PHP) was estimated via the incorporation of ^{3}H-leucine using the centrifugation method (Smith and Azam 1992). ^{3}H-leucine (Perkin-Elmer, specific activity 160 Ci mmoL^{-1}) was added at final concentration (20 nmol L^{-1}) to quadruplicate 1 mL subsamples. Blanks were established by adding 100 µL of 50% trichloroacetic acid (TCA) to duplicate blanks screw-cap microcentrifuge tubes 15 min prior to radioisotope addition. The microcentrifuge tubes were incubated at *in situ* temperature (± 1ºC) in the dark for 2 h. Incorporation of leucine in the quadruplicate tubes was stopped by adding 100 µL ice-cold 50% TCA and tubes were kept together with the blanks at –20ºC until further processing as in Smith and Azam (1992). The mean disintegrations per minute (DPM) of the TCA-killed blanks were removed from the mean DPM of the respective samples and succeeding DPM value converted into leucine incorporation rates. PHP was calculated using a conservative theoretical conversion factor of 1.55 kg C moL^{-1} Leu assuming no internal isotope dilution (Kirchman 1993). The PHP data are available at the PANGAEA repository (Baumann et al. 2021a).

Samples for prokaryotic cell abundance were collected into 2 mL cryovials, fixed with a 2% final concentration of paraformaldehyde and stored at -80°C. After thawing, 400 µL subsamples were stained with 4 µL of the fluorochrome SYBR Green I (Molecular Probes) diluted in dimethyl sulfoxide (1:10) and analysed in a FACSCalibur (Becton-Dickinson) flow cytometer. Fluorescent beads (1 µm, Polysciences) were added for internal calibration (10^{5} mL^{-1}). Prokaryotic cells were identified in green fluorescence vs side scatter cytograms. Details in **Chapter 2**.

Inorganic nutrients, chlorophyll a and particulate organic carbon

Nitrate (NO_3^-), nitrite (NO_2^-), ammonium (NH_4^+), phosphate (PO_4^{3-}) and silicic acid ($Si(OH)_4$) were quantified spectrophotometrically on a five channel continuous flow analyser (QuAAtro AutoAnalyzer, SEAL Analytical Inc., Mequon, United States). Chlorophyll *a* (Chl *a*) was measured with an HPLC Ultimate 3000 (Thermo Scientific GmbH, Schwerte, Germany). Particulate organic carbon (POC) in the water column was measured using a CN analyser (Euro EA-CN, HEKAtech). See Baumann et al. (2021b) for details. Chl *a* and POC data are available at the PANGAEA repository (Baumann et al. 2021a).

Statistical analyses

All statistical analyses and data representations were performed in R (v. 4.1.2; R Core Team, 2021). Linear regressions were performed to assess the relationships between upwelling intensity (as N addition, in μM) and the dissolved organic matter variables. Normality and homoscedasticity of residuals were tested with Shapiro-Wilk (*stats* package, v. 4.1.2) and Breusch-Pagan (*lmtest* package, v. 0.9.39; Zeileis and Hothorn, 2002) tests, respectively. Data representations were done with *ggplot2* (v. 3.3.5; Wickham, 2016).

Results

Response of primary producers

Artificial upwelling led to large phytoplankton blooms after the first deep water addition, increasing primary production and shifting the community composition towards a diatom dominated assemblage (Ortiz et al. 2022). Changes were in accordance with the intensity level of upwelling: the largest Chl *a* build-ups were registered in the singular extreme treatment, where Chl *a* reached 11.2 $\mu g \cdot L^{-1}$ on day 9 (Fig. 1a). Upwelling modes however differed in their outcomes after the first deep water addition. In the singular treatments the blooms rapidly collapsed and Chl *a* remained low until the end of the experiment, while in the recurring treatments subsequent deep water additions allowed to sustain the blooms (with oscillating Chl *a* concentrations, Fig. 1a) throughout the experiment. Particulate organic carbon (POC) concentrations in the water column (Fig. 1b) showed accumulations following the phytoplankton bloom dynamics. Singular treatments accumulated the highest POC values after the initial bloom, reaching 66 μM in the extreme intensity level, followed by a steady decrease. The response in the recurring treatments was slower but POC accumulated until day ~20 (63 μM in the extreme treatment). While the least intense levels ended with similar concentrations to those of the singular mode, in the high and extreme recurring treatments POC values were markedly higher after day 27 (maximum of 102 μM).

Dissolved organic matter concentration and elemental composition

Artificial upwelling yielded large increases in the DOM pool, in direct positive relationship with upwelling intensity (Fig. 2 and 3). Extreme treatments presented

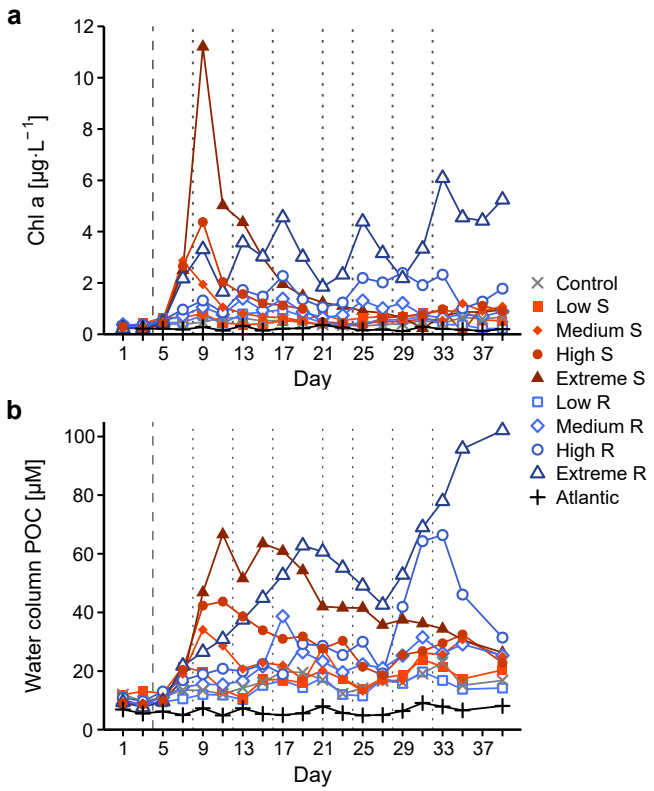

Figure 1. Chl *a* (a) and particulate organic carbon (POC) (b) concentrations during the experiment. Vertical lines indicate deep water additions of singular (dashed) and recurring (dashed and dotted) treatments.

DOC concentrations that were +70 µM compared to starting conditions (Fig. 2a). Average DOC concentrations prior to the first deep water addition on day 4 ranged between 70.6-78.1 µM. After the deep water addition DOC remained relatively stable without exceeding initial values until day 9, when concentrations started to raise in all treatments coinciding with the peak of the diatom bloom (Fig. 1). After day 9, while the bloom in the singular treatments started to collapse, DOC concentrations continued to increase, especially in the singular treatments: on day 13, the extreme, high and medium singular treatments showed the highest DOC values with 155, 109 and 106 µM respectively (Fig. 2a). After day 13, DOC in these mesocosms did not continue to increase and tended to stabilize until the end of the experiment.

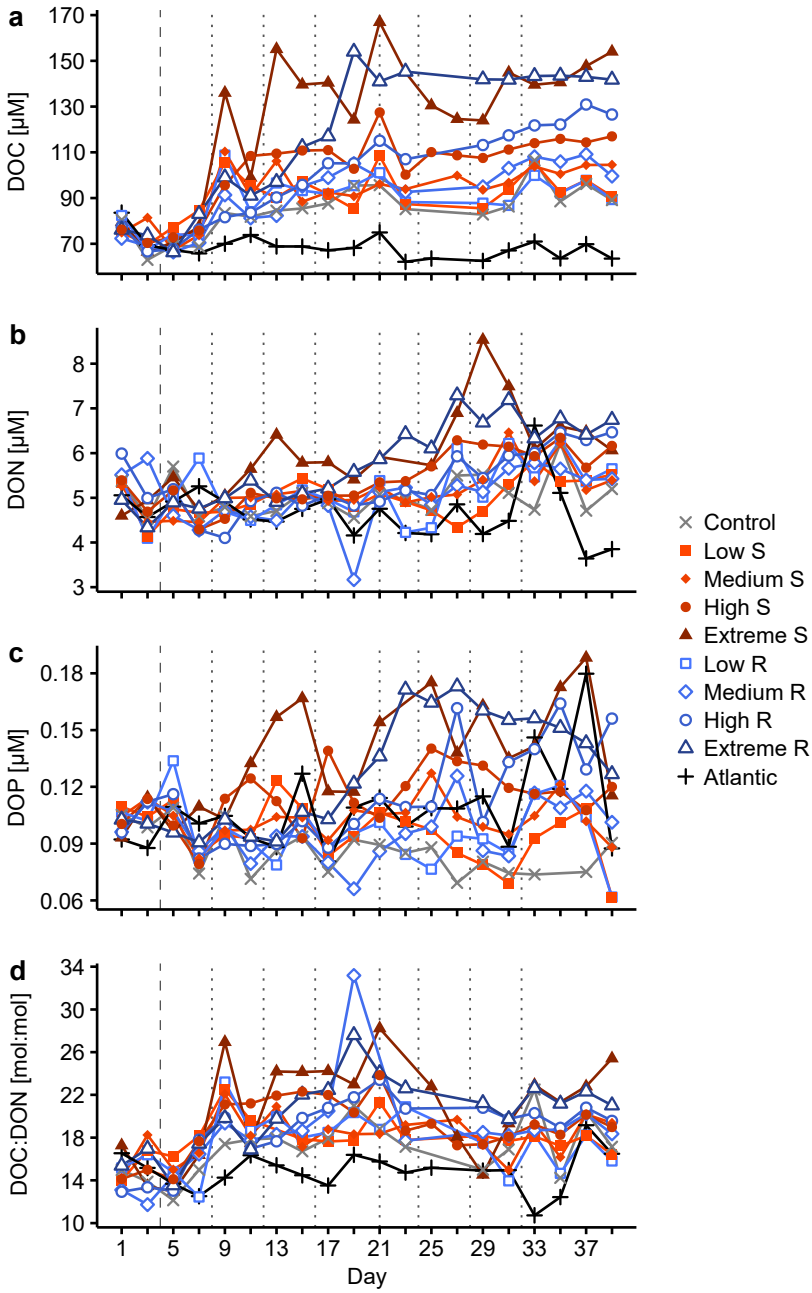

Figure 2. Changes in dissolved organic matter concentrations and elemental ratios during the experiment. Temporal evolution of a) DOC, b) DON, c) DOP, d) DOC:DON. Vertical lines indicate deep water additions of singular (dashed, day 4) and recurring (dashed and dotted) treatments. Results for DOC:DOP and DON:DOP ratios can be found in Figure S2.

In the recurring treatments, where phytoplankton abundances experienced smaller initial increases but did not collapse (Fig. 1), DOC increases were not as abrupt. Only between days 16-20, when the bloom in the extreme recurring treatment presented a major decrease, DOC displayed pronounced increases, reaching its peak on day 19 (154 µM) and subsequently sustained similar values, while the high treatment experienced a steady increase throughout the experiment (Fig. 2a). During days 33-39, average DOC values were of 143-145, 115-125, 103-106 and 95-97 µM for extreme, high, medium and low treatments, respectively. After the final deep water addition to the recurring treatments (days ≥33), average DOC concentrations showed a significant positive relationship with upwelling intensity (Fig. 3a), with a similar effect for both upwelling modes (Table S3). During the entire experiment, DOC concentrations in the control mesocosm trailed those in the low treatments, while the Atlantic remained relatively stable with far smaller values (mean ± sd = 68.5 ± 5.1 µM).

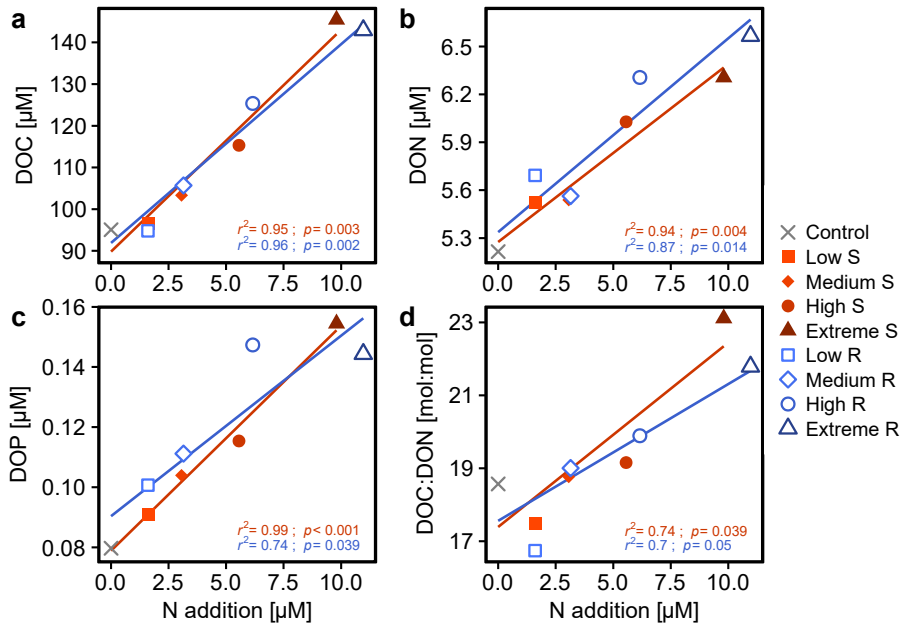

Figure 3. Effect of upwelling intensity on dissolved organic matter. Shown are linear regressions of a) DOC, b) DON, c) DOP and d) DOC:DON values against upwelling intensity (N addition) per upwelling mode. DOM values were averaged after the last deep water addition (≥day 33). The coefficient of determination (r^2) and p-value (p) of the regressions are included. Only the lines for significant regressions ($p < 0.05$) are displayed (see Table S3 for detailed test statistics). Results for DOC:DOP and DON:DOP ratios can be found in Figure S3.

Increases in DON and DOP concentrations were more subtle than in DOC (Fig. 2b and 2c). Initial values ranged between 4.65-5.70 μM and 0.102-0.109 μM, respectively. On days 11-13 DON values started to raise in the extreme singular treatment, followed by the extreme recurring treatment on day 19. These mesocosms reached maximum values of 7-8 μM during days 27-31. In contrast to DOC concentrations, DON values departed less from initial conditions and presented higher variability. Nonetheless, increasing DON concentrations were associated with increasing upwelling intensity, with similar effects for both modes (Fig. 2b and 3b, Table S3). Similarly, differences in DOP between treatments were minor until day 11, when the extreme singular treatment started to increase, reaching values above 0.15 μM and fluctuating until the end of the experiment. The extreme recurring treatment began to separate from less intense treatments on day 19, peaking during days 23-27 at ~0.17 μM and slowly decreasing towards the end (Fig. 2c). Despite variability, overall treatments subject to more intense upwelling presented higher DOP concentrations: average DOP values on days ≥33 showed significant positive relationships with upwelling intensity both for singular and recurring upwelling modes (Fig. 3c, Table S3).

The differential changes in DOC, DON and DOP were reflected in the elemental ratios (Fig. 2d and S2), with notable increases in the values of the DOC:DON and DOC:DOP ratios, leading to DOM with higher relative C content. The average DOC:DON:DOP ratio across mesocosms prior to the first deep water addition was 704:48:1 (DOC:DON ~15:1). After the addition and following the DOC build up, carbon ratios started to increase, although consistent differences between treatments were only observed for DOC:DON (Fig. 2d), but not DOC:DOP (Fig. S2). During days 13-21, DOC:DON ratios were highest, particularly in mesocosms with more intense upwelling: extreme singular and recurring treatments showed average values of 25:1 and 23:1, respectively, while low treatments only reached 19:1. Average DOC:DOP ratios ranged between 927:1-1178:1 for this same period. During days 33-39, DOC:DON values experienced a slight decrease, but still were higher than initial ratios and showed consistent differences between treatments (17:1-23:1 across intensity levels). In fact, DOC:DON showed a positive relationship with upwelling intensity (Fig. 3d). While DON:DOP values showed considerable variability and no consistent temporal trend throughout the experiment (Fig. S2), the more intense treatments tended to show lower values. After the last deep water addition, DON:DOP ratios showed negative relationships with upwelling intensity, although only significant for the singular treatments (Fig. S3).

Optical characteristics of dissolved organic matter

The chromophoric and fluorescent fractions of the dissolved organic matter presented pronounced increases in response to artificial upwelling. CDOM concentrations, as depicted by a_{254} (Fig. 4a), increased in all mesocosms once the first water addition was done (including the control despite no nutrients were added). Initial values ranged between 1.22-1.39 m^{-1} and steadily increased for most of the

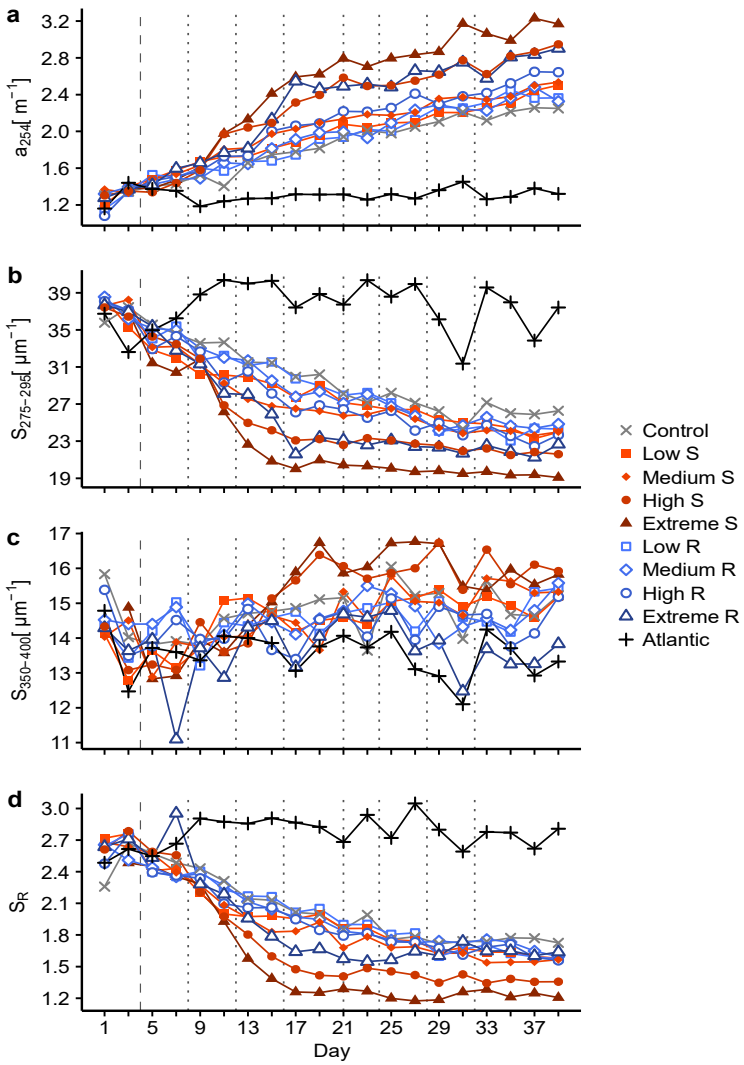

Figure 4. Changes in chromophoric dissolved organic matter during the experiment. Temporal development of a) CDOM quantity as a_{254}, b) $S_{275-295}$, c) $S_{350-400}$, and d) S_R. Vertical lines indicate deep water additions of singular (dashed) and recurring (dashed and dotted) treatments. See explanation of parameters in the Methods section.

experiment, reaching 2.90 m^{-1} (extreme recurring) and 3.17 m^{-1} (extreme singular). The extreme and high singular treatments displayed a pronounced increase on days 9-17 (during and post phytoplankton bloom, Fig. 1), and the extreme recurring treatment on days 13-17, but subsequently continued to raise at a gentler rate until the end of experiment. Resulting CDOM quantities were higher in mesocosms with more intense simulated upwelling and were overall greater in the singular treatments: recurring treatments displayed values that were comparable to the previous intensity level in singular treatments (Fig. 4a). While both upwelling modes showed significant positive relationships between a_{254} and upwelling intensity (Fig. 5a), the slope of the singular mode was steeper than the recurring one even when considering the 95% confidence interval (Table S3). The aromatic fraction of CDOM, represented by a_{325} (Fig. S4), followed patterns very similar to a_{254}, starting at 0.17-0.19 m^{-1} and ending at 0.53-0.99 m^{-1}. a_{325} showed a positive relationship with upwelling intensity (Fig. S5, Table S3).

Spectral slopes ($S_{275-295}$ and $S_{350-400}$), which provide insights into the average molecular weight of the CDOM pool, also experienced marked changes. $S_{275-295}$ (Fig. 4b) began

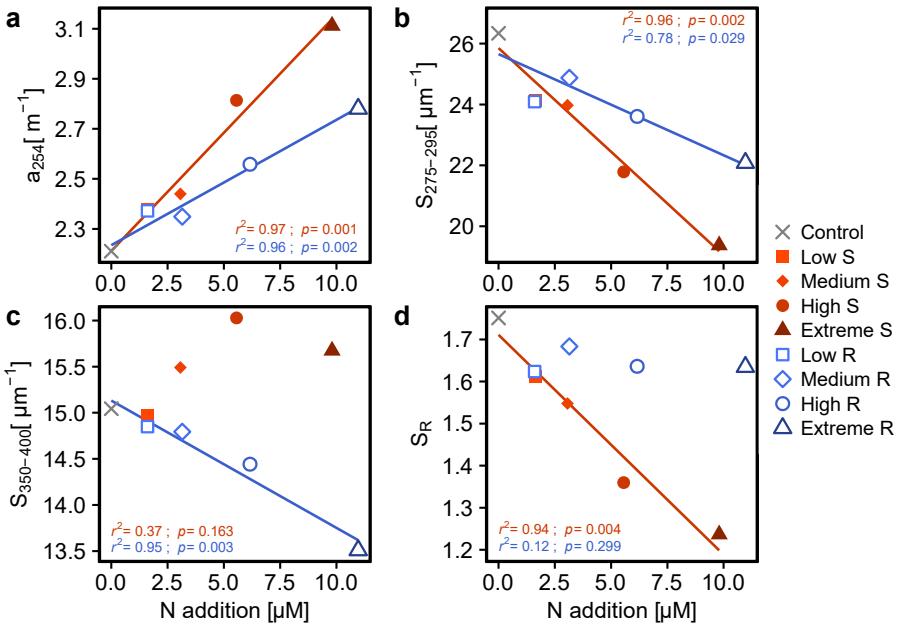

Figure 5. Linear regressions of average values after the last deep water addition to recurring treatments (≥ day 33) of a) CDOM quantity as a_{254}, b) $S_{275-295}$, c) $S_{350-400}$ and d) S_R against upwelling intensity (as N addition), per upwelling mode. The coefficient of determination (r^2) and p-value (p) of the regressions are included. Only lines for significant regressions ($p < 0.05$) are displayed. Regression parameters are detailed in Table S3.

at 36.0-37.9 μm^{-1} and decreased throughout the experiment, signalling an increase in average molecular weight, as compounds of higher molecular weight tend to absorb light at higher wavelengths, thus decreasing the slopes. Coupled with changes in a_{254}, $S_{275-295}$ in the high and extreme singular treatments showed a very pronounced decline between days 9-13, while a sharp decrease was registered on days 13-17 in the extreme recurring treatment. After day 17 values tended to stabilize in the more intense simulated upwelling treatments while less intense treatments continued to steadily decrease (Fig. 4b). The extreme singular treatment displayed the lowest $S_{275-295}$, reaching average values of 19.4 ± 0.3 μm^{-1} during days ≥33. Average $S_{275-295}$ values for this period showed significant negative relationship with upwelling intensity for both modes (Fig. 5b) but, as for a_{254}, $S_{275-295}$ values in singular treatments were comparable to the previous intensity level in recurring treatments. $S_{350-400}$ (initial values of 13.5-14.9 μm^{-1}, Fig. 4c) on the other hand presented opposite trends for each upwelling mode: while singular treatments presented increases (the extreme reaching 16-17 μm^{-1} on days 17-29), the recurring treatments tended to decrease. This resulted in different outcomes after day 33: despite the increase, singular treatments did not show a significant relationship with upwelling intensity, while recurring treatments showed a significant negative one (Fig. 5c). Resulting S_R values overall were dominated by the marked changes in $S_{275-295}$ and followed its patterns (Fig. 4d): initially at 2.48-2.74, decreases were observed specially in high and extreme singular patterns (the latter reaching minimum values close to 1.25) until day 17 and subsequently tended to stabilize. However, the different fates of $S_{350-400}$ for the two upwelling modes were reflected in S_R: at the end of the experiment, singular treatments displayed a significant relationship with upwelling intensity (Fig. 5d), but recurring ones did not and tended to converge around S_R values of 1.65 (Fig. 4d).

Fluorescence measurements provided further details into the composition of the DOM pool. Components C1 and C5 of the PARAFAC model were similar to fluorophores described as amino acid-like/tryptophan-like compounds that are at least partially bioavailable to prokaryotic consumption (Table S2). Both C1 and C5 (Fig. 6a and 6d) presented increases in the intensity of their signal across mesocosms after the first deep water addition. For C1 the extreme singular treatment experienced a fluorescence intensification that was clearly superior to any other treatment, increasing from 0.009 RU to 0.070 RU on day 15, and continued to increase until reaching 0.087 RU at the end of the experiment. Other treatments also displayed increases until day 15 (although smaller) and tended to stabilize afterwards, despite variability, ending within a range of 0.032 (high singular) and 0.044 RU (low

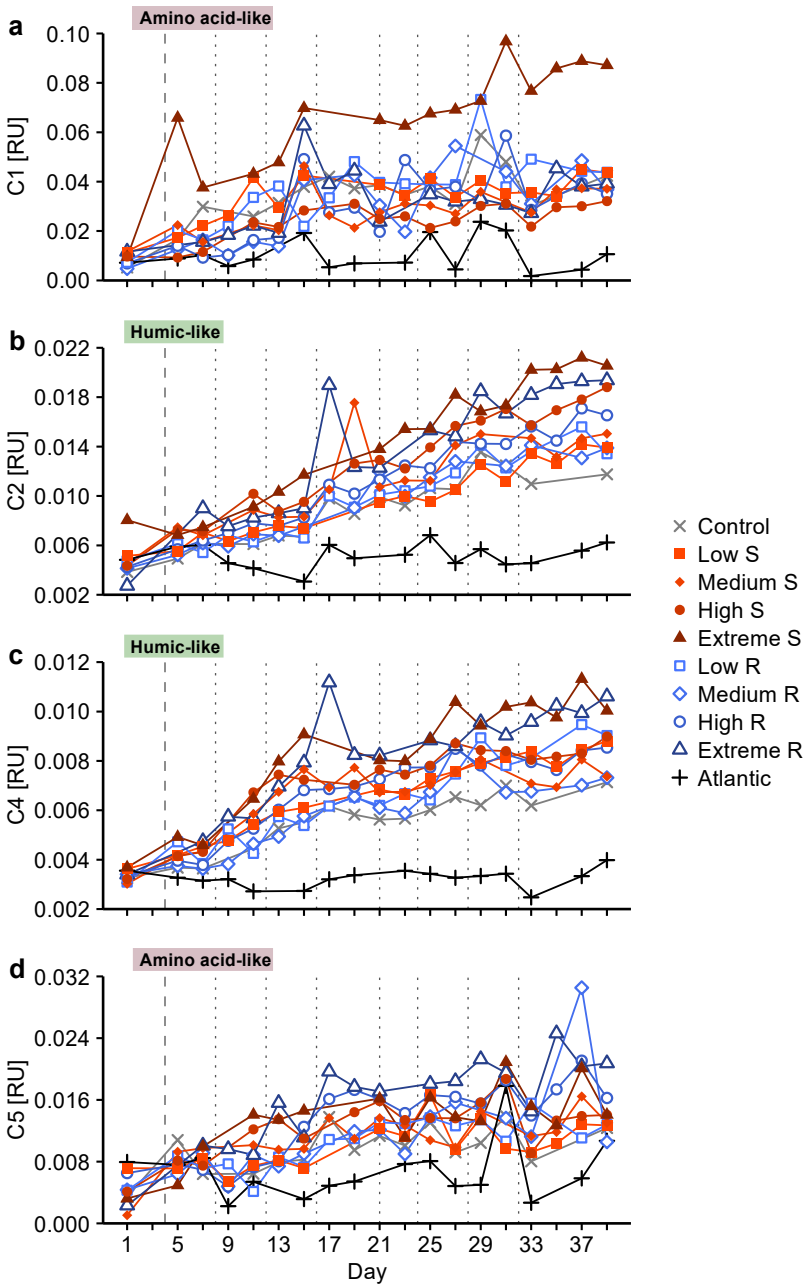

Figure 6. Changes in fluorescent dissolved organic matter during the experiment. Temporal evolution of PARAFAC components a) C1, b) C2, c) C4 and d) C5. Vertical lines indicate deep water additions of singular (dashed) and recurring (dashed and dotted) treatments.

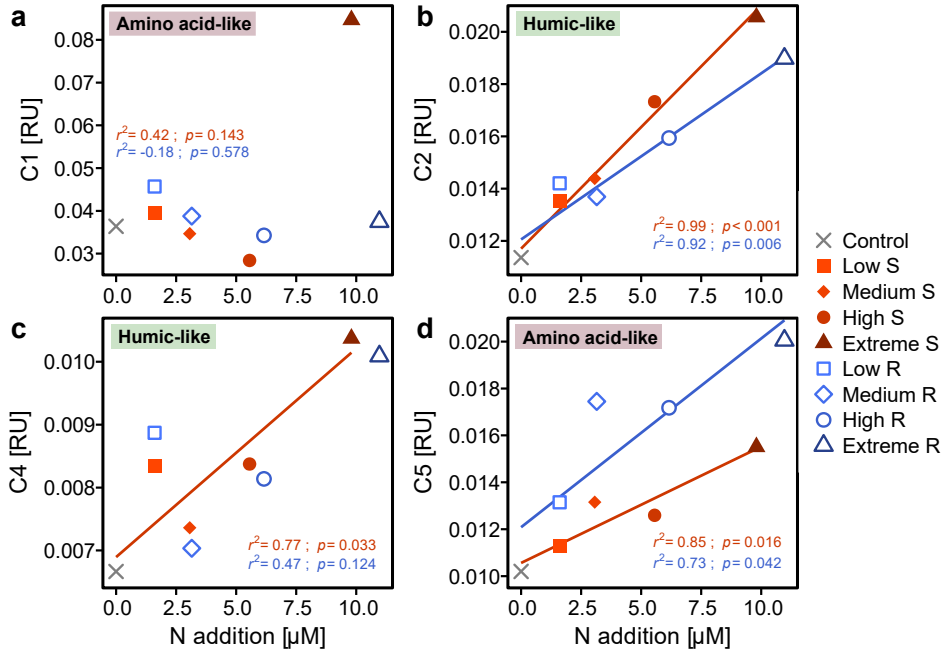

Figure 7. Linear regressions of average values after the last deep water addition to recurring treatments (≥ day 33) of FDOM components a) C1, b) C2, c) C4 and d) C5 against upwelling intensity (as N addition), per upwelling mode. The coefficient of determination (r^2) and p-value (p) of the regressions are included. Only lines for significant regressions ($p < 0.05$) are displayed. Regression parameters are detailed in Table S3.

recurring). Despite the extreme singular treatment showed markedly high values, no consistent relationship was found between C1 and upwelling intensity at the end of the experiment (Fig. 7a). For C5 (Fig. 6d) all treatments exhibited relatively similar patterns. Initial values ranged between 0.001-0.007 RU, fluorescence signals increasing until day 21 and subsequently maintaining relatively similar values, ending at 0.011-0.021 RU. C5 did display significant positive relationships with upwelling intensity for both upwelling modes (Fig. 7d).

Components representing humic-like compounds (C2 and C4), which have been associated to the microbial transformation of DOM, displayed nearly continuous increases in fluorescence signals (Fig. 6b and 6c). C2 started at values of 0.003-0.008 RU and increased throughout the experiment in all mesocosms, treatments with greater upwelling intensity exhibiting more intense fluorescence signals. Positive significant relationships were found with upwelling intensity after the final deep water addition (Fig. 7b). Singular treatments presented slightly higher values than recurring ones: e.g., during days ≥33, average C2 values for the extreme singular and

recurring treatments were 0.0206 ± 0.0005 and 0.0190 ± 0.0005 RU, respectively. C4 also displayed fluorescence signals that consistently increased throughout the experiment (Fig. 6c) and, as C2, presented significant positive relationships with upwelling intensity for both modes at the end of the experiment (Fig. 7c).

Discussion

DOC accumulation in the water column

Initial concentrations of DOC were similar to those typically found in surface waters of the Canary Islands oceanic region (Arístegui et al. 2003, 2004, 2020; Burgoa et al. 2020) and other locations in the North Atlantic subtropical gyre (Goldberg et al. 2010; Lomas et al. 2013). Concentrations quickly increased following nutrient depletion and the collapse of the diatom-dominated phytoplankton bloom (Ortiz et al. 2022). In the case of extreme treatments (~140 μM), values reached levels far exceeding DOC concentrations observed in the Canary Current upwelling system (100-110 μM, Arístegui et al. 2003; Burgoa et al. 2020). Similar DOC levels have previously been reported in deep water addition mesocosm experiments in oligotrophic waters (Zark et al. 2017a).

Diatoms are known to release DOC upon nutrient limitation (Norrman et al. 1995; Zark et al. 2017a), but the source of the observed DOC (~70 μM increase in extreme treatments by day 21) was not limited to dissolved primary production (that is, recently photosynthesized DOC). Accumulated dissolved primary production by day 21 was 20.53 μmol $C{\cdot}L^{-1}$ (11.91% of total primary production) and 6.58 μmol $C{\cdot}L^{-1}$ (5.07% of total primary production) for the extreme singular and recurring treatments, respectively (Fig. S6; Ortiz et al. 2022). Given these values, most of the DOC increase must have originated from a source other than dissolved primary production. This DOC increase in extreme singular and recurring treatments represented 43% and 58% of cumulative total primary production by day 21, respectively (35% and 55% of cumulative particulate primary production after removing the dissolved primary production contribution to the DOC increase), higher than the 23% of total new production accumulated as DOC reported by Norrman et al. (1995) during a coastal diatom bloom.

The arising question is how such vast amounts of organic carbon were channelled into the dissolved matter pool in such a short period of time (~10 days). Processes such as exudation by diatoms (Mühlenbruch et al. 2018), extracellular enzymatic

activity on particles and gel structures (Arnosti 2011), grazing and sloppy feeding (Steinberg and Landry 2017), viral lysis (Breitbart et al. 2018) and programmed cell death (Spungin et al. 2018) result in release of DOM. The large amounts of particles (including transparent exopolymer particles) that were formed following the diatom bloom (Baumann et al. 2021b) provided the substrate for prokaryotes to consume POC, and this could have contributed to the production of DOC. The stabilisation of DOC after day 21 despite continued primary production, in conjunction with sustained community respiration (Baños et al. 2022) and prokaryotic heterotrophic production (PHP) rates (Fig. S7), indicates that prokaryotes were consuming at least a fraction of the DOM pool and, consequently, at least part of the DOC accumulated in the water column could eventually be remineralised.

Increase in the relative C content of DOM

Artificial upwelling enhanced the C:N ratio in the DOM pool from ~15 to 19-27. Initial DOC:DON values (Fig. 2d) were within the range of values reported for the subtropical North Atlantic (Hansell and Carlson 2001; Valiente et al. 2022). Subsequent increases in DOC:DON ratios as a result of artificial upwelling were similar to those observed in other experimentally-induced diatom blooms (Norrman et al. 1995). This increase was probably a combination of the release of C-rich polysaccharides by diatoms (Engel 2001; Mühlenbruch et al. 2018) and the preferential degradation of DON by prokaryotes (Hach et al. 2020). The blooming diatom community itself was probably a major source of DON in the form of free amino acids, proteins and aminosugars, as suggested by the initial increase in amino acid-like fluorescence (Fig. 6; Granum et al. 2002). Over the course of the experiment the amino acid-like fluorescence was not clearly related to upwelling intensity (Fig. 6 and 7), which may indicate ongoing consumption by prokaryotes. While the organic molecules generating the humic-like fluorescence signal probably also contained N, they tend not to be degraded by prokaryotes (Lønborg et al. 2010). Amino acid-like fluorescence did not return to initial levels, meaning that a fraction of this signal corresponded to molecules that were not readily consumed by prokaryotes (Lønborg et al. 2010). Amino acid release through viral lysis (Middelboe and Jørgensen 2006) and, for recurring treatments, more constant releases of amino acid-containing molecules by the prolonged diatom blooms throughout the experiment (Ortiz et al. 2022) could have also contributed to the sustained amino acid-like fluorescence signal.

DOC:DOP ratios were also similar to previous estimates for the subtropical North Atlantic (Ammerman et al. 2003) but, as opposed to DOC:DON, no clear relationship with upwelling intensity was observed for DOC:DOP (Fig. S2 and S3). Overall, DOC:DOP values slightly increased from initial conditions and, thus, preferential DOP consumption might have existed to a certain degree (Hach et al. 2020). Prokaryotes are known to utilize DOP as a source of P through the use of alkaline phosphatases when inorganic P is limiting, as measured previously in the study area (Sebastián et al. 2004). Particulate organic matter stoichiometry also tended to shift to higher relative content of C (Baumann et al. 2021b), supporting the idea that not only the consumption of DON and DOP, but also the production of C-rich organic matter, yielded higher C content of DOM. While DOP concentrations fluctuated considerably (Fig. 2c), DON:DOP values tended to decrease with increasing upwelling intensity at the end of the experiment (Fig. S2), suggesting that DON might have been consumed over DOP to compensate for the lower N availability, as NO_3^-:PO_4^- ratios decreased after deep water additions (Fig. S8).

Shift towards high molecular weight, humic-like DOM

CDOM increases have been previously observed associated with phytoplankton production (Romera-Castillo et al. 2010), including communities in nutrient-depleted conditions after a blooming phase (Loginova et al. 2015). Hence, as with DOC, the initial post-bloom increase in a_{254} (Fig. 4a) and a_{325} (Fig. S4) was probably partly associated with DOM released by diatoms. While DOC tended to stabilize, CDOM continued to accumulate (to a greater degree in singular treatments), including an intensification of the humic-like fluorescence signal (Fig. 6). The sustained accumulation throughout the experiment seems to be the result of the generation of CDOM and humic-like FDOM as by-products of the prokaryotic reworking of organic matter (Nelson and Siegel 2013; Catalá et al. 2015b). The fact that cumulative PHP was strongly correlated with CDOM absorption, spectral slopes and humic-like FDOM intensity (Fig. 8) would support that interpretation, as cumulative PHP has been previously observed to be correlated to DOM transformation (Zark et al. 2017a).

CDOM average molecular weight also changed markedly: initial values of spectral slopes were similar to those found in other oligotrophic regions (e.g., Catalá et al. 2018) but markedly decreased after the initial bloom (Fig. 4b and 4c), suggesting an

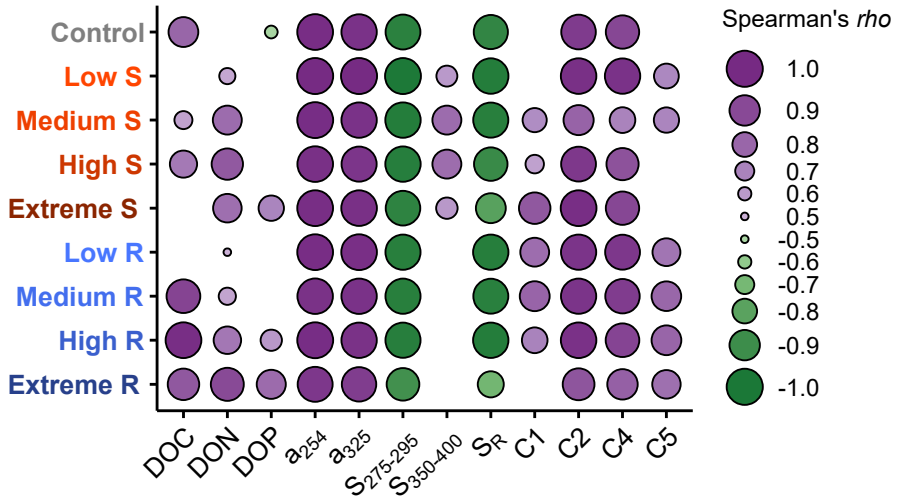

Figure 8. Relationship between cumulative prokaryotic heterotrophic production (PHP) and dissolved organic matter (DOM) parameters. Shown are Spearman's *rho* (ρ) correlation coefficients per mesocosm. Only significant correlations ($p < 0.05$) are displayed.

increase in average molecular weight (Helms et al. 2008). Artificial upwelling modes, however, had different outcomes, with higher CDOM molecular weight in the singular treatments and differences in composition (Fig. 4b and 4d). According to the size-reactivity continuum theory (Benner and Amon 2015), larger size classes of DOM (e.g., macromolecules of combined forms of carbohydrates and amino acids) tend to be preferentially degraded by prokaryotes. The degradation of this high molecular weight DOM, which here probably included polysaccharides and molecules containing amino acids, would result in the generation of CDOM (and FDOM) of higher molecular weight than what was initially present in the mesocosms, hence yielding the observed changes in spectral slopes. Similar results have been reported for the open ocean, as apparent oxygen utilization has been linked to the decreases in $S_{275\text{-}295}$ and increases in humic-like fluorescence (Catalá et al. 2015b, 2018; Martínez-Pérez et al. 2017).

Implications for carbon sequestration

Long-term nutrient addition experiments (weeks to >1 year) have shown that following large DOM accumulations, a significant fraction of it can be remineralised in the weeks following the diatom bloom, but as much as ~30% remain for at least several months (Fry et al. 1996; Meon and Kirchman 2001). Here, the fertilization

with nutrient-rich deep water caused an accumulation of DOC with no visible decrease during the duration of the experiment (~5.5 weeks). The magnitude of the excess DOC was comparable to the carbon that sunk out of the mesocosms in the form of POC (Baumann et al. 2021b), highlighting that DOC represents a pool of major importance for carbon sequestration. DOC is known to accumulate in the oligotrophic waters of the North Atlantic subtropical gyre (Goldberg et al. 2010; Lomas et al. 2013) as surface prokaryotic communities are not able to remineralize it (Carlson et al. 2004). Mesopelagic and bathypelagic prokaryotes, however, have been shown to consume surface DOC when they come into contact with it, suggesting that deep ocean prokaryotic communities possess a wider range of metabolic capabilities (Carlson et al. 2004; Sebastián et al. 2021). As artificial upwelling is not merely limited to nutrient addition but involves the translocation of deep prokaryotic communities into surface waters, their inoculation into the surface DOM pool could enhance DOC remineralization. However, this will depend on whether deep ocean prokaryotes are able to thrive when introduced among the surface prokaryotic assemblages in the course of the successions that happen during and following phytoplankton blooms (Pontiller et al. 2022).

During our experiment, while no decreases in DOC concentrations were found following the post-bloom accumulation, DOM transformation seemed to be taking place. The production of CDOM and humic-like FDOM (Fig. 4 and 6) and their correlation with cumulative PHP (Fig. 8) are indicative of ongoing microbial transformation of DOM (Nelson and Siegel 2013; Catalá et al. 2015b). This has been previously observed in mesocosm fertilization experiments also at the molecular level (Zark et al. 2017a). Oceanic DOM is known to undergo rapid molecular diversification following the consumption and transformation of newly produced organic matter by prokaryotes, resulting in an extremely diverse mixture of organic molecules (Lechtenfeld et al. 2015; Hach et al. 2020). The complex web of ecological interactions between the resulting diverse DOM and the prokaryotic community likely contributed to the stabilization of the organic matter pool (Dittmar et al. 2021). Nutrients were quickly depleted after deep water additions (Ortiz et al. 2022), and their limitation could partially explain the lack of DOM consumption (Letscher et al. 2015). Additionally, predation (Jürgens and Massana 2008) and viral infection (Breitbart et al. 2018) of prokaryotes, whose abundance markedly decreased during the diatom bloom collapse (Fig. S9), could also have reduced bulk DOM degradation rates. In conjunction, these factors could contribute to the persistence of DOC, hindering remineralization and potentially leading to its long-term storage.

The accumulated persistent DOC could be ultimately subducted below the permanent pycnocline (Boyd et al. 2019; Le Moigne 2019), leading to potential carbon sequestration. A long monitoring period (multiple weeks, months) and tracing of DOC dynamics would be required to reliably assess the fate of DOC. Additionally, while mesocosms are a useful tool to study pelagic communities in close-to-natural conditions, they cannot reproduce the multi-dimensional physical dynamics of the real ocean. Downwelling or convective mixing would need to be considered, as they transport DOC to the deep ocean (Boyd et al. 2019; Baetge et al. 2020), which is a requirement for long-term sequestration. Moreover, horizontal advection would potentially limit the accumulation of DOC, thereby reducing its concentrations and making potential downwelling less effective. All these factors would need to be considered in conjunction with POC dynamics to assess the viability of artificial upwelling as a climate mitigation measure in natural open-sea conditions.

Conclusions

The artificial upwelling of deep, nutrient-rich waters into the oligotrophic subtropical North Atlantic yielded marked increases in the DOM concentration and its carbon content, and shifts in DOM characteristics. The magnitude of the observed changes was mostly related to the upwelling intensity, as mesocosms subject to more intense upwelling presented higher concentrations of DOC. Increases over 70 μM for extreme treatments show the potential of artificial upwelling to transfer inorganic carbon to the dissolved organic fraction. The resulting DOC pool was as large as the POC that sunk in the mesocosms, highlighting the importance that DOC has for carbon sequestration estimations. Upwelling intensity led to increases in the C content of DOM relative to N and P, increases in concentration and average molecular weight of CDOM, and the intensification of humic-like FDOM signals. The generation of CDOM, and specifically humic-like FDOM, has been associated with the reworking of organic matter, suggesting ongoing transformation and molecular diversification of DOM during the experiment. The artificial upwelling mode yielded partially different outcomes: while it did not result in differences in DOC concentrations during the time period of the experiment, the treatments reproducing a singular upwelling event presented higher CDOM quantities and average molecular weight than recurring treatments, as well as differences in the spectral slope ratios. These differences in the CDOM pool likely indicate that the

singular upwelling event yielded conditions where the by-products of the microbial transformation of DOM accumulated to a greater extent than in recurring upwelling, where periodic additions of deep water resulted in sustained diatoms blooms and new inputs of DOM. Nonetheless, in both upwelling modes no decreases in DOM quantity were observed. This persistence could be associated with a combination of the molecular diversification of DOM due to microbial reworking, unfavourable environmental conditions (nutrient limitation) and inadequate metabolic capabilities of the prokaryotic communities in the mesocosms. While the temporal scale of the experiment leaves an open question regarding the mid- and long-term fate of the accumulated DOM (long-term persistence vs gradual remineralization), our results highlight the importance of considering DOC along POC when assessing the carbon sequestration potential of artificial upwelling. A monitoring period of multiple weeks/months would be required to reliably estimate the extent of DOM remineralization and studies in open-sea conditions would be necessary to include the effects of the physical processes involved in carbon export.

Supplementary material

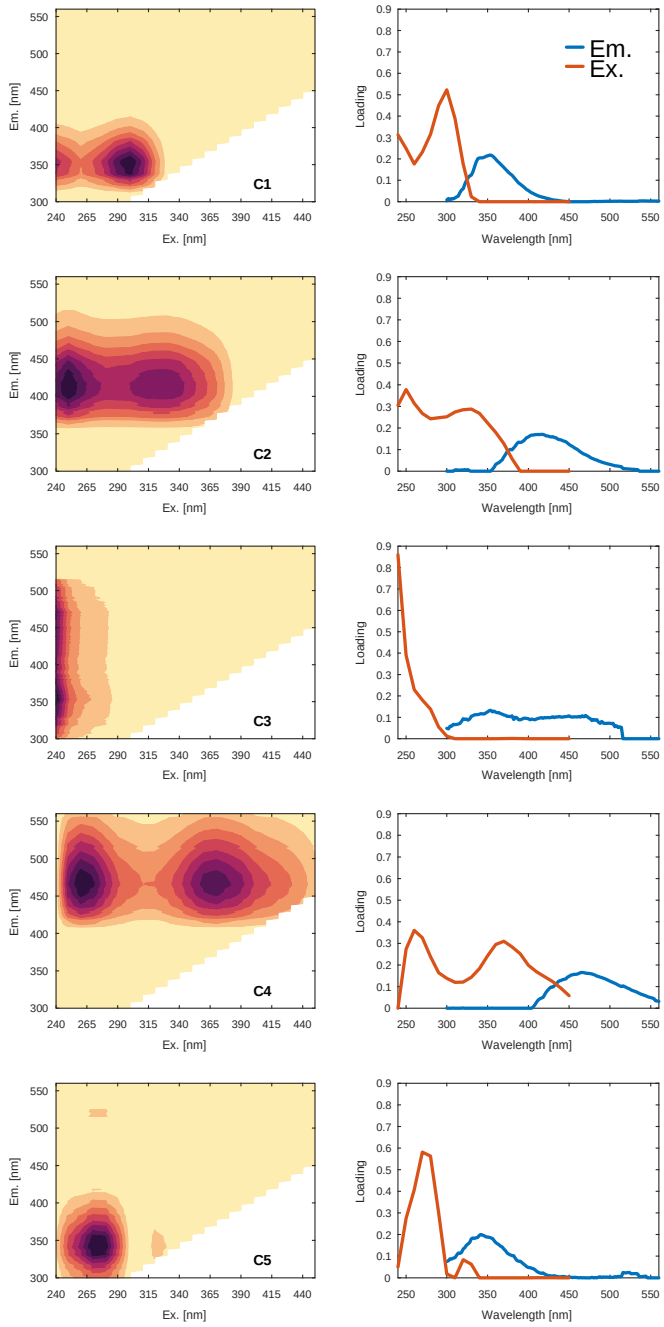

Figure S1. FDOM components derived from the PARAFAC analysis (C1, C2, C3, C4, C5; see Methods for details). In the left column, excitation-emission matrices of each component; in the right column, excitation (red) and emission (blue) spectra. The processed EEMs were analysed using the DOMFluor toolbox (v. 1.7; Stedmon and Bro, 2008) toolbox for Matlab (R2017a).

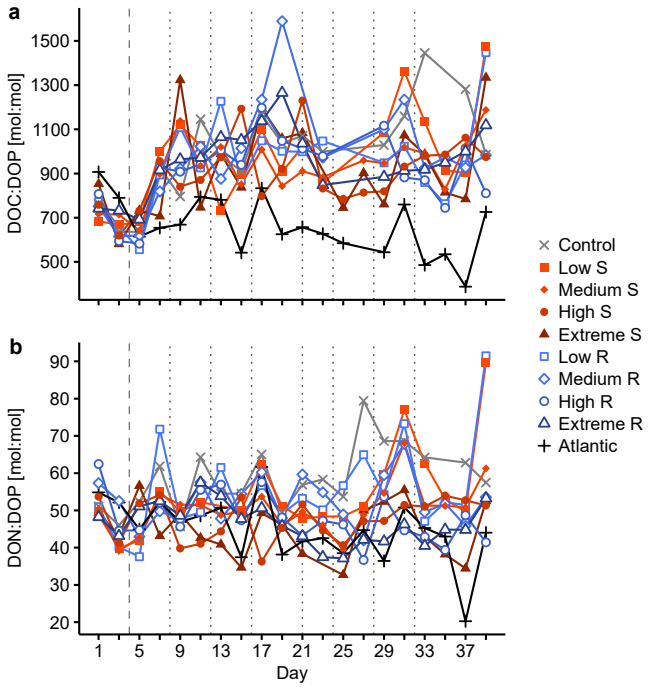

Figure S2. Changes in dissolved organic matter concentrations and ratios during the experiment. Temporal evolution of a) DOC:DOP, and b) DON:DOP. Vertical lines indicate deep water additions of singular (dashed, day 4) and recurring (dashed and dotted) treatments.

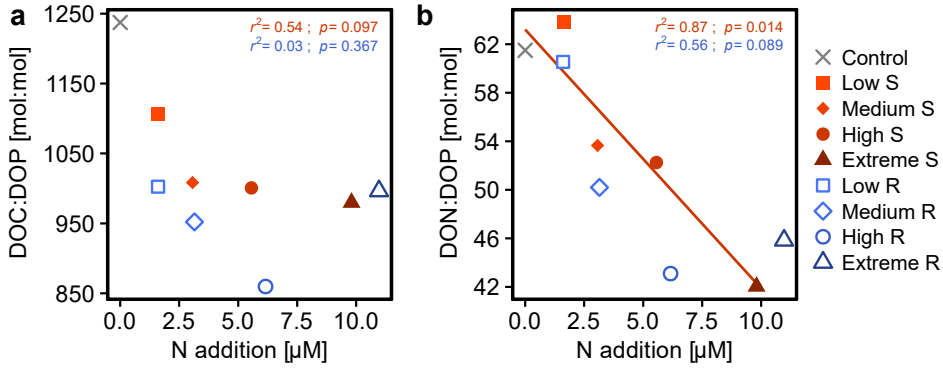

Figure S3. Effect of upwelling intensity on dissolved organic matter. Shown are linear regressions of a) DOC:DOP and b) DON:DOP values against upwelling intensity (N addition) per upwelling mode. DOM values were averaged after the last deep water addition (≥ day 33). The coefficient of determination (r^2) and p-value (p) of the regressions are included. Only the lines for significant regressions ($p < 0.05$) are displayed (see Table S3 for detailed test statistics).

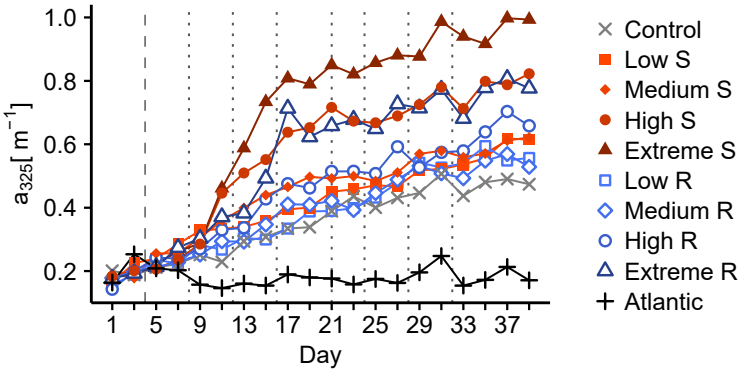

Figure S4. Temporal evolution of the absorption coefficient at 325 nm (a_{325}) during the experiment.

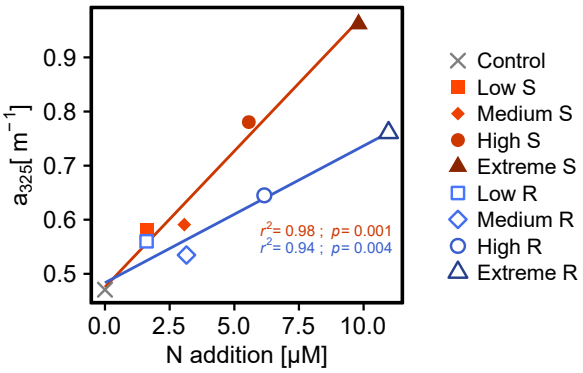

Figure S5. Linear regression of average values after the last deep water addition (≥ day 33) of a_{325} against upwelling intensity (as N addition), per upwelling mode. The coefficient of determination (r^2) and p-value (p) of the regressions are included.

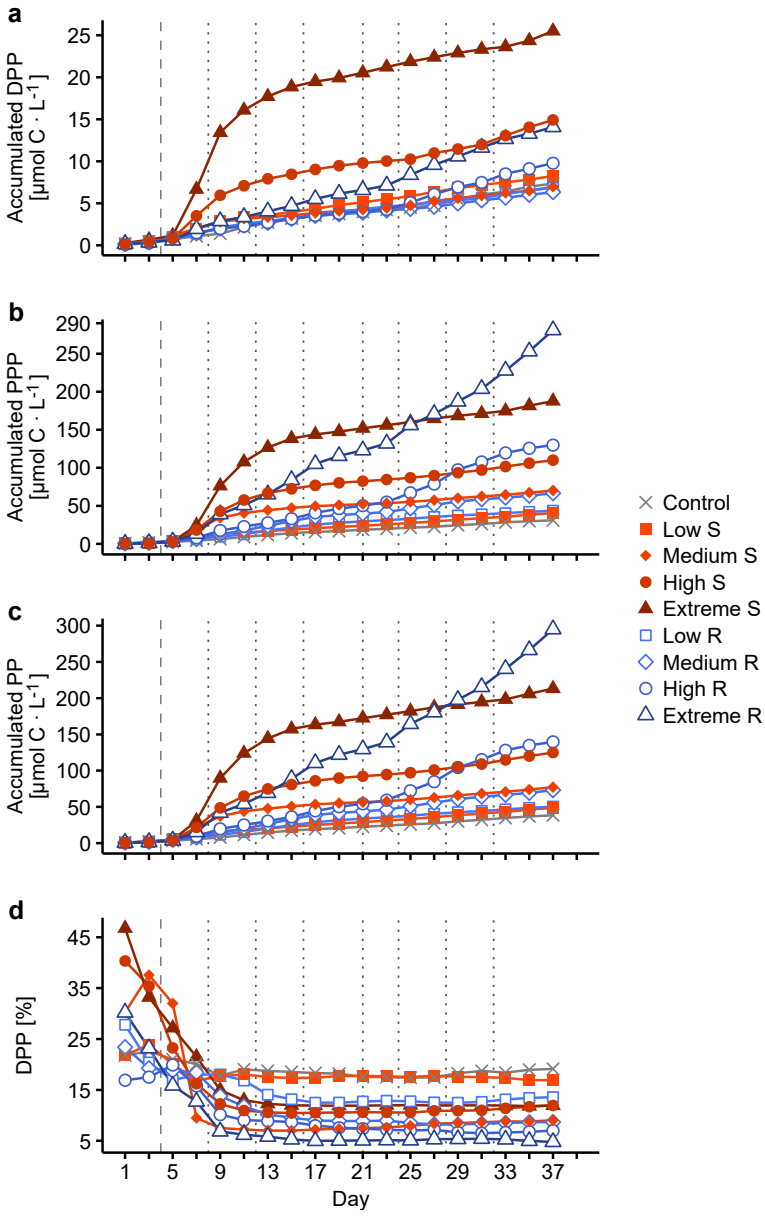

Figure S6. Temporal evolution of accumulated PP in the different fractions over the experiment. a) dissolved primary production (DPP), b) particulate primary production (PPP), c) total primary production (PP), and d) DPP as % of total PP.

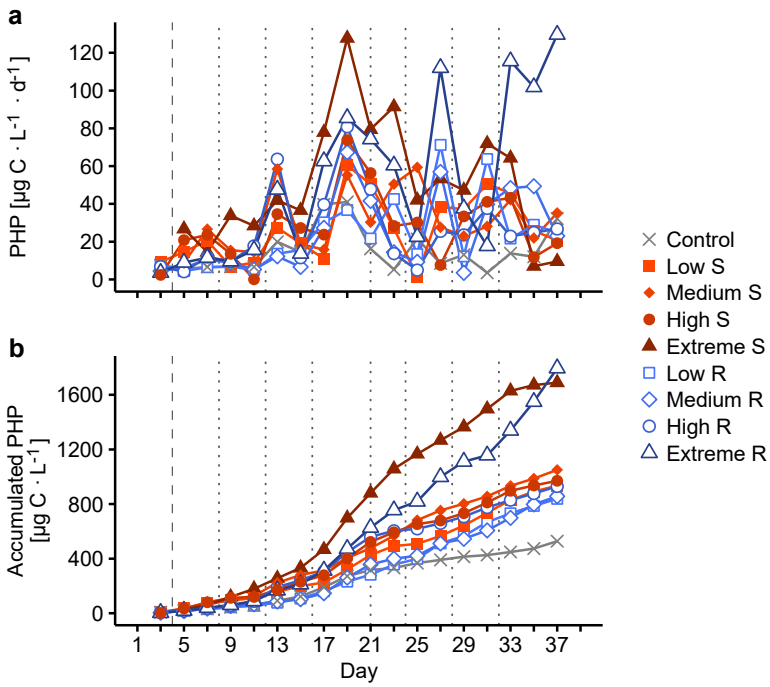

Figure S7. Temporal evolution of a) prokaryotic heterotrophic production (PHP) and b) its accumulated values.

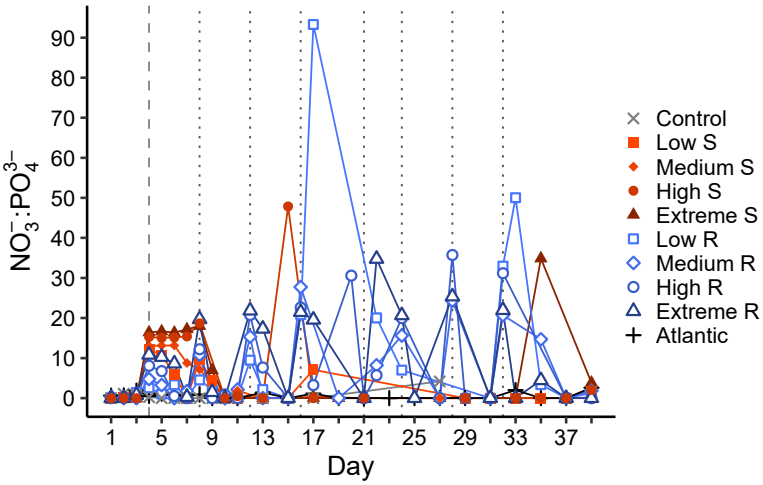

Figure S8. Temporal evolution of the NO_3^-:PO_4^{3-} ratios during the experiment.

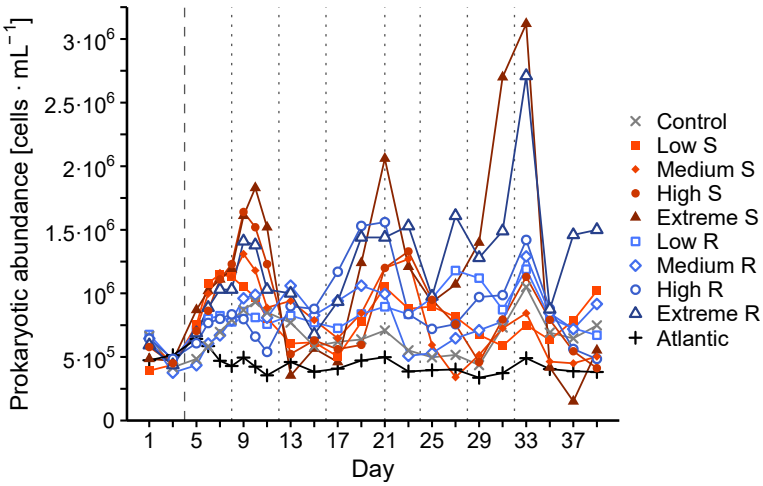

Figure S9. Temporal evolution of the abundance of prokaryotes during the experiment as determined by flow cytometry.

Table S1. Dissolved organic matter characteristics of the Deep Water employed during the artificial upwelling experiment. See Materials and methods section in the main text for details on parameters. Data from days 3-25 correspond to the first Deep Water bag (330 m) and from days 27-31 to the second Deep Water bag (280 m).

Day	DOC [μM]	DON [μM]	DOP [μM]	DOC:DON [mol:mol]	DOC:DOP [mol:mol]	DON:DOP [mol:mol]	a_{254} [m-1]	a_{325} [m-1]	$S_{275-295}$ [μm^{-1}]	$S_{350-400}$ [μm^{-1}]	S_R	C1 [RU]	C2 [RU]	C4 [RU]	C5 [RU]
3	-	4.36	52	-	-	84.5	1.29	278	24.63	11.33	2.17	-	-	-	-
7	82	3.27	0.04	25.1	2051	81.6	1.24	232	27.46	12.29	2.23	8	12	8	4
9	104.6	3.72	57	28.1	1845	65.6	1.33	233	27.82	12.59	2.21	-	-	-	-
11	116.7	4.37	78	26.7	1505	56.4	1.48	263	27.47	13.15	2.09	0.02	15	0.01	8
15	184.6	6.87	129	26.9	1432	53.3	1.9	0.44	23.39	12.6	1.86	35	16	13	11
17	-	6.84	149	-	-	45.8	-	-	-	-	-	-	-	-	-
19	178.8	4.94	119	36.2	1500	41.5	2.4	573	23.92	13	1.84	17	19	15	16
25	-	3.42	45	-	-	75.9	2.2	507	23.83	12.8	1.86	32	24	17	18
27	53.3	4.54	53	11.7	996	85	1.05	195	27.24	11.09	2.46	-	-	-	-
29	-	3.81	12	-	-	322.3	-	-	-	-	-	-	-	-	-
31	71.4	4.68	52	15.3	1371	89.8	1.08	191	28.19	12.33	2.29	11	0.01	7	3

Table S2. Characteristics of the FDOM components derived from the PARAFAC analysis, along with analogous fluorophores previously described in the literature. Components are named according to the wavelength of their emission maximum. FDOM fluorophores from the literature were identified making use of the OpenFluor database (Murphy et al. 2014), applying threshold values of the Tucker Congruence Coefficients (TCC) of 0.95 for both excitation and emission spectra. Wavelengths between parentheses represent secondary maxima.

This study			**Similar fluorophores in literature**					
Comp.	Excitation max [nm]	Emission max [nm]	Study	Comp. name	Excitation max [nm]	Emission max [nm]	$TCC_{ex\text{-}em}$	Description
C1	300 (240)	354	Chen et al. (2018)	$C_{305/344}$	305	344	0.9829	Amino acid-like. Peak T (Coble 1996).
			Catalá et al. (2015)	C3	290	340	0.9827	
			Amaral et al. (2020)	C2	300	359	0.9670	
			Amaral et al. (2016)	C3	300 (<250)	340	0.9930	
C2	250 (330)	410	Yamashita et al. (2011b)	C1	<250 (320)	422	0.9853	Humic-like, peak M (Coble 1996). Positively correlated with AOU
			Catalá et al. (2015)	C2	320	400	0.9774	
			Yamashita et al. (2011a)	C1	<260 (320)	425	0.9774	
			Chen et al. (2018)	$C_{<260(305)/404}$	<260 (305)	404	0.9721	
			Amaral et al. (2020)	C1	270 (320)	411	0.9715	
C3	<240	330-472	Murphy et al. (2008)	P4	<260	-	0.9248	Low excitation maxima, broad emission spectrum. Origin unknown. Potential fluorometer artifact.
			Yamashita et al. (2010)	C3	<260	-	0.9197	

Continued

Table S2. Continued.

This study			Similar fluorophores in literature					
Comp.	Excitation max [nm]	Emission max [nm]	Study	Comp. name	Excitation max [nm]	Emission max [nm]	$TCC_{ex\text{-}em}$	Description
C4	260 (370)	466	Chen et al. (2018)	$C_{<260(365)/476}$	<260 (365)	476	0.9815	Humic-like, mixture of A and C peaks (Coble 1996). High aromaticity.
			Yamashita et al. (2011a)	C2	365 (<260)	475	0.9658	
			Yamashita et al. (2010)	C1	<260 (370)	466	0.9523	
			Dainard et al. (2015)	C2	<260 (370)	475	0.9630	
C5	270	342	Lapierre and Del Giorgio (2014)	C6	275	334	0.9517	Amino acid-like. peak T
			Chen et al. (2018)	C5	275	338	0.9421	
			Osburn et al. (2015)	C7	280	340	0.9551	
			Wünsch et al. (2015)	C2	269	340	0.9577	Indole

Table S3. Summary of results from the linear regressions of DOM variables versus upwelling intensity (as N addition, in μM), per upwelling mode. Slope and intercept values are presented along 95% confidence intervals. r^2 is the coefficient of determination of the regression, *p* is the p-value of the regression. Significant regressions are highlighted in *italic* ($p < 0.05$) and **bold** ($p < 0.01$).

	Upwelling mode	Slope	Intercept	r^2	*p*
DOC [μM]	Singular	5.32 ± 1.98	89.8 ± 10.4	0.95	**0.003**
	Recurring	4.77 ± 1.54	91.91 ± 8.98	0.96	**0.002**
DON [μM]	Singular	0.111 ± 0.045	5.28 ± 0.24	0.94	**0.004**
	Recurring	0.121 ± 0.075	5.34 ± 0.44	0.87	*0.014*
DOP [μM]	Singular	0.0075 ± 0.0014	0.0789 ± 0.0076	0.99	**< 0.001**
	Recurring	0.0060 ± 0.0054	0.090 ± 0.032	0.74	*0.039*
DOC:DON [mol:mol]	Singular	0.51 ± 0.46	17.39 ± 2.41	0.74	*0.039*
	Recurring	0.37 ± 0.37	17.56 ± 2.19	0.7	*0.05*
DOC:DOP [mol:mol]	Singular	-22.7 ± 30.2	1157.5 ± 159.3	0.54	0.097
	Recurring	-16.8 ± 50.5	1083.2 ± 295.1	0.03	0.367
DON:DOP [mol:mol]	Singular	-2.13 ± 1.30	63.21 ± 6.85	0.87	*0.014*
	Recurring	-1.59 ± 2.05	59.2 ± 11.9	0.56	0.089
a_{254} [m^{-1}]	Singular	0.095 ± 0.025	2.21 ± 0.13	0.97	**0.001**
	Recurring	0.050 ± 0.016	2.235 ± 0.096	0.96	**0.002**
a_{325} [m^{-1}]	Singular	0.050 ± 0.013	0.475 ± 0.067	0.98	**0.001**
	Recurring	0.025 ± 0.010	0.483 ± 0.059	0.94	**0.004**
$S_{275\text{-}295}$ [μm^{-1}]	Singular	-0.68 ± 0.21	25.85 ± 1.11	0.96	**0.002**
	Recurring	-0.33 ± 0.27	25.65 ± 1.57	0.78	*0.029*
$S_{350\text{-}400}$ [μm^{-1}]	Singular	0.084 ± 0.145	15.10 ± 0.77	0.37	0.163
	Recurring	-0.14 ± 0.05	15.13 ± 0.30	0.95	**0.003**
S_R	Singular	-0.052 ± 0.020	1.71 ± 0.11	0.94	**0.004**
	Recurring	-0.0072 ± 0.0182	1.70 ± 0.11	0.12	0.299
C_{354} [RU]	Singular	0.0045 ± 0.0072	0.027 ± 0.038	0.42	0.143
	Recurring	-0.00034 ± 0.00173	0.040 ± 0.010	-0.18	0.578

Continued

Table S3. Continued.

	Upwelling mode	Slope	Intercept	r^2	*p*
C_{410} [RU]	Singular	0.00093 ± 0.00017	0.01170 ± 0.00090	0.99	< **0.001**
	Recurring	0.00064 ± 0.00029	0.0121 ± 0.0017	0.92	**0.006**
C_{466} [RU]	Singular	0.00033 ± 0.00028	0.0069 ± 0.0015	0.77	*0.033*
	Recurring	0.00025 ± 0.00037	0.0071 ± 0.0022	0.47	0.124
C_{342} [RU]	Singular	0.00050 ± 0.00032	0.0106 ± 0.0017	0.85	*0.016*
	Recurring	0.00080 ± 0.00075	0.0121 ± 0.0044	0.73	*0.042*

References

Acinas, S. G., P. Sánchez, G. Salazar, and others. 2021. Deep ocean metagenomes provide insight into the metabolic architecture of bathypelagic microbial communities. Commun. Biol. **4**: 604. doi:10.1038/s42003-021-02112-2

Amaral, V., D. Graeber, D. Calliari, and C. Alonso. 2016. Strong linkages between DOM optical properties and main clades of aquatic bacteria. Limnol. Oceanogr. **61**: 906–918. doi:10.1002/lno.10258

Amaral, V., C. Romera-Castillo, and J. Forja. 2020. Dissolved Organic Matter in the Gulf of Cádiz: Distribution and Drivers of Chromophoric and Fluorescent Properties. Front. Mar. Sci. **7**: 126. doi:10.3389/fmars.2020.00126

Ammerman, J. W., R. R. Hood, D. A. Case, and J. B. Cotner. 2003. Phosphorus deficiency in the Atlantic: An emerging paradigm in oceanography. Eos, Trans. Am. Geophys. Union **84**: 165–170. doi:10.1029/2003EO180001

Arcos-Pulido, M., A. Rodríguez-Santana, M. Emelianov, and others. 2014. Diapycnal nutrient fluxes on the northern boundary of Cape Ghir upwelling region. Deep-Sea Res. Part I Oceanogr. Res. Pap. **84**: 100–109. doi:10.1016/j.dsr.2013.10.010

Arístegui, J., E. D. Barton, M. F. Montero, M. García-Muñoz, and J. Escánez. 2003. Organic carbon distribution and water column respiration in the NW Africa-Canaries Coastal Transition Zone. Aquat. Microb. Ecol. **33**: 289–301.

Arístegui, J., E. D. Barton, P. Tett, and others. 2004. Variability in plankton community structure, metabolism, and vertical carbon fluxes along an upwelling filament (Cape Juby, NW Africa). Prog. Oceanogr. **62**: 95–113. doi:10.1016/j.pocean.2004.07.004

Arístegui, J., M. F. Montero, N. Hernández-Hernández, I. J. Alonso-González, F. Baltar, M. L. Calleja, and C. M. Duarte. 2020. Variability in Water-Column Respiration and Its Dependence on Organic Carbon Sources in the Canary Current Upwelling Region. Front. Earth Sci. **8**: 349. doi:10.3389/feart.2020.00349

Arnosti, C. 2011. Microbial Extracellular Enzymes and the Marine Carbon Cycle. Ann. Rev. Mar. Sci. **3**: 401–425. doi:10.1146/annurev-marine-120709-142731

Azam, F., and F. Malfatti. 2007. Microbial structuring of marine ecosystems. Nat. Rev. Microbiol. **5**: 782–791. doi:10.1038/nrmicro1747

Baetge, N., J. R. Graff, M. J. Behrenfeld, and C. A. Carlson. 2020. Net Community Production, Dissolved Organic Carbon Accumulation, and Vertical Export in the Western North Atlantic. Front. Mar. Sci. **7**: 227. doi:10.3389/fmars.2020.00227

Baños, I., J. Arístegui, M. Benavides, and others. 2022. Response of plankton community respiration under variable simulated upwelling events. Front. Mar. Sci. **9**: 1006010. doi:10.3389/fmars.2022.1006010

Baumann, M., M. Sswat, J. Ortiz Cortes, N. Hernández-Hernández, I. Baños Cerón, M. Vanharanta, and M. Heinemann. 2021a. KOSMOS 2018 Gran Canaria mesocosm study: water column biogeochemistry.doi:10.1594/PANGAEA.933090

Baumann, M., J. Taucher, A. J. Paul, and others. 2021b. Effect of Intensity and Mode of Artificial Upwelling on Particle Flux and Carbon Export. Front. Mar. Sci. **8**: 742142.

doi:10.3389/fmars.2021.742142

Benner, R., and R. M. W. Amon. 2015. The Size-Reactivity Continuum of Major Bioelements in the Ocean. Ann. Rev. Mar. Sci. **7**: 185–205. doi:10.1146/annurev-marine-010213-135126

Boyd, P. W., H. Claustre, M. Levy, D. A. Siegel, and T. Weber. 2019. Multi-faceted particle pumps drive carbon sequestration in the ocean. Nature **568**: 327–335. doi:10.1038/s41586-019-1098-2

Breitbart, M., C. Bonnain, K. Malki, and N. A. Sawaya. 2018. Phage puppet masters of the marine microbial realm. Nat. Microbiol. **3**: 754–766. doi:10.1038/s41564-018-0166-y

Burgoa, N., F. Machín, Á. Marrero-Díaz, Á. Rodríguez-Santana, A. Martínez-Marrero, J. Arístegui, and C. M. Duarte. 2020. Mass, nutrients and dissolved organic carbon (DOC) lateral transports off northwest Africa during fall 2002 and spring 2003. Ocean Sci. **16**: 483–511. doi:10.5194/os-16-483-2020

Carlson, C. A., S. J. Giovannoni, D. A. Hansell, S. J. Goldberg, R. Parsons, and K. Vergin. 2004. Interactions among dissolved organic carbon, microbial processes, and community structure in the mesopelagic zone of the northwestern Sargasso Sea. Limnol. Oceanogr. **49**: 1073–1083. doi:10.4319/lo.2004.49.4.1073

Catalá, T. S., X. A. Álvarez-Salgado, J. Otero, and others. 2016. Drivers of fluorescent dissolved organic matter in the global epipelagic ocean. Limnol. Oceanogr. **61**: 1101–1119. doi:10.1002/lno.10281

Catalá, T. S., A. M. Martínez-Pérez, M. Nieto-Cid, and others. 2018. Dissolved Organic Matter (DOM) in the open Mediterranean Sea. I. Basin–wide distribution and drivers of chromophoric DOM. Prog. Oceanogr. **165**: 35–51. doi:10.1016/j.pocean.2018.05.002

Catalá, T. S., I. Reche, M. Álvarez, and others. 2015a. Water mass age and aging driving chromophoric dissolved organic matter in the dark global ocean. Global Biogeochem. Cycles **29**: 917–934. doi:10.1002/2014GB005048

Catalá, T. S., I. Reche, A. Fuentes-Lema, and others. 2015b. Turnover time of fluorescent dissolved organic matter in the dark global ocean. Nat. Commun. **6:5986**. doi:10.1038/ncomms6986

Chen, M., J. Jung, Y. K. Lee, and J. Hur. 2018. Surface accumulation of low molecular weight dissolved organic matter in surface waters and horizontal off-shelf spreading of nutrients and humic-like fluorescence in the Chukchi Sea of the Arctic Ocean. Sci. Total Environ. **639**: 624–632. doi:10.1016/j.scitotenv.2018.05.205

Coble, P. G. 1996. Characterization of marine and terrestrial DOM in seawater using excitation-emission matrix spectroscopy. Mar. Chem. **51**: 325–346. doi:10.1016/0304-4203(95)00062-3

Dainard, P. G., C. Guéguen, N. McDonald, and W. J. Williams. 2015. Photobleaching of fluorescent dissolved organic matter in Beaufort Sea and North Atlantic Subtropical Gyre. Mar. Chem. **177**: 630–637. doi:10.1016/j.marchem.2015.10.004

Dittmar, T., S. T. Lennartz, H. Buck-Wiese, D. A. Hansell, C. Santinelli, C. Vanni, B. Blasius, and J.-H. Hehemann. 2021. Enigmatic persistence of dissolved organic matter in the ocean. Nat. Rev. Earth Environ. **2**: 570–583. doi:10.1038/s43017-021-00183-7

Engel, A. 2001. Carbon and nitrogen content of transparent exopolymer particles (TEP) in relation to their Alcian Blue adsorption . Mar. Ecol. Prog. Ser. **219**: 1–10.

Fawzy, S., A. I. Osman, J. Doran, and D. W. Rooney. 2020. Strategies for mitigation of climate change: a review. Environ. Chem. Lett. **18**: 2069–2094. doi:10.1007/s10311-020-01059-w

Field, C. B., M. J. Behrenfeld, J. T. Randerson, and P. Falkowski. 1998. Primary production of the biosphere: Integrating terrestrial and oceanic components. Science (80-.). **281**: 237–240. doi:10.1126/science.281.5374.237

Fry, B., C. S. Hopkinson Jr., A. Nolin, B. Norrman, and U. L. Zweifel. 1996. Long-term decomposition of DOC from experimental diatom blooms. Limnol. Oceanogr. **41**: 1344–1347. doi:10.4319/lo.1996.41.6.1344

Goldberg, S. J., C. A. Carlson, B. Bock, N. B. Nelson, and D. A. Siegel. 2010. Meridional variability in dissolved organic matter stocks and diagenetic state within the euphotic and mesopelagic zone of the North Atlantic subtropical gyre. Mar. Chem. **119**: 9–21. doi:10.1016/j.marchem.2009.12.002

Granum, E., S. Kirkvold, and S. M. Myklestad. 2002. Cellular and extracellular production of carbohydrates and amino acids by the marine diatom Skeletonema costatum: diel variations and effects of N depletion. Mar. Ecol. Prog. Ser. **242**: 83–94.

Hach, P. F., H. K. Marchant, A. Krupke, and others. 2020. Rapid microbial diversification of dissolved organic matter in oceanic surface waters leads to carbon sequestration. Sci. Rep. **10**: 13025. doi:10.1038/s41598-020-69930-y

Hansell, D. A., and C. A. Carlson. 2001. Biogeochemistry of total organic carbon and nitrogen in the Sargasso Sea: control by convective overturn. Deep Sea Res. Part II Top. Stud. Oceanogr. **48**: 1649–1667. doi:10.1016/S0967-0645(00)00153-3

Hansell, D. A., C. A. Carlson, D. J. Repeta, and R. Schlitzer. 2009. Dissolved organic matter in the ocean: A controversy stimulates new insights. Oceanography **22**: 202–211.

Hansen, H. P., and F. Koroleff. 1999. Determination of nutrients, p. 159–228. *In* K. Grasshoff, K. Kremling, and M. Ehrhardt [eds.], Methods of Seawater Analysis. Wiley Verlag Chemie GmbH.

Helms, J. R., A. Stubbins, E. M. Perdue, N. W. Green, H. Chen, and K. Mopper. 2013. Photochemical bleaching of oceanic dissolved organic matter and its effect on absorption spectral slope and fluorescence. Mar. Chem. **155**: 81–91. doi:10.1016/j.marchem.2013.05.015

Helms, J. R., A. Stubbins, J. D. Ritchie, E. C. Minor, D. J. Kieber, and K. Mopper. 2008. Absorption spectral slopes and slope ratios as indicators of molecular weight, source, and photobleaching of chromophoric dissolved organic matter. Limnol. Oceanogr. **53**: 955–969. doi:10.4319/lo.2008.53.3.0955

Jacox, M. G., C. A. Edwards, E. L. Hazen, and S. J. Bograd. 2018. Coastal Upwelling Revisited: Ekman, Bakun, and Improved Upwelling Indices for the U.S. West Coast. J. Geophys. Res. Ocean. **123**: 7332–7350. doi:10.1029/2018JC014187

Johnson, K. S., R. Michael Gordon, and K. H. Coale. 1997. What controls dissolved iron concentrations in the world ocean? Mar. Chem. **57**: 137–161. doi:10.1016/S0304-4203(97)00043-1

Jürgens, K., and R. Massana. 2008. Protistan Grazing on Marine Bacterioplankton, p. 383–441. *In* Microbial Ecology of the Oceans.

Kirchman, D. L. 1993. Leucine Incorporation as a Measure of Biomass Production by Heterotrophic Bacteria, p. 509–512. *In* P.F. Kemp, B.F. Sherr, E.B. Sherr, and J.J. Cole [eds.], Handbook of Methods in Aquatic Microbial Ecology. CRC Press.

Lapierre, J. F., and P. A. Del Giorgio. 2014. Partial coupling and differential regulation of biologically

and photochemically labile dissolved organic carbon across boreal aquatic networks. Biogeosciences **11**: 5969–5985. doi:10.5194/bg-11-5969-2014

Lawaetz, A. J., and C. A. Stedmon. 2009. Fluorescence intensity calibration using the Raman scatter peak of water. Appl. Spectrosc. **63**: 936–940. doi:10.1366/000370209788964548

Lechtenfeld, O. J., N. Hertkorn, Y. Shen, M. Witt, and R. Benner. 2015. Marine sequestration of carbon in bacterial metabolites. Nat. Commun. **6**: 6711. doi:10.1038/ncomms7711

Letscher, R. T., A. N. Knapp, A. K. James, C. A. Carlson, A. E. Santoro, and D. A. Hansell. 2015. Microbial community composition and nitrogen availability influence DOC remineralization in the South Pacific Gyre. Mar. Chem. **177**: 325–334. doi:10.1016/j.marchem.2015.06.024

Levitus, S., M. E. Conkright, J. L. Reid, R. G. Najjar, and A. Mantyla. 1993. Distribution of nitrate, phosphate and silicate in the world oceans. Prog. Oceanogr. **31**: 245–273. doi:10.1016/0079-6611(93)90003-V

Loginova, A. N., C. Borchard, J. Meyer, H. Hauss, R. Kiko, and A. Engel. 2015. Effects of nitrate and phosphate supply on chromophoric and fluorescent dissolved organic matter in the Eastern Tropical North Atlantic: a mesocosm study. Biogeosciences **12**: 6897–6914. doi:10.5194/bg-12-6897-2015

Lomas, M. W., N. R. Bates, R. J. Johnson, A. H. Knap, D. K. Steinberg, and C. A. Carlson. 2013. Two decades and counting: 24-years of sustained open ocean biogeochemical measurements in the Sargasso Sea. Deep Sea Res. Part II Top. Stud. Oceanogr. **93**: 16–32. doi:10.1016/j.dsr2.2013.01.008

Lønborg, C., and X. A. Álvarez-Salgado. 2014. Tracing dissolved organic matter cycling in the eastern boundary of the temperate North Atlantic using absorption and fluorescence spectroscopy. Deep Sea Res. Part I Oceanogr. Res. Pap. **85**: 35–46. doi:10.1016/j.dsr.2013.11.002

Lønborg, C., X. A. Álvarez-Salgado, K. Davidson, S. Martínez-García, and E. Teira. 2010. Assessing the microbial bioavailability and degradation rate constants of dissolved organic matter by fluorescence spectroscopy in the coastal upwelling system of the Ría de Vigo. Mar. Chem. **119**: 121–129. doi:10.1016/j.marchem.2010.02.001

Martínez-Pérez, A. M., X. A. Álvarez-Salgado, J. Arístegui, and M. Nieto-Cid. 2017. Deep-ocean dissolved organic matter reactivity along the Mediterranean Sea: does size matter? Sci. Rep. **7**: 5687. doi:10.1038/s41598-017-05941-6

Maruyama, S., T. Yabuki, T. Sato, K. Tsubaki, A. Komiya, M. Watanabe, H. Kawamura, and K. Tsukamoto. 2011. Evidences of increasing primary production in the ocean by Stommel's perpetual salt fountain. Deep-Sea Res. Part I Oceanogr. Res. Pap. **58**: 567–574. doi:10.1016/j.dsr.2011.02.012

McGillicuddy, D. J., L. A. Anderson, N. R. Bates, and others. 2007. Eddy/Wind interactions stimulate extraordinary mid-ocean plankton blooms. Science (80-.). **316**: 1021–1026. doi:10.1126/science.1136256

Meon, B., and D. L. Kirchman. 2001. Dynamics and molecular composition of dissolved organic material during experimental phytoplankton blooms. Mar. Chem. **75**: 185–199. doi:10.1016/S0304-4203(01)00036-6

Middelboe, M., and N. O. G. Jørgensen. 2006. Viral lysis of bacteria: an important source of dissolved amino acids and cell wall compounds. J. Mar. Biol. Assoc. United Kingdom **86**: 605–612. doi:DOI: 10.1017/S0025315406013518

Le Moigne, F. A. C. 2019. Pathways of Organic Carbon Downward Transport by the Oceanic Biological Carbon Pump. Front. Mar. Sci. **6**: 634. doi:10.3389/fmars.2019.00634

Mühlenbruch, M., H.-P. Grossart, F. Eigemann, and M. Voss. 2018. Mini-review: Phytoplankton-derived polysaccharides in the marine environment and their interactions with heterotrophic bacteria. Environ. Microbiol. **20**: 2671–2685. doi:10.1111/1462-2920.14302

Murphy, K. R., C. A. Stedmon, T. D. Waite, and G. M. Ruiz. 2008. Distinguishing between terrestrial and autochthonous organic matter sources in marine environments using fluorescence spectroscopy. Mar. Chem. **108**: 40–58. doi:10.1016/j.marchem.2007.10.003

Murphy, K. R., C. A. Stedmon, P. Wenig, and R. Bro. 2014. OpenFluor- An online spectral library of auto-fluorescence by organic compounds in the environment. Anal. Methods **6**: 658–661. doi:10.1039/c3ay41935e

Nelson, N. B., and D. A. Siegel. 2013. The Global Distribution and Dynamics of Chromophoric Dissolved Organic Matter. Ann. Rev. Mar. Sci. **5**: 447–476. doi:10.1146/annurev-marine-120710-100751

Norrman, B., U. L. Zwelfel, C. S. Hopkinson Jr., and F. Brian. 1995. Production and utilization of dissolved organic carbon during an experimental diatom bloom. Limnol. Oceanogr. **40**: 898–907. doi:10.4319/lo.1995.40.5.0898

Ortiz, J., J. Arístegui, N. Hernández-Hernández, M. Fernández-Méndez, and U. Riebesell. 2022. Oligotrophic Phytoplankton Community Effectively Adjusts to Artificial Upwelling Regardless of Intensity, but Differently Among Upwelling Modes. Front. Mar. Sci. **9**: 880550. doi:10.3389/fmars.2022.880550

Osburn, C. L., M. P. Mikan, J. R. Etheridge, M. R. Burchell, and F. Birgand. 2015. Seasonal variation in the quality of dissolved and particulate organic matter exchanged between a salt marsh and its adjacent estuary. J. Geophys. Res. Biogeosciences **120**: 1430–1449. doi:10.1002/2014JG002897

Pan, Y. W., W. Fan, D. H. Zhang, and others. 2016. Research progress in artificial upwelling and its potential environmental effects. Sci. China Earth Sci. **59**: 236–248. doi:10.1007/s11430-015-5195-2

Polovina, J. J., E. A. Howell, and M. Abecassis. 2008. Ocean's least productive waters are expanding. Geophys. Res. Lett. **35**: L03618. doi:10.1029/2007GL031745

Pontiller, B., S. Martínez-García, V. Joglar, and others. 2022. Rapid bacterioplankton transcription cascades regulate organic matter utilization during phytoplankton bloom progression in a coastal upwelling system. ISME J. **16**: 2360–2372. doi:10.1038/s41396-022-01273-0

R Core Team. 2021. R: A language and environment for statistical computing. R Foundation for Statistical Computing, Vienna, Austria. URL https://www.R-project.org/.

Riebesell, U., J. Czerny, K. Von Bröckel, and others. 2013. Technical Note: A mobile sea-going mesocosm system - New opportunities for ocean change research. Biogeosciences **10**: 1835–1847. doi:10.5194/bg-10-1835-2013

Romera-Castillo, C., H. Sarmento, X. A. Álvarez-Salgado, J. M. Gasol, and C. Marraséa. 2010. Production of chromophoric dissolved organic matter by marine phytoplankton. Limnol. Oceanogr. **55**: 446–454. doi:10.4319/lo.2010.55.1.0446

Sebastián, M., J. Arístegui, M. F. Montero, J. Escanez, and F. Xavier Niell. 2004. Alkaline phosphatase activity and its relationship to inorganic phosphorus in the transition zone of the North-western

African upwelling system. Prog. Oceanogr. **62**: 131–150. doi:10.1016/j.pocean.2004.07.007

Sebastián, M., I. Forn, A. Auladell, M. Gómez-Letona, M. M. Sala, J. M. Gasol, and C. Marrasé. 2021. Differential recruitment of opportunistic taxa leads to contrasting abilities in carbon processing by bathypelagic and surface microbial communities. Environ. Microbiol. **23**: 190–206. doi:10.1111/1462-2920.15292

Severin, T., F. Kessouri, M. Rembauville, and others. 2017. Open-ocean convection process: A driver of the winter nutrient supply and the spring phytoplankton distribution in the Northwestern Mediterranean Sea. J. Geophys. Res. Ocean. **122**: 4587–4601. doi:10.1002/2016JC012664

Sharp, J. H., E. T. Peltzer, M. J. Alperin, and others. 1993. Procedures subgroup report. Mar. Chem. **41**: 37–49. doi:10.1016/0304-4203(93)90104-V

Shepherd, J., D. Iglesias-Rodriguez, and A. Yool. 2007. Geo-engineering might cause, not cure, problems. Nature **449**: 781. doi:10.1038/449781a

Smith, D., and F. Azam. 1992. A simple, economical method for measuring bacterial protein synthesis rates in seawater using. Mar. Microb. food webs **6**: 107–114.

Spungin, D., N. Belkin, R. A. Foster, and others. 2018. Programmed cell death in diazotrophs and the fate of organic matter in the western tropical South Pacific Ocean during the OUTPACE cruise. Biogeosciences **15**: 3893–3908. doi:10.5194/bg-15-3893-2018

Stedmon, C. A., and R. Bro. 2008. Characterizing dissolved organic matter fluorescence with parallel factor analysis: A tutorial. Limnol. Oceanogr. Methods **6**: 572–579. doi:10.4319/lom.2008.6.572

Stedmon, C. A., S. Markager, and R. Bro. 2003. Tracing dissolved organic matter in aquatic environments using a new approach to fluorescence spectroscopy. Mar. Chem. **82**: 239–254. doi:10.1016/S0304-4203(03)00072-0

Steinberg, D. K., and M. R. Landry. 2017. Zooplankton and the Ocean Carbon Cycle. Ann. Rev. Mar. Sci. **9**: 413–444. doi:10.1146/annurev-marine-010814-015924

Sunagawa, S., L. P. Coelho, S. Chaffron, and others. 2015. Structure and function of the global ocean microbiome. Science (80-.). **348**: 1261359. doi:10.1126/science.1261359

Thomas, C., G. Cauwet, and J.-F. Minster. 1995. Dissolved organic carbon in the equatorial Atlantic Ocean. Mar. Chem. **49**: 155–169. doi:10.1016/0304-4203(94)00061-H

Valiente, S., B. Fernández-Castro, R. Campanero, and others. 2022. Dissolved and suspended organic matter dynamics in the Cape Verde Frontal Zone (NW Africa). Prog. Oceanogr. **201**: 102727. doi:10.1016/j.pocean.2021.102727

Wickham., H. 2016. ggplot2: Elegant Graphics for Data Analysis. Springer-Verlag New York.

Williamson, P., D. W. R. Wallace, C. S. Law, and others. 2012. Ocean fertilization for geoengineering: A review of effectiveness, environmental impacts and emerging governance. Process Saf. Environ. Prot. **90**: 475–488. doi:10.1016/j.psep.2012.10.007

Wünsch, U. J., K. R. Murphy, and C. A. Stedmon. 2015. Fluorescence Quantum Yields of Natural Organic Matter and Organic Compounds: Implications for the Fluorescence-based Interpretation of Organic Matter Composition. Front. Mar. Sci. **2**: 98. doi:10.3389/fmars.2015.00098

Yamashita, Y., R. M. Cory, J. Nishioka, K. Kuma, E. Tanoue, and R. Jaffé. 2010. Fluorescence characteristics of dissolved organic matter in the deep waters of the Okhotsk Sea and the

northwestern North Pacific Ocean. Deep-Sea Res. Part II Top. Stud. Oceanogr. **57**: 1478–1485. doi:10.1016/j.dsr2.2010.02.016

Yamashita, Y., B. D. Kloeppel, J. Knoepp, G. L. Zausen, and R. Jaffé. 2011a. Effects of Watershed History on Dissolved Organic Matter Characteristics in Headwater Streams. Ecosystems **14**: 1110–1122. doi:10.1007/s10021-011-9469-z

Yamashita, Y., A. Panton, C. Mahaffey, and R. Jaffé. 2011b. Assessing the spatial and temporal variability of dissolved organic matter in Liverpool Bay using excitation–emission matrix fluorescence and parallel factor analysis. Ocean Dyn. **61**: 569–579. doi:10.1007/s10236-010-0365-4

Yool, A., J. G. Shepherd, H. L. Bryden, and A. Oschlies. 2009. Low efficiency of nutrient translocation for enhancing oceanic uptake of carbon dioxide. J. Geophys. Res. Ocean. **114**: C08009. doi:10.1029/2008JC004792

Zark, M., N. K. Broda, T. Hornick, H.-P. Grossart, U. Riebesell, and T. Dittmar. 2017a. Ocean Acidification Experiments in Large-Scale Mesocosms Reveal Similar Dynamics of Dissolved Organic Matter Production and Biotransformation. Front. Mar. Sci. **4**: 271. doi:10.3389/fmars.2017.00271

Zark, M., J. Christoffers, and T. Dittmar. 2017b. Molecular properties of deep-sea dissolved organic matter are predictable by the central limit theorem: Evidence from tandem FT-ICR-MS. Mar. Chem. **191**: 9–15. doi:10.1016/j.marchem.2017.02.005

Zeileis, A., and T. Hothorn. 2002. Diagnostic Checking in Regression Relationships. R News **2**: 7–10.

Zhang, D., W. Fan, J. Yang, Y. Pan, Y. Chen, H. Huang, and J. Chen. 2016. Reviews of power supply and environmental energy conversions for artificial upwelling. Renew. Sustain. Energy Rev. **56**: 659–668. doi:10.1016/j.rser.2015.11.041

Chapter 2

Prokaryotic successions under simulated upwelling

Prokaryotic successional patterns are consistent under variable simulated upwelling scenarios

Markel Gómez-Letona, Javier Arístegui, Ulf Riebesell and Marta Sebastián

Manuscript

Heterotrophic prokaryotes drive the tempo of dissolved organic matter processing in the ocean, and they have been shown to follow a substrate-controlled succession during phytoplankton blooms. However, knowledge on how repeatable these succession patterns are under upwelling events of varying strength and temporal extent is lacking. We simulated upwellings of varying intensity and duration (singular pulse vs recurring) in a total of 8 scenarios by adding nutrient-rich mesopelagic waters into large-scale mesocosms containing surface waters of the subtropical Eastern North Atlantic. A monitoring period of close to 6 weeks showed that phytoplankton blooms had diverging outcomes depending on the upwelling mode: singular treatments presented a unique, short-lived bloom while in the recurring ones elevated phytoplanktonic biomass and primary production were sustained in time (in both cases bloom strength was proportional to upwelling intensity). Prokaryotic abundances were positively related to upwelling intensity and presented three main peaks in all treatments. In contrast, trends in cell-specific activity were markedly different for the two modes: a single, post-bloom peak in the singular mode as opposed to lower proportion of active cells but more sustained in time in the recurring mode. Successional patterns were surprisingly similar regardless of upwelling intensity and mode, with five prokaryotic assemblages sequentially proliferating during the experiment. While the dominant taxa within the successional assemblages differed mostly between the particle-associated and the free-living fractions, upwelling modes also displayed some variability in composition. Our results unveil that despite diverse taxa might dominate prokaryotic communities during differing phytoplankton blooms and subsequent organic matter cycling, they share common succession patterns even between the particle-associated and free-living fractions.

Introduction

Phytoplankton can form large blooms under favourable environmental conditions, a process which has been extensively studied both in the field and experimentally (e.g., Boyd et al. 2000; Leblanc et al. 2016; Sundby et al. 2016; Taucher et al. 2018; Behrenfeld and Boss 2018; Horvat et al. 2022). During blooming episodes, these autotrophic microorganisms fix large amounts of inorganic carbon into organic matter through photosynthesis. Part of the newly fixed organic matter eventually returns to the marine environment through the release of organic compounds by phytoplankton (Mühlenbruch et al. 2018), prokaryotic extracellular enzymatic activity on particles (Arnosti 2011) and, especially during bloom termination, through grazing (Steinberg and Landry 2017) and viral lysis (Kuhlisch et al. 2022). This way, organic matter becomes available to prokaryotic organisms (bacteria and archaea), which in turn transform, consume and incorporate it, channelling it back into the marine trophic web in a process known as the microbial loop (Azam et al. 1983; Fenchel 2008).

Prokaryotic communities harbour a myriad of metabolisms that allow them to utilise different organic matter compounds (Moran 2015). Thus, while communities tend to be dominated by a small number of taxa at any given time, shifts in composition and gene expression occur following changes in nutrient and organic matter concentrations (Teeling et al. 2012; Needham and Fuhrman 2016; Pontiller et al. 2022). For instance, the oligotrophic specialist SAR11 clade usually thrives in surface waters with low nutrient concentrations (Giovannoni 2017), while copiotrophic bacteria like Alteromonadales and Flavobacteriales take advantage of sudden bursts of organic matter (Buchan et al. 2014). In addition to quantity, organic matter composition has also been suggested as one of the main factors driving the taxonomic and transcriptional successions of prokaryotes, as taxa tend to specialise in particular sets of compounds (Teeling et al. 2012; Sharma et al. 2014; Pontiller et al. 2022). The resulting microbial landscape during phytoplankton blooms is one in which resources are partitioned among different taxa during the consecutive stages of the blooming episode. Thus, tracking the evolution of standing stocks, activity and taxonomic composition of prokaryotic communities is key to advance our understanding of the cycling of organic matter during phytoplankton blooms in different oceanic environments.

Studying prokaryotic community dynamics during phytoplankton blooms is of major relevance in coastal upwelling regions, as they constitute one of the most

productive ecosystems in the global ocean (Carr and Kearns 2003; Demarcq 2009). While such systems are characterised by high primary production supported by nutrient-rich deep waters, the intensity and temporal extent of upwelling can markedly vary between and within systems, influencing their productivity regime: from short-term events to seasonal to year-round, with varying degrees of upwelling strength (Cropper et al. 2014; Desbiolles et al. 2014; Bode et al. 2019). Moreover, coastal upwelling systems can present intense mesoscale activity in the form of upwelling filaments and eddies, which may transport nutrients, organic matter and planktonic communities from the coast to the open ocean (Arístegui et al. 2004; Santana-Falcón et al. 2016; Amos et al. 2019).

The input of nutrients through coastal upwelling and associated processes are hence variable in intensity and duration, largely influencing the development of phytoplankton blooms. To test how prokaryotes responded to variable upwelling conditions, we used large-scale mesocosms where we introduced nutrient-rich waters from the upper mesopelagic into oligotrophic surface waters, simulating combinations of upwelling intensity (from 1.6 μM to 10.5 μM of nitrogen) and duration (single pulse vs recurring upwelling), for a total of eight upwelling scenarios. We measured the temporal dynamics of abundance, physiological status and taxonomic composition of prokaryotic communities, hypothesising that prokaryotic successions would differ in relation to the blooming events occurring under the different upwelling scenarios.

Materials and methods

Experimental setup and sampling

Nine KOSMOS (Kiel Off-Shore Mesocosms for Ocean Simulations; Riebesell et al. 2013) were deployed in Gando Bay (27° 55′ 41″ N, 15° 21′ 55″ W, Gran Canaria, Canary Islands) during the autumn of 2018 as part of the Ocean artUp project. Mesocosms were filled with in situ oligotrophic water (mean ± sd volume = 43.775 ± 1.352 m^3) and monitored for 39 days, during which nutrient-rich deep water was added to them to simulate upwelling. Deep water was collected off Gran Canaria from 330 m (on day -10) and 280 m depth (on day 23), and additions to the mesocosms were done in two different treatment modes (Table 1): a singular mode (mesocosms M3, M7, M9, M1; denoted here with an *S*), consisting of a single deep-water addition (on day 4), and a recurring mode (mesocosms M2, M4, M6, M8;

Table 1. Information of the treatments applied to each mesocosm. Total additions of deep water (as absolute values and % relative to the volume of the mesocosms), nitrogen (N), phosphorus (P) and silica (Si). N, P and Si values include both inorganic and organic forms.

Mesocosm	Upwelling mode	Upwelling intensity	Added deep water volume [m^3]	Added deep water volume [%]*	Added N [$\mu mol \cdot L^{-1}$]	Added P [$\mu mol \cdot L^{-1}$]	Added Si [$\mu mol \cdot L^{-1}$]
M5	Control		0.0	0.0	0.00	0.000	0.00
M3	Singular	Low	2.8	6.4	1.62	0.094	0.74
M7		Medium	5.3	12.0	3.07	0.177	1.41
M9		High	9.8	22.4	5.56	0.325	2.63
M1		Extreme	17.2	39.2	9.80	0.567	4.58
M2	Recurring	Low	2.8	6.3	1.61	0.094	0.69
M4		Medium	5.6	12.7	3.15	0.187	1.35
M6		High	11.2	25.6	6.16	0.363	2.64
M8		Extreme	22.4	51.1	10.97	0.682	4.96

** Considering average mesocosm volume of 43.775 m^3*

denoted here with an *R*), in which consecutive deep-water additions were performed (on days 4, 8, 12, 16, 21, 24, 28 and 32). For each upwelling mode, four levels of intensity were simulated, with increasing quantities of deep water added to them: low (M3, M2), medium (M7, M4), high (M9, M6) and extreme (M1, M8), resulting in an intensity range of approximately 1.6–10.5 μM in terms of nitrogen addition (Table 1). For the same intensity level, the singular and recurring modes had similar amounts of total nutrients added during the experiment, yielding comparable treatments (Table 1). No deep water was added to M5 (Control) and ambient waters outside of the mesocosms were monitored during regular sampling (Atlantic). Integrated samples of the water column within the mesocosms were collected using depth-integrated water samplers (IWS, HYDRO-BIOS, Kiel). A detailed description of the experimental set up and sampling procedures can be found in Baumann et al. (2021).

Prokaryotic abundances and viability

Abundance of prokaryotic cells was quantified by flow cytometry. Samples were collected into 2 mL cryovials, fixed with paraformaldehyde at a final concentration of 2% (v/v) and kept at -80°C until further processing. Samples were thawed and analysed in a FACSCalibur flow cytometer (Becton-Dickinson), staining subsamples (400 μL) with 4 μL of the SYBR Green I fluorochrome (Molecular Probes) diluted in dimethyl sulfoxide (1:10). Fluorescent beads (1 μm, Polysciences) were added for internal calibration (10^5 mL^{-1}). High and low nucleic acid content (HNA and LNA, respectively) prokaryotic cells were identified in green vs red fluorescence and green fluorescence vs side scatter cytograms. Additionally, nano- and picophytoplankton abundances were determined by analysing subsamples with no staining, and subgroups identified in red vs orange fluorescence and red fluorescence vs side scatter cytograms.

Viability of prokaryotic cells was quantified by nucleic-acid double-staining using SYBR Green I and propidium iodide (Falcioni et al. 2008) following Baltar et al. (2010a). Viable (intact cell membrane; live and potentially active) and non-viable (compromised cell membrane; dead or injured) cell populations were identified in green vs red fluorescence cytograms.

Single cell translational activity of prokaryotes

The single-cell translational (i.e., protein-synthesising) activity of prokaryotes was assessed by BioOrthogonal Non-Canonical Amino acid Tagging (BONCAT) following Leizeaga et al. (2017). For each sampling time and mesocosm two replicates and a control (9 mL each) were incubated with L-Homopropargylglycine (HPG) at a final concentration of 1 μM for 2h at in situ temperature. The control was fixed with paraformaldehyde prior to HPG addition at a final concentration of 2% (v/v), and replicates were likewise fixed to finalise incubations, after which they were left overnight at 4°C. Samples were then gently filtered through polycarbonate filters with a pore size of 0.2 μm (Whatman Nuclepore). Filters were washed thrice with sterile ultrapure water, labelled and stored at -80°C until further processing.

Filters were subsequently processed by submerging them in a pre-boiled agarose solution (0.1 % w/w) to ensure cell attachment to the filters and avoid cell loss during downstream processing. After drying the filters at 37°C they were dehydrated with ethanol (96%, v/v). Cells were then permeabilised with 1) freshly prepared lysozyme solution (10 $mg{\cdot}mL^{-1}$; 0.05 M EDTA, 0.1 M Tris-HCL) for 1h at 37°C and 2)

achromopeptidase (60 $U \cdot mL^{-1}$; 0.01 M NaCl, 0.01 M Tris-HCl, pH 8.0) for 30' at 37°C (Sekar et al. 2003). Filters were subsequently washed with sterile ultrapure water and ethanol (96%, v/v). Next, Cu(I)-catalyzed click chemistry was performed. A dye premix was prepared with 10 μL of 20 mM copper sulfate solution ($CuSO_4 \cdot 5H_2O$), 8 μL of 1 mM Alexa594 azide dye (ThermoFisher) and 20 μL of 50 mM Tris[(1-hydroxypropyl-1H-1,2,3-triazol-4-yl)methyl]amine (THPTA), and left to react in the dark at room temperature for 3'. A solution combining 100 μL of freshly prepared 10 mM sodium ascorbate solution in phosphate buffered saline (PBS), 100 μL of freshly prepared 10 mM aminoguanidine hydrochloride solution in PBS, and 1.77 mL of PBS solution was prepared in the meantime. For the click reaction mix, the dye premix and the PBS-ascorbate-aminoguanidine solution were combined, gently inverting the tube twice to ensure homogenisation. The click reaction mix was then quickly added to a 1.5 mL tube containing a triangular filter piece of each sample, filling the entire tube and its cap to avoid air bubbles and hence maintain reducing conditions. Furthermore, after closing the tube the cap was sealed with parafilm to ensure no air exchange happened. The tube was placed in the dark at room temperature for 30' to let the click reaction take place. Filters were subsequently washed thrice with PBS and once each with ethanol at 50, 70 and 96% (v/v). A final 1h wash with a solution of PBS:ethanol (1:1) was performed to reduce the background fluorescence signal. Filters were counterstained with 4′,6-diamidino-2-phenylindole (DAPI; 1 $\mu g \cdot mL^{-1}$ final concentration), placed in microscope slides with antifading reagent (77% glycerol, 15% VECTASHIELD and 8% 20x PBS) and covered with glass covers.

Image acquisition to quantify translationally active cells was done in black and white with a Zeiss Axio Imager.Z2m Epifluorescence Microscope connected to a Zeiss camera (AxioCam MRm, Carl Zeiss MicroImaging, S.L., Barcelona, Spain) at 630× magnification, along with the AxioVision software. A Colibri LED light source (Carl Zeiss) with multiple light-emitting diodes was used, capturing all images at excitation of both 1) 385 nm for DAPI and 2) 590 nm for Alexa594, adjusting exposure time to optimise cell detection. Images analysis to quantify total (DAPI) and translationally active (BONCAT+) cells was carried out with the ACMEtool software following Leizeaga et al. (2017).

DNA sampling, extraction and sequencing

Seawater samples for DNA sequencing were collected in acid-cleaned plastic canisters (mean ± sd = 3.0 ± 1.3 L). Samples were prefiltered through a 200 μm mesh to remove any large organisms and subsequently filtered using a peristaltic pump through a set of polycarbonate filters (Whatman Nuclepore) with a pore size of 3.0 and 0.2 μm, resulting in a size fractionation of 0.2-3.0 μm (hereafter '0.2 μm' size fraction) and 3.0-200 μm (hereafter '3.0 μm' size fraction). Upon filtration, filters were stored in autoclaved safe-lock tubes and kept at -80°C until further processing.

DNA extraction from samples was performed using the DNeasy Plant Mini Kit (Qiagen) following instructions by the manufacturer. To increase extraction yield, the procedure was slightly modified to include a pre-treatment of samples that consisted of 1) an initial (triple) freeze fracture step, 2) bead beating with autoclaved zirconia (0.1 mm) and glass (0.5 mm) beads (Sigma-Aldrich) for 5', and 3) a proteinase-k (Sigma-Aldrich) treatment at 55°C for 1h. Three polycarbonate filters with no sample were also subject to the extraction protocol to act as negative controls. After completing the full procedure, DNA concentration in the extract was quantified with an Eppendorf D30 BioPhotometer. Extraction aliquots of samples and negative controls were dispensed into PCR plates (VWR) and these were sealed with adhesive aluminium foil.

The extracted DNA was sequenced for the V4 and V5 regions of the 16S rRNA gene (16S rDNA) using the universal primers '515F' and '926R' (Parada et al. 2016). Amplified regions were sequenced with the Illumina MiSeq platform (paired-end reads; 2 × 250 bp) at the Argonne National Laboratory (Lemont, IL, USA).

16S amplicon sequence analysis

Bioinformatic analyses were performed at the Marine Bioinformatics platform (Marbits, marbits.icm.csic.es) of the Institut de Ciències del Mar (ICM-CSIC, Barcelona). *Cutadapt* (Martin 2011) was used to ensure primers were not present in the sequences. All subsequent analyses were performed in R (v. 4.0; R Core Team 2021). The *DADA2* package (Callahan et al. 2016) was used to process the amplicon sequence data (*trunclen* = (240, 155), *maxEE* = (2, 8), *minOverlap* = 15). Briefly, *DADA2* models errors in the Illumina-sequenced amplicon reads to infer exact amplicon sequence variants (ASV) down to one nucleotide difference. Taxonomic assignation of ASVs was carried out using the 'assignTaxonomy' function (*minBoot* = 50), with SILVA v. 138.1 (arb-silva.de) as the training set. Identification of

contaminant sequences was performed using the *decontam* package (Davis et al. 2018) combining the frequency and prevalence methods (*threshold* = 0.2). After all the processing, the average sequencing depth of samples was 13678 (sd = 4831, n = 252). Samples with at least 2500 reads were preserved for downstream analyses (n = 247).

Statistical analyses

All statistical analyses were carried out in R (v. 4.1.2, R Core Team 2021). Non-metric multidimensional scaling (NMDS) was performed with the *metaMDS* function (*vegan* package, v. 2.5.7, Oksanen et al. 2020) to assess similarities in prokaryotic community composition among samples. A Bray-Curtis dissimilarity matrix (*vegdist* function, *vegan*) estimated from a rarefied ASV count table of 5000 counts (sample n = 241) that was based on 100 permutations (*rrarefy.perm* function, *EcolUtils* package, v. 0.1, Salazar 2022) was used for the analysis. Dissimilarities between day 3 (last preaddition sampling) and the rest of the samples within each size fraction were considered, and differences between treatments were evaluated by means of Kruskal-Wallis and post-hoc Conover tests, correcting p-values with the Bonferroni method (*kruskalTest* and *kwAllPairsConoverTest* functions, *PMCMRplus* package, v. 1.9.6; Pohlert 2022). Diversity indicators of richness and Pielou index were estimated with the *richness* and *evenness* functions (*microbiome* package, v. 1.16.0, Lahti and Shetty 2019), respectively, using the same rarefied table.

Prokaryotic community succession patterns induced by upwelling were analysed by Fuzzy C-Means Clustering (Bezdek 1981). Unlike hard clustering, where each element is allocated to a unique cluster, in fuzzy clustering elements are assigned a membership score for all clusters concurrently (from 0 = no membership, to 1 = full membership), allowing for a more detailed evaluation of cluster classifications. Fuzzy clustering was performed individually for each treatment and size fraction combination using the *cmeans* function (*e1071* package, v. 1.7.9, Meyer et al. 2021). The fuzzifier parameter *m* was estimated following Schwämmle and Jensen (2010), resulting in a value (excluding deep waters) of 1.290 ± 0.025 (mean ± sd). The choice of the number of clusters (*k*) was based on several cluster selection indices (Within Cluster Sum of Squared Error, Simple Structure Index (*cascadeKM* function, *vegan*, Dimitriadou et al. 2002) and Normalized Partition Coefficient (*vegclustIndex* function, *vegan*, Bezdek 1981)), aided by the knowledge of the biogeochemical processes happening in the mesocosms (Fig S1). For this analysis, a centred log-ratio (CLR) transformed ASV count table was used with an added pseudocount of 1 (*clr*

function, *compositions* package, v. 2.0.4, van den Boogaart et al. 2022). From that table, only ASVs representing at least 0.1% of reads in one sample were considered. To cluster ASVs according to their temporal patterns and exclude the influence of abundance levels, the CLR-transformed abundance of each ASV was centred and scaled by subtracting its mean and dividing by its standard deviation. The resulting clusters were named following the same convention across all treatments and size fractions. For each treatment and size fraction combination, the relationship between specific environmental parameters and prokaryotic community successions was assessed by means of Mantel tests (*mantel* function, *vegan*, Legendre and Legendre 2012). The two dissimilarity matrices of samples required for the tests (here based on Euclidean distances) were estimated from 1) CLR-transformed ASV count table and 2) individual environmental parameters. Mantel tests were run with the Spearman method based on 9999 permutations.

Ancillary environmental parameters

Nitrate (NO_3^-), nitrite (NO_2^-), ammonium (NH_4^+), phosphate (PO_4^{3-}) and silicic acid ($Si(OH)_4$) were quantified spectrophotometrically on a five channel continuous flow analyser (QuAAtro AutoAnalyzer, SEAL Analytical Inc., Mequon, United States). Total chlorophyll *a* (Chl *a*) was measured with an HPLC Ultimate 3000 (Thermo Scientific GmbH, Schwerte, Germany). Concentrations of particulate organic matter in the water column were quantified using a CN analyser (Euro EA-CN, HEKAtech). Prokaryotic heterotrophic production (PHP) was estimated from ^{3}H-leucine incorporation using the centrifugation method (Smith and Azam 1992). These methods are described in detail in Baumann et al. (2021). Fractionated Chl *a* concentrations (0.2-2.0 μm, 2.0-20 μm, >20 μm) were determined with a Turner Design AU-10 fluorometer (Ortiz et al. 2022).

Details of the dissolved organic matter (DOM) characterisation can be found in Chapter 1. Briefly, dissolved organic carbon (DOC) concentrations were determined with a Shimadzu TOC-5000 analyser (Sharp et al. 1993). Dissolved organic nitrogen (DON) and phosphorus (DOP) concentrations were quantified spectrophotometrically on a continuous flow analyser (QuAAtro AutoAnalyzer) following Hansen and Koroleff (1999). Absorbance measurements for the characterisation of chromophoric dissolved organic matter were performed using a USB2000+UV-VIS-ES Spectrometer (Ocean Optics) alongside a liquid waveguide capillary cell (World Precision Instruments). Absorption coefficients (a_{254}, a_{325}) and spectral slopes ($S_{275\text{-}295}$, $S_{350\text{-}400}$, S_R) at wavelengths of interest were calculated following

previous works (Helms et al. 2008; Catalá et al. 2018). Fluorescence measurements for the characterisation of fluorescent dissolved organic matter were conducted with a Fluoromax-4 spectrofluorometer (Jobin Yvon Horiba). Fluorescence components were defined applying a parallel factor analysis (Stedmon and Bro 2008), resulting in two amino acid-like components (C1, C5) and two humic-like components (C2, C4) (see Chapter 1 for details).

Results

Biogeochemical context

The addition of nutrient-rich deep waters led to large phytoplankton blooms (proportional to the simulated upwelling intensity). Chl *a* concentrations (Fig. 1a) peaked on day 9, the highest values being registered in the singular extreme treatment. Diatoms dominated the phytoplankton blooms of all treatments, leading to increases in primary production rates (Ortiz et al. 2022). In the singular treatments the blooms collapsed after day 9 and did not recover, but in the recurring treatments the periodic deep water additions allowed the blooms to persist until the end of the experiments, albeit with oscillating Chl *a* concentrations and primary production rates (Ortiz et al. 2022). Particulate organic matter concentrations in the water column accumulated following the phytoplankton blooms (Baumann et al. 2021). The singular treatments presented the highest particulate organic carbon (POC) values after the initial bloom (Fig. S2), followed by a steady decrease until the end of the experiment. In the recurring treatments increases were slower but POC accumulated until day ~20. Approaching the end of the experiment, the low to high recurring treatments converged to similar concentrations as those measured in the singular mode, but particulate organic matter markedly accumulated in the extreme recurring treatment (Fig. S2). This accumulation, accompanied by increases in Chl *a* and primary production rates, was associated with a coccolithophorid bloom (Ortiz et al. 2022).

The DOM pool also showed marked changes (see Chapter 1 for details). Dissolved organic carbon (DOC) concentrations (Fig. S2) greatly increased after days 7–9, especially during the decay of the initial blooms (days 11–17), until day ~19, when DOC tended to stabilise until the end of the experiment. In the extreme treatments DOC accumulations were most remarkable, reaching ~140 μM, meaning that DOC doubled relative to initial concentrations. Dissolved organic nitrogen (DON) and phosphorus (DOP) values also increased, although more moderately, and displayed variability (see Fig. 2 of Chapter 1). The optical characterisation of DOM showed

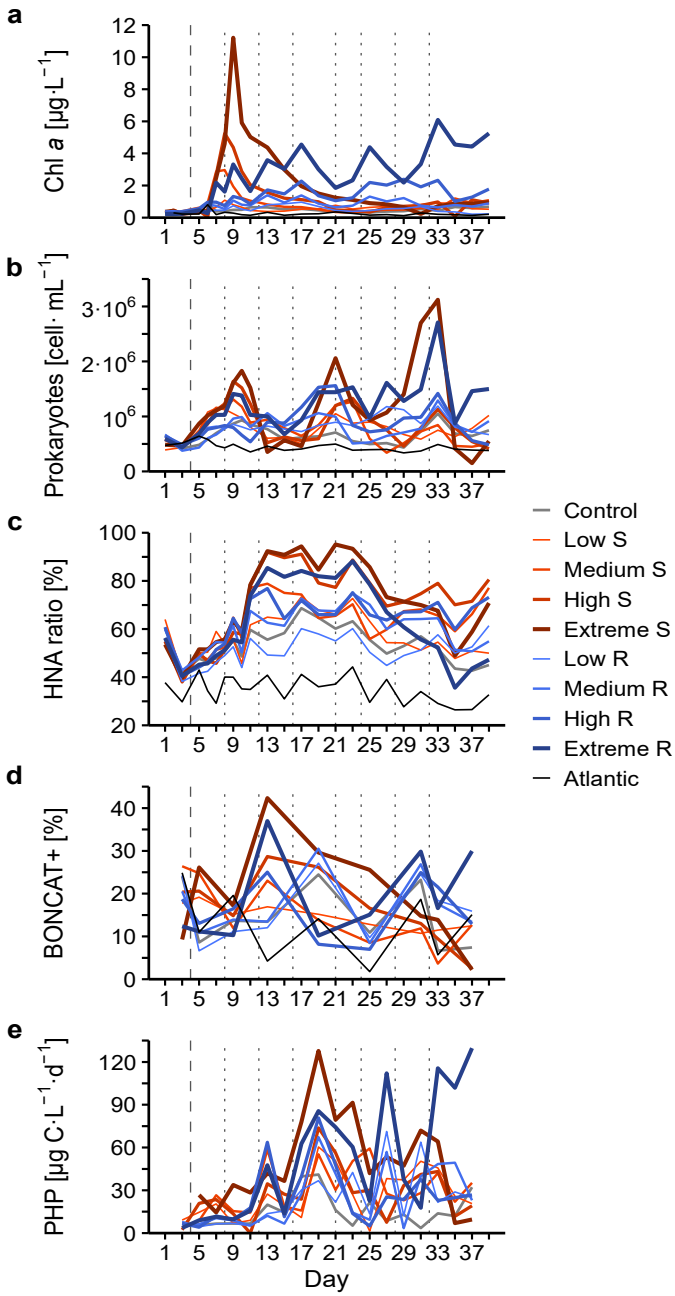

Figure 1. Temporal dynamics of relevant biological variables. a) Chlorophyll *a* (Chl *a*) concentration, b) abundance of prokaryotes, c) relative abundance of high nucleic acid content (HNA) prokaryotes, d) relative abundance of prokaryotic cells actively synthesizing proteins (BONCAT+ cells), and e) prokaryotic heterotrophic production (PHP). Vertical lines represented deep water additions in singular (dashed) and recurring treatments (dashed and dotted).

sustained accumulations of chromophoric DOM, along an increase in its average molecular weight (see Fig. 4 of Chapter 1). While proportional to upwelling intensity, these changes were more pronounced in the singular mode. Fluorescence measurements also showed uninterrupted accumulations of humic-like fluorescent DOM. Amino acid-like fluorescence on the other hand increased during the initial bloom and its subsequent collapse but remained fairly stable afterwards. Chromophoric and humic-like fluorescent DOM were found to be positively correlated to cumulative prokaryotic heterotrophic production (Fig. 8 of Chapter 1).

Prokaryotic abundance, viability and activity

Prokaryotic abundance (Fig. 1b) was 3.8–4.9 · 10^5 cells · mL^{-1} prior to the first deep water addition. Despite differences in magnitude, all mesocosms followed similar trends, regardless of the treatment: cell counts increased and first peaked on days 9–10 (up to 1.8 · 10^6 cells · mL^{-1} in the extreme singular), slightly later than the initial diatom blooms (days 8–9). Like the diatom blooms, abundance of prokaryotic cells greatly decreased on days 13–17 in the singular treatments and, to a lesser extent, in the recurring ones, falling back to approximately initial values. Subsequently, a new abundance peak was registered around day 21 (maximum of 2.1 · 10^6 cells · mL^{-1}) and a third one on day 33 (particularly evident in both extreme treatments, 3.1 · 10^6 cells · mL^{-1} in the singular, 2.7 · 10^6 cells · mL^{-1} in the recurring). Prokaryotic abundance in all treatments then dropped to 4.1–10.2 · 10^5 cells · mL^{-1} except in the extreme recurring treatment (1.5 · 10^6 cells · mL^{-1}). The percentage of viable prokaryotes (i.e., those with intact cell membranes) was high throughout the experiment (>85%) but overall followed a three peak pattern similar to prokaryotic abundance (correlations between abundance and viability were significant in the extreme treatments, Fig. S3).

The percentage of high nucleic acid content prokaryotes (HNA, Fig. 1c) also presented similar dynamics across treatments. From 38–43 % just before the initial deep water addition, the percentage steadily grew until day 10. Following the bloom collapse and the first major drop in prokaryotic abundances, the proportion of HNA cells markedly increased according to upwelling intensity. This increase was more pronounced in the singular treatments, where the percentage of HNA cells exceeded 90% for the high and extreme intensities by day 13, in contrast to 71–84% for the equivalent recurring levels. After day 23, the proportion of HNA cells declined in all treatments. Owing to a late recovery, HNA cells at the end of the experiment presented a clearly higher contribution than at the start in most treatments, although

with considerable dispersion (45–81%), the singular mode overall displaying higher values than the recurring.

The proportion of protein-synthesising prokaryotes (BONCAT+ cells, Fig. 1d) started around 10–25% of total cells. The fraction of BONCAT+ cells increased on day 13, with the extreme treatments reaching ~40%. After day 13 the upwelling modes showed two different outcomes: while the fraction of BONCAT+ cells steadily decreased in the singular mode (falling below 5% in the high and extreme treatments at the end of the experiment), the recurring mode registered values that oscillated between 10–30% BONCAT+ cells, with a notable peak at the end of the experiment in the recurring extreme treatment. Bulk activity levels, measured as PHP (Fig. 1e), started at 5.7 ± 2.5 $\mu g\ C \cdot L^{-1} \cdot d^{-1}$. While presenting only a small increase on day 13, they subsequently peaked on day 19 (128 $\mu g\ C \cdot L^{-1} \cdot d^{-1}$in the extreme singular treatment), coinciding with the raise of the second prokaryotic abundance peak. Recurring treatments displayed another PHP increase on day 27. While in most mesocosms a late increase around day 33 was followed by a decrease, the extreme recurring treatment showed very high PHP rates during the final days, reaching 130 $\mu g\ C \cdot L^{-1} \cdot d^{-1}$.

General prokaryotic community composition

The composition of prokaryotic communities was overwhelmingly dominated by bacteria and presented two main general patterns: a temporal evolution of the mesocosm communities throughout the whole experiment and a clear divide between the two size fractions (Fig. 2a). Taxonomic composition of initial communities within each size fraction was similar among treatments and ambient waters (Fig. 2a and S4). They clearly differed, however, with the deep waters, despite sharing an important number of ASVs (Fig. S5). The addition of deep water and the subsequent dynamics within mesocosm communities greatly altered the structure of the prokaryotic assemblages. Bray-Curtis dissimilarities between day 3 (last pre-addition sampling) and the rest of the samples showed that major changes occurred following deep water additions (Fig. 2b). Overall, dissimilarities increased with time and were larger in the 3.0 μm size fraction, although differences relative to ambient waters were smaller in the 3.0 μm size fraction than in the 0.2 μm one. Despite a slight positive relation between treatment intensity and dissimilarity (Fig. 2b), there were no significant differences in community structure among mesocosms of the same upwelling mode ($p > 0.05$, Post-hoc Conover test, adjusted by Bonferroni

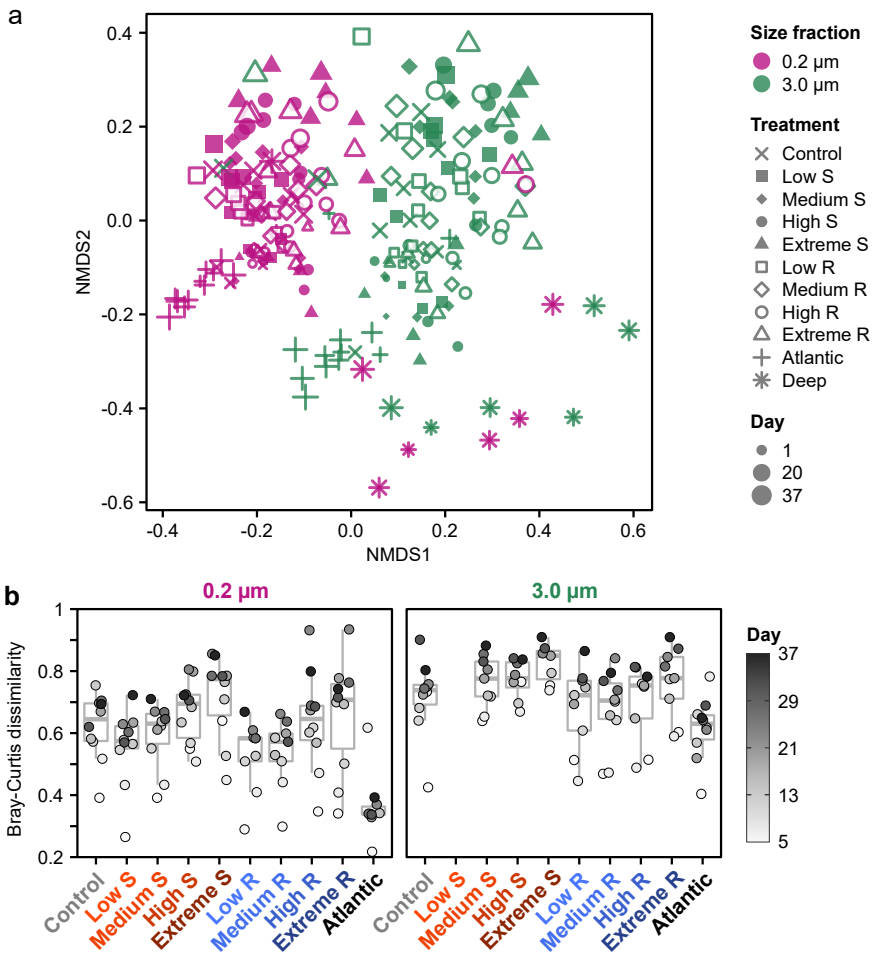

Figure 2. Dynamics in the community structure of prokaryotic communities in the mesocosms. a) Distribution of samples in the NMDS space according to their taxonomic composition, based on Bray-Curtis dissimilarities between samples estimated from a rarefied ASV table (5000 counts). Each point corresponds to a sample, colour representing the size fraction, shape the experimental treatment and size the sampling day. 'Atlantic' corresponds to environmental waters outside of the mesocosms and 'Deep' to the deep waters employed for the additions. b) Bray-Curtis dissimilarities between day 3 (last pre-addition sampling) and the rest of the samplings, within each treatment and size fraction, estimated from the same rarefied table. The 3.0 µm size fraction of the Low S treatment is missing due to insufficient sequencing depth for day 3. Colourmap indicates the sampling day. Boxplots in the background summarise dissimilarities for each treatment: the horizontal line corresponds to the median; the lower and upper hinges correspond to the 25th and 75th percentiles; the upper (lower) whisker extends from the hinge to the largest (smallest) value no further than 1.5 * IQR from the hinge, where IQR is the inter-quartile range, i.e., the distance between the 25th and 75th percentiles.

method). Significant differences were also absent when comparing upwelling modes (grouping mesocosms under singular vs recurring modes within each size fraction).

The diversity of the prokaryotic communities also presented important changes over time. In the 0.2 µm size fraction, ASV richness (Fig. 3a) showed a decrease with time in all treatments (particularly in the first half of the experiment), from 855 ± 73 at the start to 497 ± 75 at the end (Fig. 3a). Changes in the Pielou evenness index were not as marked (Fig. 3b), from 0.764 ± 0.026 at the start to 0.719 ± 0.046 at the end, with a relatively quick recovery from the pronounced decrease caused by the first deep water addition. This meant that despite the decrease in richness the members of the 0.2 µm size fraction were distributed in a similarly even manner. The 3.0 µm size fraction tended to be more diverse (as defined by richness): initial richness and Pielou indices were higher than in the 0.2 µm size fraction (1031 ± 134 and 0.806 ± 0.018, respectively), experienced a large drop coinciding with the bloom following the first deep water addition, particularly in all the singular treatments and the extreme

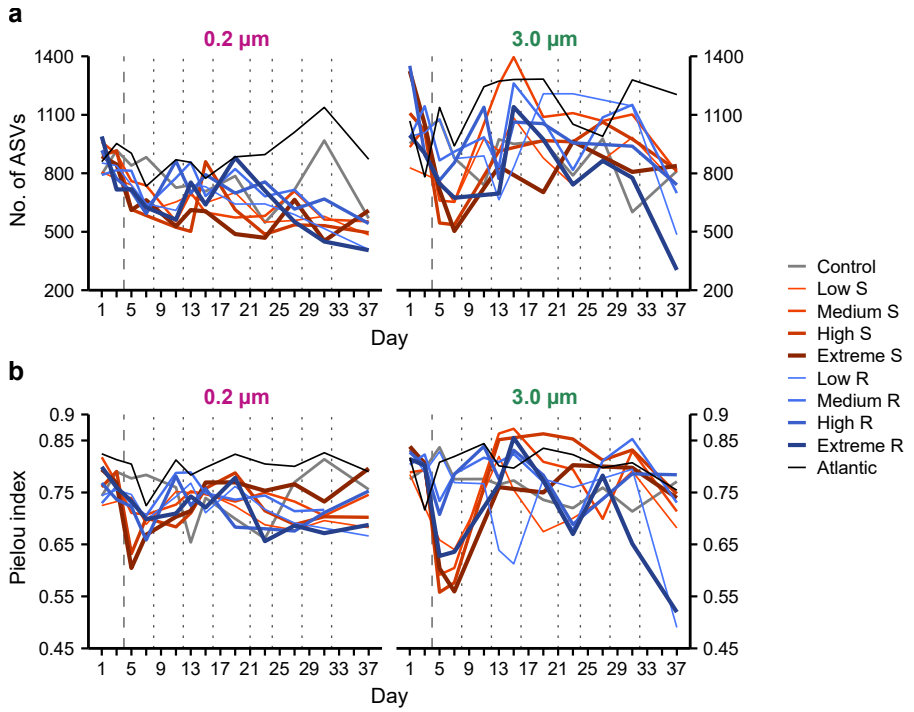

Figure 3. Temporal dynamics of prokaryotic diversity in the 0.2 µm (left panel) and 3 µm (right panel) size fractions. a) species richness as number of ASVs, and b) Pielou evenness index. Vertical lines represented deep water additions in the singular (dashed) and recurring treatments (dashed and dotted). Count table was rarefied down to 5000 reads to estimate indices.

recurrent treatment, and then quickly recovered. Only at the end of the experiment did values decrease, mainly in the extreme (and low) recurring treatment (Extreme R: richness = 311 and Pielou = 0.521). Thus, as opposed to the 0.2 μm size fraction, in the 3.0 μm one both richness and evenness remained closer to those of the initial communities most of the time.

Temporal succession patterns

Under the different simulated upwelling intensities and modes, the initial communities underwent dramatic changes in their taxonomic composition. By means of fuzzy clustering of the temporal trends we identified that the changes observed in Figs. 2 and 3 corresponded to prokaryotic successions formed by 4-5 assemblages of ASVs. These ASV clusters shared common patterns across all treatments and size fractions (Fig. 4, S6 and S7): 1) an initial community (named '*Initial'*), 2) a post-initial-addition cluster dominating on days 5-7 (named '*Postaddition'* for simplicity; only well resolved in singular treatments, but present in recurring ones too, see e.g., the elbow in the initial cluster in Fig. 4), 3) a cluster peaking during the demise (decline, for recurring treatments) of the initial blooms (days 11-19, '*Postbloom*'), 4) a fourth one usually occurring during days 19-27 ('*Intermediate*'), and 5) a final cluster dominating towards the end of the experiment ('*Final'*, with varying degrees of temporal extension). ASVs belonging to each cluster of the prokaryotic succession process usually dominated the community during their peak, representing on average 54.9 ± 14.1 % of reads (Fig. 4 and S8).

Initial communities were associated with environmental conditions typical of oligotrophic surface waters: low Chl *a* (0.2–0.4 mg · m^{-3}), prokaryotic abundance (~4 · 10^5 cells · mL^{-1}) and POC (5–10 μM), and DOC concentrations around 70–80 μM. While dominating the preaddition days (1-3), their abundance quickly decreased after simulated upwelling was initiated, representing a very reduced number of reads from that moment onwards (Fig. 4, S6 and S8). The most representative ASVs of the initial clusters (membership > 0.75) throughout all treatments in the 0.2 μm size fraction belonged to multiple Flavobacteriales (mainly *Aurantivirga*, but also *Formosa*, and NS4, NS5 and NS2b marine groups; Fig. S9 and S10), Rhodobacterales (chiefly HIMB11 genus, Fig. S11 and S12), Actinomarinales, the SAR11 clade (Clades Ia, Ib) and Synechococcales (*Synechococcus*, *Prochlorococcus*) (Fig. 6a-b and S14). All these taxa represented a notable fraction of the community at the start of the experiment (Figs. 5 and S13). In the 3.0 μm size fraction, Flavobacteriales (NS9 marine group, *Aurantivirga*, and *Formosa*) were prominent, accompanied by

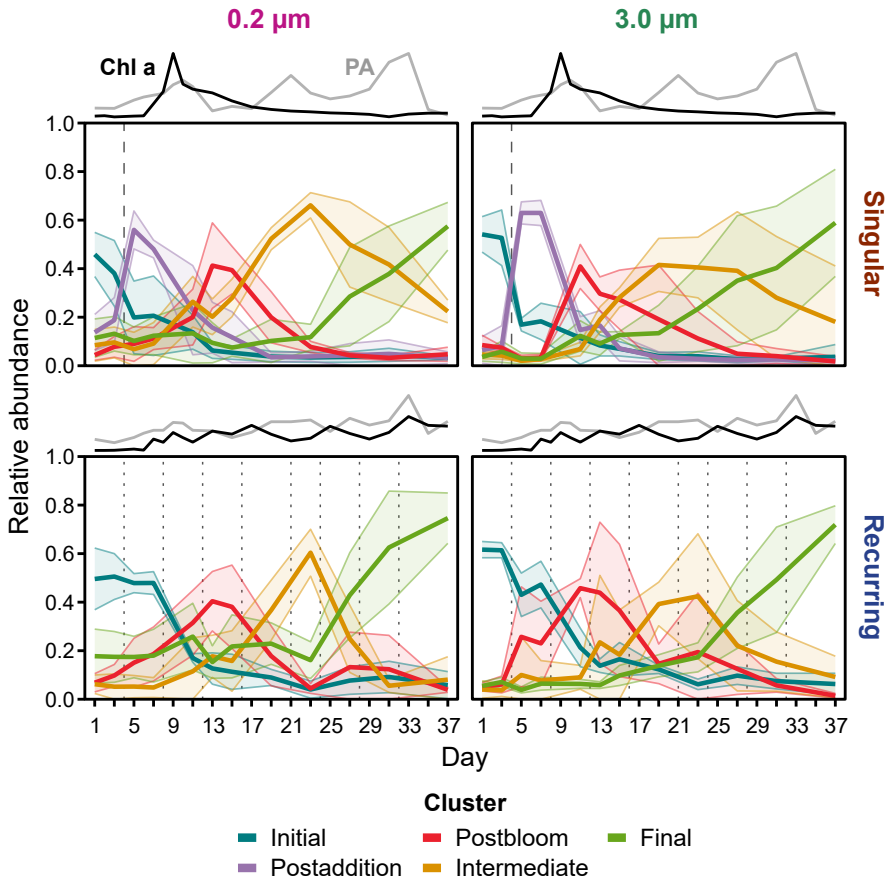

Figure 4. Combined relative abundance of ASVs assigned to each cluster, averaged per upwelling mode (Singular = upper row; Recurring = lower row) and size fraction (0.2 µm = left column; 3.0 µm = right column). The shaded area around lines represents the ± standard deviation of averaged values for the different intensity treatments. Lines on top of plots show scaled Chl *a* (black) and prokaryotic abundance (PA, grey) values (from extreme treatments, in arbitrary units). Deep water additions are shown as dashed (singular) and dotted lines (recurring). Detailed results for all individual treatments are available in Fig. S8.

Pirellulales (*Rubripirellula*), Chitinophagales (unidentified Saprospiraceae) and Rhodobacterales (most notably *Cognatishimia*) (Fig. 6c-d and S14). In the singular treatments, which received the largest unique pulses of upwelling (Table 1), the initial community was quickly overtaken by prokaryotes linked to deep waters: in both size fractions two Rhodobacterales ASVs from the *Sulfitobacter* genus (which dominated initial deep waters, Fig. S14) were disproportionately abundant (32-45% of reads). Other Rhodobacterales (*Shimia*, *Planktotalea*, *Pseudooceanicola*) and

Pseudomonadales (*Pseudohongiella*) were also characteristic of the postaddition communities. The prominence of Rhodobacterales during this phase was evident from the large relative abundance represented by the order (Fig. 5). Post-addition ASVs held considerable abundances approximately until day 7, but markedly decreased afterwards (Fig. 4). In the recurring treatments, these deep water-derived ASVs also peaked on days 5-7, but due to their lower abundances the postaddition cluster was not well resolved and they were instead grouped within initial or postbloom ASVs (Fig. 6).

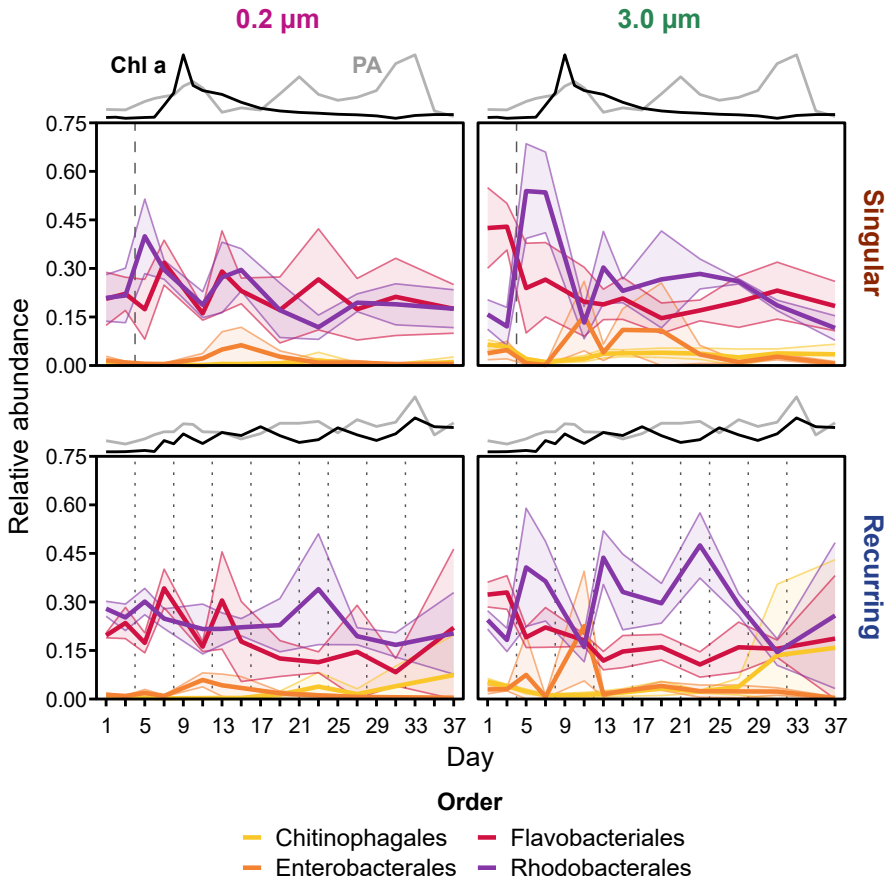

Figure 5. Combined relative abundance of ASVs assigned to major orders associated with DOM cycling during blooms, averaged per upwelling mode (Singular = upper row; Recurring = lower row) and size fraction (0.2 µm = left column; 3.0 µm = right column). The shaded area around lines represents the ± standard deviation of averaged values for the different intensity treatments. Lines on top of plots show scaled Chl *a* (black) and prokaryotic abundance (PA, grey) values (from extreme treatments, in arbitrary units). Deep water additions are shown as dashed (singular) and dotted lines (recurring).

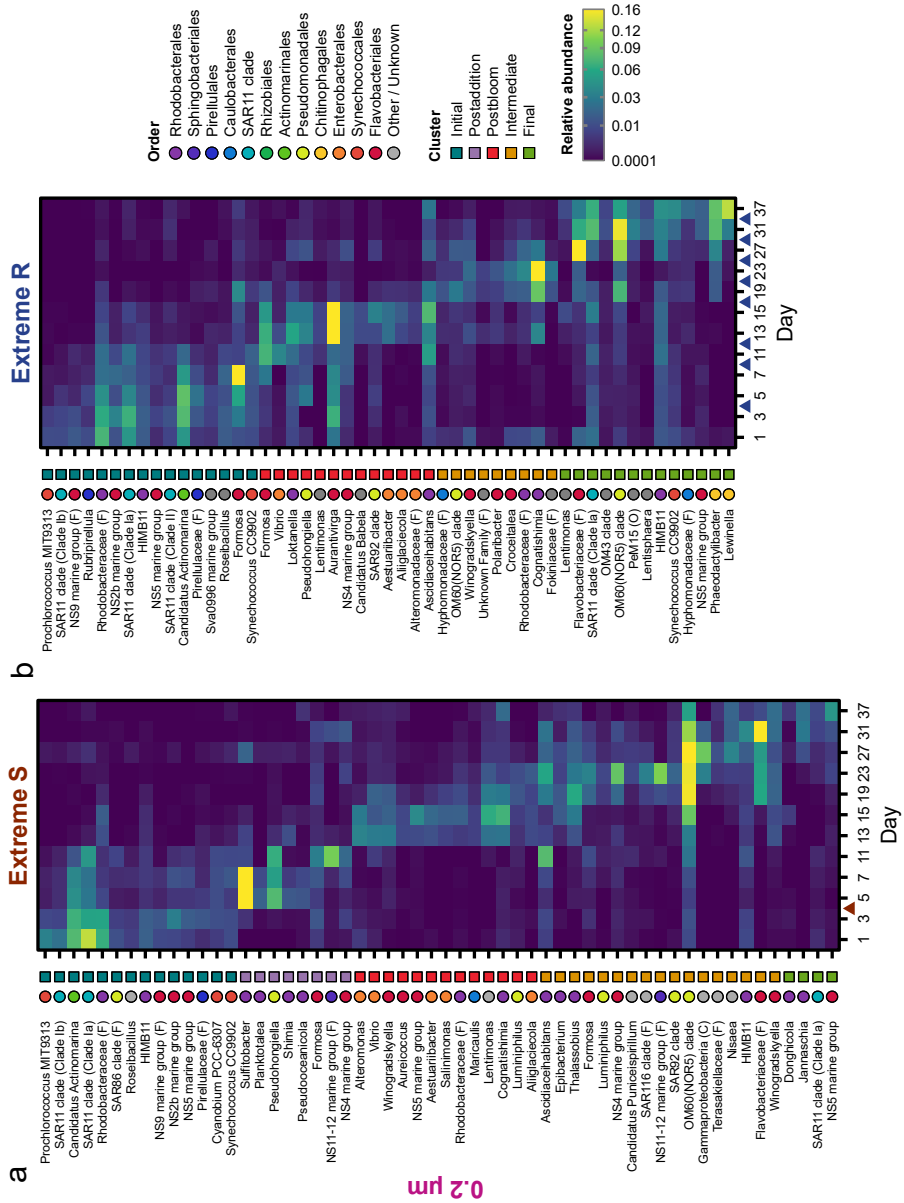

Figure 6. Succession patterns of most relevant prokaryotic taxa in extreme treatments. a) extreme singular, 0.2 µm; b) extreme recurring, 0.2 µm; c) extreme singular, 3.0 µm; and d) extreme recurring, 3.0 µm. For each treatment and size fraction, ASVs with a membership value over 0.75 were merged by genera (when possible; otherwise, at the most detailed taxonomic level available, as indicated next to their name: F = family, O = order, C = class). From those, taxa representing at least 0.5% of reads in more than 1 sample within each treatment and size fraction are shown.

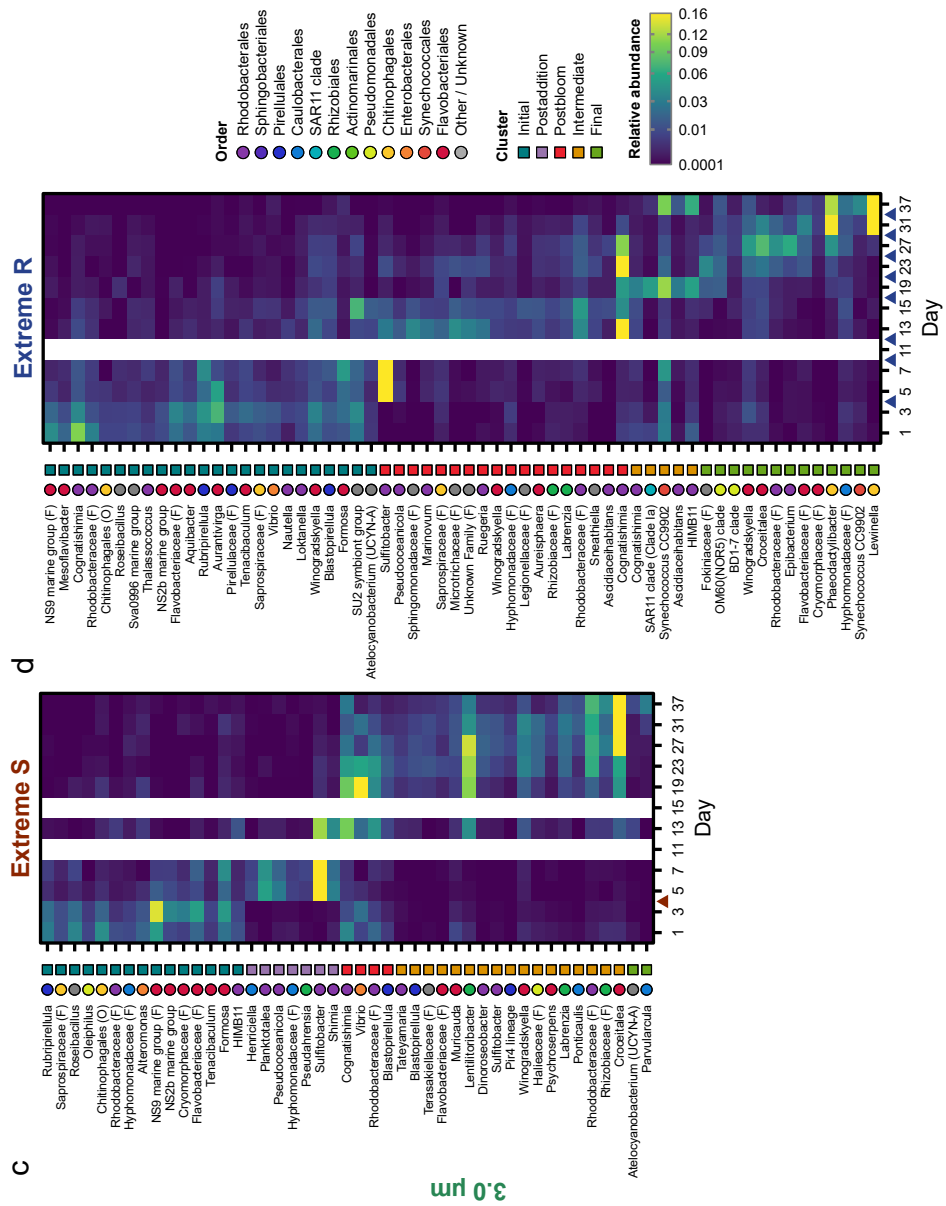

Figure 6. Continued. Colourmap represents relative abundance of taxa (note that to aid visualisation 1) the scale is square-root-transformed and 2) out of bounds outlier values have been assigned the colours of the upper and lower limits of the colourmap). Coloured dots represent the taxonomic order of taxa, and coloured squares their cluster assignation. A complete figure with all the treatments is shown as Fig. S14.

During the termination of the initial diatom blooms (or decrease, in the case of the recurring treatments) a new assemblage of ASVs increased in abundance (postbloom cluster), following drops in prokaryotic counts, increases in DOC and, depending on upwelling mode, decreases (singular) and increases (recurring) in POC (Fig. 4 and S8). The 0.2 μm size fraction of the extreme treatments was mainly dominated by multiple Flavobacteriales (especially *Formosa* on days 7-13, followed on days 13-19 by other genera, with a strong peak of *Aurantivirga* in the recurring), some Rhodobacterales (*Cognatishimia* in the singular treatment, *Ascidiaceihabitans* in the recurring), Enterobacterales (multiple genera, chiefly *Vibrio* and *Alteromonas*) and Sphingobacteriales (Fig. 6a-b, see S14 for details of all treatments). In the 3.0 μm size fraction, there were some differences between upwelling modes: singular treatments prominently featured *Vibrio* (Enterobacterales) and *Cognatishimia* (Rhodobacterales), whereas the recurring treatments had a large representation of *Cognatishimia* (resulting in a marked increase of Rhodobacterales relative abundance, Fig. 5) and multiple other ASVs from diverse orders (Fig. 6c-d and S14). Notably, Enterobacterales were mostly restricted to this postbloom phase in both size fractions, presenting clearly higher abundances in the 3.0 μm one (Fig. 5 and 6).

On days 19-25, coinciding with the stabilisation of DOC concentrations, and the onset and demise of the second prokaryotic abundance peak, the intermediate cluster was found in most mesocosms, albeit it tended to be stronger in the 0.2 μm size fraction and in the singular treatments (Fig. S7 and S8). In these treatments the intermediate cluster was dominated by members of the OM60(NOR5) clade (among other Pseudomonadales), Flavobacteriales (mainly NS4 marine group and *Formosa*), Rhodobacterales (*Thalassobius* and *Ascidiaceihabitans*), and Puniceispirillales (SAR116 clade). ASVs belonging to the SAR11 clade displayed variability across treatments (Fig. S13 and S14), appearing in the intermediate cluster of the low, medium and high treatments, but not in the extreme (Fig. S14). In the same size fraction of the recurring treatments, *Cognatishimia* dominated the intermediate cluster, together with several Flavobacteriales ASVs (including *Winogradskyella*). In contrast, Pseudomonadales only irregularly appeared (see Fig. S14 for all treatments). The 3.0 μm size fraction of the singular treatment was initially dominated by *Lentilitoribacter* (among other Rhizobiales) and ended up dominated by *Croceitalea* (Flavobacteriales) (Fig. 6c, S9 and S10). In the recurring treatments, Rhodobacterales (again, predominantly *Cognatishimia*) were the most relevant taxa in both size fractions. Despite *Aurantivirga* (Flavobacteriales) being the largest contributor to deep water during this period (Fig. S14), it did not feature among taxa in the recurring intermediate clusters.

During the final days of the experiment, different outcomes were observed for extreme treatments. Days > 27 were characterised by low Chl *a,* POC, and prokaryotic activity levels in the singular treatments, while DOC remained high. This final cluster was dominated by Flavobacteriales (NS4 and NS5 marine groups) and Rhodobacterales (HIMB11 and *Jannaschia*) in the 0.2 μm size fraction. In the 3.0 μm size fraction, *Croceitalea* (Flavobacteriales) ended as the most prominent taxa in the singular treatments, although its abundance decreased with decreasing upwelling intensity (Fig. S10). Similarly, unidentified Rhodobacterales tended to display higher abundances with increasing upwelling intensity (Fig. S12). Caulobacterales (mainly Hyphomonadaceae), and Synechococcales (*Synechococcus*) were abundant in both size fractions (Fig. S13 and S14), especially in the low and medium treatments. In the extreme recurring treatment on the other hand, the prokaryotic community shifted to be dominated by Chitinophagales ASVs from the *Lewinella* and *Phaeodactylibacter* genera. This was especially evident in the 3.0 μm size fraction (Fig. 5 and 6d), where they represented more than 50% of the community by day 37. As opposed to the singular mode, *Croceitalea* had far smaller presence among Flavobacteriales taxa in the recurring treatments at the end of the experiment (Fig. S10). Unidentified Rhodobacterales had also reduced abundances and were instead displaced mainly by HIMB11 in the 3.0 μm size fraction of the recurring extreme treatment (Fig. S11). As with the singular treatments, *Synechococcus* were also found in high abundances in the recurring ones (Fig. S14).

Relationship between prokaryotic community composition and biogeochemical variables

Taxonomic successions were strongly related to the organic matter pools in each of the treatments (Fig. 7). Correlations were highest with chromophoric DOM (a_{254}, a_{325}, $S_{275\text{-}295}$, S_R), especially in the 0.2 μm size fraction and in the singular treatments. Likewise, changes in taxonomic composition were highly associated with changes in humic-like fluorescent DOM (C2, C4) and, to a lesser extent, DOC and protein-like fluorescent DOM. In the case of POM concentrations, significant correlations were found with POC and PON, which tended to be stronger for the recurring treatments. Changes in Chl *a* concentrations, biogenic silica and added nutrient concentrations displayed higher correlations with taxonomic changes in the recurring treatments for both size fractions, suggesting a relationship with the sustained phytoplankton blooms. On the other hand, taxonomic changes in the singular treatments seemed more related to the variability in picophytoplankton, particularly

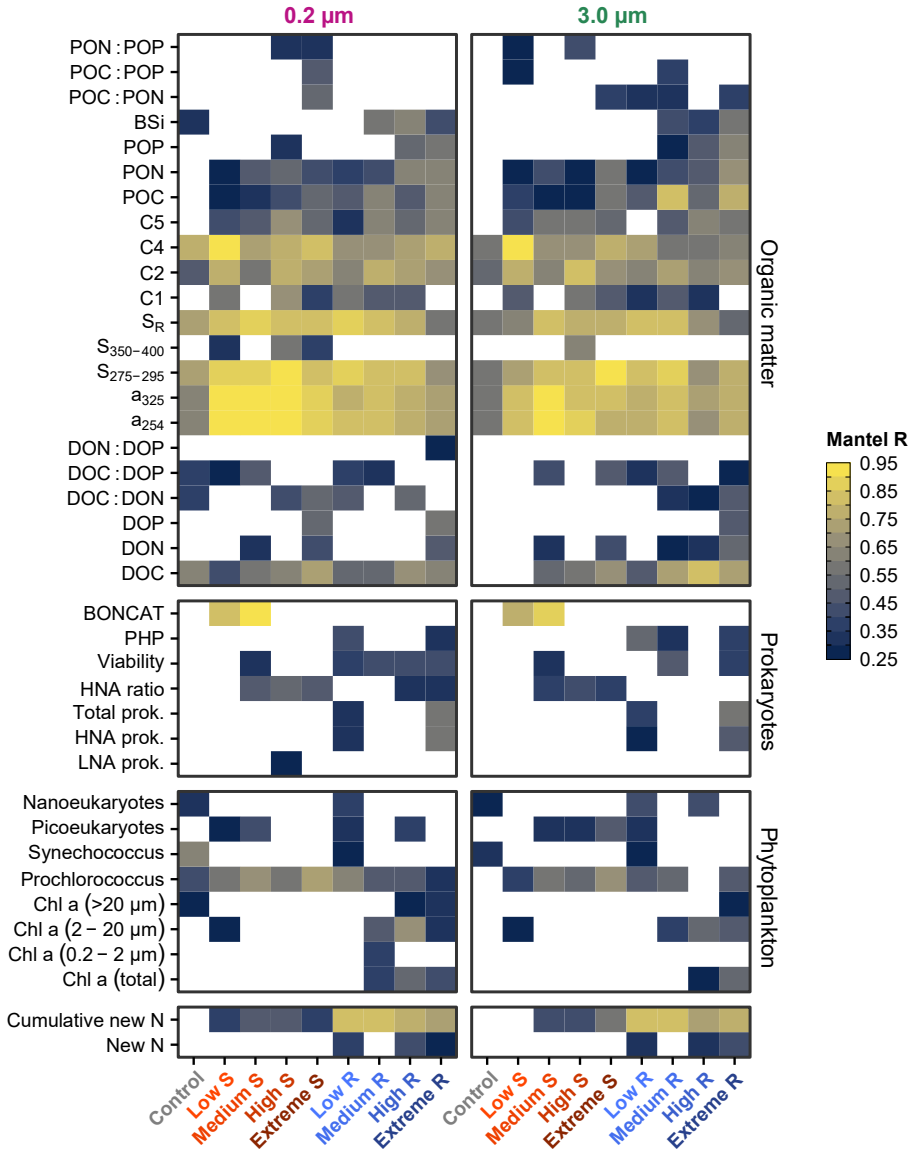

Figure 7. Relationship between prokaryotic community composition and biogeochemical parameters. For each treatment and size fraction, Mantel test results between sample dissimilarity matrices (Euclidean distance) based on 1) the CLR-transformed ASV abundance table and 2) the individual biogeochemical parameters are shown. Only values of significant ($p < 0.05$) results are displayed.

Prochlorococcus, counts. No clear patterns were found with prokaryotic abundances (HNA, LNA, or total counts) but taxonomic changes displayed significant correlations with viability in the recurring treatments and with HNA% in the singular treatments, especially in the 0.2 μm size fraction.

Discussion

Consistent prokaryotic succession patterns regardless upwelling mode

Phytoplankton blooms are known to heavily influence the standing stocks and activity of prokaryotic communities (Buchan et al. 2014). Our observations were no exception, as initial prokaryotic populations went from abundances common to the subtropical eastern North Atlantic and the Canary Islands (Fig. 2; Bode et al. 2001; Baltar et al. 2012) to over 10^6 cells · mL^{-1} following the simulated upwelling and the initiation of diatom blooms. Changes in prokaryotic abundance slightly trailed those of the diatom blooms, reaching maximum values about one day after the peak in Chl *a* and primary production (Fig. 1; Ortiz et al. 2022a). While typically prokaryotic abundances peak during phytoplankton bloom termination and are maintained for some time afterwards (Buchan et al. 2014), here communities across treatments quickly decreased after reaching their peak. Given that conditions during bloom collapse are favourable for prokaryotic growth due to major DOM releases, the decrease in prokaryotic abundance was probably related to a rapid top-down control through grazing by flagellates and/or viral infection (Riemann et al. 2000). In that regard, the considerable viability drops around day 13 likely reflect these top-down mortality losses (Fig. S3). Despite the decrease in total abundance, the fraction of prokaryotes that were actively synthesising proteins overall peaked during the bloom collapse, evidencing that a considerable part of those present were active (Fig. 2d). In fact, in stark contrast to initial conditions (Fig. 8a), clusters of highly active prokaryotes were observed attached to gel structures and particles (Fig. 8b), indicating that they were consuming and transforming the organic matter made available by the decaying phytoplankton (Fig. 1a and Fig. S2; Engel et al. 2002; Mühlenbruch et al. 2018; Baumann et al. 2021). The postbloom activity peak also coincided with the rise of HNA prokaryotes (Fig. 1c), which on some occasions have been described as the community fraction displaying higher activity (Servais et al. 2003).

Prokaryotic community successions during phytoplankton blooms are thought to be tightly coupled with the different algal bloom stages (Zhou et al. 2019). Yet, we

observed surprisingly similar succession patterns among treatments, despite the differences in bloom outcomes regarding the timing of the bloom peak, its intensity and duration (Fig. 4). Concurrent second (days 19-23) and third (day 33) prokaryotic abundance peaks were observed across treatments, and these were paired, particularly in the case of the second peak, with high PHP rates (Fig. 1e). Correlations between PHP and optical properties of DOM indicated that all prokaryotic communities were transforming the DOM pool (see Chapter 1 for more details). It probably involved, however, DOM from partially different sources depending on upwelling mode: in singular treatments, DOM accumulated mostly during the collapse of the initial bloom, and likely consisted of polysaccharides (Mühlenbruch et al. 2018). In contrast, in the recurring treatments the sustained blooms probably led to continuous releases of low molecular weight compounds (such as amino acids and small carbohydrates) alongside polysaccharides (Thornton 2014; Mühlenbruch et al. 2018). Ultimately, DOM did not decrease in neither of the upwelling modes (Fig. S2), suggesting that during the time the experiment lasted prokaryotic DOM remineralisation was balanced with its production regardless of bloom dynamics. At the end of the experiment, a notable shift in the prokaryotic community composition occurred in the extreme recurring treatment concurrent with a coccolithophorid bloom (Ortiz et al. 2022): active filamentous prokaryotes (usually ranging between 10-25 μm) were found in high abundances, an observation that contrasted with the low activity in the singular extreme treatment (Figs. 8c and 8d). The presence of these active filamentous prokaryotes coincided with a dramatic increase in bulk prokaryotic heterotrophic production rates (Fig. 1e) and POC concentration (Fig. S2).

Taxonomic successions within the prokaryotic community

Initial free-living communities (0.2 μm size fraction) were characterised by oligotrophic specialists belonging to the SAR11 clade, Synechococcales and Actinomarinales (Giovannoni 2017; Becker et al. 2019; Teoh et al. 2020; López-Pérez et al. 2020) and versatile Rhodobacterales adapted to low nutrient conditions such as HIMB11 (Durham et al. 2014; Smith et al. 2019). Within the 3.0 μm size fraction, which mostly comprises the particle-attached fraction of the community but can also involve filament-forming prokaryotes (Fig. 8), multiple Flavobacteriales (chiefly NS9 marine group, *Aurantivirga*), Rhodobacterales (*Cognatishimia*) and Pirellulales (*Rubripirellula*) were prominent, all orders known to colonise particles and form biofilms (Haiwei and Ann 2014; Faria et al. 2018; Duret et al. 2019). These initial

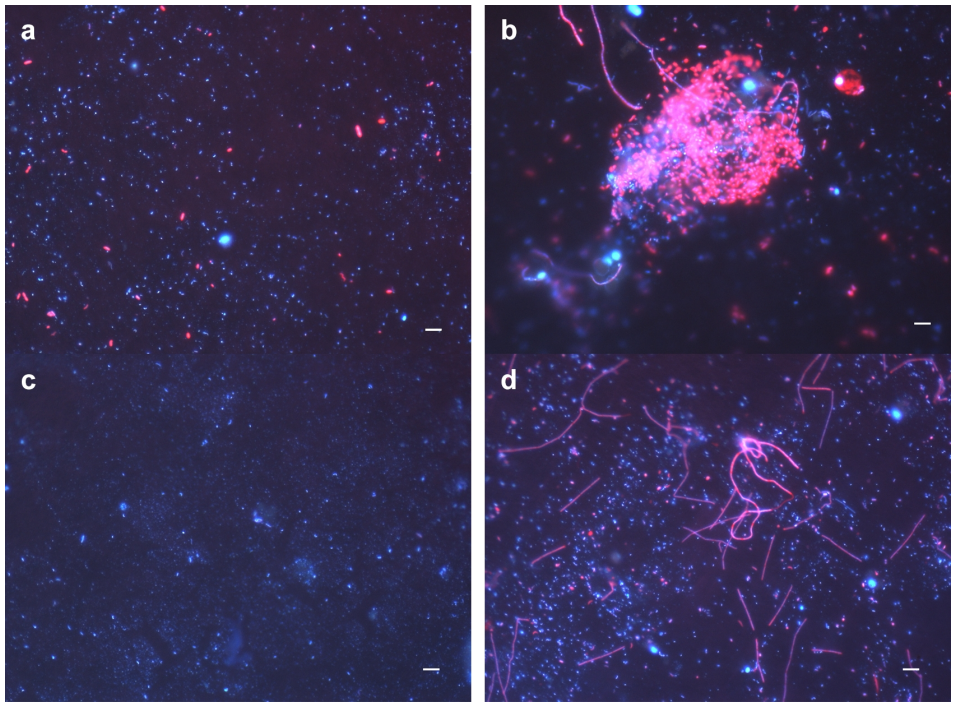

Figure 8. Changes in single-cell protein synthesizing activity, spatial distribution and morphology of prokaryotes during the experiment. Pictures show the combined signal of 4′,6-diamidino-2-phenylindole (DAPI; all cells, blue) and Alexa594 (BONCAT; protein-synthesising cells, red): a) Extreme S (day 3), b) Extreme S (day 13), c) Extreme S (day 37) and d) Extreme R (day 37). Scale bars (bottom right of each panel) represent 5 μm.

communities, however, declined following the marked environmental changes after the initiation of simulated upwelling. Immediately after the first deep water additions, both size fractions were dominated by two ASVs assigned to the *Sulfitobacter* genera (Rhodobacterales), which have been described to have a particle-associated lifestyle (Sorokin 1995; LeCleir et al. 2014). Their sudden increase in numbers was related to their dominance in the deep water at that time, presenting a stronger signal in treatments with larger deep water additions. Nonetheless, *Sulfitobacter* ASVs could not sustain abundances in surface conditions for long and quickly disappeared. Other Rhodobacterales such as *Planktotalea* and *Shimia* presented similar patterns.

Among the first responders to the diatom blooms were *Formosa*, a Flavobacteriales genus known to be highly efficient consuming laminarin, an storage polysaccharide with widespread presence in marine phytoplankton, including diatoms (Unfried et al. 2018; Becker et al. 2020). During the decay of the blooms, copiotrophic opportunists

were dominant. Enterobacterales were most prominent in the more intense treatments where higher quantities of DOM were released, with *Alteromonas* (in the free-living fraction) and *Vibrio* (in the free-living and particle-attached fraction) as the primary genera, agreeing with their ability to make use of sudden inputs of organic matter (Main et al. 2015; Hou et al. 2018; Reintjes et al. 2020). Enterobacterales members were notably more abundant in the particle-attached size fraction (Fig. 5), evidencing their ability to colonise particulate organic matter, including phytoplankton cells (Ivars-Martínez et al. 2008; Grimes et al. 2009; Boeuf et al. 2019). Free-living *Formosa* continued to be abundant and were accompanied by other Flavobacteriales (*Aurantivirga*, *Winogradskyella*, and NS5 marine group) known to utilise polysaccharides (Krüger et al. 2019; Alejandre-Colomo et al. 2020; Priest et al. 2022). During this phase, *Croceitalea* started to rise, displaying a clear affinity for decaying particles, as markedly higher abundances were observed in the singular treatments with higher upwelling intensity, in opposition to the recurring mode where new particulate primary production was more sustained during the experiment (Ortiz et al. 2022). While this genus has been previously found in marine particles and they seem to have all the characteristic attributes of Flavobacteriales (Kwon et al. 2016; Su et al. 2017), lack of detailed information about their metabolism prevents explaining their success colonising particles during the decay and senescence of the large diatom blooms in the singular upwelling mode.

The end of the postbloom phase was marked by yet another shift in the community composition of both size fractions. The free-living community prominently featured members of the Pseudomonadales OM60 clade, a group common in marine surface waters which includes members capable of complementing their heterotrophic metabolism with aerobic anoxygenic photosynthesis (Fuchs et al. 2007; Yan et al. 2009). Members of the OM60 clade have been postulated to be able to degrade aromatic compounds (Mou et al. 2007; Jang et al. 2011), which potentially accumulated in the mesocosm as suggested by the increase in chromophoric and humic-like fluorescent DOM (Catalá et al. 2018; see Chapter 1 for more details). Besides the persistence of several Flavobacteriales and Rhodobacterales (Fig. 5), members of the oligotrophic initial communities (SAR11, *Synechococcus*) made a return, particularly in the least intense treatments (Fig. S14), signalling some potential nutrient limitation. The particle-attached community of the singular treatments presented clear increases in Pirellulales (*Blastopirellula* and Pir4 lineage) and Rhizobiales (*Labrenzia* and *Lentilitoribacter*), taxa that include prokaryotes able to perform nitrate reduction in suboxic and anoxic conditions (Coates and Wyman 2017; Dedysh et al. 2020). This suggests that low-oxygen conditions were probably

created in the suspended and slow-sinking particles that remained in the water column at this time, which were in fact more porous in the singular treatments (Baumann et al. 2021), favouring the creation of microenvironments. The prevalence of potentially aerobic *Croceitalea* (Su et al. 2017) among the taxa attached to these particles suggests an heterogeneity of microenvironments created during particle degradation. *Cognatishimia* represented a notable fraction of the communities, especially in the recurring treatments. While this may be partially explained by their high abundances in the deep water inocula, closely related prokaryotes have been described as aerobic heterotrophs capable of particle attachment and biofilm formation, and have been observed associated to diatoms (Behringer et al. 2018; Pujalte et al. 2018; Arahal et al. 2019). The final days were marked by a major increase in two Saprospiraceae genera (*Lewinella* and *Phaeodactylibacter*) in the extreme recurring treatment, especially in the 3.0 μm size fraction. By timing and morphology (Khan et al. 2007; Chen et al. 2014), they matched the highly active filamentous prokaryotes observed by fluorescence microscopy (Fig. 8d), suggesting that their high abundances in the 3.0 μm size fraction were likely due to their filamentous nature, rather than a particle-attached life style. Both Saprospiraceae genera have been found associated with phytoplankton (Lee et al. 2018; Pontiller et al. 2022), and here their rise coincided with a coccolithophorid bloom (Ortiz et al. 2022) and a marked increase in prokaryotic heterotrophic production (Fig. 1e). Saprospiraceae have been observed to display high peptidase transcription during the senescence phase of diatom blooms (Pontiller et al. 2022), and expression of transcripts related to degradation of aromatic molecules has also been reported for *Phaeodactylibacter* (Lee et al. 2018). This might offer them an advantage over other taxa although the specific reasons behind their proliferation coupled to the coccolithophorid bloom are unknown.

Prokaryotic communities thus showed taxonomic changes that suggest functional successions related to the transformation of the organic matter pool during the different phases of the phytoplankton blooms (Pontiller et al. 2022). This was further implied by the clear correlations between community composition and the DOM quantities and characteristics (and to a lesser extent, POM concentrations) (Fig. 7). Free-living communities shifted from oligotrophic specialists to various copiotrophic prokaryotes that thrive consuming the DOM produced during phytoplankton blooms (both during the bloom growth and decay). Subsequently, bloom specialists were accompanied by prokaryotes with likely more varied metabolisms, including the ability to degrade aromatic compounds, the presence of which was suggested by the optical characteristics of DOM (see Chapter 1 for more details). Ultimately, some

oligotrophic taxa regained presence too. The prokaryotic successional patterns were consistent in both upwelling modes despite the remarkably different bloom developments, which showed dissimilarities in biomass, primary production and Chl *a* (Ortiz et al. 2022). Thus, it seems that, beyond phytoplankton composition (Teeling et al. 2016), bloom characteristics had little effect on successional dynamics. Instead, succession seemed more coupled with preceding organic matter accumulation (which tended to be similar in both modes), or the interplay of substrate availability and trophic interactions (Gralka et al. 2020), viral lysis (Chen et al. 2019; Szabo et al. 2022) or predation (Allers et al. 2007), rather than with the concurrent bloom state. In particle-attached bacteria, composition shifts suggesting changing conditions in the colonised particles were parallel to those observed in the free-living community, hinting that the temporal dynamics of both size fractions were coupled. Overall, similarities in successional patterns and in their composition suggest low functional redundancy among taxa, as otherwise reoccurrence would be considerably reduced due to functionally similar taxa indistinctly replacing each other (Fuhrman et al. 2006). A degree of functional redundancy (particularly among closely related taxa) probably existed, however, and could account for the observed taxonomic variability among treatments together with differences in environmental conditions between blooms and contingencies during microbial interactions (for instance, equal initial conditions can yield starkly different viral infection dynamics in phytoplankton blooms; Vincent et al. 2021).

The observed percentage of active cells during the postbloom peak (~45% in the extreme singular treatment) was lower than expected given the amount of resources available for the prokaryotes. The low substrate concentration used for the BONCAT incubations in the context of very high cell densities (close to $2 \cdot 10^{-6}$ cells $\cdot$ mL^{-1} in the extreme singular treatment) and amino acid uptake competition by highly active diatoms (Fig. S15) (Mulholland and Lomas 2008; Rogato et al. 2015) probably decreased the substrate uptake by prokaryotes and, hence, reduced the sensitivity level of the method. Thus, rather than a precise estimate of the fraction of active cells, our BONCAT results should be considered as an indicator of single-cell activity changes within the prokaryotic communities. Still, the marked activity differences between prokaryotes across and, most importantly, within specific communities (Fig. 8) evidence contrasting contributions to organic matter cycling by distinct prokaryotic groups. The observed activity changes probably involved energy obtention through respiration too as cell-specific respiration rates have been shown to vary three orders of magnitude between taxa within the same community, with relatively minor taxa (e.g., Rhodobacterales) disproportionately contributing to the

community level respiration (Munson-McGee et al. 2022). Among those, Flavobacteriales have been identified to increase their contribution to respiration during and after phytoplankton blooms, highlighting their relevance in carbon cycling under upwelling.

Our results provide insight into successional patterns in prokaryotic communities during blooms of different intensity and duration, suggesting that successions occur in a predictable manner. This could help understand community dynamics under different environmental scenarios, which is a critical step in the context of global change.

Conclusions

The simulation of upwelling through the addition of nutrient-rich mesopelagic waters to oligotrophic surface waters yielded different phytoplankton blooms depending on the experimental treatment: a single pulse of upwelled waters resulted in relatively short-lived, but large blooms, while recurring upwelling yielded sustained blooming episodes. Despite the contrasting bloom outcomes, the observed prokaryotic successional patterns were notably similar. All treatments displayed three cycles of prokaryotic proliferation and demise, with abundance levels positively related to upwelling intensity. Contrary to what is typically observed during phytoplankton blooms, prokaryotic abundance peaks were brief, implying that trophic controls (grazing, viral infection) played a major role in modulating prokaryotic abundance. Taxonomic successional patterns were very similar across treatments: the initial oligotrophic community was mostly replaced by mesopelagic prokaryotes following the first deep water addition, and these quickly gave way to bloom specialists, which peaked during the termination (or decrease in the recurring treatments) of the initial phytoplankton bloom. A fourth, intermediate assemblage of prokaryotes (with members potentially able to degrade aromatic compounds) prevailed after the postbloom period, and yet another shift in composition lead to a final group of prokaryotes that dominated at the end of the experiment. These changes, along their relationship to DOM and POM, imply consistent functional successions across communities during organic matter transformation (both in the free-living and particle-attached size fractions). The fact that many taxa were shared between the different treatments suggests that there was low functional redundancy among prokaryotes during organic matter transformation. Albeit successional patterns across upwelling scenarios were similar, variability in cell-specific activity between and within communities indicate contrasting contributions by different taxa

to carbon cycling. In conjunction, our results are relevant to understand prokaryotic community successions and organic matter cycling during phytoplankton blooms under varying upwelling conditions.

Supplementary material

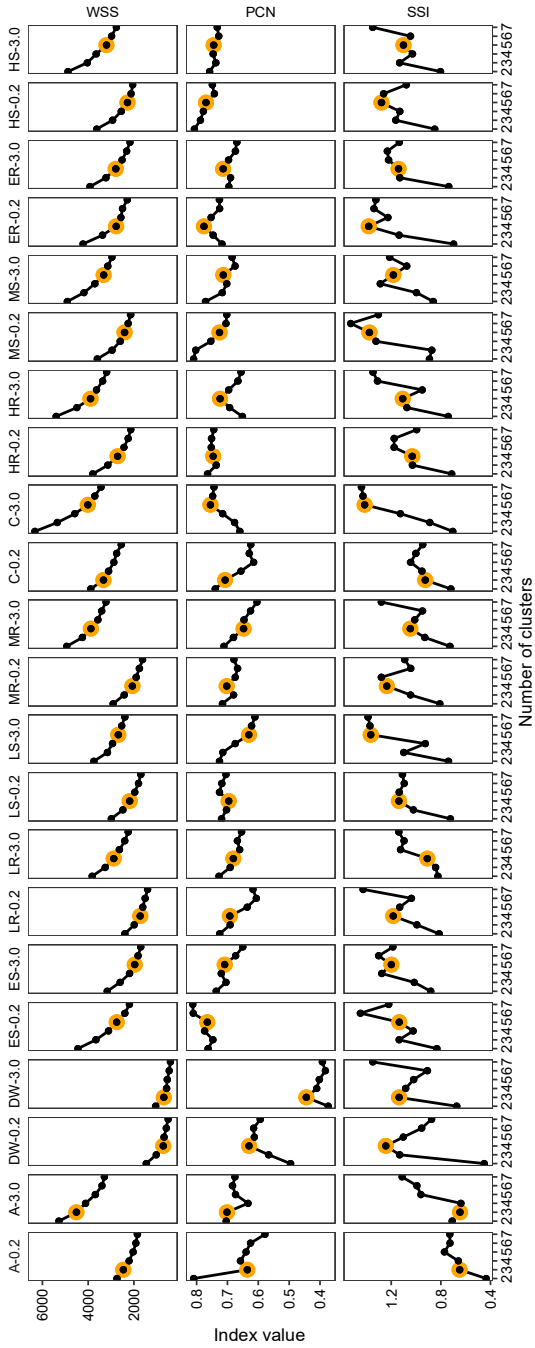

Figure S1. Results of the cluster selection indices, per treatment and size fraction. Within Cluster Sum of Squared Error (WSS), Normalized Partition Coefficient (PCN) and Simple Structure Index (SSI). The chosen cluster number is indicated with an orange circle. Treatments are denoted by the first letter of each word, along with the corresponding size fraction number.

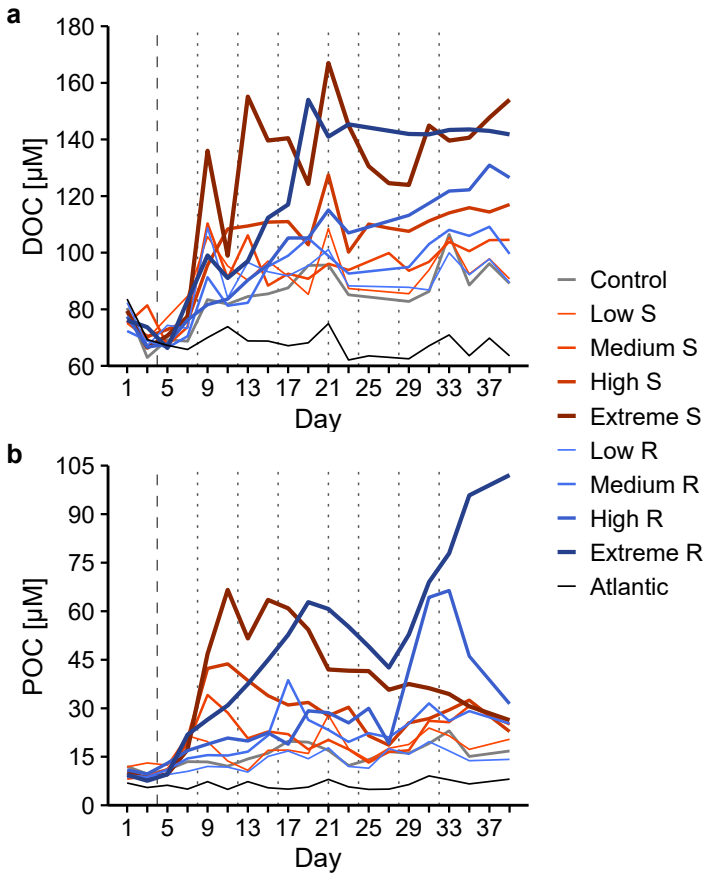

Figure S2. Evolution of a) dissolved organic carbon (DOC) and b) particulate organic carbon (POC) during the experiment. Data from **Chapter 1** and Baumann et al. (2021), respectively (see *Materials and methods* section in the main text).

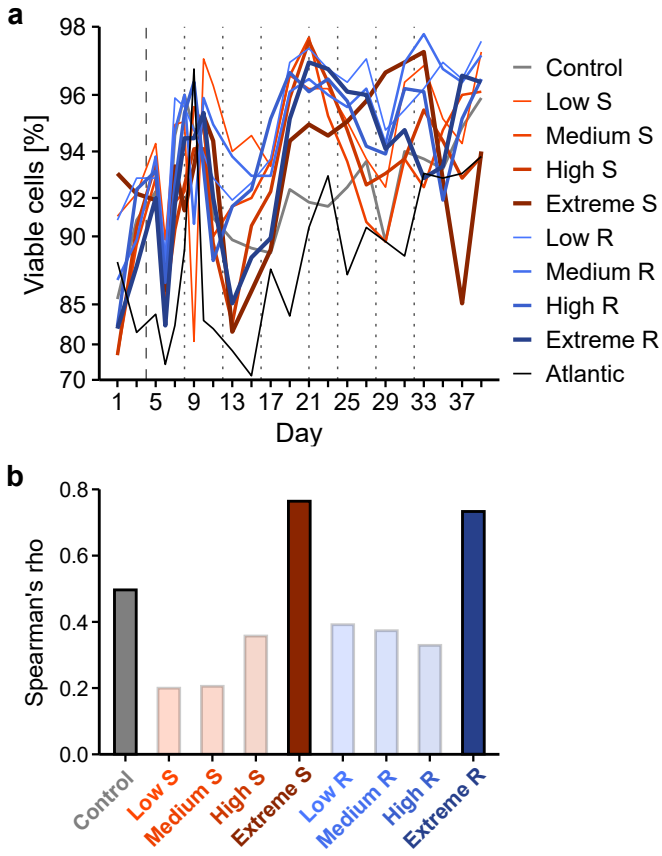

Figure S3. Viability of prokaryotic cells. a) evolution of the percentage of viable cells (i.e., with intact cell membrane) within the prokaryotic community during the experiment. b) correlation (Spearman's rho) between cell viability and (log_{10}-transformed) prokaryotic abundance. Bar transparency represents correlation significance (solid = p-value < 0.05; transparent otherwise).

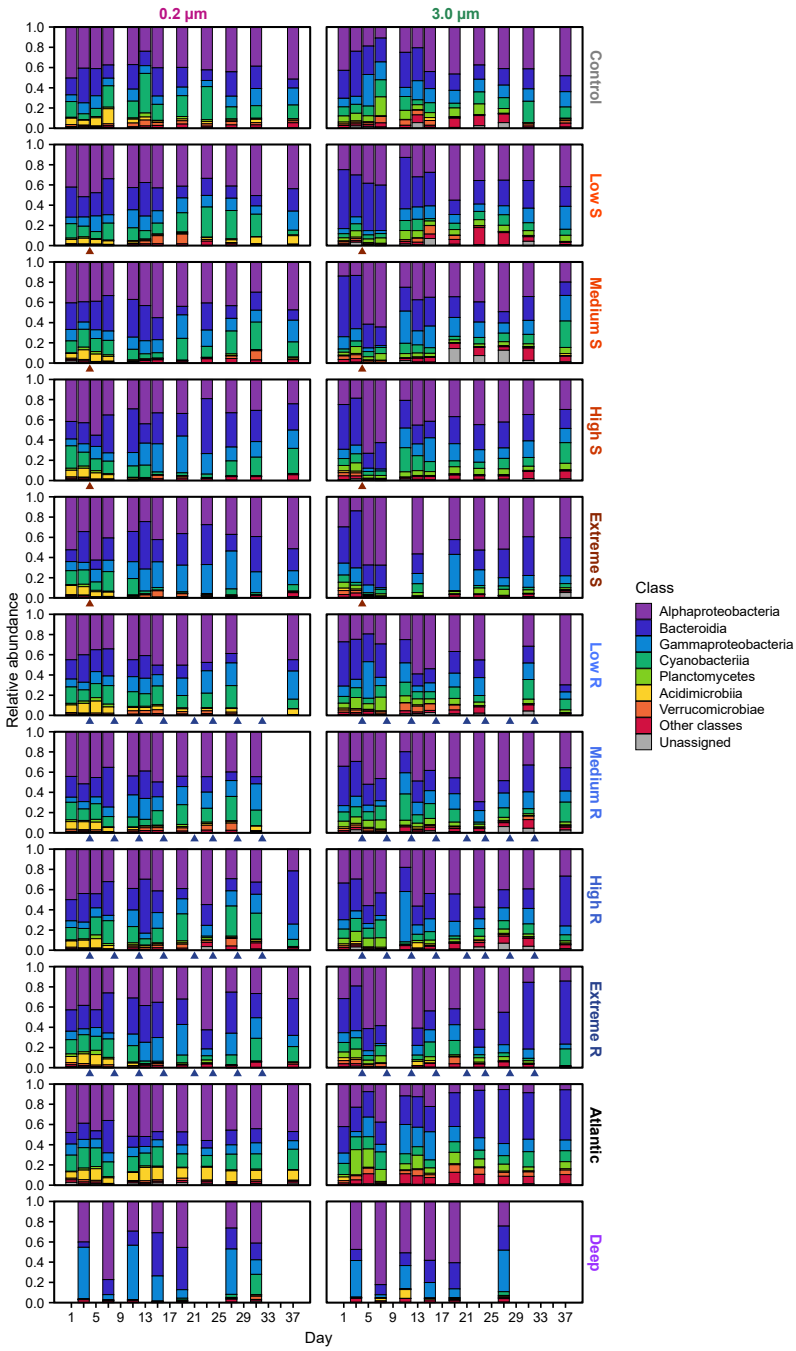

Figure S4. Temporal evolution of the relative abundance of prokaryotes by taxonomic class, per mesocosm and size fraction. Triangles represent deep water additions.

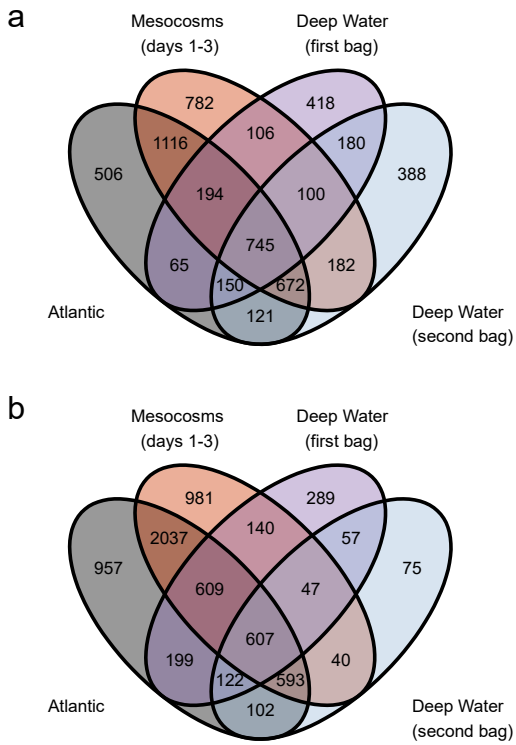

Figure S5. Share of ASVs between surface and deep waters. For mesocosms only samples prior to deep water additions are considered.

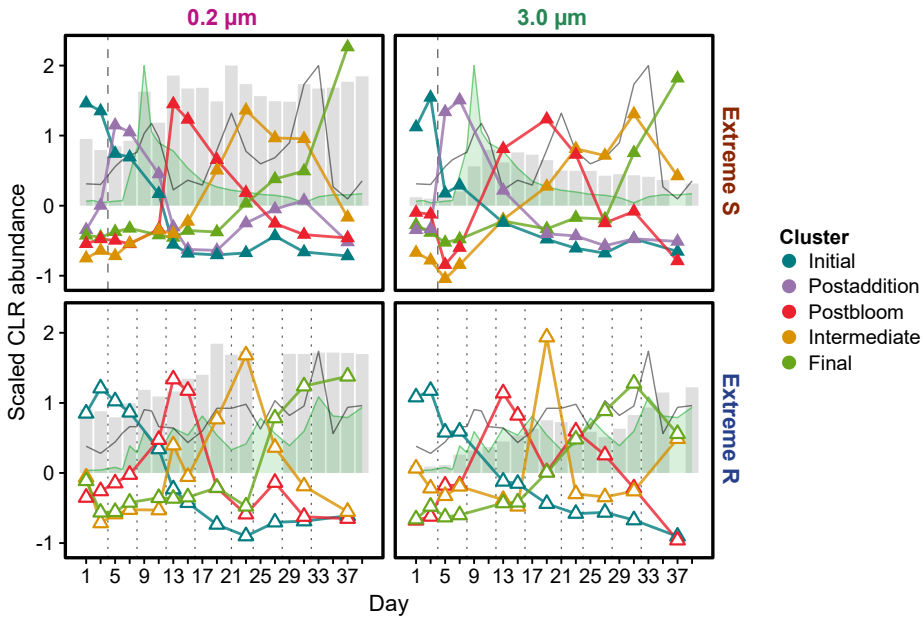

Figure S6. Succession patterns within the prokaryotic communities. Evolution of ASV cluster centroids in extreme treatments is shown in the foreground, colour coded. In the background DOC (grey columns, 0.2 µm panels), POC (grey columns, 3.0 µm panels), total Chl *a* (green area, all panels), and prokaryotic abundance data (grey line, all panels) are shown in arbitrary units, as context. Scales for DOC and POC concentrations are equivalent. Deep water additions are shown as dashed (singular) and dotted lines (recurring). Cluster centroid patterns for all treatments are available in Fig. S7.

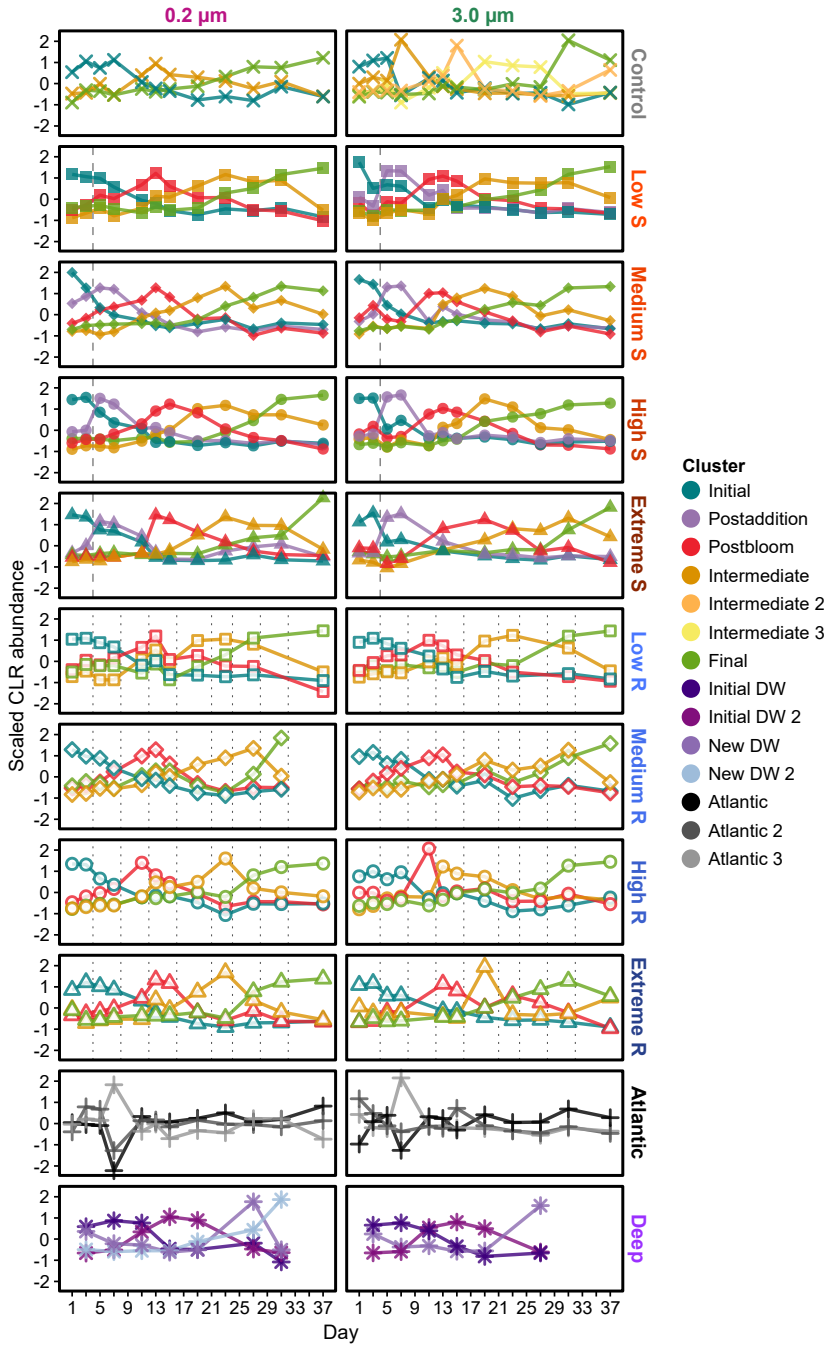

Figure S7. Temporal patterns of the cluster centroids obtained by fuzzy clustering of ASVs representing >0.1% in at least one sample (within each treatment). ASVs were assigned to the cluster in which they displayed the highest membership.

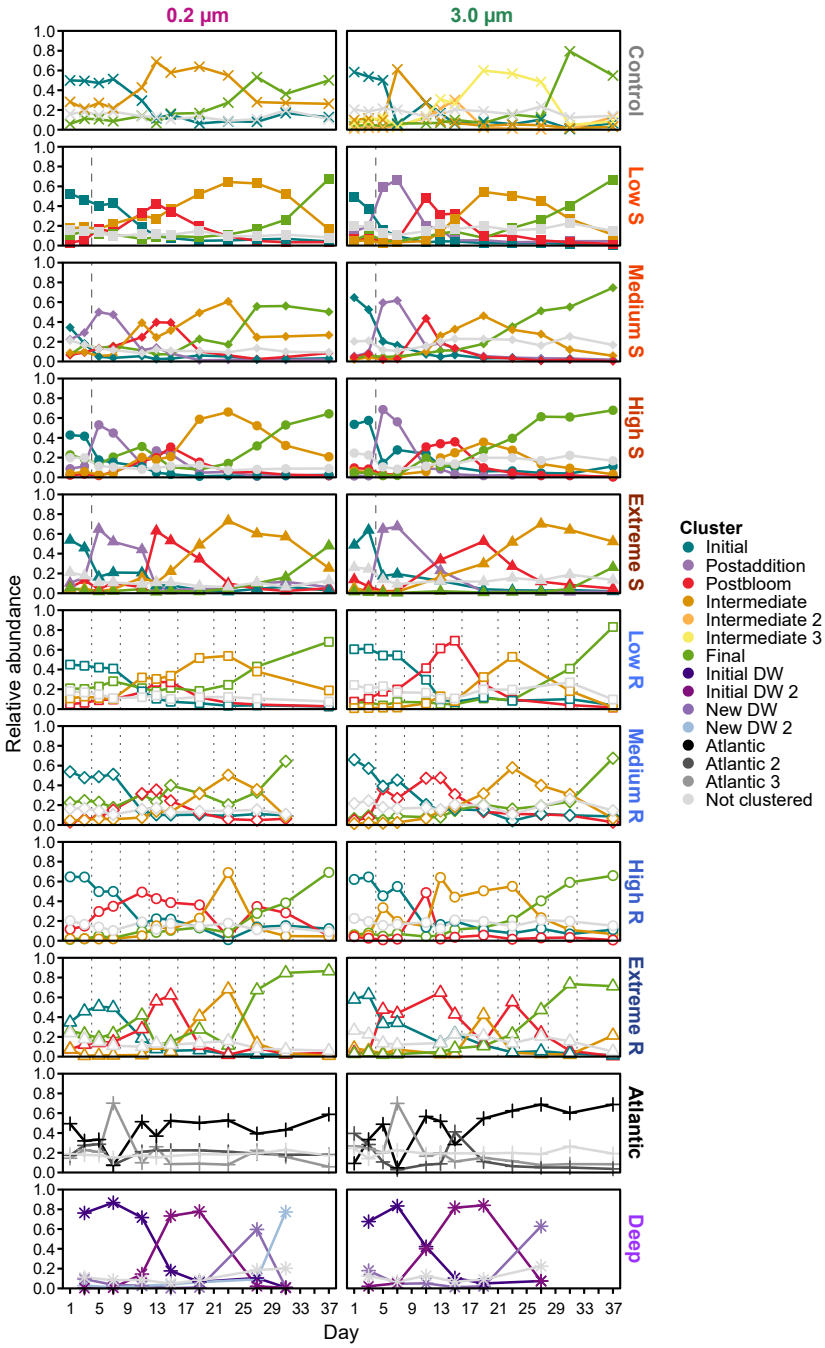

Figure S8. Relative abundance of ASVs contributing to each cluster. ASVs that were not included in the clustering (i.e., not exceeding >0.1% in any sample) are represented as 'Not clustered'.

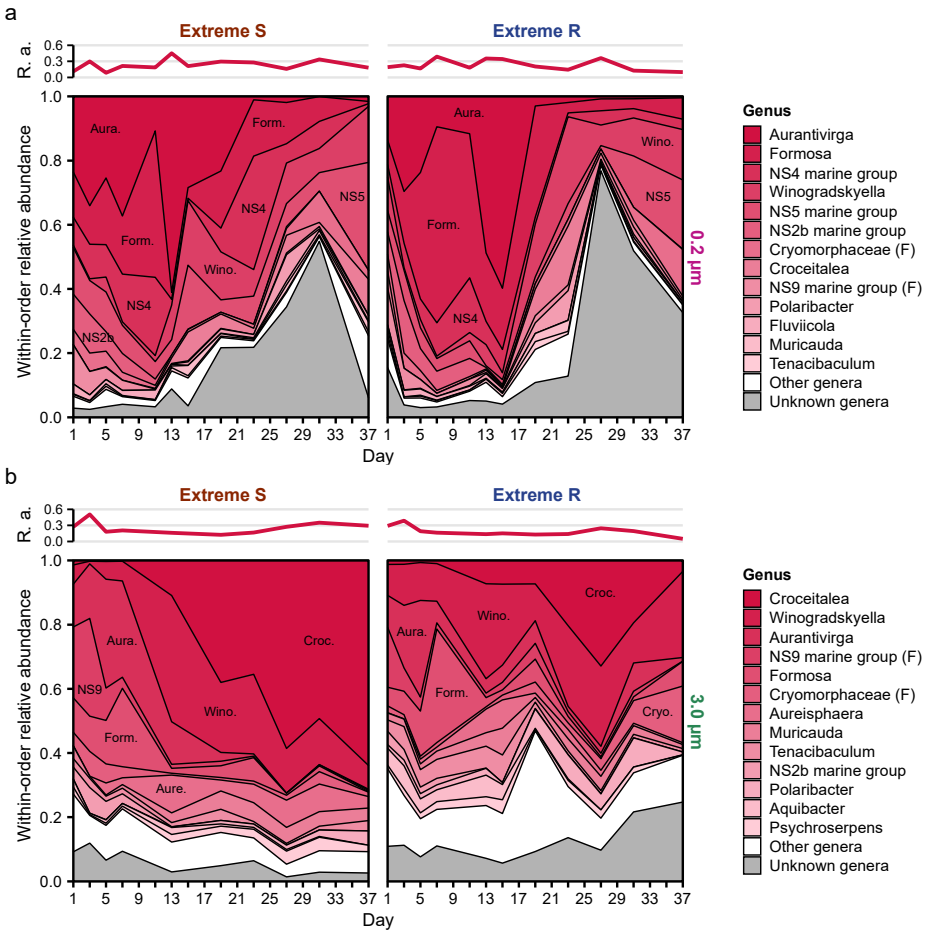

Figure S9. Detailed evolution of Flavobacteriales ASVs. Area plots show the relative abundance of Flavobacteriales genera within that taxonomic order, and line plots on top represent the relative abundance of the Flavobacteriales order as a whole within prokaryotic community. Results are shown separately for the 0.2 µm (a) and 3.0 µm size fractions (b).

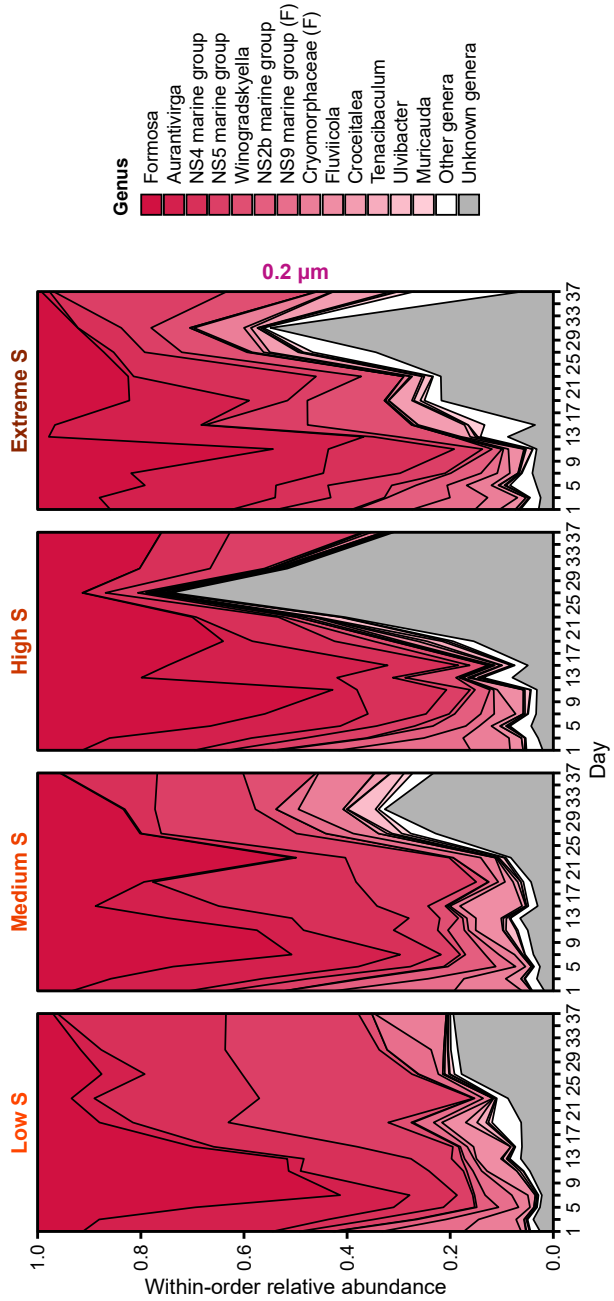

Figure S10. Detailed evolution of Flavobacteriales ASVs. Area plots show the relative abundance of Flavobacteriales genera within that taxonomic order. The contribution of each genus is displayed in descending order as shown in the legend. Results are shown separately for the 0.2 µm and 3.0 µm size fractions. This page: 0.2 µm size fraction of singular treatments.

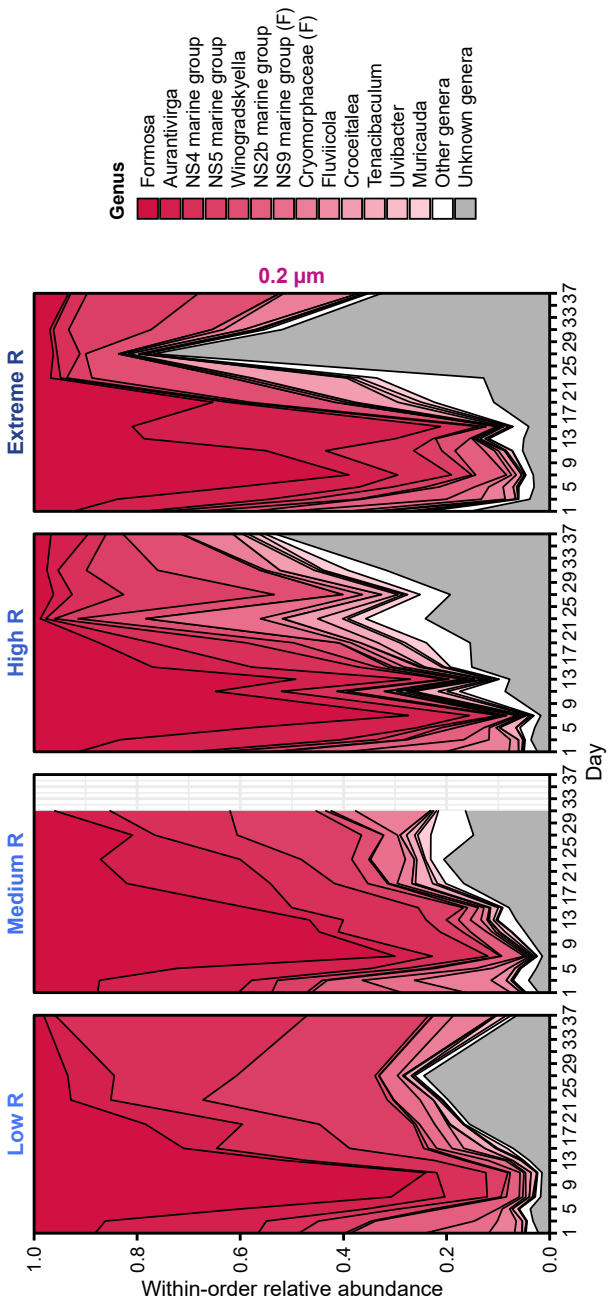

Figure S10. Continued. Detailed evolution of Flavobacteriales ASVs. Area plots show the relative abundance of Flavobacteriales genera within that taxonomic order. The contribution of each genus is displayed in descending order as shown in the legend. Results are shown separately for the 0.2 µm and 3.0 µm size fractions. This page: 0.2 µm size fraction of recurring treatments.

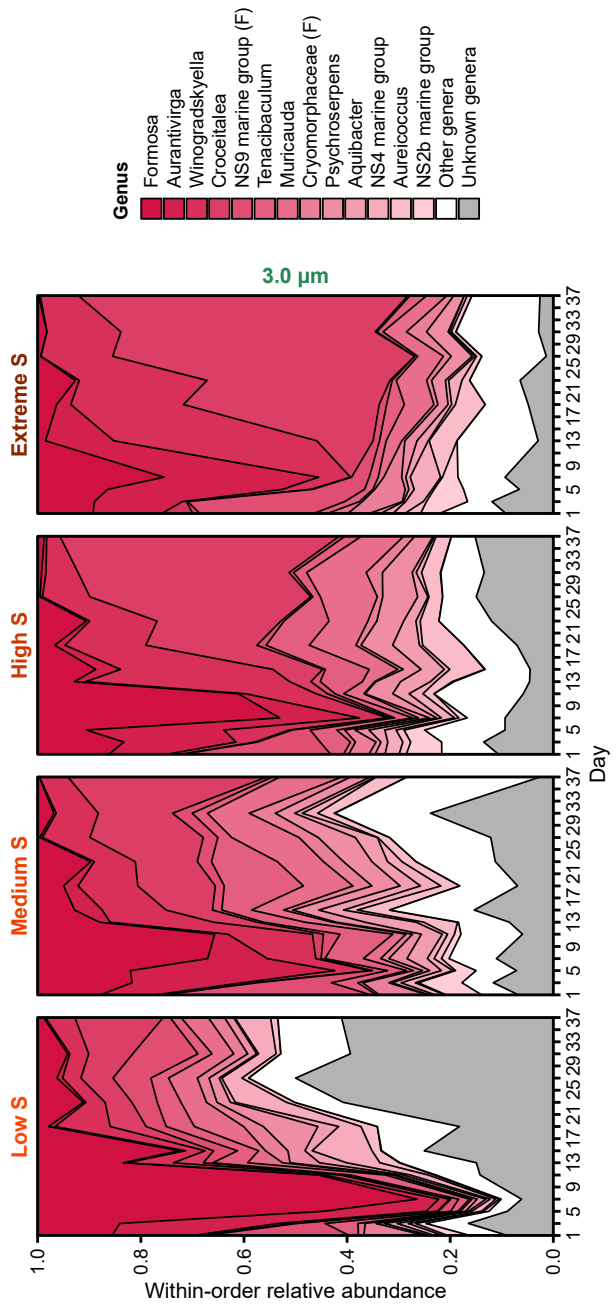

Figure S10. Continued. Detailed evolution of Flavobacteriales ASVs. Area plots show the relative abundance of Flavobacteriales genera within that taxonomic order. The contribution of each genus is displayed in descending order as shown in the legend. Results are shown separately for the 0.2 µm and 3.0 µm size fractions. This page: 3.0 µm size fraction of singular treatments.

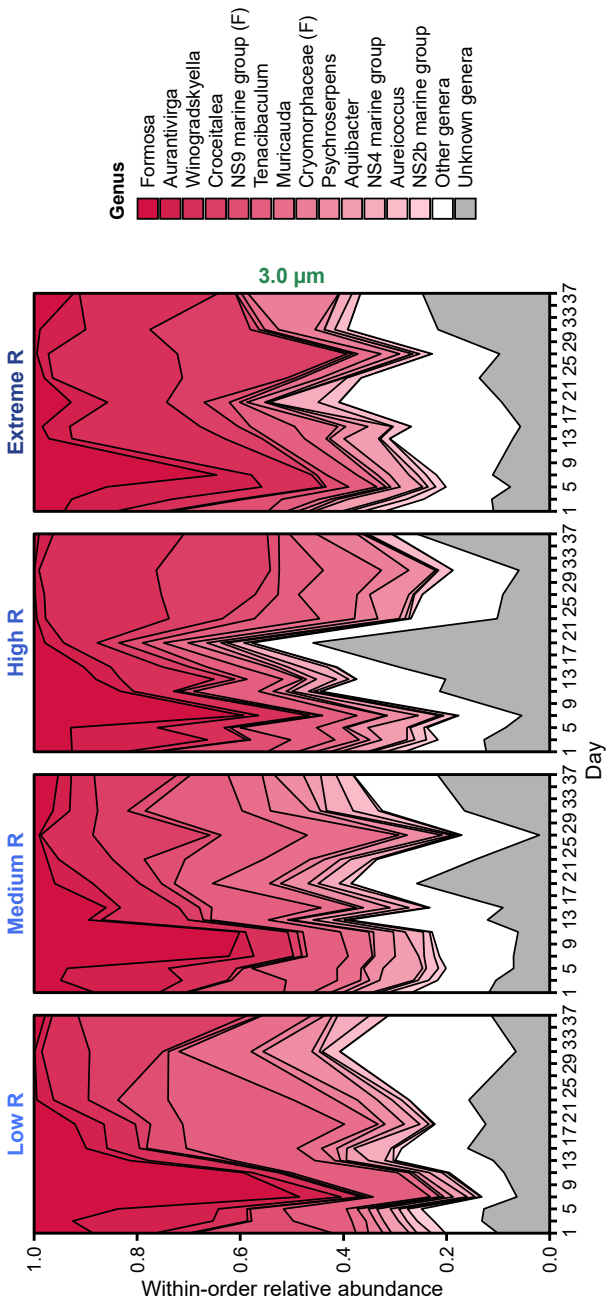

Figure S10. Continued. Detailed evolution of Flavobacteriales ASVs. Area plots show the relative abundance of Flavobacteriales genera within that taxonomic order. The contribution of each genus is displayed in descending order as shown in the legend. Results are shown separately for the 0.2 µm and 3.0 µm size fractions. This page: 3.0 µm size fraction of recurring treatments.

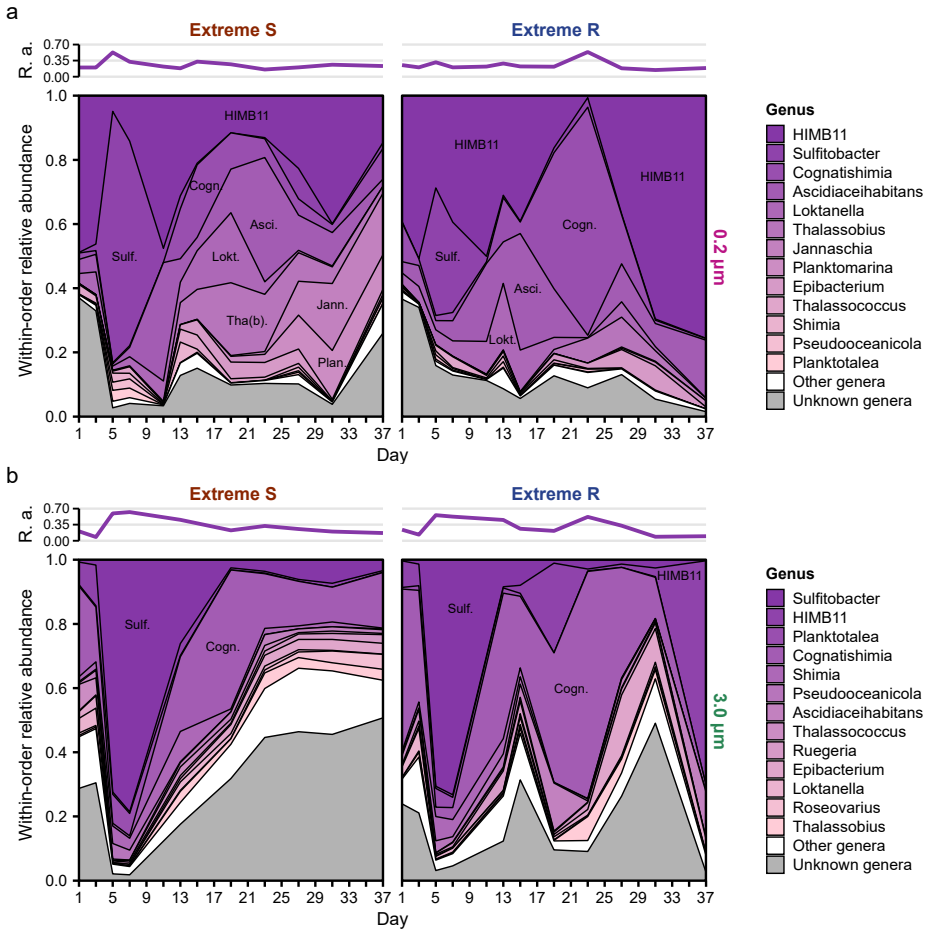

Figure S11. Detailed evolution of Rhodobacterales ASVs. Area plots show the relative abundance of Rhodobacterales genera within that taxonomic order, and line plots on top represent the relative abundance of the Rhodobacterales order as a whole within prokaryotic community. Results are shown separately for the 0.2 µm (a) and 3.0 µm size fractions (b).

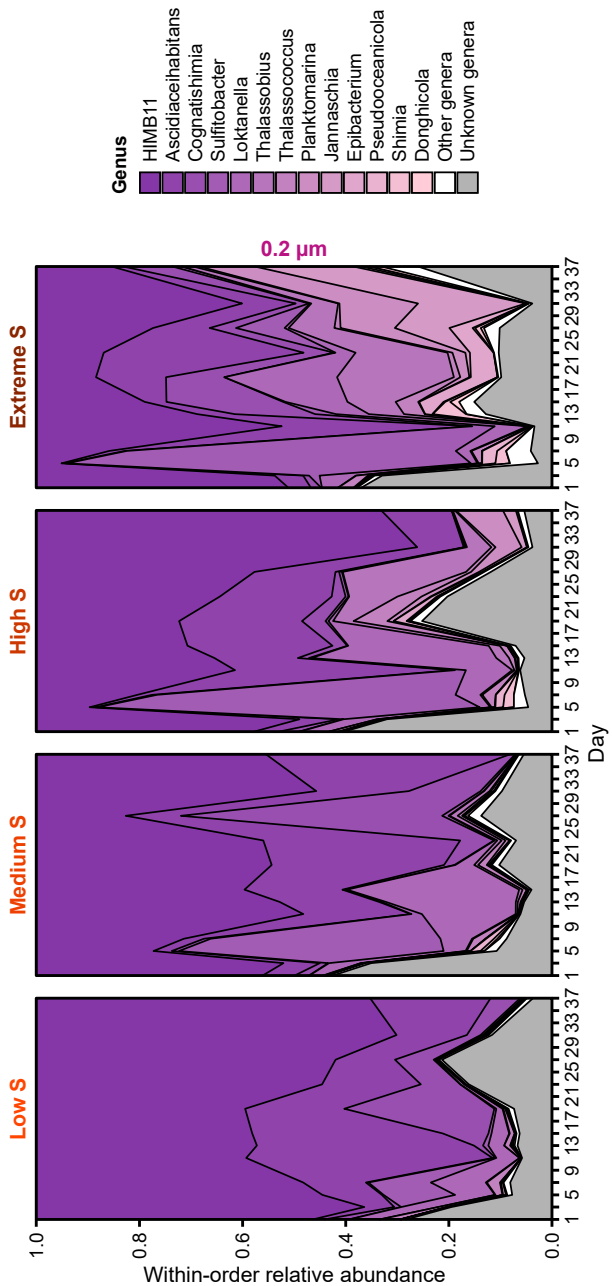

Figure S12. Detailed evolution of Rhodobacterales ASVs. Area plots show the relative abundance of Rhodobacterales genera within that taxonomic order. The contribution of each genus is displayed in descending order as shown in the legend. Results are shown separately for the 0.2 µm and 3.0 µm size fractions. This page: 0.2 µm size fraction of singular treatments.

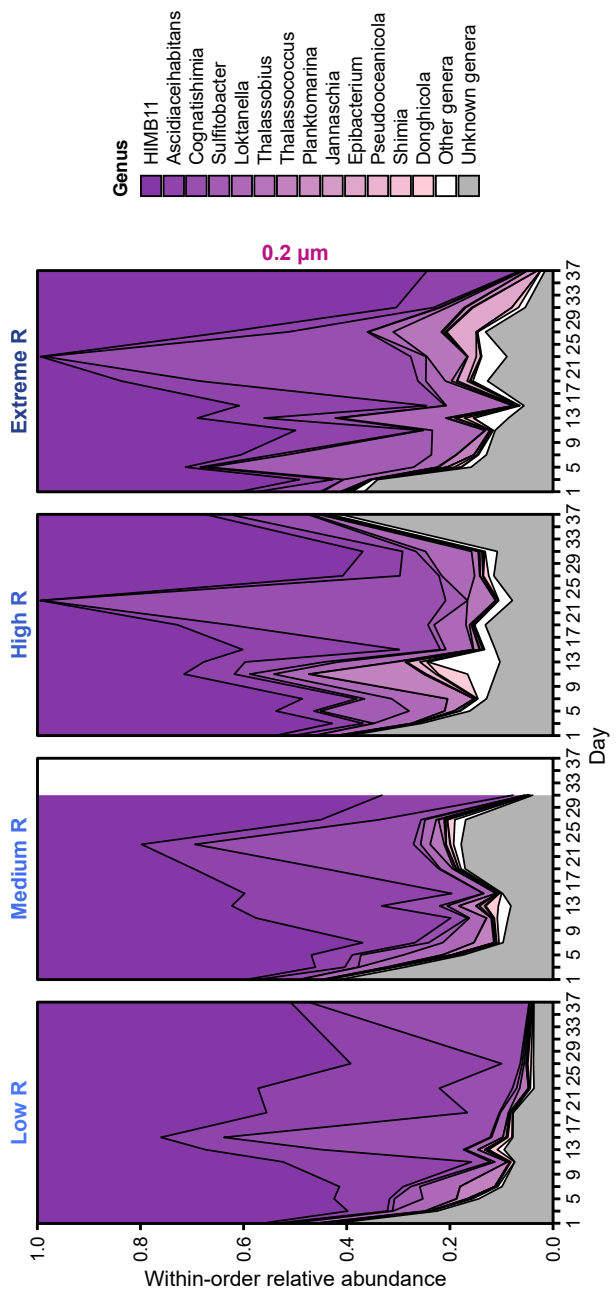

Figure S12. Continued. Detailed evolution of Rhodobacterales ASVs. Area plots show the relative abundance of Rhodobacterales genera within that taxonomic order. The contribution of each genus is displayed in descending order as shown in the legend. Results are shown separately for the 0.2 µm and 3.0 µm size fractions. This page: 0.2 µm size fraction of recurring treatments.

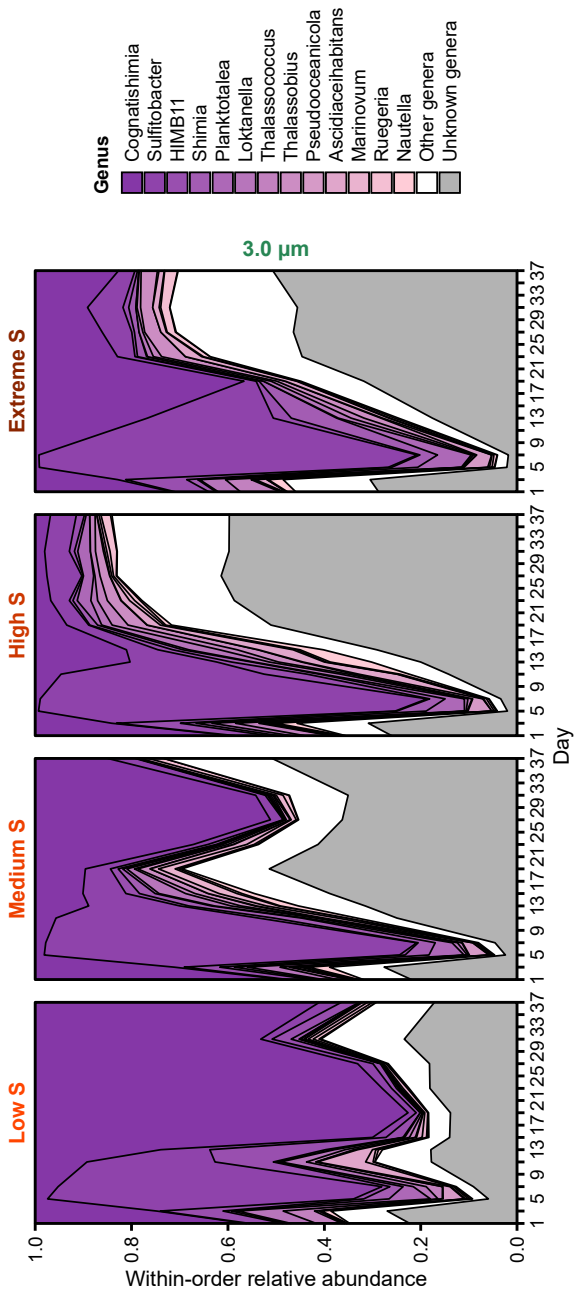

Figure S12. Continued. Detailed evolution of Rhodobacterales ASVs. Area plots show the relative abundance of Rhodobacterales genera within that taxonomic order. The contribution of each genus is displayed in descending order as shown in the legend. Results are shown separately for the 0.2 µm and 3.0 µm size fractions. This page: 3.0 µm size fraction of singular treatments.

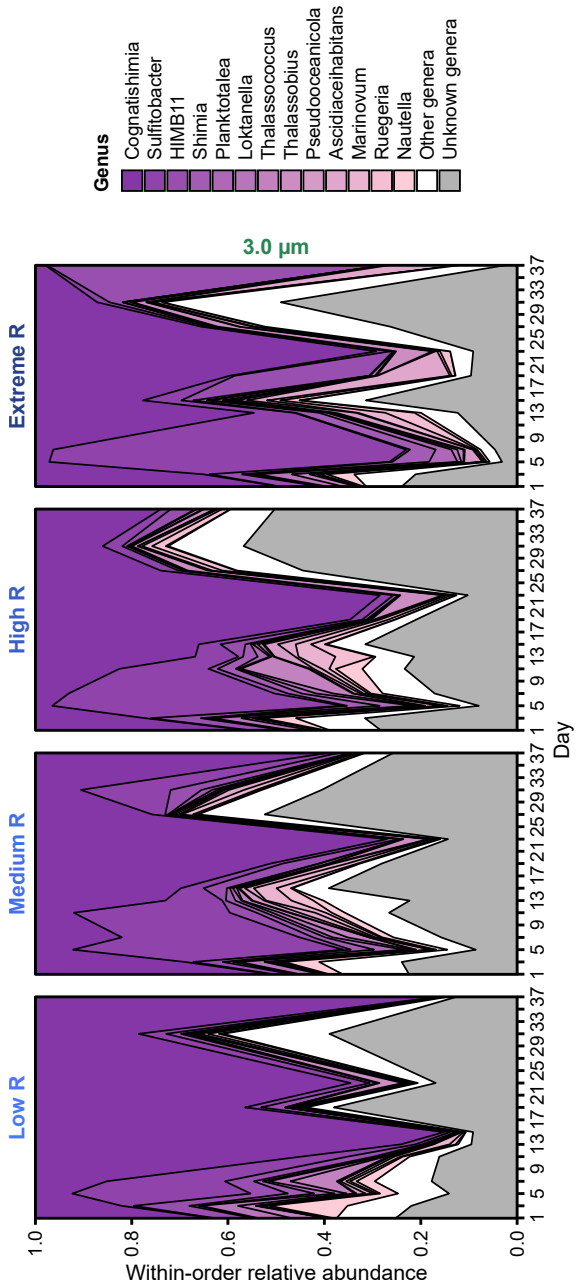

Figure S12. Continued. Detailed evolution of Rhodobacterales ASVs. Area plots show the relative abundance of Rhodobacterales genera within that taxonomic order. The contribution of each genus is displayed in descending order as shown in the legend. Results are shown separately for the 0.2 µm and 3.0 µm size fractions. This page: 3.0 µm size fraction of recurring treatments.

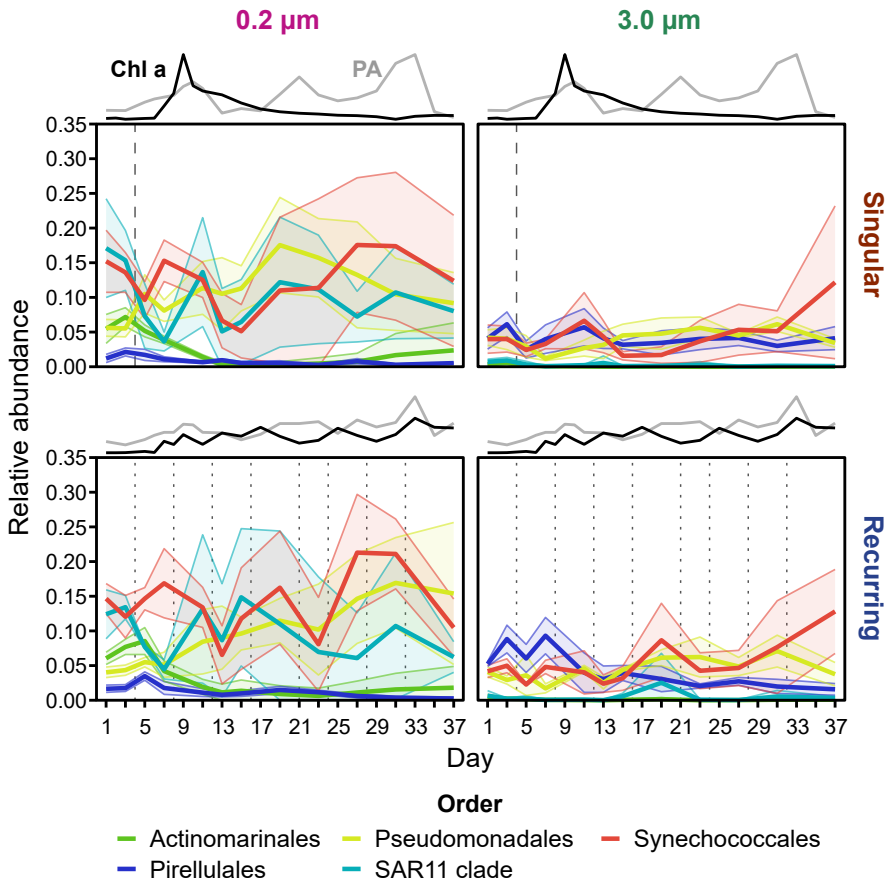

Figure S13. Combined relative abundance of ASVs assigned to major orders associated with oligotrophic/mesotrophic conditions, averaged per upwelling mode (Singular = upper row; Recurring = lower row) and size fraction (0.2 µm = left column; 3.0 µm = right column). The shaded area around lines represents the ± standard deviation of averaged values. Lines on top of plots show scaled Chl *a* (black) and prokaryotic abundance (grey) values (from extreme treatments, in arbitrary units). Deep water additions are shown as dashed (singular) and dotted lines (recurring).

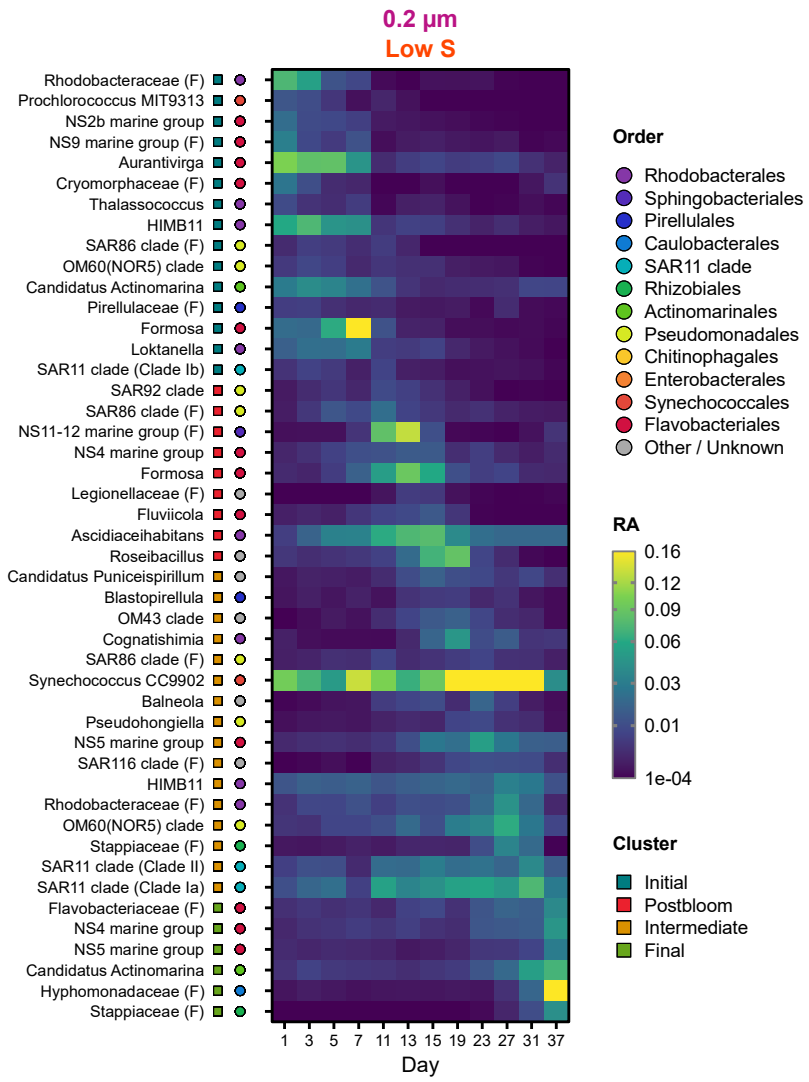

Figure S14. Succession patterns of most relevant prokaryotic taxa. Results are shown per treatment and size fraction as indicated on top of each panel. For each treatment and size fraction, ASVs with a membership value over 0.75 were merged by genera (when possible; otherwise, at the most detailed taxonomic level available, as indicated next to their name: F = family, O = order, C = class). From those, taxa representing at least 0.5% of reads in more than 1 sample within each treatment and size fraction are shown. Colourmap represents relative abundance (RA) of taxa (note that to aid visualisation 1) the scale is square−root−transformed and 2) out of bounds outlier values have been assigned the colours of the upper and lower limits of the colourmap). Coloured dots represent the taxonomic order of taxa, and cluster assignations are displayed next to taxa names. Results for the singular and recurring modes of each intensity level are shown paired in adjacent pages to aid comparison (this page: 0.2 µm size fraction of the low singular treatment).

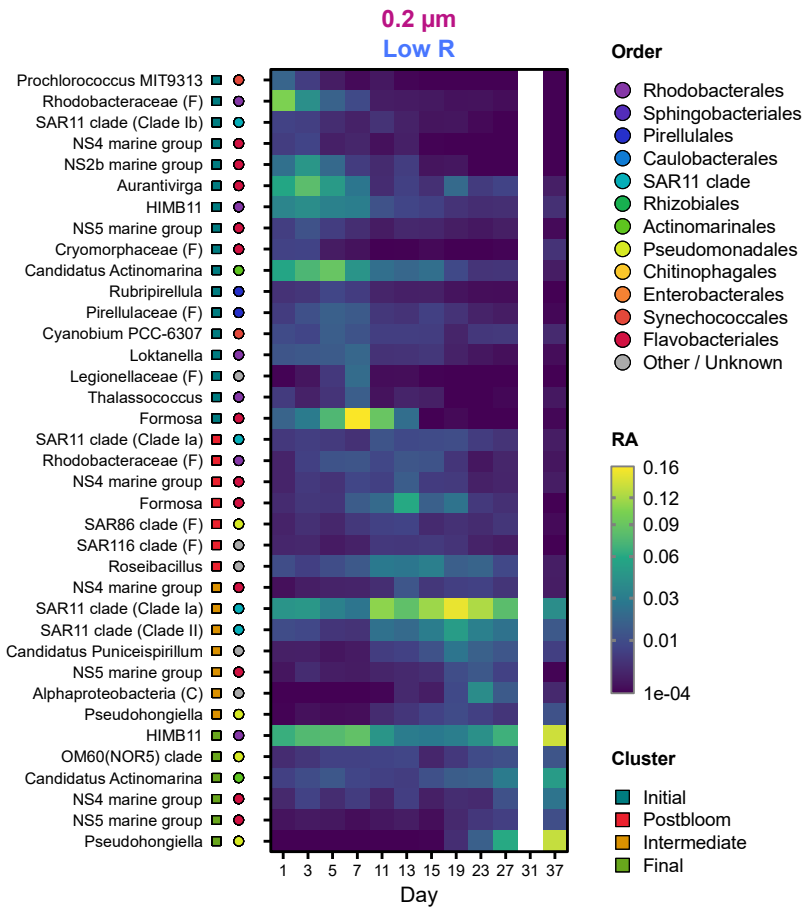

Figure S14. Continued. 0.2 µm size fraction of the low recurring treatment.

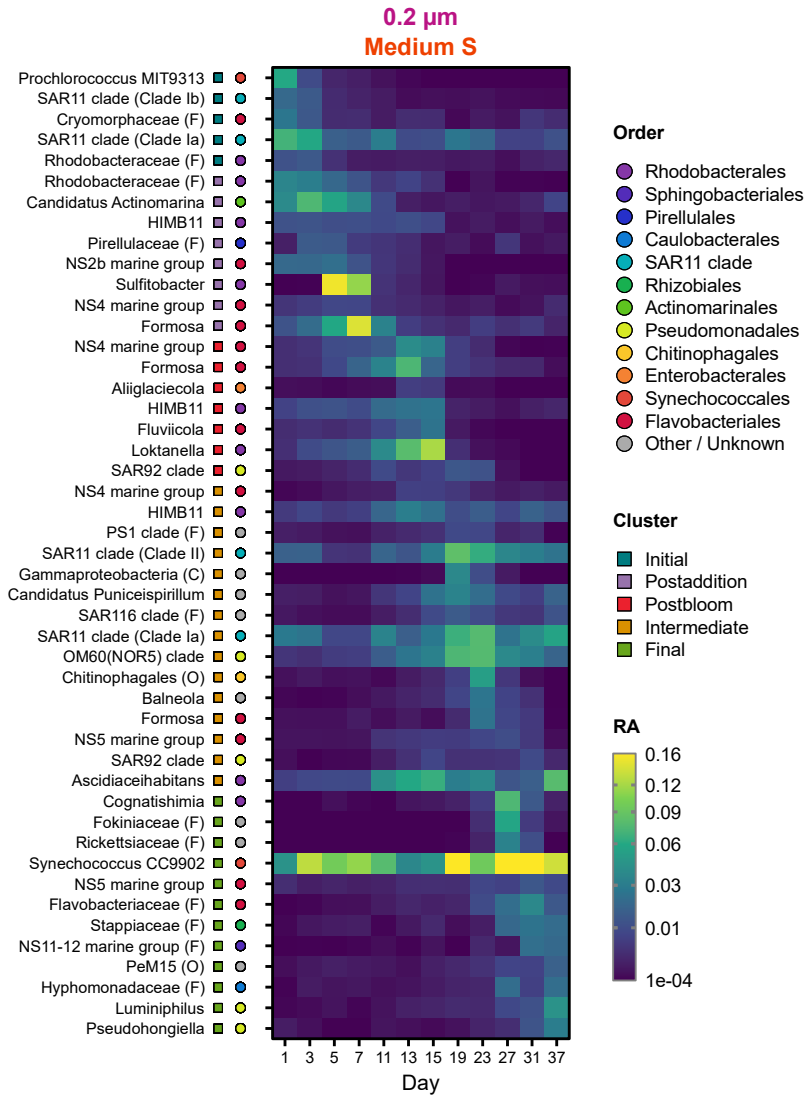

Figure S14. Continued. Succession patterns of most relevant prokaryotic taxa. Results are shown per treatment and size fraction as indicated on top of each panel. For each treatment and size fraction, ASVs with a membership value over 0.75 were merged by genera (when possible; otherwise, at the most detailed taxonomic level available, as indicated next to their name: F = family, O = order, C = class). From those, taxa representing at least 0.5% of reads in more than 1 sample within each treatment and size fraction are shown. Colourmap represents relative abundance (RA) of taxa (note that to aid visualisation 1) the scale is square−root−transformed and 2) out of bounds outlier values have been assigned the colours of the upper and lower limits of the colourmap). Coloured dots represent the taxonomic order of taxa, and cluster assignations are displayed next to taxa names. Results for the singular and recurring modes of each intensity level are shown paired in adjacent pages to aid comparison (this page: 0.2 µm size fraction of the medium singular treatment).

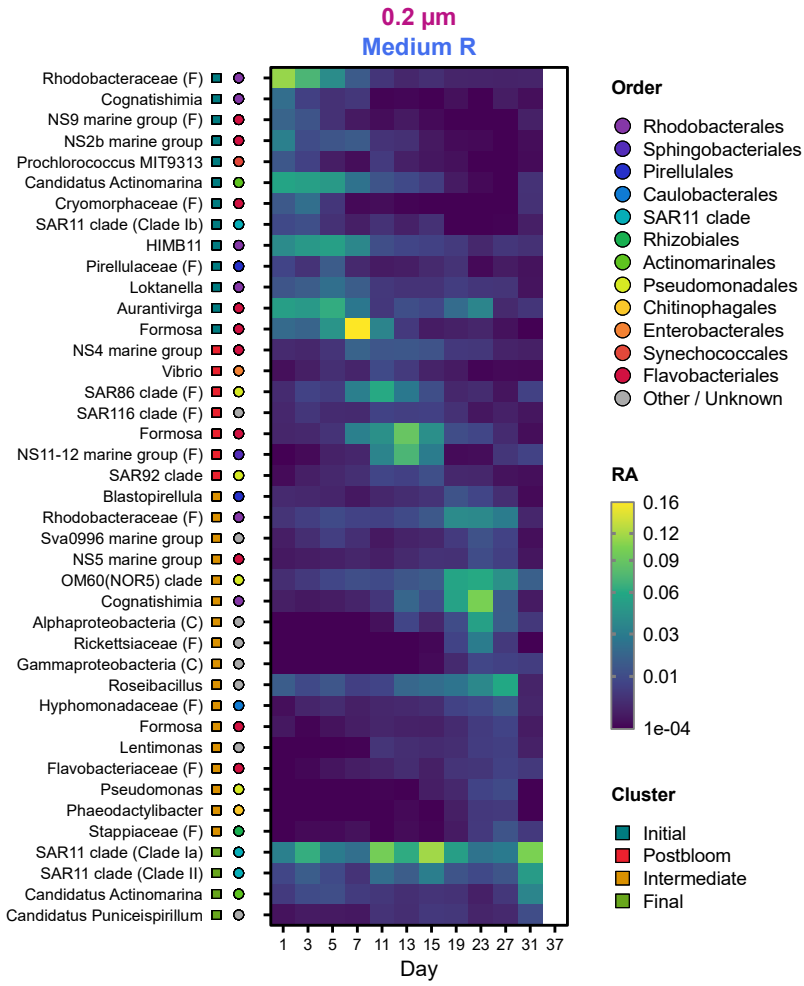

Figure S14. Continued. 0.2 µm size fraction of the medium recurring treatment.

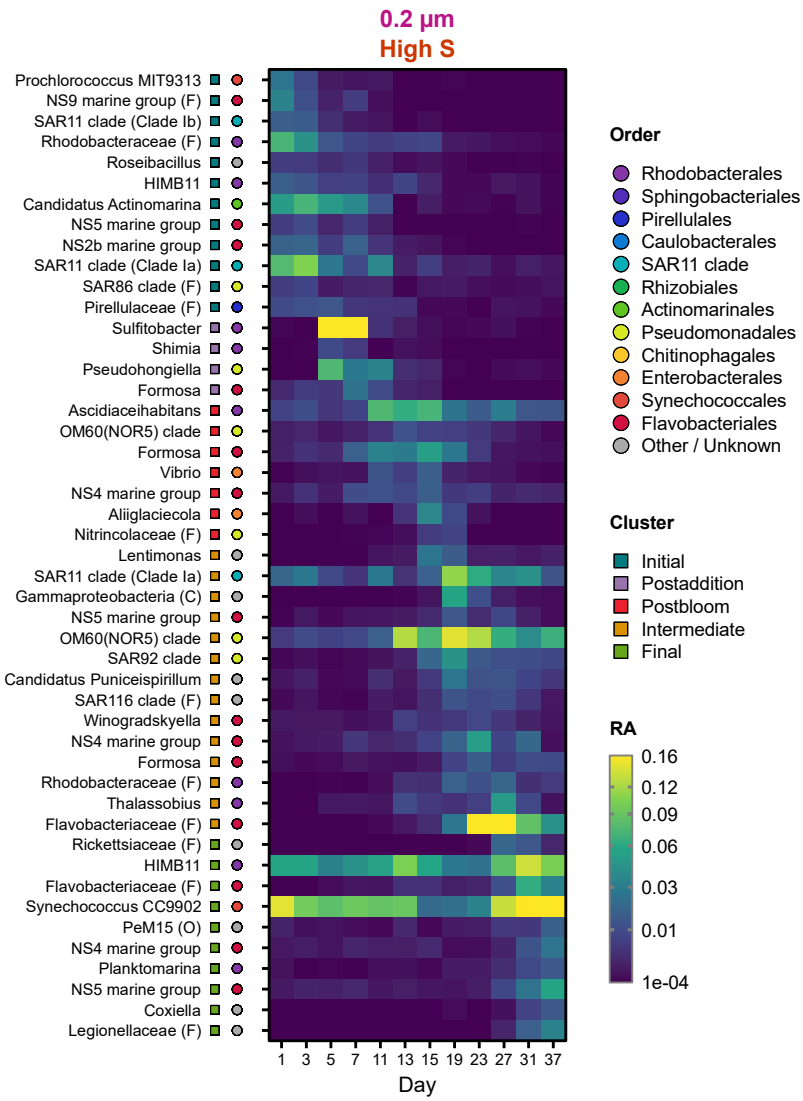

Figure S14. Continued. Succession patterns of most relevant prokaryotic taxa. Results are shown per treatment and size fraction as indicated on top of each panel. For each treatment and size fraction, ASVs with a membership value over 0.75 were merged by genera (when possible; otherwise, at the most detailed taxonomic level available, as indicated next to their name: F = family, O = order, C = class). From those, taxa representing at least 0.5% of reads in more than 1 sample within each treatment and size fraction are shown. Colourmap represents relative abundance (RA) of taxa (note that to aid visualisation 1) the scale is square−root−transformed and 2) out of bounds outlier values have been assigned the colours of the upper and lower limits of the colourmap). Coloured dots represent the taxonomic order of taxa, and cluster assignations are displayed next to taxa names. Results for the singular and recurring modes of each intensity level are shown paired in adjacent pages to aid comparison (this page: 0.2 µm size fraction of the high singular treatment).

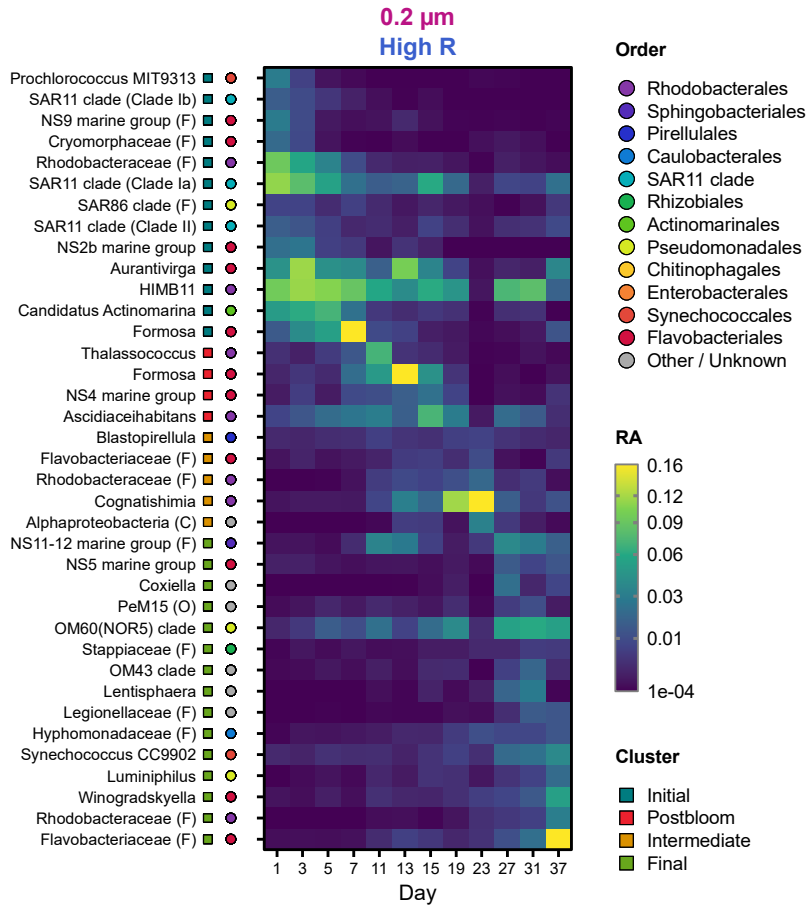

Figure S14. Continued. 0.2 µm size fraction of the high recurring treatment.

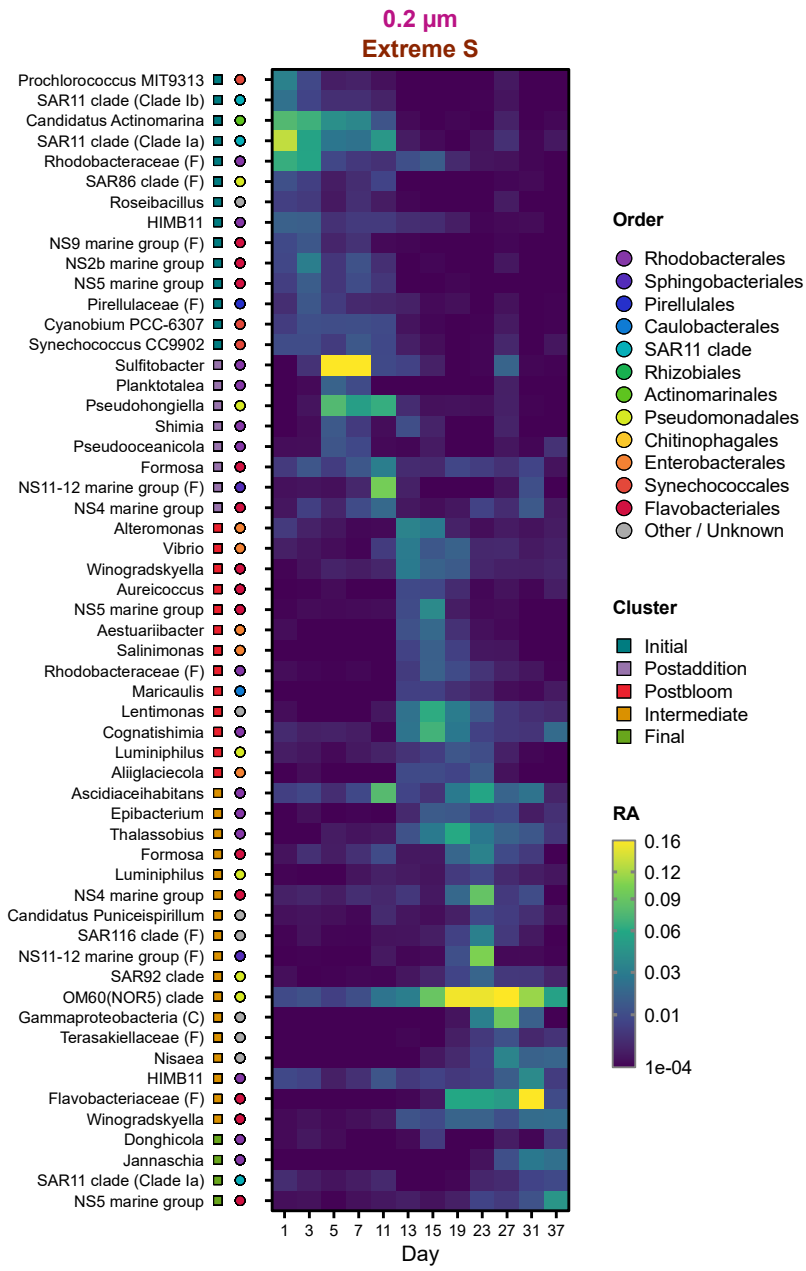

Figure S14. Continued. For each treatment and size fraction, ASVs with a membership value over 0.75 were merged by genera (when possible; otherwise, at F = family, O = order, C = class). From those, taxa representing at least 0.5% of reads in more than 1 sample within each treatment and size fraction are shown. Colourmap represents relative abundance (RA) of taxa. Coloured dots represent the order of taxa, and cluster assignations are displayed next to taxa names. The singular and recurring modes of each intensity level are shown paired in adjacent pages (this page: 0.2 µm size fraction of the extreme singular treatment).

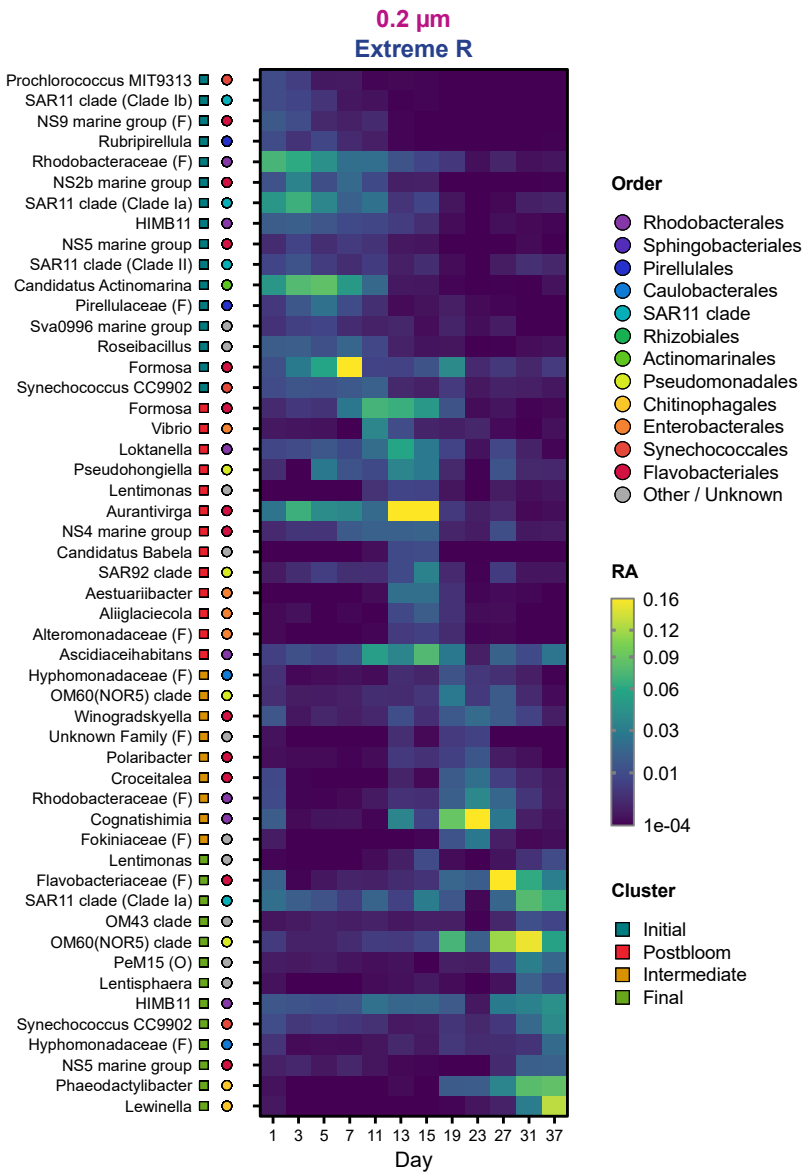

Figure S14. Continued. 0.2 µm size fraction of the extreme recurring treatment.

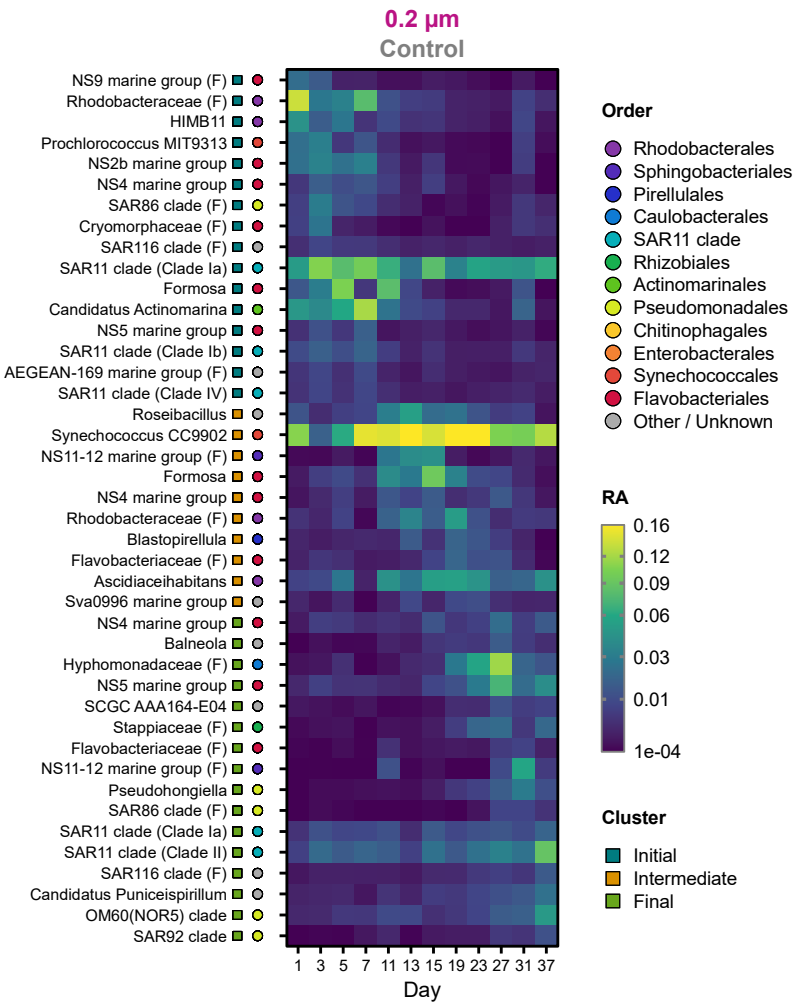

Figure S14. Continued. Succession patterns of most relevant prokaryotic taxa. Results are shown per treatment and size fraction as indicated on top of each panel. For each treatment and size fraction, ASVs with a membership value over 0.75 were merged by genera (when possible; otherwise, at the most detailed taxonomic level available, as indicated next to their name: F = family, O = order, C = class). From those, taxa representing at least 0.5% of reads in more than 1 sample within each treatment and size fraction are shown. Colourmap represents relative abundance (RA) of taxa (note that to aid visualisation 1) the scale is square−root−transformed and 2) out of bounds outlier values have been assigned the colours of the upper and lower limits of the colourmap). Coloured dots represent the taxonomic order of taxa, and cluster assignations are displayed next to taxa names. Results for the singular and recurring modes of each intensity level are shown paired in adjacent pages to aid comparison (this page: 0.2 µm size fraction of the control treatment).

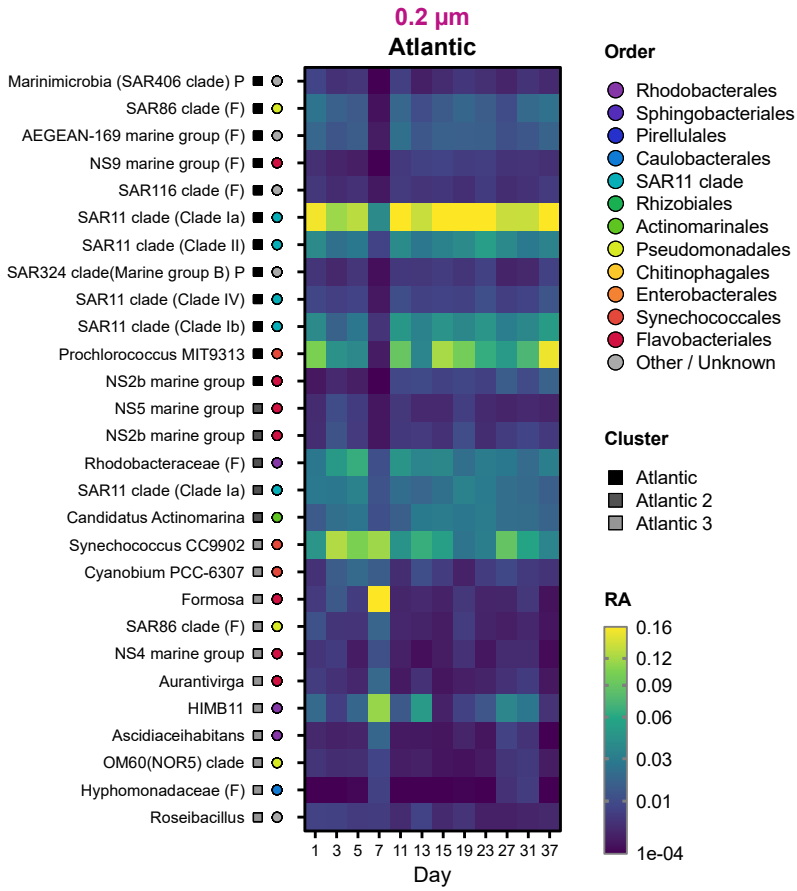

Figure S14. Continued. 0.2 µm size fraction of the Atlantic (ambient waters).

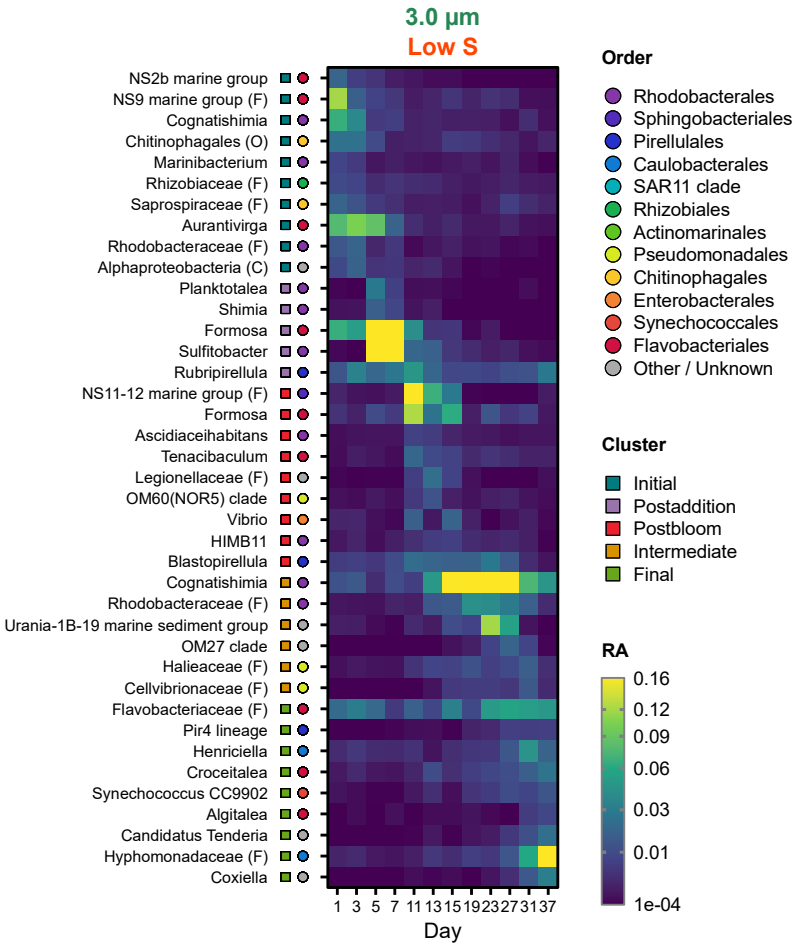

Figure S14. Continued. Succession patterns of most relevant prokaryotic taxa. Results are shown per treatment and size fraction as indicated on top of each panel. For each treatment and size fraction, ASVs with a membership value over 0.75 were merged by genera (when possible; otherwise, at the most detailed taxonomic level available, as indicated next to their name: F = family, O = order, C = class). From those, taxa representing at least 0.5% of reads in more than 1 sample within each treatment and size fraction are shown. Colourmap represents relative abundance (RA) of taxa (note that to aid visualisation 1) the scale is square−root−transformed and 2) out of bounds outlier values have been assigned the colours of the upper and lower limits of the colourmap). Coloured dots represent the taxonomic order of taxa, and cluster assignations are displayed next to taxa names. Results for the singular and recurring modes of each intensity level are shown paired in adjacent pages to aid comparison (this page: 3.0 µm size fraction of the low singular treatment).

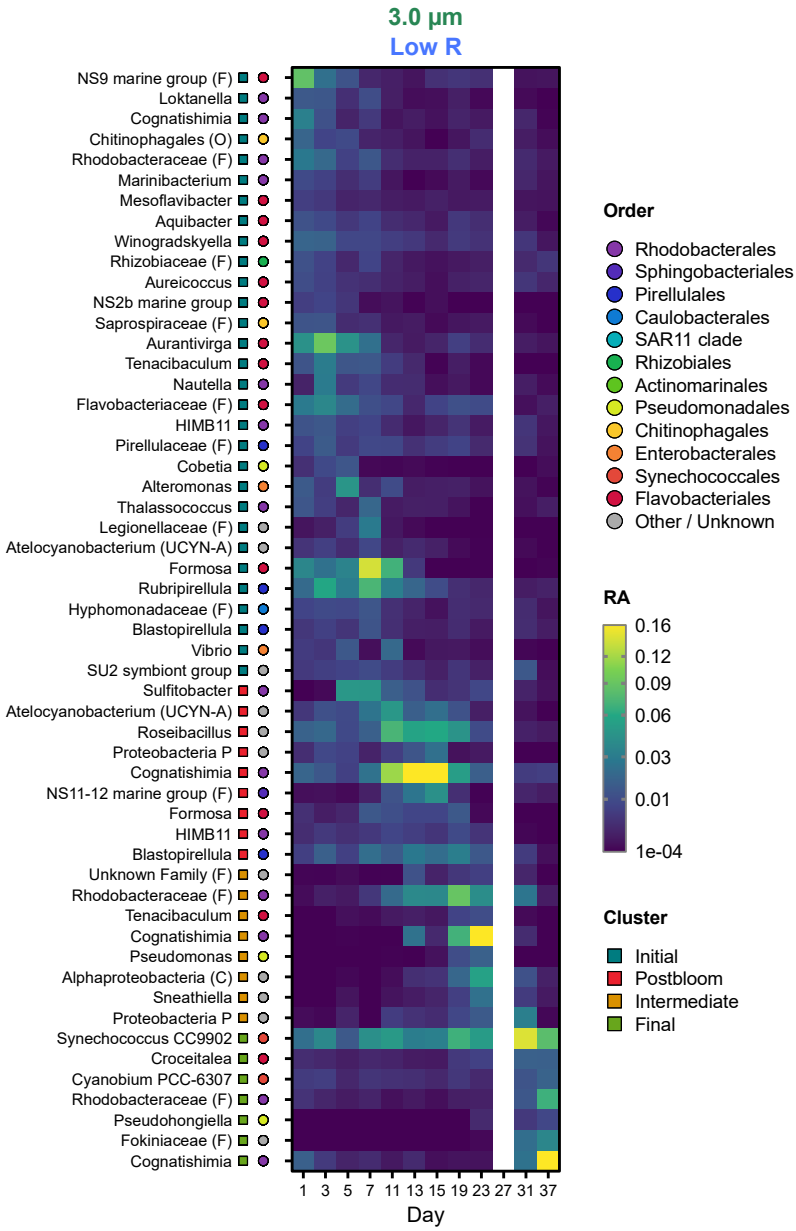

Figure S14. Continued. 3.0 µm size fraction of the low recurring treatment

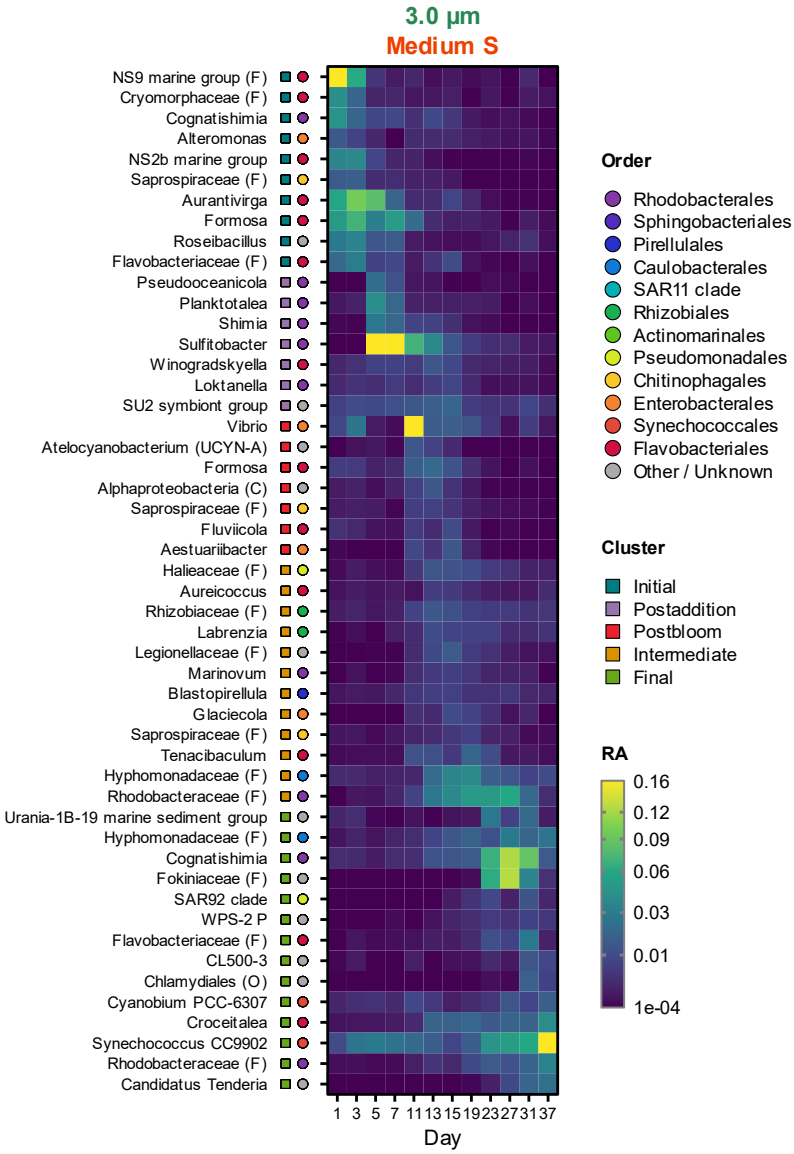

Figure S14. Continued. For each treatment and size fraction, ASVs with a membership value over 0.75 were merged by genera (when possible; otherwise, at F = family, O = order, C = class). From those, taxa representing at least 0.5% of reads in more than 1 sample within each treatment and size fraction are shown. Colourmap represents relative abundance (RA) of taxa (note that to aid visualisation 1) the scale is square−root−transformed and 2) out of bounds outlier values have been assigned the colours of the upper and lower limits of the colourmap). Coloured dots represent the taxonomic order of taxa, and cluster assignations are displayed next to taxa names. Results for the singular and recurring modes of each intensity level are shown paired in adjacent pages to aid comparison (this page: 3.0 µm size fraction of the medium singular treatment).

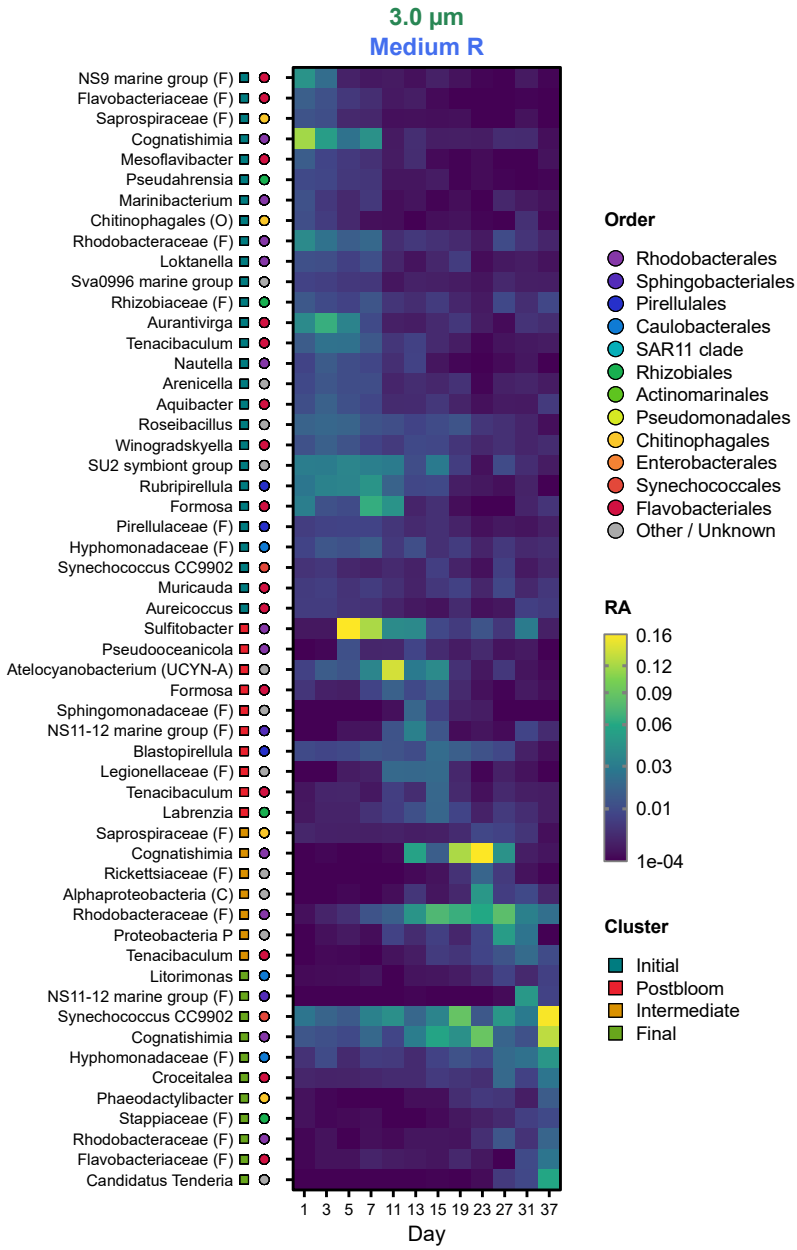

Figure S14. Continued. 3.0 µm size fraction of the medium recurring treatment

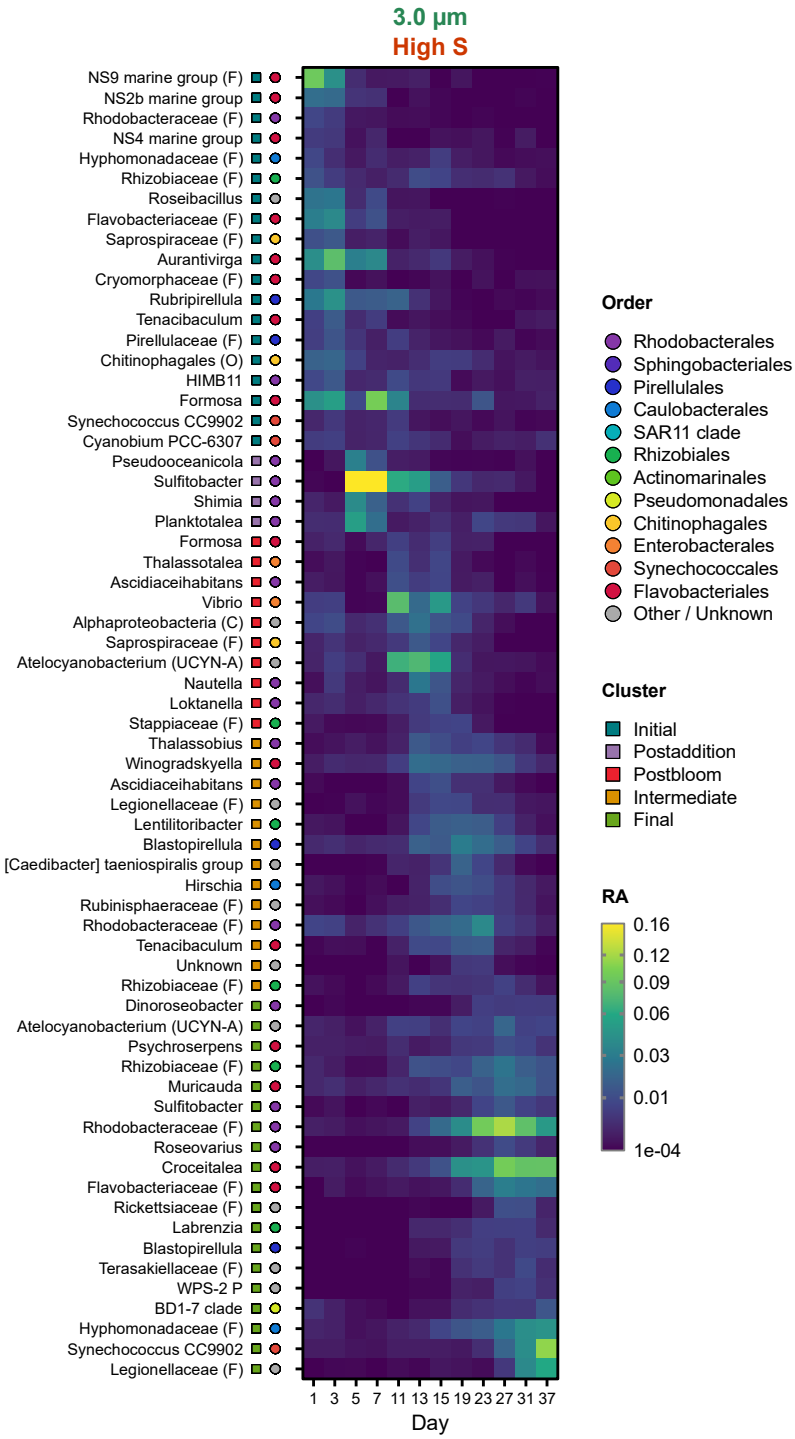

Figure S14. Continued. Succession patterns of most relevant prokaryotic taxa. RA = relative abundance. 3.0 µm size fraction of the high singular treatment.

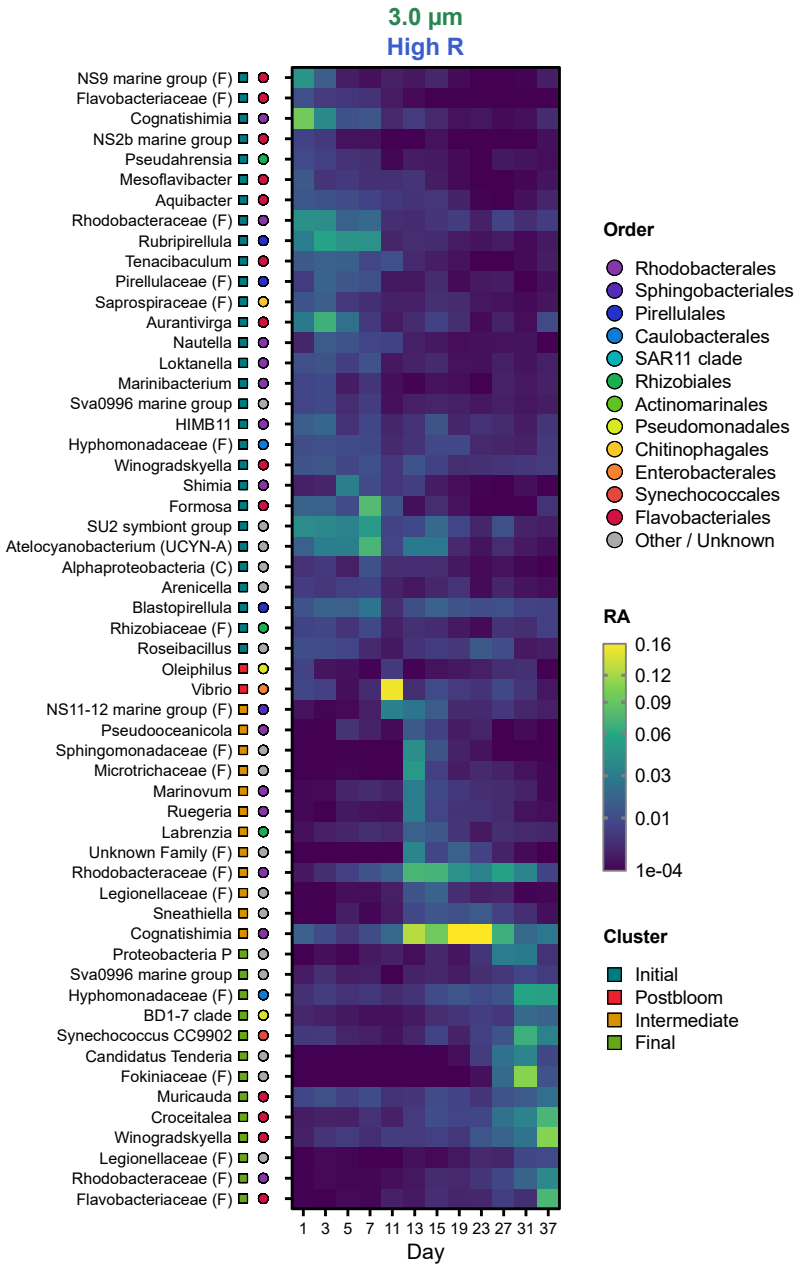

Figure S14. Continued. 3.0 µm size fraction of the high recurring treatment.

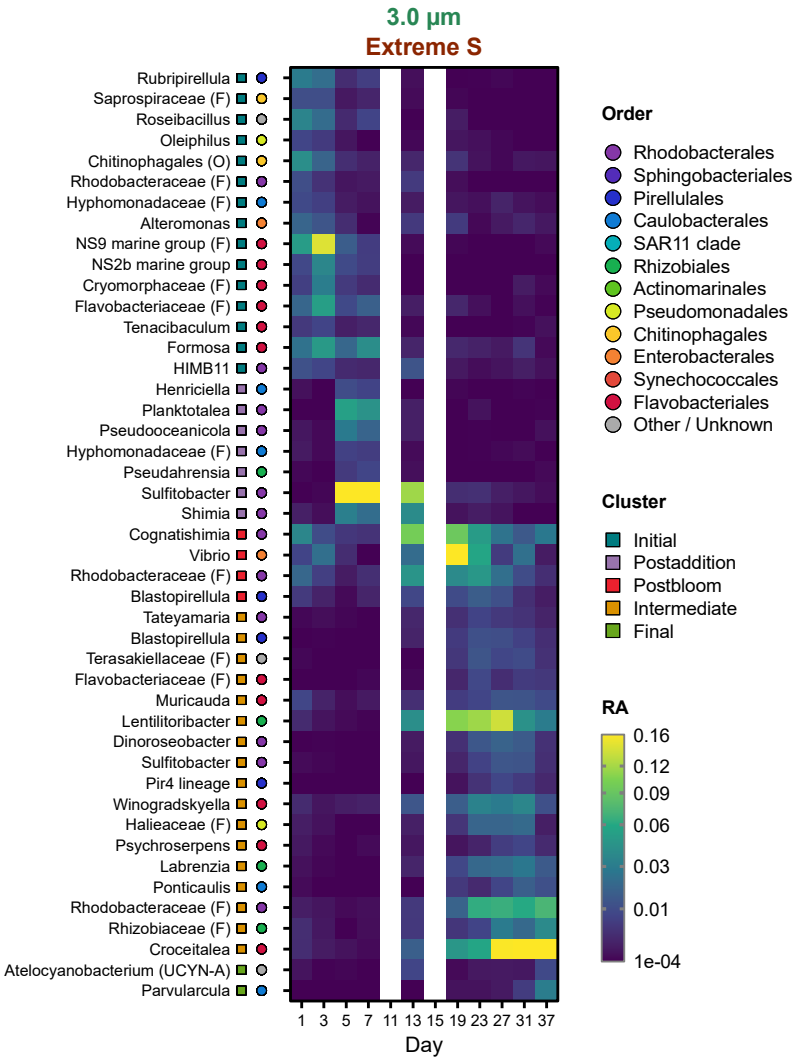

Figure S14. Continued. Succession patterns of most relevant prokaryotic taxa. Results are shown per treatment and size fraction as indicated on top of each panel. For each treatment and size fraction, ASVs with a membership value over 0.75 were merged by genera (when possible; otherwise, at the most detailed taxonomic level available, as indicated next to their name: F = family, O = order, C = class). From those, taxa representing at least 0.5% of reads in more than 1 sample within each treatment and size fraction are shown. Colourmap represents relative abundance (RA) of taxa (note that to aid visualisation 1) the scale is square−root−transformed and 2) out of bounds outlier values have been assigned the colours of the upper and lower limits of the colourmap). Coloured dots represent the taxonomic order of taxa, and cluster assignations are displayed next to taxa names. Results for the singular and recurring modes of each intensity level are shown paired in adjacent pages to aid comparison (this page: 3.0 µm size fraction of the extreme singular treatment).

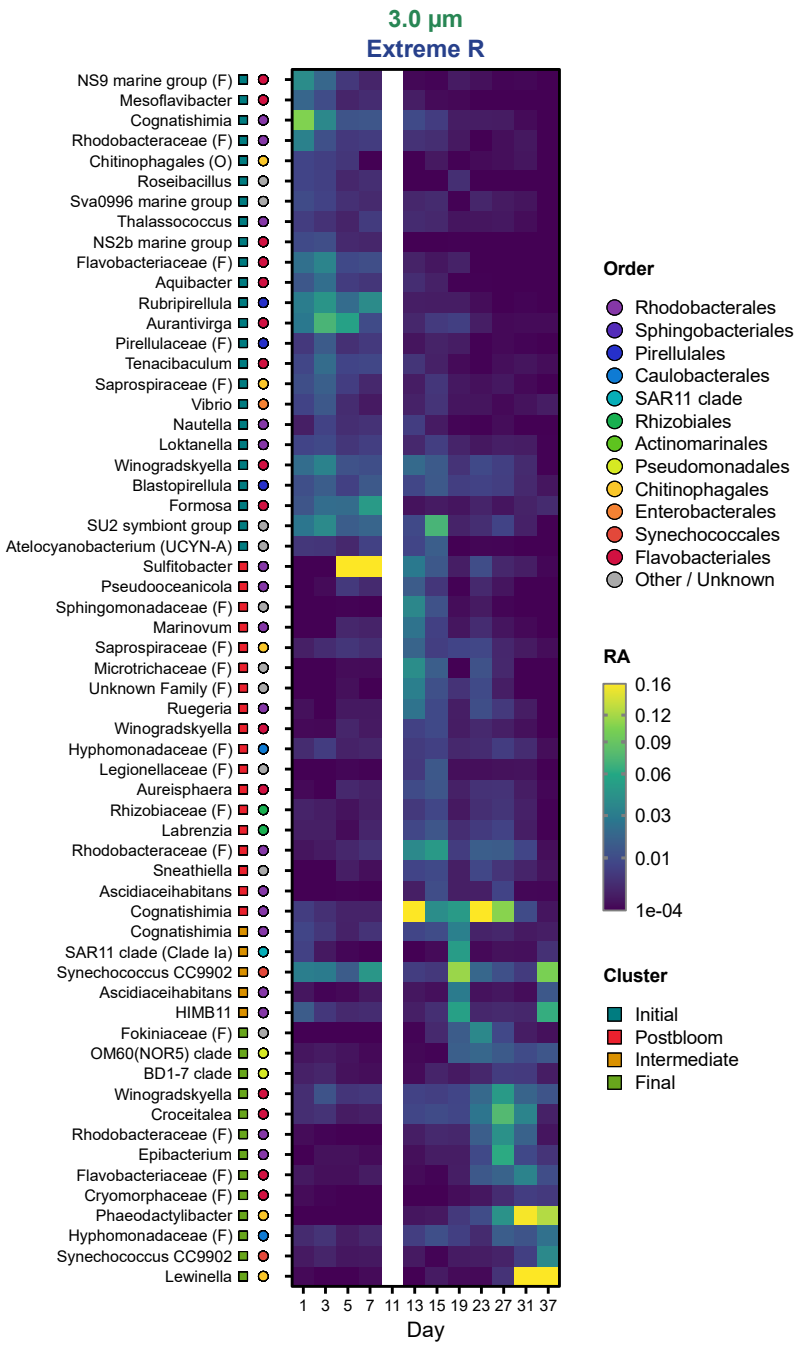

Figure S14. Continued. 3.0 µm size fraction of the extreme recurring treatment

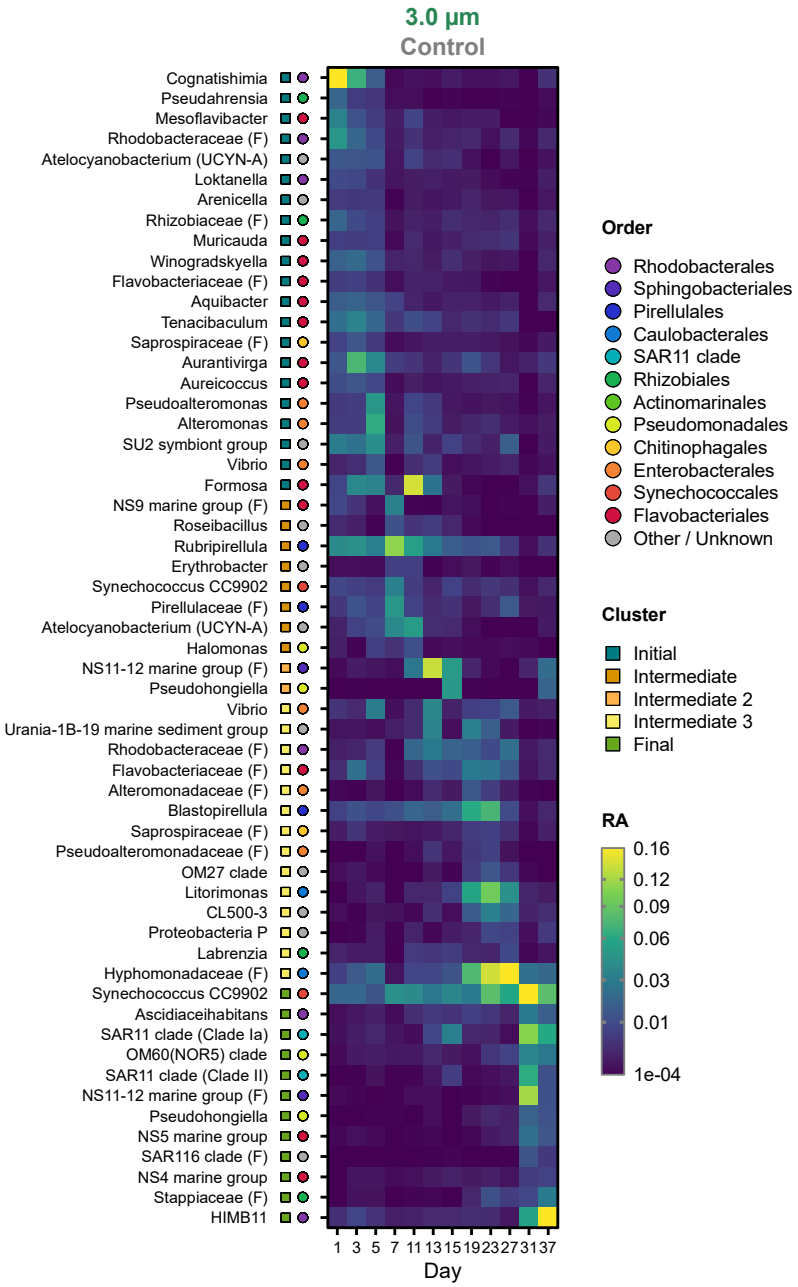

Figure S14. Continued. Succession patterns of most relevant prokaryotic taxa. ASVs with a membership value over 0.75 were merged by genera (when possible; otherwise, at F = family, O = order, C = class). From those, taxa representing at least 0.5% of reads in more than 1 sample within each treatment and size fraction are shown. Colourmap represents relative abundance (RA) of taxa Coloured dots represent the taxonomic order of taxa, and cluster assignations are displayed next to taxa names. 3.0 µm size fraction of the control treatment.

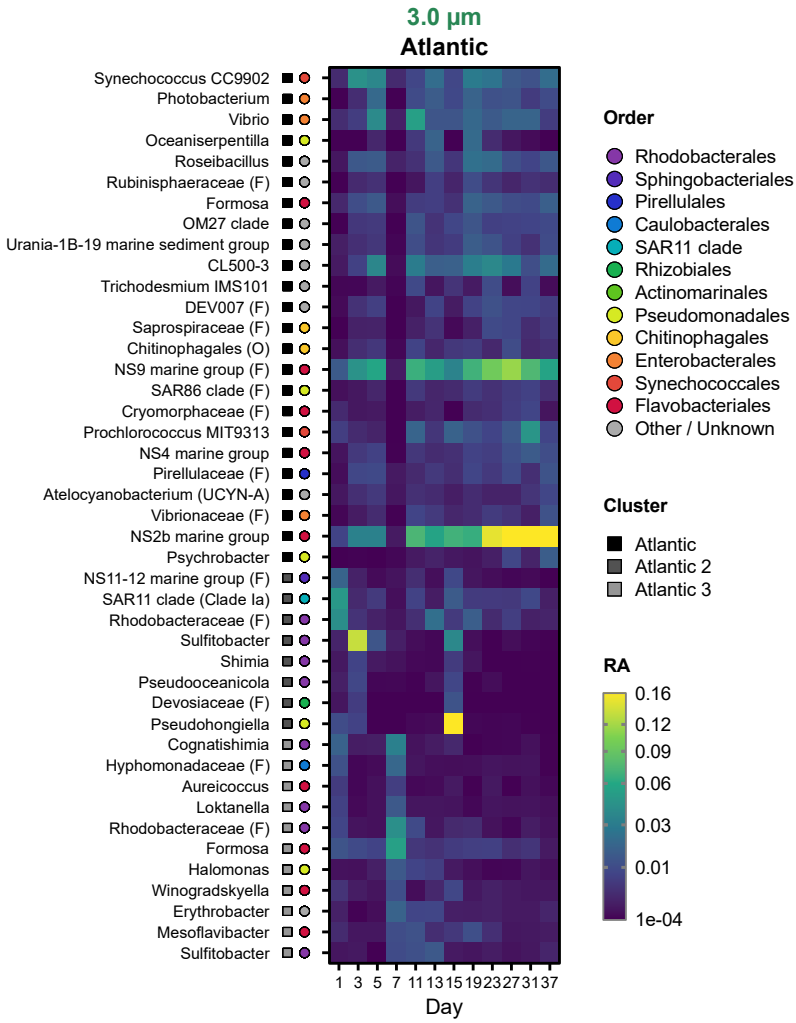

Figure S14. Continued. 3.0 µm size fraction of the Atlantic (ambient waters).

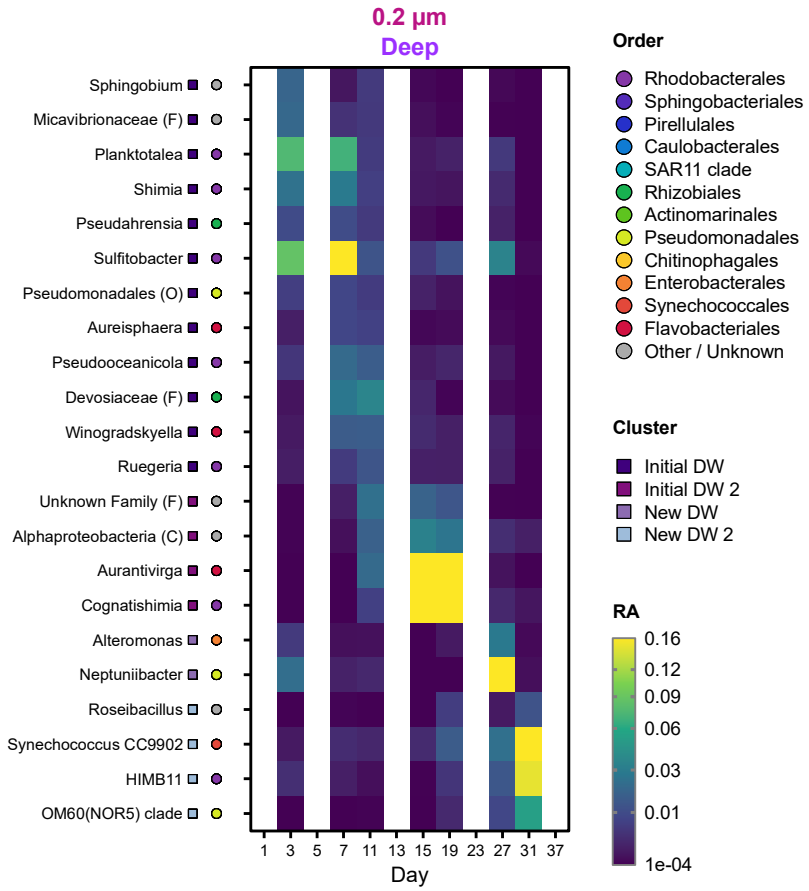

Figure S14. Continued. Succession patterns of most relevant prokaryotic taxa. Results are shown per treatment and size fraction as indicated on top of each panel. For each treatment and size fraction, ASVs with a membership value over 0.75 were merged by genera (when possible; otherwise, at the most detailed taxonomic level available, as indicated next to their name: F = family, O = order, C = class). From those, taxa representing at least 0.5% of reads in more than 1 sample within each treatment and size fraction are shown. Colourmap represents relative abundance (RA) of taxa (note that to aid visualisation 1) the scale is square−root−transformed and 2) out of bounds outlier values have been assigned the colours of the upper and lower limits of the colourmap). Coloured dots represent the taxonomic order of taxa, and cluster assignations are displayed next to taxa names. Results for the deep water used to simulate upwelling are shown paired in adjacent pages to aid comparison (this page: 0.2 µm size fraction).

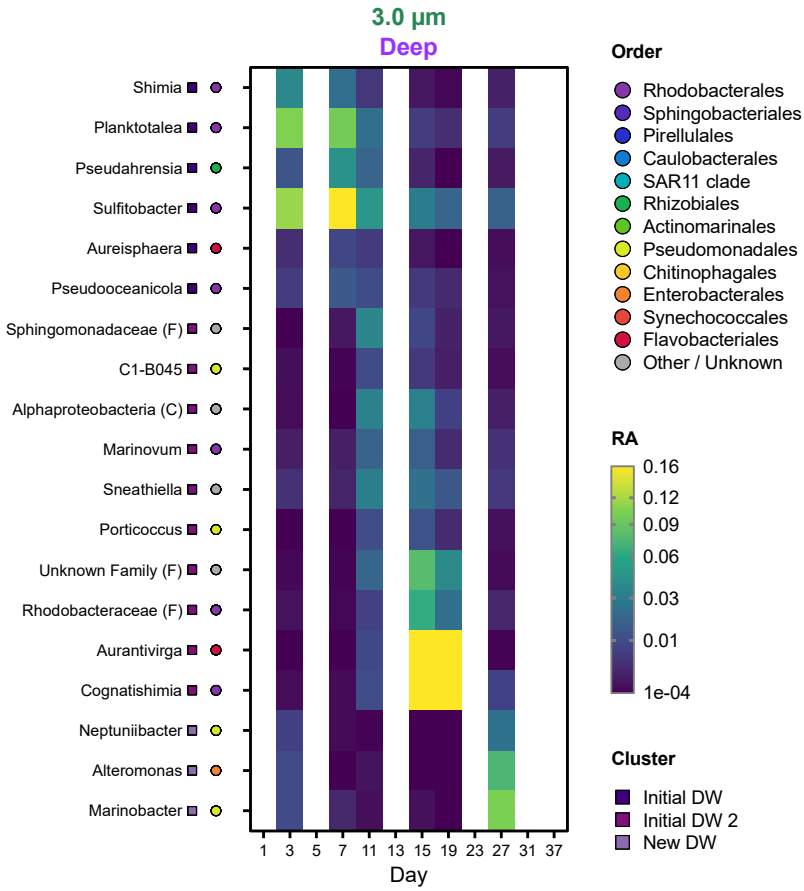

Figure S14. Continued. 3.0 µm size fraction of the deep water.

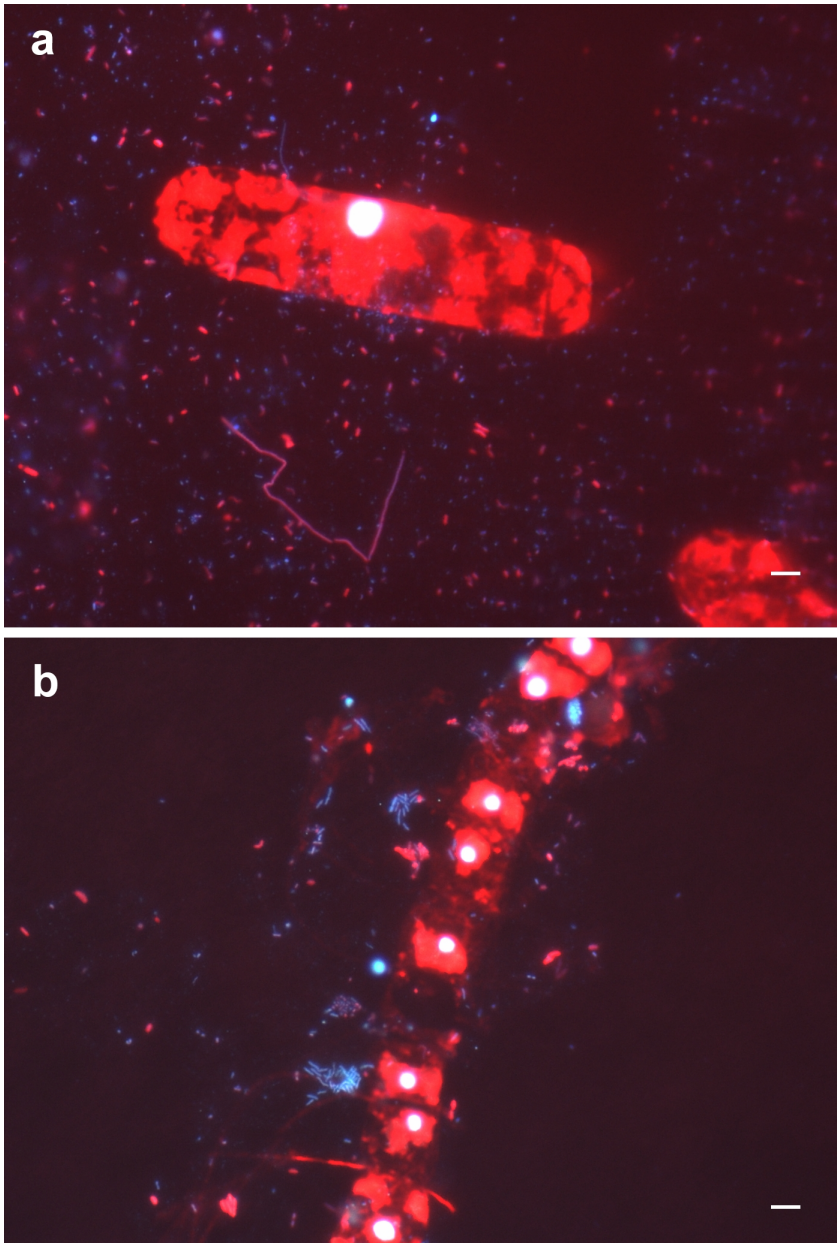

Figure S15. Protein synthesizing activity in diatoms during the experiment. Pictures show the combined signal of 4′,6-diamidino-2-phenylindole (DAPI; all cells, blue) and Alexa594 (BONCAT, protein-synthesising cells, red): a) Extreme R (day 13), b) Extreme S (day 13). Scale bars (bottom right of each panel) represent 5 μm.

References

Alejandre-Colomo, C., T. Viver, M. Urdiain, B. Francis, J. Harder, P. Kämpfer, R. Amann, and R. Rosselló-Móra. 2020. Taxonomic study of nine new Winogradskyella species occurring in the shallow waters of Helgoland Roads, North Sea. Proposal of Winogradskyella schleiferi sp. nov., Winogradskyella costae sp. nov., Winogradskyella helgolandensis sp. nov., Winogradskyella v. Syst. Appl. Microbiol. **43**: 126128. doi:10.1016/j.syapm.2020.126128

Allers, E., L. Gómez-Consarnau, J. Pinhassi, J. M. Gasol, K. Šimek, and J. Pernthaler. 2007. Response of Alteromonadaceae and Rhodobacteriaceae to glucose and phosphorus manipulation in marine mesocosms. Environ. Microbiol. **9**: 2417–2429. doi:10.1111/j.1462-2920.2007.01360.x

Amos, C. M., R. M. Castelao, and P. M. Medeiros. 2019. Offshore transport of particulate organic carbon in the California Current System by mesoscale eddies. Nat. Commun. **10**: 4940. doi:10.1038/s41467-019-12783-5

Arahal, D. R., A. La Mura, T. Lucena, L. Rodrigo-Torres, R. Aznar, and M. J. Pujalte. 2019. Shimia thalassica sp. nov., and reclassification of Pseudopelagicola gijangensis as Shimia gijangensis comb. nov., and Thalassobius activus as Cognatishimia activa comb. nov. Int. J. Syst. Evol. Microbiol. **69**: 3405–3413. doi:10.1099/ijsem.0.003629

Arístegui, J., E. D. Barton, P. Tett, and others. 2004. Variability in plankton community structure, metabolism, and vertical carbon fluxes along an upwelling filament (Cape Juby, NW Africa). Prog. Oceanogr. **62**: 95–113. doi:10.1016/j.pocean.2004.07.004

Arnosti, C. 2011. Microbial Extracellular Enzymes and the Marine Carbon Cycle. Ann. Rev. Mar. Sci. **3**: 401–425. doi:10.1146/annurev-marine-120709-142731

Azam, F., T. Fenchel, J. Field, J. Gray, L. Meyer-Reil, and F. Thingstad. 1983. The Ecological Role of Water-Column Microbes in the Sea. Mar. Ecol. Prog. Ser. **10**: 257–263. doi:10.3354/meps010257

Baltar, F., J. Arístegui, J. M. Gasol, and G. J. Herndl. 2012. Microbial functioning and community structure variability in the mesopelagic and epipelagic waters of the subtropical northeast Atlantic Ocean. Appl. Environ. Microbiol. **78**: 3309–3316. doi:10.1128/AEM.07962-11

Baltar, F., J. Arístegui, J. M. Gasol, I. Lekunberri, and G. J. Herndl. 2010. Mesoscale eddies: Hotspots of prokaryotic activity and differential community structure in the ocean. ISME J. **4**: 975–988. doi:10.1038/ismej.2010.33

Baumann, M., J. Taucher, A. J. Paul, and others. 2021. Effect of Intensity and Mode of Artificial Upwelling on Particle Flux and Carbon Export. Front. Mar. Sci. **8**: 742142. doi:10.3389/fmars.2021.742142

Becker, J. W., S. L. Hogle, K. Rosendo, and S. W. Chisholm. 2019. Co-culture and biogeography of Prochlorococcus and SAR11. ISME J. **13**: 1506–1519. doi:10.1038/s41396-019-0365-4

Becker, S., J. Tebben, S. Coffinet, K. Wiltshire, M. H. Iversen, T. Harder, K.-U. Hinrichs, and J.-H. Hehemann. 2020. Laminarin is a major molecule in the marine carbon cycle. Proc. Natl. Acad. Sci. **117**: 6599–6607. doi:10.1073/pnas.1917001117

Behrenfeld, M. J., and E. S. Boss. 2018. Student's tutorial on bloom hypotheses in the context of phytoplankton annual cycles. Glob. Chang. Biol. **24**: 55–77. doi:10.1111/gcb.13858

Behringer, G., M. A. Ochsenkühn, C. Fei, J. Fanning, J. A. Koester, and S. A. Amin. 2018. Bacterial Communities of Diatoms Display Strong Conservation Across Strains and Time. Front.

Microbiol. **9**: 659. doi:10.3389/fmicb.2018.00659

Bezdek, J. C. 1981. Pattern Recognition with Fuzzy Objective Function Algorithms, 1st ed. Plenum Press.

Bode, A., M. Álvarez, M. Ruíz-Villarreal, and M. M. Varela. 2019. Changes in phytoplankton production and upwelling intensity off A Coruña (NW Spain) for the last 28 years. Ocean Dyn. **69**: 861–873. doi:10.1007/s10236-019-01278-y

Bode, A., S. Barquero, M. Varela, J. G. Braun, and D. de Armas. 2001. Pelagic bacteria and phytoplankton in oceanic waters near the Canary Islands in summer. Mar. Ecol. Prog. Ser. **209**: 1–17.

Boeuf, D., B. R. Edwards, J. M. Eppley, and others. 2019. Biological composition and microbial dynamics of sinking particulate organic matter at abyssal depths in the oligotrophic open ocean. Proc. Natl. Acad. Sci. **116**: 11824–11832. doi:10.1073/pnas.1903080116

van den Boogaart, K. G., R. Tolosana-Delgado, and M. Bren. 2022. compositions: Compositional Data Analysis. R package version 2.0-4. https://CRAN.R-project.org/package=compositions.

Boyd, P. W., A. J. Watson, C. S. Law, and others. 2000. A mesoscale phytoplankton bloom in the polar Southern Ocean stimulated by iron fertilization. Nature **407**: 695–702. doi:10.1038/35037500

Buchan, A., G. R. LeCleir, C. A. Gulvik, and J. M. González. 2014. Master recyclers: features and functions of bacteria associated with phytoplankton blooms. Nat. Rev. Microbiol. **12**: 686–698. doi:10.1038/nrmicro3326

Callahan, B. J., P. J. McMurdie, M. J. Rosen, A. W. Han, A. J. A. Johnson, and S. P. Holmes. 2016. DADA2: High-resolution sample inference from Illumina amplicon data. Nat. Methods **13**: 581–583. doi:10.1038/nmeth.3869

Carr, M. E., and E. J. Kearns. 2003. Production regimes in four Eastern Boundary Current systems. Deep-Sea Res. Part II Top. Stud. Oceanogr. **50**: 3199–3221. doi:10.1016/j.dsr2.2003.07.015

Catalá, T. S., A. M. Martínez-Pérez, M. Nieto-Cid, and others. 2018. Dissolved Organic Matter (DOM) in the open Mediterranean Sea. I. Basin–wide distribution and drivers of chromophoric DOM. Prog. Oceanogr. **165**: 35–51. doi:10.1016/j.pocean.2018.05.002

Chen, X., R. Ma, Y. Yang, N. Jiao, and R. Zhang. 2019. Viral Regulation on Bacterial Community Impacted by Lysis-Lysogeny Switch: A Microcosm Experiment in Eutrophic Coastal Waters. Front. Microbiol. **10**: 1763. doi:10.3389/fmicb.2019.01763

Chen, Z., X. Lei, Q. Lai, and others. 2014. Phaeodactylibacter xiamenensis gen. nov., sp. nov., a member of the family Saprospiraceae isolated from the marine alga Phaeodactylum tricornutum. Int. J. Syst. Evol. Microbiol. **64**: 3496–3502. doi:10.1099/ijs.0.063909-0

Coates, C. J., and M. Wyman. 2017. A denitrifying community associated with a major, marine nitrogen fixer. Environ. Microbiol. **19**: 4978–4992. doi:10.1111/1462-2920.14007

Cropper, T. E., E. Hanna, and G. R. Bigg. 2014. Spatial and temporal seasonal trends in coastal upwelling off Northwest Africa, 1981-2012. Deep-Sea Res. Part I Oceanogr. Res. Pap. **86**: 94–111. doi:10.1016/j.dsr.2014.01.007

Davis, N. M., Di. M. Proctor, S. P. Holmes, D. A. Relman, and B. J. Callahan. 2018. Simple statistical identification and removal of contaminant sequences in marker-gene and metagenomics data. Microbiome **6**: 226. doi:10.1186/s40168-018-0605-2

Dedysh, S. N., I. S. Kulichevskaya, A. V Beletsky, A. A. Ivanova, W. I. C. Rijpstra, J. S. S. Damsté, A. V

Mardanov, and N. V Ravin. 2020. Lacipirellula parvula gen. nov., sp. nov., representing a lineage of planctomycetes widespread in low-oxygen habitats, description of the family Lacipirellulaceae fam. nov. and proposal of the orders Pirellulales ord. nov., Gemmatales ord. nov. and Isosph. Syst. Appl. Microbiol. **43**: 126050. doi:10.1016/j.syapm.2019.126050

Demarcq, H. 2009. Trends in primary production, sea surface temperature and wind in upwelling systems (1998-2007). Prog. Oceanogr. **83**: 376–385. doi:10.1016/j.pocean.2009.07.022

Desbiolles, F., B. Blanke, and A. Bentamy. 2014. Short-term upwelling events at the western African coast related to synoptic atmospheric structures as derived from satellite observations. J. Geophys. Res. Ocean. **119**: 461–483. doi:10.1002/2013JC009278

Dimitriadou, E., S. Dolničar, and A. Weingessel. 2002. An examination of indexes for determining the number of clusters in binary data sets. Psychometrika **67**: 137–159. doi:10.1007/BF02294713

Duret, M. T., R. S. Lampitt, and P. Lam. 2019. Prokaryotic niche partitioning between suspended and sinking marine particles. Environ. Microbiol. Rep. **11**: 386–400. doi:10.1111/1758-2229.12692

Durham, B. P., J. Grote, K. A. Whittaker, and others. 2014. Draft genome sequence of marine alphaproteobacterial strain HIMB11, the first cultivated representative of a unique lineage within the Roseobacter clade possessing an unusually small genome. Stand. Genomic Sci. **9**: 632–645. doi:10.4056/sigs.4998989

Engel, A., S. Goldthwait, U. Passow, and A. Alldredge. 2002. Temporal decoupling of carbon and nitrogen dynamics in a mesocosm diatom bloom. Limnol. Oceanogr. **47**: 753–761. doi:10.4319/lo.2002.47.3.0753

Falcioni, T., S. Papa, and J. M. Gasol. 2008. Evaluating the flow-cytometric nucleic acid double-staining protocol in realistic situations of planktonic bacterial death. Appl. Environ. Microbiol. **74**: 1767–79. doi:10.1128/AEM.01668-07

Faria, M., N. Bordin, J. Kizina, J. Harder, D. Devos, and O. M. Lage. 2018. Planctomycetes attached to algal surfaces: Insight into their genomes. Genomics **110**: 231–238. doi:10.1016/j.ygeno.2017.10.007

Fenchel, T. 2008. The microbial loop – 25 years later. J. Exp. Mar. Bio. Ecol. **366**: 99–103. doi:10.1016/j.jembe.2008.07.013

Fuchs, B. M., S. Spring, H. Teeling, and others. 2007. Characterization of a marine gammaproteobacterium capable of aerobic anoxygenic photosynthesis. Proc. Natl. Acad. Sci. **104**: 2891–2896. doi:10.1073/pnas.0608046104

Fuhrman, J. A., I. Hewson, M. S. Schwalbach, J. A. Steele, M. V Brown, and S. Naeem. 2006. Annually reoccurring bacterial communities are predictable from ocean conditions. Proc. Natl. Acad. Sci. **103**: 13104–13109. doi:10.1073/pnas.0602399103

Giovannoni, S. J. 2017. SAR11 Bacteria: The Most Abundant Plankton in the Oceans. Ann. Rev. Mar. Sci. **9**: 231–255. doi:10.1146/annurev-marine-010814-015934

Gralka, M., R. Szabo, R. Stocker, and O. X. Cordero. 2020. Trophic Interactions and the Drivers of Microbial Community Assembly. Curr. Biol. **30**: R1176–R1188. doi:10.1016/j.cub.2020.08.007

Grimes, D. J., C. N. Johnson, K. S. Dillon, A. R. Flowers, N. F. Noriea, and T. Berutti. 2009. What Genomic Sequence Information Has Revealed About Vibrio Ecology in the Ocean—A Review. Microb. Ecol. **58**: 447–460. doi:10.1007/s00248-009-9578-9

Haiwei, L., and M. M. Ann. 2014. Evolutionary Ecology of the Marine Roseobacter Clade. Microbiol. Mol. Biol. Rev. **78**: 573–587. doi:10.1128/MMBR.00020-14

Hansen, H. P., and F. Koroleff. 1999. Determination of nutrients, p. 159–228. *In* K. Grasshoff, K. Kremling, and M. Ehrhardt [eds.], Methods of Seawater Analysis. Wiley Verlag Chemie GmbH.

Helms, J. R., A. Stubbins, J. D. Ritchie, E. C. Minor, D. J. Kieber, and K. Mopper. 2008. Absorption spectral slopes and slope ratios as indicators of molecular weight, source, and photobleaching of chromophoric dissolved organic matter. Limnol. Oceanogr. **53**: 955–969. doi:10.4319/lo.2008.53.3.0955

Horvat, C., D. R. Jones, S. Iams, D. Schroeder, D. Flocco, and D. Feltham. 2022. The frequency and extent of sub-ice phytoplankton blooms in the Arctic Ocean. Sci. Adv. **3**: e1601191. doi:10.1126/sciadv.1601191

Hou, S., M. López-Pérez, U. Pfreundt, and others. 2018. Benefit from decline: the primary transcriptome of Alteromonas macleodii str. Te101 during Trichodesmium demise. ISME J. **12**: 981–996. doi:10.1038/s41396-017-0034-4

Ivars-Martínez, E., A. B. Martín-Cuadrado, G. D'Auria, A. Mira, S. Ferriera, J. Johnson, R. Friedman, and F. Rodríguez-Valera. 2008. Comparative genomics of two ecotypes of the marine planktonic copiotroph Alteromonas macleodii suggests alternative lifestyles associated with different kinds of particulate organic matter. ISME J. **2**: 1194–1212. doi:10.1038/ismej.2008.74

Jang, Y., H.-M. Oh, I. Kang, K. Lee, S.-J. Yang, and J.-C. Cho. 2011. Genome sequence of strain IMCC3088, a proteorhodopsin-containing marine bacterium belonging to the OM60/NOR5 clade. J. Bacteriol. **193**: 3415–3416. doi:10.1128/JB.05111-11

Khan, S. T., Y. Fukunaga, Y. Nakagawa, and S. Harayama. 2007. Emended descriptions of the genus Lewinella and of Lewinella cohaerens, Lewinella nigricans and Lewinella persica, and description of Lewinella lutea sp. nov. and Lewinella marina sp. nov. Int. J. Syst. Evol. Microbiol. **57**: 2946–2951. doi:10.1099/ijs.0.65308-0

Krüger, K., M. Chafee, T. Ben Francis, T. Glavina del Rio, D. Becher, T. Schweder, R. I. Amann, and H. Teeling. 2019. In marine Bacteroidetes the bulk of glycan degradation during algae blooms is mediated by few clades using a restricted set of genes. ISME J. **13**: 2800–2816. doi:10.1038/s41396-019-0476-y

Kuhlisch, C., G. Schleyer, N. Shahaf, F. Vincent, D. Schatz, and A. Vardi. 2022. Viral infection of algal blooms leaves a unique metabolic footprint on the dissolved organic matter in the ocean. Sci. Adv. **7**: eabf4680. doi:10.1126/sciadv.abf4680

Kwon, S.-K., H. G. Lee, M.-J. Kwak, and J. F. Kim. 2016. Genome sequence of the marine flavobacterium Croceitalea dokdonensis DOKDO 023 that contains proton- and sodium-pumping rhodopsins. Mar. Genomics **26**: 1–3. doi:10.1016/j.margen.2015.11.011

Lahti, L., and S. Shetty. 2019. microbiome R package, version 1.16.0 http://microbiome.github.io.

Leblanc, K., V. Cornet, M. Caffin, M. Rodier, A. Desnues, H. Berthelot, K. Turk-Kubo, and J. Heliou. 2016. Phytoplankton community structure in the VAHINE mesocosm experiment. Biogeosciences **13**: 5205–5219. doi:10.5194/bg-13-5205-2016

LeCleir, G. R., J. M. DeBruyn, E. W. Maas, P. W. Boyd, and S. W. Wilhelm. 2014. Temporal changes in particle-associated microbial communities after interception by nonlethal sediment traps. FEMS Microbiol. Ecol. **87**: 153–163. doi:10.1111/1574-6941.12213

Lee, M. D., E. A. Webb, N. G. Walworth, F.-X. Fu, N. A. Held, M. A. Saito, and D. A. Hutchins. 2018.

Transcriptional Activities of the Microbial Consortium Living with the Marine Nitrogen-Fixing Cyanobacterium Trichodesmium Reveal Potential Roles in Community-Level Nitrogen Cycling. Appl. Environ. Microbiol. **84**. doi:10.1128/AEM.02026-17

Legendre, P., and L. Legendre. 2012. Numerical Ecology, Elsevier.

Leizeaga, A., M. Estrany, I. Forn, and M. Sebastián. 2017. Using click-chemistry for visualizing in situ changes of translational activity in planktonic marine bacteria. Front. Microbiol. **8**: 2360. doi:10.3389/fmicb.2017.02360

López-Pérez, M., J. M. Haro-Moreno, J. Iranzo, and F. Rodriguez-Valera. 2020. Genomes of the "Candidatus Actinomarinales" Order: Highly Streamlined Marine Epipelagic Actinobacteria. mSystems **5**: e01041-20. doi:10.1128/mSystems.01041-20

Main, C. R., L. R. Salvitti, E. B. Whereat, and K. J. Coyne. 2015. Community-Level and Species-Specific Associations between Phytoplankton and Particle-Associated Vibrio Species in Delaware's Inland Bays. Appl. Environ. Microbiol. **81**: 5703–5713. doi:10.1128/AEM.00580-15

Martin, M. 2011. Cutadapt removes adapter sequences from high-throughput sequencing reads. EMBnet.journal. doi:10.14806/ej.17.1.200

Meyer, D., E. Dimitriadou, K. Hornik, A. Weingessel, and F. Leisch. 2021. e1071: Misc Functions of the Department of Statistics, Probability Theory Group (Formerly: E1071), TU Wien. R package version 1.7-9. https://CRAN.R-project.org/package=e1071.

Moran, M. A. 2015. The global ocean microbiome. Science, **350**: aac8455. doi:10.1126/science.aac8455

Mou, X., R. E. Hodson, and M. A. Moran. 2007. Bacterioplankton assemblages transforming dissolved organic compounds in coastal seawater. Environ. Microbiol. **9**: 2025–2037. doi:10.1111/j.1462-2920.2007.01318.x

Mühlenbruch, M., H.-P. Grossart, F. Eigemann, and M. Voss. 2018. Mini-review: Phytoplankton-derived polysaccharides in the marine environment and their interactions with heterotrophic bacteria. Environ. Microbiol. **20**: 2671–2685. doi:10.1111/1462-2920.14302

Mulholland, M. R., and M. W. Lomas. 2008. Nitrogen Uptake and Assimilation, p. 303–384. *In* D.G. Capone, D.A. Bronk, M.R. Mulholland, and E.J.B.T.-N. in the M.E. (Second E. Carpenter [eds.], Nitrogen in the Marine Environment. Academic Press.

Munson-McGee, J. H., M. R. Lindsay, E. Sintes, and others. 2022. Decoupling of respiration rates and abundance in marine prokaryoplankton. Nature. doi:10.1038/s41586-022-05505-3

Needham, D. M., and J. A. Fuhrman. 2016. Pronounced daily succession of phytoplankton, archaea and bacteria following a spring bloom. Nat. Microbiol. **1**: 16005. doi:10.1038/nmicrobiol.2016.5

Oksanen, J., F. G. Blanchet, M. Friendly, and others. 2020. vegan: Community Ecology Package. R package version 2.5-7. https://CRAN.R-project.org/package=vegan.

Ortiz, J., J. Arístegui, N. Hernández-Hernández, M. Fernández-Méndez, and U. Riebesell. 2022. Oligotrophic Phytoplankton Community Effectively Adjusts to Artificial Upwelling Regardless of Intensity, but Differently Among Upwelling Modes. Front. Mar. Sci. **9**: 880550. doi:10.3389/fmars.2022.880550

Parada, A. E., D. M. Needham, and J. A. Fuhrman. 2016. Every base matters: Assessing small subunit rRNA primers for marine microbiomes with mock communities, time series and global field samples. Environ. Microbiol. **18**: 1403–1414. doi:10.1111/1462-2920.13023

Pohlert, T. 2022. PMCMRplus: Calculate Pairwise Multiple Comparisons of Mean Rank Sums Extended. R package version 1.9.6. https://CRAN.R-project.org/package=PMCMRplus.

Pontiller, B., S. Martínez-García, V. Joglar, and others. 2022. Rapid bacterioplankton transcription cascades regulate organic matter utilization during phytoplankton bloom progression in a coastal upwelling system. ISME J. **16**: 2360–2372. doi:10.1038/s41396-022-01273-0

Priest, T., A. Heins, J. Harder, R. Amann, and B. M. Fuchs. 2022. Niche partitioning of the ubiquitous and ecologically relevant NS5 marine group. ISME J. **16**: 1570–1582. doi:10.1038/s41396-022-01209-8

Pujalte, M. J., T. Lucena, L. Rodrigo-Torres, and D. R. Arahal. 2018. Comparative Genomics of Thalassobius Including the Description of Thalassobius activus sp. nov., and Thalassobius autumnalis sp. nov. Front. Microbiol. **8**: 2645. doi:10.3389/fmicb.2017.02645

R Core Team. 2021. R: A language and environment for statistical computing. R Foundation for Statistical Computing, Vienna, Austria. URL https://www.R-project.org/.

Reintjes, G., B. M. Fuchs, M. Scharfe, K. H. Wiltshire, R. Amann, and C. Arnosti. 2020. Short-term changes in polysaccharide utilization mechanisms of marine bacterioplankton during a spring phytoplankton bloom. Environ. Microbiol. **22**: 1884–1900. doi:10.1111/1462-2920.14971

Riebesell, U., J. Czerny, K. Von Bröckel, and others. 2013. Technical Note: A mobile sea-going mesocosm system - New opportunities for ocean change research. Biogeosciences **10**: 1835–1847. doi:10.5194/bg-10-1835-2013

Riemann, L., G. F. Steward, and F. Azam. 2000. Dynamics of bacterial community composition and activity during a mesocosm diatom bloom. Appl. Environ. Microbiol. **66**: 578–587. doi:10.1128/AEM.66.2.578-587.2000

Rogato, A., A. Amato, D. Iudicone, M. Chiurazzi, M. I. Ferrante, and M. R. D'Alcalà. 2015. The diatom molecular toolkit to handle nitrogen uptake. Mar. Genomics **24**: 95–108. doi:10.1016/j.margen.2015.05.018

Salazar, G. 2022. EcolUtils: Utilities for community ecology analysis. R package version 0.1. https://github.com/GuillemSalazar/EcolUtils.

Santana-Falcón, Y., M. Benavides, P. Sangrà, E. Mason, E. D. Barton, A. Orbi, and J. Arístegui. 2016. Coastal–offshore exchange of organic matter across the Cape Ghir filament (NW Africa) during moderate upwelling. J. Mar. Syst. **154**: 233–242. doi:10.1016/j.jmarsys.2015.10.008

Schwämmle, V., and O. N. Jensen. 2010. A simple and fast method to determine the parameters for fuzzy c–means cluster analysis. Bioinformatics **26**: 2841–2848. doi:10.1093/bioinformatics/btq534

Sekar, R., A. Pernthaler, J. Pernthaler, F. Warnecke, T. Posch, and R. Amann. 2003. An Improved Protocol for Quantification of Freshwater Actinobacteria by Fluorescence In Situ Hybridization. Appl. Environ. Microbiol. **69**: 2928–2935. doi:10.1128/AEM.69.5.2928-2935.2003

Servais, P., E. O. Casamayor, C. Courties, P. Catala, N. Parthuisot, and P. Lebaron. 2003. Activity and diversity of bacterial cells with high and low nucleic acid content. Aquat. Microb. Ecol. **33**: 41–51. doi:10.3354/ame033041

Sharma, A. K., J. W. Becker, E. A. Ottesen, and others. 2014. Distinct dissolved organic matter sources induce rapid transcriptional responses in coexisting populations of Prochlorococcus, Pelagibacter and the OM60 clade. Environ. Microbiol. **16**: 2815–2830. doi:10.1111/1462-2920.12254

Sharp, J. H., E. T. Peltzer, M. J. Alperin, and others. 1993. Procedures subgroup report. Mar. Chem. **41**: 37–49. doi:10.1016/0304-4203(93)90104-V

Smith, A. F., B. Rihtman, R. Stirrup, E. Silvano, M. A. Mausz, D. J. Scanlan, and Y. Chen. 2019. Elucidation of glutamine lipid biosynthesis in marine bacteria reveals its importance under phosphorus deplete growth in Rhodobacteraceae. ISME J. **13**: 39–49. doi:10.1038/s41396-018-0249-z

Smith, D., and F. Azam. 1992. A simple, economical method for measuring bacterial protein synthesis rates in seawater using. Mar. Microb. food webs **6**: 107–114.

Sorokin, D. Y. 1995. Sulfitobacter pontiacus gen. nov., sp. nov. —— A new heterotrophic bacterium from the black sea, specialized on sulfite oxidation. Microbiology **64**: 295–305.

Stedmon, C. A., and R. Bro. 2008. Characterizing dissolved organic matter fluorescence with parallel factor analysis: A tutorial. Limnol. Oceanogr. Methods **6**: 572–579. doi:10.4319/lom.2008.6.572

Steinberg, D. K., and M. R. Landry. 2017. Zooplankton and the Ocean Carbon Cycle. Ann. Rev. Mar. Sci. **9**: 413–444. doi:10.1146/annurev-marine-010814-015924

Su, Y., M. Yu, Q. Ren, Z. Sun, Y. Zhang, X. Yang, Y. Wang, and X.-H. Zhang. 2017. Croceitalea marina sp. nov., isolated from marine particles of Yellow Sea, and emended description of the genera Croceitalea. Int. J. Syst. Evol. Microbiol. **67**: 4253–4259. doi:10.1099/ijsem.0.002298

Sundby, S., K. F. Drinkwater, and O. S. Kjesbu. 2016. The North Atlantic Spring-Bloom System—Where the Changing Climate Meets the Winter Dark. Front. Mar. Sci. **3**: 28. doi:10.3389/fmars.2016.00028

Szabo, R. E., S. Pontrelli, J. Grilli, J. A. Schwartzman, S. Pollak, U. Sauer, and O. X. Cordero. 2022. Historical contingencies and phage induction diversify bacterioplankton communities at the microscale. Proc. Natl. Acad. Sci. **119**: e2117748119. doi:10.1073/pnas.2117748119

Taucher, J., J. Arístegui, L. T. Bach, W. Guan, M. F. Montero, A. Nauendorf, E. P. Achterberg, and U. Riebesell. 2018. Response of Subtropical Phytoplankton Communities to Ocean Acidification Under Oligotrophic Conditions and During Nutrient Fertilization. Front. Mar. Sci. **5**: 330. doi:10.3389/fmars.2018.00330

Teeling, H., B. M. Fuchs, D. Becher, and others. 2012. Substrate-Controlled Succession of Marine Bacterioplankton Populations Induced by a Phytoplankton Bloom. Science, **336**: 608–611. doi:10.1126/science.1218344

Teeling, H., B. M. Fuchs, C. M. Bennke, and others. 2016. Recurring patterns in bacterioplankton dynamics during coastal spring algae blooms A.A. Brakhage [ed.]. Elife **5**: e11888. doi:10.7554/eLife.11888

Teoh, F., B. Shah, M. Ostrowski, and I. Paulsen. 2020. Comparative membrane proteomics reveal contrasting adaptation strategies for coastal and oceanic marine Synechococcus cyanobacteria. Environ. Microbiol. **22**: 1816–1828. doi:10.1111/1462-2920.14876

Thornton, D. C. O. 2014. Dissolved organic matter (DOM) release by phytoplankton in the contemporary and future ocean. Eur. J. Phycol. **49**: 20–46. doi:10.1080/09670262.2013.875596

Unfried, F., S. Becker, C. S. Robb, and others. 2018. Adaptive mechanisms that provide competitive advantages to marine bacteroidetes during microalgal blooms. ISME J. **12**: 2894–2906. doi:10.1038/s41396-018-0243-5

Vincent, F., M. Gralka, G. Schleyer, and others. 2021. Viral infection switches the balance between

bacterial and eukaryotic recyclers of organic matter during algal blooms. bioRxiv 2021.10.25.465659. doi:10.1101/2021.10.25.465659

Yan, S., B. M. Fuchs, S. Lenk, J. Harder, J. Wulf, N.-Z. Jiao, and R. Amann. 2009. Biogeography and phylogeny of the NOR5/OM60 clade of Gammaproteobacteria. Syst. Appl. Microbiol. **32**: 124–139. doi:10.1016/j.syapm.2008.12.001

Zhou, J., G.-F. Chen, K.-Z. Ying, H. Jin, J.-T. Song, and Z.-H. Cai. 2019. Phycosphere Microbial Succession Patterns and Assembly Mechanisms in a Marine Dinoflagellate Bloom. Appl. Environ. Microbiol. **85**. doi:10.1128/AEM.00349-19

Chapter 3

Surface productivity governs deep ocean viability

Surface productivity gradients govern changes in the viability of deep ocean prokaryotes across the tropical and subtropical Atlantic

Markel Gómez-Letona, Javier Arístegui, Nauzet Hernández-Hernández, María Pérez-Lorenzo, Xosé Antón Alvarez-Salgado, Eva Teira, Marta Sebastián

Limnology and Oceanography, 2022. doi: 10.1002/lno.12248

Prokaryotes represent a major fraction of marine biomass and play a key role in the global carbon cycle. We studied the vertical profiles (0-3500 m) of abundance, viability, and activity of prokaryotic communities along a productivity gradient in the subtropical and tropical Atlantic to assess whether there is a vertical linkage between surface productivity regimes and deep ocean prokaryotic communities. We found that latitudinal changes in the vertical patterns of cytometric variables were coupled with surface productivity: higher prokaryotic abundances and viabilities, and smaller cell sizes were observed below highly productive surface waters, an effect reaching down to the bathypelagic layer. Leucine uptake rates in deep waters showed no clear relationship with surface productivity. Changes in resource and energy allocation to growth vs. maintenance in hostile environments, cell-size-dependent metabolic requirements and variability in leucine to carbon conversion may all be part of the array of factors involved in controlling the prokaryotic activity patterns that were measured. Our work adds to the recent findings that highlight the importance of vertical connectivity for prokaryotic communities in the dark ocean and unveils a remarkable impact of surface conditions in the viability of deep ocean prokaryotes. This is a key aspect when considering metabolic rates of prokaryotic communities in the bathypelagic realm.

Introduction

Prokaryotes represent a key component of marine ecosystems. At abundances typically ranging from thousands to millions of cells per millilitre, they conform a major fraction of the biomass of marine organisms (Whitman et al. 1998; Bar-On et al. 2018) and make use of a wide variety of energy and carbon sources (Moran 2015), driving global biogeochemical cycles. While prokaryotes are distributed along the entire water column, their abundance and activity are not constant. Epipelagic communities exhibit markedly higher abundances, biomass and production rates, lower percentages of cells with high nucleic acid content, and smaller cell sizes than those in meso- and bathypelagic waters (Arístegui et al. 2009). Nonetheless, given the vast volume of water encompassed by the dark ocean, prokaryotes in this realm are responsible for 75% and 50% of the ocean's prokaryotic biomass and production, respectively (Arístegui et al. 2009), underlining the importance of considering dark ocean communities when studying the carbon cycle in the ocean.

In surface open-ocean waters the organic matter consumed by prokaryotes stems either from *in situ* primary production or from lateral advection from coastal adjacent regions (Santana-Falcón et al. 2020). In the dark ocean, however, while chemolithoautotrophy (Baltar et al. 2010c) or carbon excretion by diel vertical migrants (Steinberg et al. 2008) may significantly contribute as carbon sources, the vertical flux of particles that escape remineralisation in the photic layer is assumed to be the main source of organic carbon (Boyd et al. 2019). These particles have diverse origins: they may consist of phytoplankton cells (Guidi et al. 2009), zooplankton faecal pellets (Turner 2015) or polymer gel structures (Verdugo 2012). Not only they are a source of organic matter to deep ocean layers, but also act as vectors that vertically connect prokaryotic communities (Mestre et al. 2018; Ruiz-González et al. 2020). However, a link between surface productivity or particle flux and prokaryotic biomass or production in the dark ocean has not always been found (Arístegui et al. 2009 and references therein; Herndl and Reinthaler 2013). Episodic vertical inputs and lateral advection of organic matter have been suggested as possible explanations for this lack of relationship (Yokokawa et al. 2013; Smith et al. 2018).

Alternatively, the time of response of deep ocean prokaryotes to organic matter inputs might vary between and within communities. This could be due to changes in the physiological status of individual cells, which can range from death, to limited activity or active growth (del Giorgio and Gasol 2008). For instance, the percentage of viable prokaryotes within a community (those with intact cell membranes, a

measure of their physiological status) in epipelagic waters has been previously associated with the release of organic matter by senescent phytoplankton (Lasternas and Agustí 2014), although it is not known if dark ocean communities respond in a similar way. Viability estimates in meso- and bathypelagic waters are scarce, but point to a reduction of viability with depth, from >80% in surface waters down to 10-40% (Gasol et al. 2009; Baltar et al. 2012), probably related to the more adverse conditions found in the dark realm (high pressure, low temperature, reduced organic carbon availability). Thus, assessing what drives the variability in the physiological status of dark ocean communities is key to adequately understand their bulk metabolic rates, including their response (or lack of response) to the vertical flux of organic matter.

To study the potential link between the physiological status of dark ocean prokaryotes and surface productivity, we studied prokaryotic communities along a section crossing the tropical and subtropical Atlantic Ocean, from the surface down to 3500 m. The studied region is complex, with a considerable number of currents (Brandt et al. 2008) and water masses (Pérez et al. 2001; Álvarez et al. 2014). Remarkably, it presents a strong surface productivity gradient, comprising both oligotrophic waters and areas directly under the influence of the Northwest African upwelling system, where high export rates of sinking particles have been reported (Fischer et al. 2020). We determined the abundance and viability of prokaryotic communities, estimated their cell size, and measured leucine incorporation rates, to assess whether these variables were affected by changes in surface productivity, evaluating the degree to which the standing stock and, more importantly, the metabolic status of deep prokaryotic communities were linked to epipelagic waters.

Materials and methods

Study area

During the MAFIA cruise (*Migrants and Active Flux In the Atlantic ocean*, April 2015, on board R/V Hespérides) seawater samples were collected at 13 stations along a section crossing a productivity gradient in the subtropical and tropical Atlantic (13°S – 27°N, Fig. 1). Sample collection was performed using a General Oceanics oceanographic rosette equipped with PVC Niskin bottles alongside a Seabird 911-plus CTD, a Seapoint Chlorophyll Fluorometer and a Seabird-43 Dissolved Oxygen Sensor. The chlorophyll *a* (°) values provided by the fluorometer were based on the factory calibration.

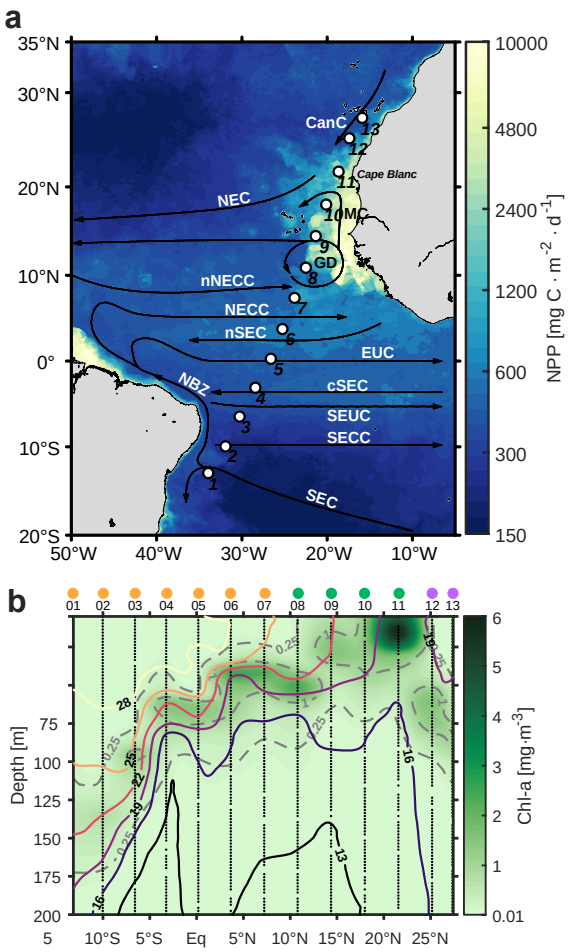

Figure 1. Surface productivity during the MAFIA cruise. (a) Sampling stations (1-13). The underlying colour map represents net primary production estimates for April 2015 (Eppley-VGPM model, MODIS dataset, Oregon State University, http://sites.science.oregonstate.edu/ocean.productivity/). Major ocean currents in the study region (based on Stramma and Schott, 1999 and Brandt et al. 2008) are also displayed: CanC, Canary Current; NEC, North Equatorial Current; MC, Mauritanian Current; GD, Guinea Dome; nNECC, northern North Equatorial Counter Current; NECC, North Equatorial Counter Current; nSEC, northern South Equatorial Current; EUC, Equatorial Under Current; NBZ, North Brazil Current; cSEC, central South Equatorial Current; SEUC, South Equatorial Under Current; SECC, South Equatorial Counter Current; SEC, South Equatorial Current. (b) Chl-a concentrations (derived from the CTD fluorometer) and potential temperature isotherms (in °C) in the epipelagic layer along the cruise section. Dashed isolines represent Chl *a* concentrations. Dots on top of station numbers represent station groups: 'South' (light orange), Guinea Dome-Cape Blanc ('Guinea Dome-Cape Blanc', green), 'North' (violet).

Prokaryotic cell abundance, size and viability

Seawater samples for measuring the abundance of prokaryotes were collected in all stations at 22 depths, from surface down to 3500 m (or bottom, when above this depth). Samples were collected into 1.2 mL cryovials, fixed with a 2% final concentration of formaldehyde, after keeping them 30 min at 4°C, and then stored frozen in liquid nitrogen. After 24 h they were analysed in a FACSCalibur (Becton-Dickinson) flow cytometer. Subsamples (400 µL) were stained with 4 µL of the fluorochrome SYBR Green I (Molecular Probes) diluted in dimethyl sulfoxide (1:10). Fluorescent beads (1 µm, Polysciences) were added for internal calibration (10^5 mL^{-1}). High and low nucleic acid content (HNA and LNA, respectively) prokaryotic cells were identified in green vs red fluorescence and green fluorescence vs side scatter cytograms. Average cell volumes (in μm^3) were estimated from side scatter based on the relationship described by Calvo-Díaz and Morán (2006) assuming spherical shape:

$$Cell\ volume = \frac{4}{3} \times \pi \times \left[\frac{0.908 + 0.34 \times \log_{10}(Relative\ side\ scatter)}{2} \right]^3$$

Where *Relative side scatter* is the (side scatter of prokaryotes)/(side scatter of beads) ratio. An in-house calibration was applied to transform relative side scatter values from Polysciences-bead-referenced to Molecular-Probes-bead-referenced ($[\text{Relative side scatter}]_{MP} = 2.201 \times [\text{Relative side scatter}]_{PS}$). Prokaryotic biomass was then estimated applying the volumetric relationship (Norland 1993):

$$pg\ C \cdot cell^{-1} = 0.12 \times (cell\ volume)^{0.7}$$

Prokaryotic cell viability was studied as an approach to assess the physiological status of cells, classifying them as viable (intact cell membrane; live and potentially active) and non-viable (compromised cell membrane; dead or injured). Viability was determined by nucleic-acid double-staining using SYBR Green I and propidium iodide (Falcioni et al. 2008) following Baltar et al. (2010a). Stained unfixed samples were analysed in the cytometer immediately after sample collection from the Niskin bottles to minimise membrane damage by depressurisation. The effect of depressurisation on cell membranes has been observed to be minimal within the first few hours, especially if the pressure change is done gradually (Park and Clark 2002; Quéric et al. 2004), as it occurs during the rosette retrieval. Viable and non-viable cell populations were identified in green vs red fluorescence cytograms.

Prokaryotic activity

Prokaryotic activity was quantified by measuring tritiated leucine incorporation (Kirchman et al. 1985). The centrifugation and filtration methods (Smith and Azam 1992) were applied for samples collected at ≤1000 m and >1000 m depth, respectively. For the centrifugation method, 1 mL of sample was incubated (3-12 h, 4 replicates and 2 blanks) with a final leucine concentration of 20 nM. For epipelagic samples (≤150 m) this was done with lukewarm leucine (1:10 dilution) and for mesopelagic samples (300-1000 m) with hot leucine (1:1 dilution). For the filtration method, samples of 40 mL were incubated (12-24 h, 2 replicates and 1 blank) with a final concentration of 5 nM (hot leucine, 1:1). The employed leucine had a specific activity of 112 Ci·mmol^{-1}. See Fig. S1 for a comparison of results obtained through both methods. Incubations were stopped by adding trichloroacetic acid to a final concentration of 5% for the centrifugation method and formaldehyde to a final concentration of 2% for the filtration method. For the latter, filters were then washed twice with trichloroacetic acid (50%). After centrifugation/filtration, a scintillation cocktail was added to the samples and the disintegrations per minute (dpm) were computed employing a Wallac scintillation counter with quenching correction, using an external standard. Dpm were converted to leucine incorporation rates based on the equation:

$$mmol\ Leu \cdot L^{-1} \cdot h^{-1} = 4.5^{-13} \times \left(dpm_{sample} - dpm_{blank}\right) \times SA^{-1} \times T^{-1} \times V^{-1}$$

where 4.5^{-13} is the number of curies per dpm (constant), SA is the specific activity of the leucine solution, T is the incubation time in hours and V is the incubation volume in litres. Specific leucine incorporation rates per viable cell were estimated making use of the results from the nucleic-acid double-staining protocol (see above).

Multiparameter Water Mass Analysis

The contribution of water masses in each sample deeper than 100 m was objectively quantified using of the optimum multiparameter analysis described in detail in **Chapter 4**. Briefly, based on previous hydrographic studies in the area (Álvarez et al. 2014; Catalá et al. 2015), twelve source water types were identified in the collected water samples (Fig. S2, Table S1): Salinity Maximum Water, Madeira Mode Water, Equatorial Water, Eastern North Atlantic Central Water of 15°C and 12°C, Subpolar Mode Water, Mediterranean Water, Antarctic Intermediate Water of 5°C and 3.1°C, Circumpolar Deep Water and North Atlantic Deep Water of 4.6°C and 2°C. The contribution of each of them to each sample is quantified by solving a set of four

conservative linear mixing equations defined by potential temperature (θ), salinity (S), silicate (SiO_4H_4) and the conservative NO tracer (= $O_2 + R_N \cdot NO_3$ with $R_N = 9.3$; Broecker 1974; Álvarez et al. 2014) (Table S2), plus a fifth equation that constrained the sum of the water mass contributions to 1. The resulting distribution of water masses in the study area can be found in Fig. S2. Archetype values of physical and biogeochemical variables were estimated for each water mass as weighed means based on the contribution of water masses to each sample (Álvarez-Salgado et al. 2013; Catalá et al. 2015).

Statistical analyses

All statistical analyses were carried out in R (v. 3.6.0, R Core Team 2019). To assess the relationship between surface productivity and the prokaryotic community, linear regressions were calculated for cytometric variables and leucine incorporation rates using surface Chl *a* (average within the upper 20 m) as the independent variable. Regressions were estimated separately for epipelagic (0-200 m), mesopelagic (200-1000 m) and bathypelagic (1000-3000 m) layers, using averaged (for HNA%, cell size, viability, and cell specific leucine incorporation) and integrated (for abundances and bulk leucine incorporation) values of the dependent variables for each depth range. Integrated values were calculated multiplying data values by the distance in meters between data points, based on an interpolated grid (see Fig. 2 and 4) estimated with DIVA (Troupin et al. 2012) in Matlab (R2017a) (see Supplementary Methods for details).

Log-log linear regressions of prokaryotic abundances and leucine incorporation vs depth were estimated (including samples of ≥10 m depth) to evaluate vertical trends. Regressions were estimated both jointly for the entire dataset and grouping stations based on surface productivity gradients (see section *Surface productivity gradient along the cruise section* for details): stations 1-7, with low surface Chl *a* values, were grouped as 'South'; stations 8-11, with high Chl *a* values, as 'Guinea Dome-Cape Blanc'; and stations 12-13, again with low Chl *a* values, as 'North'.

Results

Surface productivity gradient along the cruise section

The oceanographic section crossed regions with markedly different productivity regimes, as depicted by net primary production estimates and Chl *a* patterns (Fig. 1). Stations in the southern end of the section (1-2), off the coast of Brazil, presented conditions typically associated to oligotrophic waters, with low surface Chl *a* values (0.03-0.07 $mg{\cdot}m^{-3}$) and a Deep Chlorophyll Maximum (DCM) located at ~135 m depth, showing concentrations that barely exceeded 0.5 $mg{\cdot}m^{-3}$. Despite consistently showing low surface Chl *a* values, stations 3-7 presented an increasing trend, from 0.04-0.06 $mg{\cdot}m^{-3}$ at station 3 to 0.11-0.19 $mg{\cdot}m^{-3}$ at station 7. A parallel shoaling and strengthening of the DCM were evident, from 95 m (1.2 $mg{\cdot}m^{-3}$) at station 3 to 40 m (2.3 $mg{\cdot}m^{-3}$) at station 7. At stations 8-11 surface Chl *a* concentrations markedly increased, transitioning to highly productive waters: from 0.25-1.3 $mg{\cdot}m^{-3}$ in the Guinea Dome area (stations 8-9) to 1.4-1.5 $mg{\cdot}m^{-3}$ at station 10 and 4.8-5.9 $mg{\cdot}m^{-3}$ at Cape Blanc (station 11). These stations showed the shallowest DCMs, with Cape Blanc peaking at 15 m and 5.9 $mg{\cdot}m^{-3}$. Entering the oligotrophic Canary Current, stations 12-13 presented a sharp decrease in Chl *a* values (0.19-0.24 $mg{\cdot}m^{-3}$), while the DCM became deeper and weaker (85 m and 1.1 $mg{\cdot}m^{-3}$ at station 13).

Spatial distribution patterns of cytometric signatures

Prokaryotic abundances (Fig. 2a) showed decreasing numbers of cells with depth in all stations (log-log slope vs depth = -0.816 ± 0.035; Table 1). Concentrations in epipelagic waters were always above 10^5 $cells{\cdot}mL^{-1}$ with peaks exceeding 10^6 $cells{\cdot}mL^{-1}$ in surface samples in stations 6, 9, 10 and, especially, 11 (Cape Blanc area), where concentrations reached $2{\cdot}10^6$ $cell{\cdot}mL^{-1}$. Despite the widespread decrease with depth, prokaryotic abundances displayed latitudinal differences in the dark ocean too: increasing values were observed from the tropical South Atlantic (10^5 $cells{\cdot}mL^{-1}$ at ~300 m and $<2.5{\cdot}10^4$ $cells{\cdot}mL^{-1}$ below 1000-1500 m) to the Cape Blanc area (10^5 $cells{\cdot}mL^{-1}$ at ~700 m and $>2.5{\cdot}10^4$ $cells{\cdot}mL^{-1}$ in the entire water column). Indeed, there was a significantly positive relationship between surface Chl *a* concentrations and integrated prokaryotic abundances in the epipelagic, mesopelagic, and bathypelagic layers (Fig. 3a, Table S2). These gradients were reflected in changes in log-log slopes ('South' = -0.823 ± 0.042 vs 'Guinea Dome-Cape Blanc' = -0.783 ± 0.045; Table 1; Fig. S3) and the archetype prokaryotic cell abundances of the water masses (Table 2; see Fig. S2 for a scheme of the distribution of water masses along the

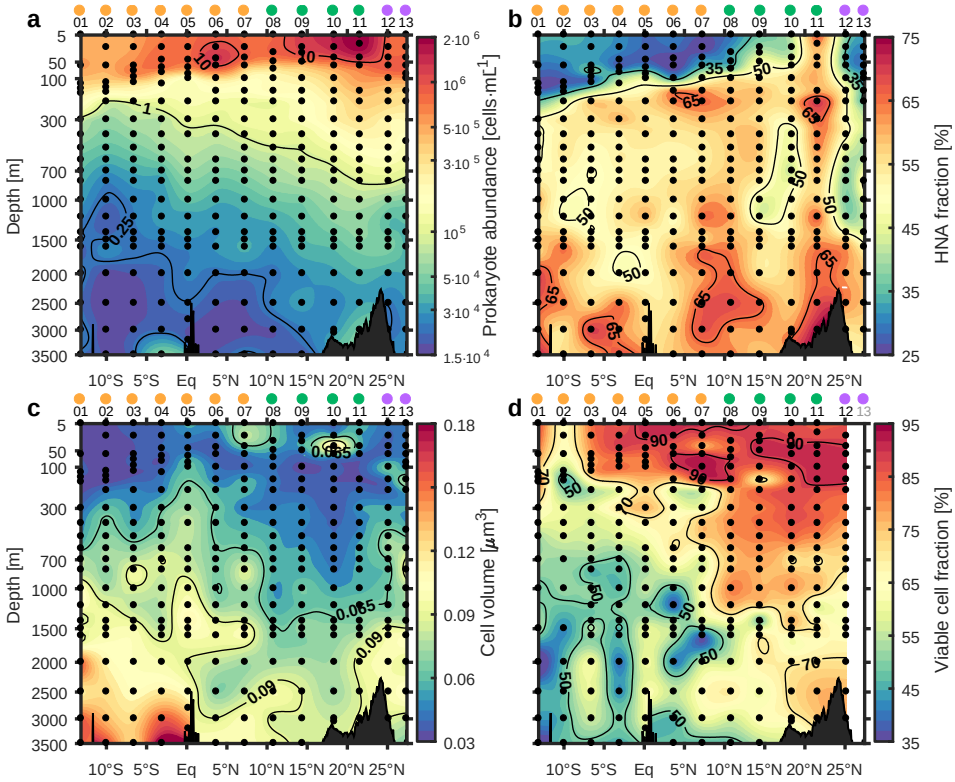

Figure 2. Characterisation of the prokaryotic community by flow cytometry. (a) Total prokaryotic cell abundance. Labels on contour lines are in 10^5. (b) Fraction of the community represented by HNA prokaryotes. (c) Mean volume of prokaryotic cells. (d) Viability of prokaryotic cells as per nucleic-acid double-staining (see methods). Black dots represent locations of collected samples and resulting estimates. Dots on top of station numbers represent station groups: 'South' (light orange), 'Guinea Dome-Cape Blanc' (green), 'North' (violet). Data interpolation was performed with DIVA in Matlab (R2017a).

section): the Salinity Maximum Water (134 ± 11 m) in the southern part of the section, presented markedly lower values (27.4 ± 3.2·10^4 cells·mL^{-1}) than the Madeira Mode Water (130 ± 17 m; 38.0 ± 5.6·10^4 cells·mL^{-1}), found in the northern part. Similarly, the Antarctic Intermediate Water of 5°C (713 ± 47 m) showed lower archetype prokaryotic abundances than the Subpolar Mode Water (696 ± 56 m), the former presenting 5.8 ± 0.5·10^4 cells·mL^{-1} and the latter 9.5 ± 0.8·10^4 cells·mL^{-1}. Bathypelagic water masses were distributed along the entire section and, thus, their differences were only depth-dependent (Table 2), but intra-water mass latitudinal changes were evident (Fig. 2a, Fig. S2).

Table 1. Log-log regressions of prokaryotic abundances (as cells · mL^{-1}) and leucine incorporation rates (as pmol Leu · L^{-1} · d^{-1}) vs depth, for samples of ≥10 m. Results are presented for the entire dataset ('All') and by station group: 'South' (stations 1-7), 'Guinea Dome-Cape Blanc' (8-11) and 'North' (12-13, if available). *Slope* and *Intercept* estimates are presented alongside 95% confidence intervals. r^2 is the adjusted coefficient of determination, p the p-value of the regression and n the number of samples per regression.

Variable	Station group	Slope	Intercept	r^2	p	n
HNA prokaryotes	All	-0.691 ± 0.037	6.514 ± 0.102	0.84	<0.001	261
	South	-0.661 ± 0.039	6.328 ± 0.108	0.89	<0.001	142
	Guinea Dome-Cape Blanc	-0.724 ± 0.055	6.742 ± 0.151	0.90	<0.001	82
	North	-0.693 ± 0.079	6.608 ± 0.215	0.90	<0.001	37
LNA prokaryotes	All	-0.923 ± 0.038	7.107 ± 0.105	0.90	<0.001	261
	South	-0.953 ± 0.049	7.107 ± 0.136	0.91	<0.001	142
	Guinea Dome-Cape Blanc	-0.848 ± 0.045	6.956 ± 0.125	0.95	<0.001	82
	North	-0.921 ± 0.076	7.307 ± 0.207	0.94	<0.001	37
All prokaryotes	All	-0.816 ± 0.035	7.149 ± 0.096	0.89	<0.001	261
	South	-0.823 ± 0.042	7.075 ± 0.117	0.91	<0.001	142
	Guinea Dome-Cape Blanc	-0.783 ± 0.045	7.153 ± 0.124	0.94	<0.001	82
	North	-0.820 ± 0.069	7.305 ± 0.188	0.94	<0.001	37
Viable prokaryotes	All	-0.916 ± 0.048	7.241 ± 0.131	0.86	<0.001	231
	South	-0.950 ± 0.050	7.204 ± 0.140	0.92	<0.001	129
	Guinea Dome-Cape Blanc	-0.868 ± 0.058	7.255 ± 0.160	0.92	<0.001	82
	North	-0.870 ± 0.118	7.354 ± 0.322	0.93	<0.001	20
Leucine incorporation	All	-1.261 ± 0.097	4.213 ± 0.269	0.81	<0.001	152
	South	-1.331 ± 0.122	4.447 ± 0.342	0.83	<0.001	98
	Guinea Dome-Cape Blanc	-1.148 ± 0.154	3.830 ± 0.424	0.81	<0.001	54
	North	-	-	-	-	-

Prokaryotic biomass (Fig. S4) was largely governed by cell abundances. Surface values increased from 5-7 μgC·L^{-1} in the south to 15-20 μgC·L^{-1} towards the Guinea Dome area, peaking at Cape Blanc at 36 μgC·L^{-1}. As abundance patterns, while decreasing with depth, biomass also displayed a latitudinal gradient in both the mesopelagic and bathypelagic layers, producing significant positive relationships with Chl *a* in epi-, meso- and bathypelagic layers (Table S3). Resulting archetype values for the Antarctic Intermediate Water of 5°C and the Subpolar Mode Water were 1.03 ± 0.09 and 1.49 ± 0.11 μgC·L^{-1}, respectively, while in bathypelagic waters biomasses below 0.55 μgC·L^{-1} in the south contrasted with values of 0.6-1 μgC·L^{-1} in the north.

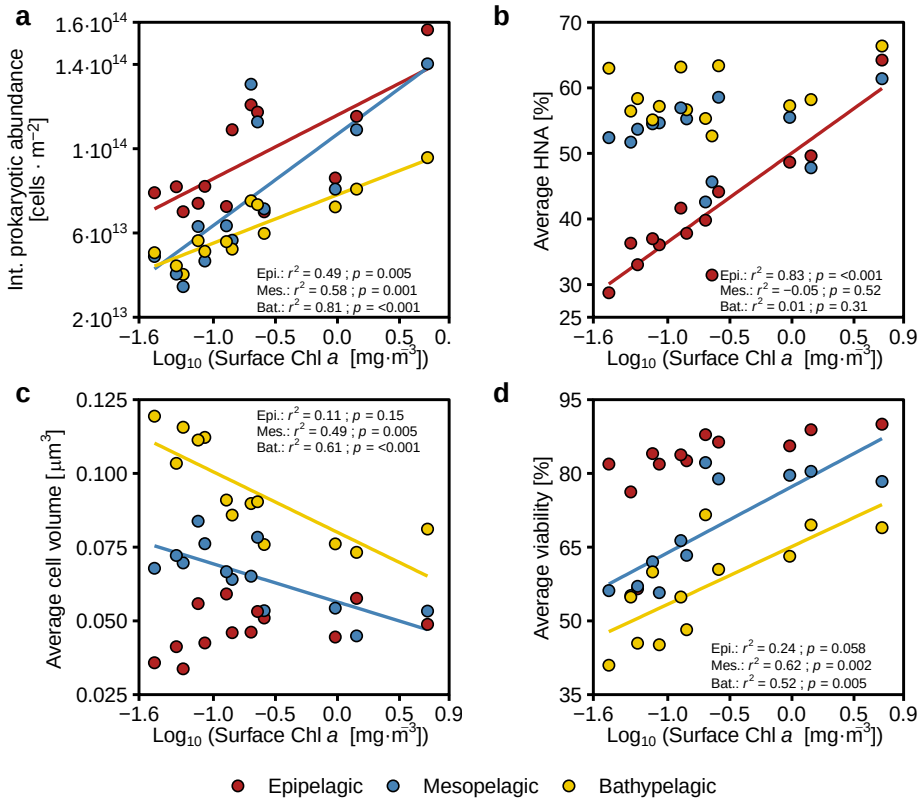

Figure 3. Linear regressions between surface Chl-a concentrations (averaged within the first 20 m, as proxy for productivity) and cytometric variables: (a) integrated prokaryotic abundance, (b) average HNA cell percentage, (c) average cell volume, and (d) average cell viability. Regressions estimated separately for epipelagic (≤200 m), mesopelagic (>200 m and ≤1000 m) and bathypelagic (>1000 m and ≤3000 m) layers. Regression lines are only shown for significant (p < 0.05) results. Regression parameters are presented in Table S3.

Surface communities were dominated by LNA cells (in many cases exceeding 65% of counts) except in station 11 (Fig. 2b). An increase of HNA contribution was observed from the southern stations across the Guinea Dome area towards Cape Blanc. In the dark ocean, HNA prokaryotes overall dominated the community (Fig. 2b), their contribution increasing with depth and reaching >65% in some bathypelagic samples. This was evident too from the different log-log slopes (Table 1), as the abundance of LNA prokaryotes (-0.923 ± 0.038) decreased markedly faster than HNA prokaryotes (-0.691 ± 0.037). While HNA contribution in station 11 was >50% in the entire water column (with particularly high values (75%) at the bottom), in stations 12 and 13 HNA contributions were back below 50% (down to ~1500 m). However, no significant relationship was observed between surface Chl *a* and average HNA % in the dark ocean, only the epipelagic layer showing a significant positive relationship (Fig. 3b, Table S3).

The average cell volume (Fig. 2c) of prokaryotic communities was lowest in surface waters, with values of 0.030-0.060 μm^3 that were rather uniform along the entire cruise section, resulting in no significant relationship with Chl *a* concentrations (Fig. 3c, Table S3). Cell volumes overall increased with depth, although with clear latitudinal differences: in stations 1-7 and 12-13, volumes of >0.065 μm^3 were reached between 300-700 m depth, while in stations 8-11 such volumes were only present below 1200-1500 m. These latitudinal differences in deep waters were reflected in significant negative relationships with surface Chl *a* concentrations, both in the meso- and bathypelagic layers (Fig. 3c, Table S3). This was also evident in archetype cell volumes of water masses, e.g., the Antarctic Intermediate Water of 5°C and the Subpolar Mode Water presented values of 0.0710 ± 0.0035 and 0.0582 ± 0.0034 μm^3, respectively (Table 2). The highest average cell volumes were observed in bathypelagic waters of stations 1-7, most samples exceeding 0.090 μm^3 (some reaching >0.15 μm^3)

The fraction of viable cells (presenting intact cell membranes) was highest in epipelagic waters with widespread >70% contributions to the total number of detected cells and peaks exceeding 90% (Fig. 2d). Viability however consistently decreased with depth along the section (log-log slopes of -0.916 ± 0.048, Table 1), following the opposite pattern to cell volume. Stations 1-7 showed quick decreases in the abundance of viable cells (log-log slope = -0.950 ± 0.050; Table 1, Fig. S3), with proportions <70% immediately below the epipelagic layer, and <50% below ~1000 m in many samples, especially in stations 1-4. In stations 8-12 on the contrary (log-log slope in 'Guinea Dome-Cape Blanc' = -0.868 ± 0.058; Table 1, Fig. S3), viabilities

above 70% were measured down to ~1000 m. This produced archetype viabilities of 61.4 ± 2.4 % and 76.1 ± 2.4 for the Antarctic Intermediate Water of 5°C and the Subpolar Mode Water, respectively. This gradient along the section was consistent down to 3500 m, were values of 35-50% in stations 1-2 contrasted with >70% in samples close to the bottom at stations 10-12. These changes yielded significant positive relationships between surface Chl *a* and cell viability in the meso- and bathypelagic waters (Fig. 3d, Table S3). Epipelagic viability also displayed a positive relationship with surface Chl *a* (Fig. 3d), although it was not significant.

Leucine incorporation rates (Fig. 4a), a measure of prokaryotic activity, decreased drastically with depth (log-log slope = -1.261 ± 0.097; Table 1). Overall leucine incorporation rates were greater than 150 pmol Leu·L^{-1}·d^{-1} in the upper 50 m of the water column, with peaks at stations 4 (564 pmol Leu·L^{-1}·d^{-1}), 7 (420 pmol Leu·L^{-1}·d^{-1}

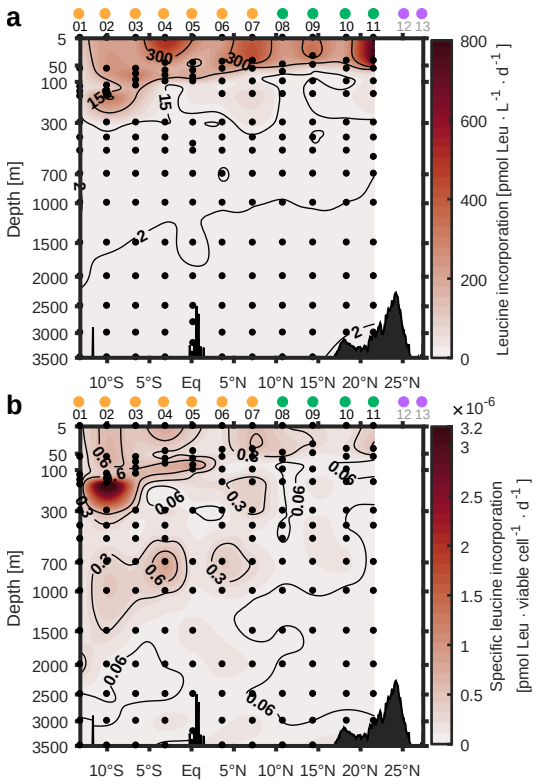

Figure 4. Prokaryotic activity as leucine incorporation rates. (a) Bulk leucine incorporation rate, (b) Specific leucine incorporation rate per viable cell (contour lines are in 10^{-6}). Black dots represent locations of collected samples and resulting estimates. Dots on top of station numbers represent station groups: 'South' (light orange), 'Guinea Dome-Cape Blanc' (green), 'North' (violet). Data interpolation was performed with DIVA in Matlab (R2017a).

^{1}), 9 (377 pmol Leu·L^{-1}·d^{-1}), and 11 (823 pmol Leu·L^{-1}·d^{-1}). Rates decreased to 15 pmol Leu·L^{-1}·d^{-1} by 300 m and to 2 pmol Leu·L^{-1}·d^{-1} by 1000-1500 m depth. No consistent latitudinal differences were observed in mesopelagic samples, but overall leucine incorporation rates in the bathypelagic were higher in the south, with the exception of samples close to the bottom at stations 9-11. Log-log slopes vs. depth in 'South' and 'Guinea Dome-Cape Blanc' stations, although different, had considerable confidence intervals (-1.331 ± 0.122 and -1.148 ± 0.154, respectively; Table 1), and no significant relationships were found between leucine incorporation rates and surface Chl *a* concentrations (Fig. S5a, Table S3).

Specific leucine incorporation rates per viable cell (Fig. 4b) tended to be higher in the southern end of the section. In epipelagic waters specific rates were widely above $0.3{\cdot}10^{-6}$ pmol Leu·viable $cell^{-1}$·d^{-1} in stations 1-5, with multiple samples exceeding 0.6 pmol Leu·viable $cell^{-1}$·d^{-1}. In stations 8-11 values were lower and barely exceed $0.3{\cdot}10^{-6}$ pmol Leu·viable $cell^{-1}$·d^{-1}. In mesopelagic samples specific leucine incorporation rates per viable cell ranged between $(0.06\text{-}0.3){\cdot}10^{-6}$ pmol Leu·viable $cell^{-1}$·d^{-1} and were slightly greater in the south, although no clear differences were observed between water masses (Subpolar Mode Water = $(0.103 \pm 0.029){\cdot}10^{-6}$ and Antarctic Intermediate Water of 5°C = $(0.228 \pm 0.070){\cdot}10^{-6}$ pmol Leu·viable $cell^{-1}$·d^{-1}, Table 2). As bulk leucine incorporation rates, viable cell specific rates in bathypelagic waters tended to increase towards the south, overall exceeding $0.06{\cdot}10^{-6}$ pmol Leu·viable $cell^{-1}$·d^{-1}, while stations 8-11 mostly showed specific rates below $0.06{\cdot}10^{-6}$ pmol Leu·viable $cell^{-1}$·d^{-1}, except samples close to the bottom. Average viable cell specific rates in bathypelagic waters did show a (weak) negative relationship with surface Chl *a* (Fig. S5b, Table S3).

Discussion

The oceanographic section studied encompassed widely diverse environments along the tropical and subtropical Atlantic, from the oligotrophic tropical south Atlantic to the highly productive waters of the Cape Blanc area in the Northwest African upwelling system (Fig. 1a; Carr and Kearns 2003). The transition from waters of low to high productivity was well captured by the increasing concentrations of Chl *a* measured in epipelagic waters from stations 1 to 11, along with a shoaling of the DCM (Fig. 1b). In a companion work with data collected during the same cruise, we report intense fluorescence signals of protein-like dissolved organic matter at stations 8, 9, 11 and 12 for the entire water column (see details in **Chapter 4**). These findings

suggest vertical transport of organic matter from the surface into the dark ocean in the Guinea Dome-Cape Blanc region, in agreement with previous studies with sediment traps reporting high sinking particle fluxes (Fischer et al. 2020).

Observed prokaryotic abundances (Fig. 2a) were in the range of those previously described for eastern tropical and subtropical North Atlantic for epipelagic (>10^5 cells·mL^{-1}), mesopelagic (10^4-10^5 cells·mL^{-1}) and bathypelagic (10^4 cells·mL^{-1}) waters (Varela et al. 2008; Baltar et al. 2010b, 2012). The vertical decrease in cell abundances of the different prokaryotic groups (total, LNA, HNA), evaluated with log-log relationship vs. depth (Table 1), yielded slope values that were in the range of those reported in the literature (Gasol et al. 2009; Arístegui et al. 2009). HNA and LNA groups had markedly different slopes, which resulted in increases in the relative contribution of HNA cells with depth. Prokaryotic cell volume increase with depth has also been documented before, although our estimated cell volumes were higher (La Ferla et al. 2012, 2015) or lower (Morán et al. 2015) than previous observations. The increases in the proportion of HNA prokaryotes and cell volume with depth agree with previous studies (Van Wambeke et al. 2011; La Ferla et al. 2012), and can be interpreted as an increase in the contribution of larger prokaryotic cells, with bigger genomes (Bouvier et al. 2007). The homogeneous profile of high % of HNA cells (>60%) observed close to Cape Blanc (Fig. 2b, station 11) was similar to the profile reported by Gasol et al. (2009) for the same area and points to the presence of copiotrophic taxa in the epipelagic waters mostly influenced by the upwelling system. HNA cells have also been related to higher activity (Servais et al. 2003), which would go in line with the very high leucine incorporation measured in station 11 (Fig. 4a).

Descriptions of prokaryotic viability in the deep ocean are scarce and this is, to the authors knowledge, the most extensive study of cell viabilities in a large-scale sampling effort that includes bathypelagic samples. The relative contribution of viable prokaryotes to total counts in epipelagic waters (>80%, Fig. 2d) was similar to prior estimates within the eastern subtropical North Atlantic (Baltar et al. 2012). A previous study in the eastern subtropical Atlantic showed a positive relationship between epipelagic viability of prokaryotes and the release of organic matter by senescent phytoplankton, which was higher in oligotrophic waters (Lasternas and Agustí 2014). Here lower values were observed in waters with low productivity, although no significant linear relationship was found between cell viability in epipelagic waters and surface Chl *a*. Out of the epipelagic layer, trends of vertical decreases in prokaryotic viability have been documented, with viability values as low as 10-40% (Gasol et al. 2009; Baltar et al. 2012), comparable to the minimum values

observed here in the southern end of the transect. This vertical trend points to harsher conditions (low temperature, high pressure, reduced DOM availability) for prokaryotes in deep ocean environments (Herndl and Reinthaler 2013). While depressurisation during sample collection could have an effect in cell viability, we considered this effect to be minimal as samples were analysed before the change in pressure could have had a significant negative impact on cell membranes (Quéric et al. 2004, see Materials and methods section for further information).

In the deep ocean, cell viability, abundance and volume displayed latitudinal trends matching surface productivity gradients (as defined by Chl *a* concentrations; Fig. 3). The tendency to more abundant, more viable and smaller cells in the mesopelagic and bathypelagic layers under highly productive surface waters with important vertical flux of particles (Fischer et al. 2020) suggests a remarkable effect of sinking particles in the prokaryotic communities of the dark ocean. While a link between surface productivity and abundance/biomass of deep ocean prokaryotes has been found before (Hansell and Ducklow 2003; Yokokawa et al. 2013), our results demonstrate that surface productivity also exerts a major imprint on their physiological status. The effect of vertical connectivity would be twofold, including the transport of both resources and microorganisms. Sinking particles would introduce organic matter, including its release by senescent phytoplankton cells (Lasternas and Agustí 2014; Agustí et al. 2015), fuelling prokaryotes and allowing them to attain higher viabilities. Besides the well-known high particle fluxes in the Northwest African upwelling area (Fischer et al. 2020), this vertical input was further suggested by the correspondence between meso- and bathypelagic protein-like fluorescent dissolved organic matter (resembling peak T, Coble 1996) and surface productivity proxies in the study area (see **Chapter 4**), in a similar manner to other oceanic regions (Ruiz-González et al. 2020). Moreover, the sinking particles could also act as vectors, transporting particle-attached prokaryotes from epipelagic communities to the dark ocean, yielding communities more similar to each other than in regions with low vertical transport (Mestre et al. 2018). This could also help explain the smaller size of deep ocean prokaryotes under the more productive stations. The changes in viability of deep ocean prokaryotes under different productivity regimes have important implications. The assessment of the physiological status of individual cells (whether they are dead or alive, or displaying various degrees of activity) is key to correctly understand processes at the community level (Sebastián and Gasol 2019). Our estimates indicate that the metabolic processes in meso- and bathypelagic waters are not driven by the entire community, only by a varying fraction of it, which will depend on the surface

productivity regime. This underlines the importance of considering a wide oceanographic context when studying dark ocean prokaryotes.

The magnitude of leucine incorporation rates in the epipelagic (10^{1}-10^{2} pmol Leu·L^{-1}·d^{-1}), mesopelagic (10^{0}-10^{1} pmol Leu·L^{-1}·d^{-1}) and bathypelagic layers (10^{-1}-10^{0} pmol Leu·L^{-1}·d^{-1}) was in the same range as previous studies in the eastern subtropical and tropical North Atlantic (Varela et al. 2008; De Corte et al. 2010). The log-log slope for the entire dataset was also similar to other slopes reported in the literature for the global ocean (Arístegui et al. 2009). An exception to the decreasing rates of leucine incorporation with depth was found in samples close to the bottom at stations 9-11, which showed relatively high rates that might have been fuelled by resuspension (Fischer et al. 2009; Ziervogel et al. 2016) or by the arrival of fast sinking particles (Boeuf et al. 2019). We found absent (for bulk rates) or negative (for cell specific rates in the bathypelagic) relationships between surface productivity and leucine incorporation in the dark ocean (Fig. S5, Table S3), manifesting that, while the vertical connection between surface productivity and prokaryotic viability was evident, the connection with heterotrophic activity was unclear. These findings are in line with previous studies that found positive but weak relationships between vertical particle flux and prokaryotic production in the mesopelagic, but none in the bathypelagic (Yokokawa et al. 2013).

The unclear relationship between surface productivity and prokaryotic heterotrophic activity may be due to methodological limitations, since prokaryotic production is estimated from metabolic rates, but sometimes metabolism might not be directed to cell-growth but to cell maintenance (Carlson et al. 2007; Giering and Evans 2022). Particularly in hostile environmental conditions, with low resources and energy supply, prokaryotes have been found to achieve lower growth efficiencies (del Giorgio and Cole 1998). In these situations, resources and energy are directed in greater proportions to the maintenance of cell structures and functionality, instead of biomass production and growth (Carlson et al. 2007). The bathypelagic waters of stations 1-4 showed minimum cell viability ratios, in agreement with expected harsher conditions due to potential low external inputs of organic substrates in these oligotrophic waters. The relatively high specific leucine incorporation rates in the deep waters of these southern stations might thus be linked to metabolism directed to maintenance, rather than growth and cell division. Moreover, larger prokaryotes have greater metabolic requirements than smaller ones (del Giorgio and Gasol 2008), and we indeed found that high average values of specific leucine incorporation in the bathypelagic were associated with high average cell sizes (Fig. 2, 3 and S6). There is

increasing evidence that leucine-to-carbon conversion factors are highly variable in the ocean, decreasing with depth and increasing with water productivity (del Giorgio and Cole 1998; Orta-Ponce et al. 2021; Giering and Evans 2022). Considering these trends, the negative relationship between leucine incorporation in bathypelagic samples and surface productivity would not directly translate to prokaryotic heterotrophic production, as lower conversion factors could be expected in the southern stations relative to the Guinea Dome-Cape Blanc area. This would potentially result in higher production rates under the productive waters, which would agree with the other trends of increased viability and cell numbers. Thus, variations in the leucine-to-carbon conversion factors probably explain the lack of relationship between surface productivity and prokaryotic heterotrophic activity (as measured by leucine incorporation) in the dark realm.

Conclusions

We studied the abundance, cell size, viability and heterotrophic metabolism of prokaryotic communities from surface down to 3500 m depth along a primary productivity gradient in the subtropical and tropical Atlantic. Our results show that deeper waters tended to harbour communities with reduced cell concentrations and viability, but larger cell sizes and high nucleic acid content. The trends were coupled with changes along surface productivity: waters under highly productive areas presented higher cell counts and viability, and lower average cell sizes, than waters under oligotrophic zones. These relationships were significant down to the bathypelagic zone (and were reflected in the archetype values of water masses), highlighting the extent of the vertical connectivity along the water column. The heterotrophic metabolism, however, was not equally affected: while bulk leucine incorporation rates displayed no significant relationship with surface productivity, cell specific rates showed a negative relationship in bathypelagic waters. Energy and resource allocation to cellular maintenance processes under adverse environmental conditions (likely resulting in low conversion of the incorporated leucine into biomass), and dependence of metabolic requirements on cell size could influence the conversion of leucine incorporation into carbon production. Our work provides further evidence on the link between the productivity regime of surface waters and dark ocean processes. The effect of surface productivity on the viability of dark ocean prokaryotes is particularly relevant, as the physiological status of the prokaryotes will determine who drives metabolic processes at the community level and, hence, dark ocean biogeochemical cycles.

Supplementary material

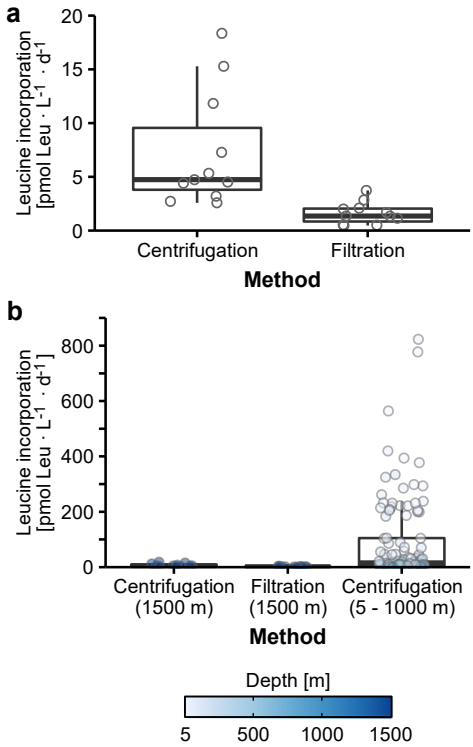

Figure S1. Comparison of leucine incorporation rates based on centrifugation and filtration methods. (a) Comparison of the leucine incorporation rates for the samples collected at 1500 m, where both methods were used. (b) Comparison of the same results but including the leucine incorporation rates for the upper 1000 m for perspective.

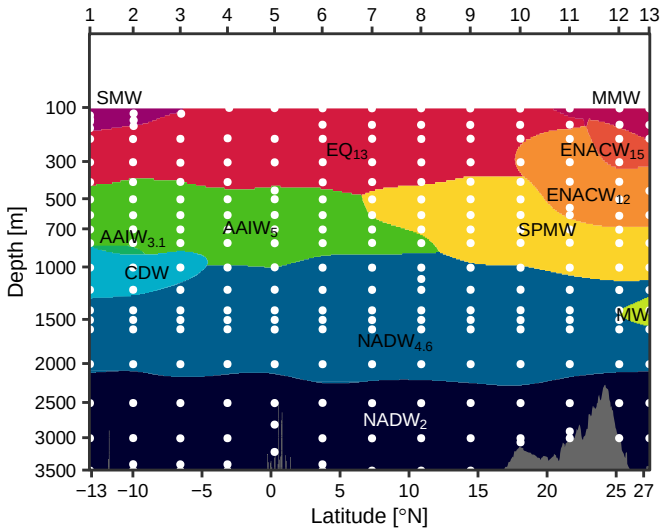

Figure S2. Distribution of the water masses in the study section. Acronyms are as follows: Salinity Maximum Water (SMW), Madeira Mode Water (MMW), Equatorial Water (EQ_{13}), Eastern North Atlantic Central Water of 15°C ($ENACW_{15}$) and 12°C ($ENACW_{12}$), Subpolar Mode Water (SPMW), Mediterranean Water (MW), Antarctic Intermediate Water of 5°C ($AAIW_5$) and 3.1°C ($AAIW_{3.1}$), Circumpolar Deep Water (CDW) and North Atlantic Deep Water of 4.6°C ($NADW_{4.6}$) and 2°C ($NADW_2$). Approximate area in which each water mass has their highest contribution is shown. Dots represent samples of the physical and geochemical variables included in the optimum multiparameter analysis. Note that the vertical scale is square root-transformed to allow for a better visualisation of the results. Numbers on top correspond to stations in Fig. 1 in the main text. Data interpolation was performed with DIVA in Matlab (R2017a).

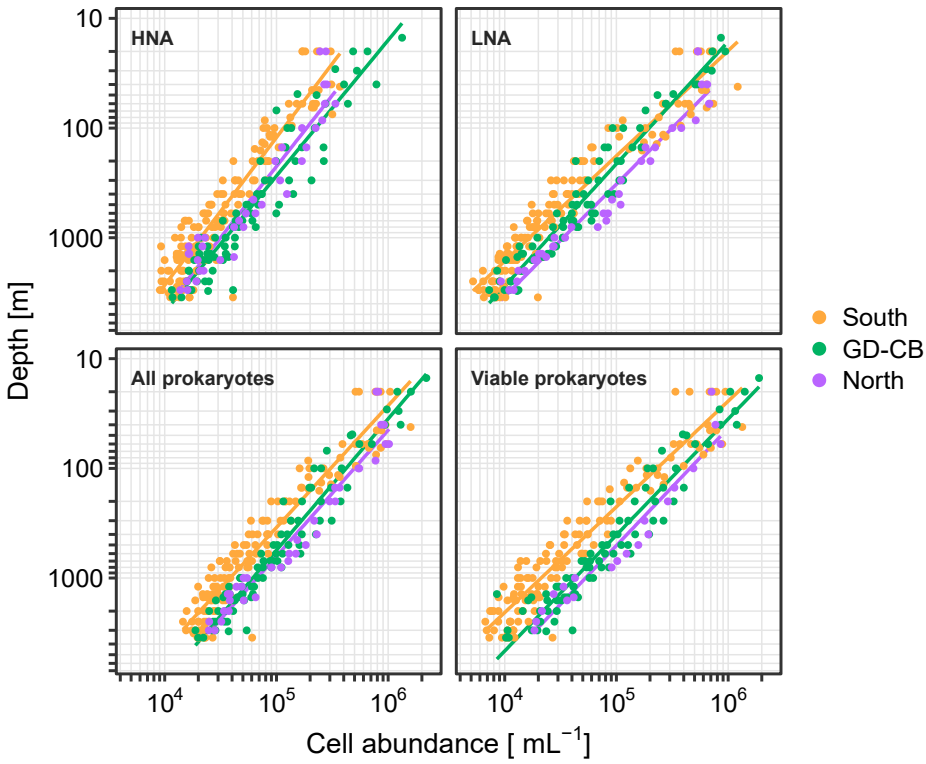

Figure S3. Log-log regressions of prokaryotic abundances vs depth (for samples of ≥10 m), by station group: 'South' (stations 1-7; light orange), 'GD-CB' (Guinea Dome-Cape Blanc, 8-11; green) and 'North' (12-13, if available; violet). The regression parameters can be found in Table 1 in the main text.

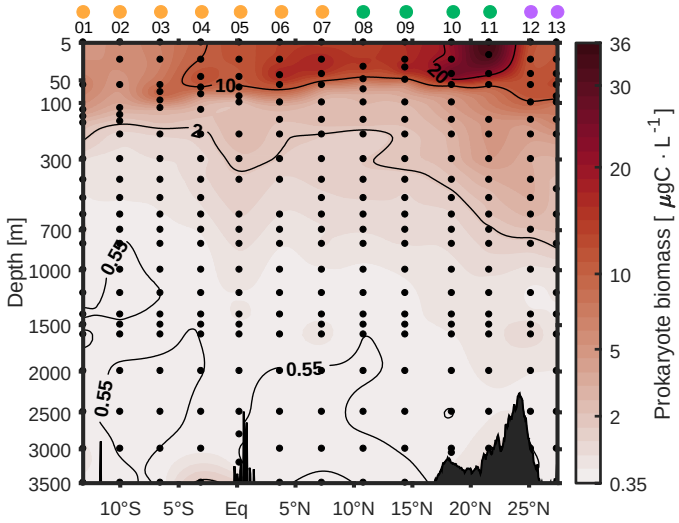

Figure S4. Biomass of prokaryotes. Black dots represent collected samples. Dots on top of station numbers represent station groups: 'South' (light orange), 'Guinea Dome-Cape Blanc' (green), 'North' (violet). Data interpolation was performed with DIVA in Matlab (R2017a).

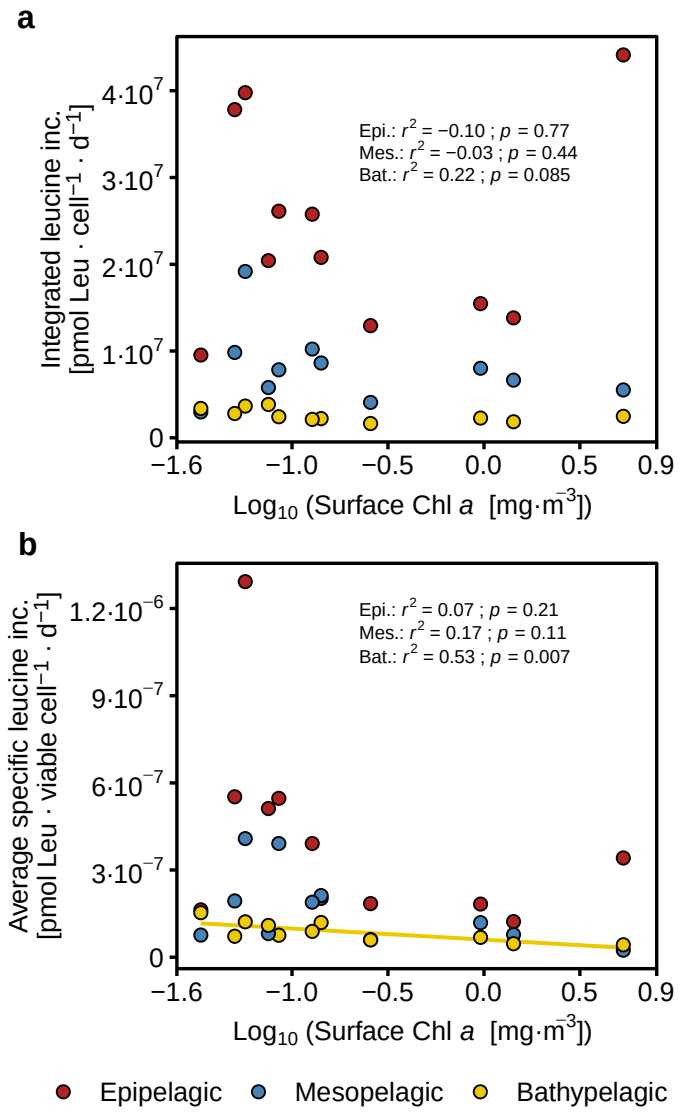

Figure S5. Linear regressions between surface Chl *a* concentrations (averaged within the first 20 m, as proxy for productivity) and metabolic variables: a) integrated leucine incorporation rate, b) average viable cell specific leucine incorporation rate. Regressions estimated separately for epipelagic (≤200 m), mesopelagic (>200 m and ≤1000 m) and bathypelagic (>1000 m and ≤3000 m) layers. Regression lines are only shown for significant ($p < 0.05$) results. Regression parameters are presented in Table S3.

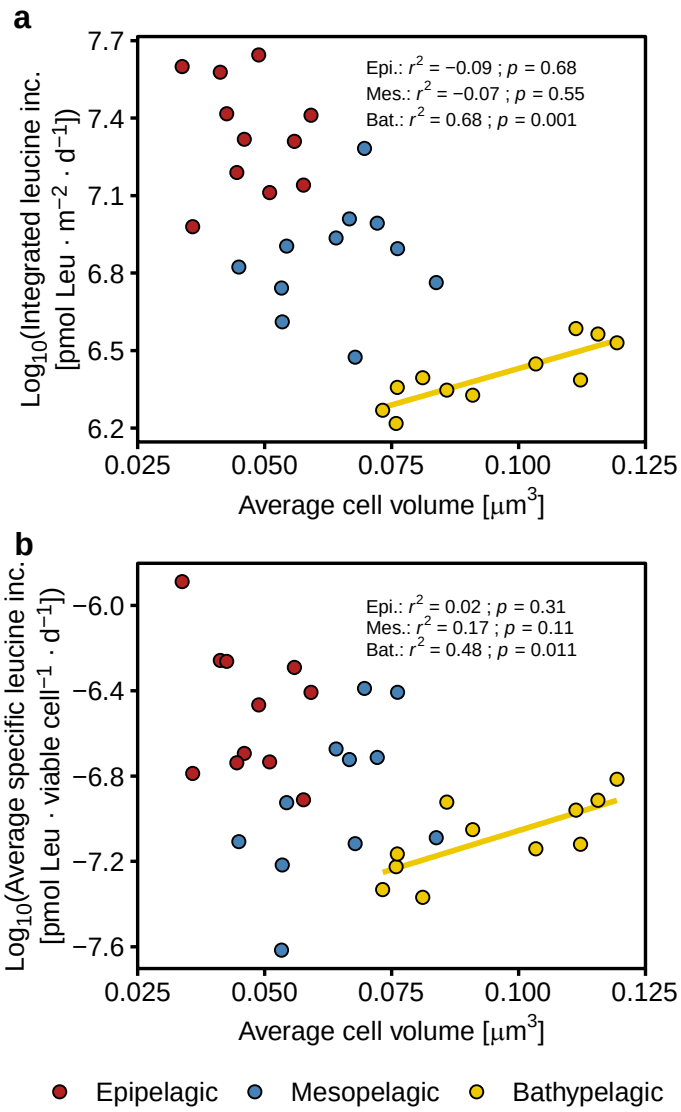

Figure S6. Linear regression between average cell volume and a) integrated leucine incorporation rate, and b) average viable cell specific leucine incorporation, estimated separately for epipelagic (≤200 m), mesopelagic (>200 m and ≤1000 m) and bathypelagic (>1000 m and ≤3000 m) layers. Regression lines are only shown for significant ($p < 0.05$) results.

Table S1. Water types intercepted during the MAFIA cruise, brief description of source point where they belong to, characteristics, and some references with more details about their origin and circulation.

Name	Source	Characteristics	SWT	References
Salinity Maximum Water	Tropical area (12–22°S)	Warmest (27°C) mode water in the SAO, formed by evaporation, transported westward to America with SEC	SMW	Worthington (1976), Stramma and England (1999), Mémery et al. (2000)
Equatorial Atlantic Central Water (13°C)	Eastern South Atlantic, near Namibia	Formed by mixing of low salinity water outcropped further south with overlying high salinity water. Transported by the South Equatorial current to the Equator and along the Brazilian coast by the North Brazil current.	EQ_{13}	Tsuchiya (1986)
Madeira Mode Water	Madeira Mode Water	Mode water formed near the Madeira Island	MMW	Siedler et al. (1987)
Eastern North Atlantic Central water	Eastern North Atlantic Subtropical gyre	Mode waters defining the upper (15°C) and lower (12°C) limits of the subtropical ENACW formed between the area of the Azores and Portugal currents.	$ENACW_{15}$ $ENACW_{12}$	Harvey (1982), Pollard and Pu (1985), Ríos et al. (1992), Álvarez-Salgado et al. (2013)
Mediterranean Water	Gulf of Cadiz	Formed in the Gulf of Cadiz by entrainment of Eastern North Atlantic Central water on the high-salinity outflow from the Mediterranean Sea, spreads at 800–1300 m, S > 36 and θ ~ 11–12 °C.	MW	Zenk (1975), Ambar and Howe (1979), Castro et al. (1998), Álvarez-Salgado et al. (2013)
Antarctic Intermediate Water	Pacific Ocean north of the Sub-Antarctic Front & Malvinas-Brazil Confluence.	Formed north of the Subantarctic Front (SAF) and east of the Drake Passage by ventilation of the Subantarctic Mode Water (SAMW) formed in the Southeast Pacific.	$AAIW_{5.0}$ $AAIW_{3.1}$	McCartney (1982), Piola and Gordon (1989), Talley (1996)
Circumpolar Deep Water	Antarctic Circumpolar Current	Also named Common Water, formed by mixing in the Antarctic Circumpolar current of mid-depth Indian, Pacific and Atlantic deep water with WSDW and NADW.	CDW	Montgomery (1958), Georgi (1981), Broecker et al. (1985)
North Atlantic Deep Water	North Atlantic Ocean	Carried into the South Atlantic by the Deep Western Boundary Current (DWBC). Characterized by salinity maximum and silicate minimum (4.6°C); and θ–S discontinuity and oxygen maximum (2.0 °C). Defined at their entry in the South Atlantic Ocean off South America.	$NADW_{4.6}$ $NADW_{2.0}$	Wüst (1935), Speer and McCartney (1992), Friedrichs et al. (1994)

Table S2. Thermohaline and chemical characteristics (average value ± uncertainty) of the water types (WT) introduced in the OMP analysis of the water masses intercepted during the MAFIA cruise. Water mass acronyms stand for: Salinity Maximum Water (SMW), Madeira Mode Water (MMW), Equatorial Water (EQ_{13}), Eastern North Atlantic Central Water of 15°C ($ENACW_{15}$) and 12°C ($ENACW_{12}$), Subpolar Mode Water (SPMW), Mediterranean Water (MW), Antarctic Intermediate Water of 5°C ($AAIW_5$) and 3.1°C ($AAIW_{3.1}$), Circumpolar Deep Water (CDW) and North Atlantic Deep Water of 4.6°C ($NADW_{4.6}$) and 2°C ($NADW_2$).

WT	θ_i (°C)	S_i	SiO_4H_{4i} (μmol kg^{-1})	NO_i (μmol kg^{-1})
SMW [a]	27.0 ± 0.1	37.50 ± 0.01	1.1 ± 0.5	206 ± 3
MMW [b]	20.0 ± 0.5	37.00 ± 0.04	0.4 ± 0.3	225 ± 10
EQ_{13} [a]	13.0 ± 0.1	35.20 ± 0.01	5.3 ± 0.7	315 ± 3
$ENACW_{15}$ [b]	15.3 ± 0.4	36.10 ± 0.02	2.2 ± 1.7	264 ± 8
$ENACW_{12}$ [c]	12.2 ± 0.4	35.66 ± 0.02	4.9 ± 0.2	322 ± 8
SPMW [c]	8.2 ± 0.4	35.23 ± 0.01	14.5 ± 0.4	386 ± 7
MW [c]	11.8 ± 0.1	36.50 ± 0.01	7.2 ± 0.7	304 ± 9
$AAIW_5$ [a]	5.00 ± 0.08	34.14 ± 0.01	7.0 ± 0.7	482 ± 3
$AAIW_{3.1}$ [a]	3.10 ± 0.08	34.12 ± 0.01	16.4 ± 0.7	558 ± 3
CDW [a]	1.60 ± 0.03	34.720 ± 0.003	110.6 ± 0.9	497 ± 1
$NADW_{4.6}$ [a]	4.6 ± 0.1	35.020 ± 0.005	7.3 ± 0.5	426 ± 2
$NADW_2$ [a]	2.02 ± 0.03	34.910 ± 0.003	28.2 ± 0.9	446 ± 1

[a] Álvarez et al. (2014)

[b] Álvarez and Álvarez-Salgado (2009); Lønborg and Álvarez-Salgado (2014)

[c] Pérez et al. (2001); Álvarez and Álvarez-Salgado (2009)

Table S3. Results from the regressions of cytometric and metabolic variables vs log-transformed surface Chl *a* values. Regressions were performed by layer, with integrated values for variables with units referenced to volume and averaged values otherwise. *Slope* and *Intercept* estimates are presented alongside 95% confidence intervals. r^2 is the adjusted coefficient of determination, *p* the p-value of the regression. Regressions are shown in Fig. 3, S5 and S6.

		Layer	Slope	Intercept	r^2	*p*
$Log_{10}(Chl\ a_{srf})$	Prokaryotic abundance	Epipelagic	$(3.02 \pm 1.89)\cdot10^{13}$	$(1.16 \pm 0.18)\cdot10^{14}$	0.49	0.005
		Mesopelagic	$(4.34 \pm 2.27)\cdot10^{13}$	$(1.07 \pm 0.21)\cdot10^{14}$	0.58	0.001
		Bathypelagic	$(2.29 \pm 0.69)\cdot10^{13}$	$(7.81 \pm 0.64)\cdot10^{13}$	0.81	<0.001
	HNA%	Epipelagic	13.56 ± 3.86	50.06 ± 3.58	0.83	<0.001
		Mesopelagic	1.62 ± 5.31	54.25 ± 4.91	-0.05	0.517
		Bathypelagic	1.93 ± 3.98	60.04 ± 3.69	0.01	0.309
	Cell volume	Epipelagic	0.0053 ± 0.0075	0.051 ± 0.007	0.11	0.148
		Mesopelagic	-0.013 ± 0.008	0.056 ± 0.007	0.49	0.005
		Bathypelagic	-0.020 ± 0.010	0.080 ± 0.009	0.61	<0.001
	Viability	Epipelagic	7.47 ± 7.79	87.35 ± 7.36	0.24	0.058
		Mesopelagic	13.43 ± 6.94	77.31 ± 6.56	0.62	0.002
		Bathypelagic	11.74 ± 7.25	65.13 ± 6.85	0.52	0.005
	Biomass	Epipelagic	$(5.30 \pm 2.72)\cdot10^{5}$	$(1.70 \pm 0.25)\cdot10^{6}$	0.59	0.001
		Mesopelagic	$(5.41 \pm 4.30)\cdot10^{5}$	$(1.64 \pm 0.40)\cdot10^{6}$	0.36	0.018
		Bathypelagic	$(3.08 \pm 2.14)\cdot10^{5}$	$(1.57 \pm 0.20)\cdot10^{6}$	0.43	0.009
	Leucine incorporation rate	Epipelagic	$(1.68 \pm 12.64)\cdot10^{6}$	$(2.54 \pm 1.22)\cdot10^{7}$	-0.10	0.770
		Mesopelagic	$(-1.63 \pm 4.51)\cdot10^{6}$	$(6.93 \pm 4.35)\cdot10^{6}$	-0.03	0.435
		Bathypelagic	$(-5.66 \pm 6.62)\cdot10^{5}$	$(2.22 \pm 0.64)\cdot10^{6}$	0.22	0.085
	Leucine incorporation rate per viable cell	Epipelagic	$(-1.96 \pm 3.30)\cdot10^{-7}$	$(2.71 \pm 3.19)\cdot10^{-7}$	0.07	0.212
		Mesopelagic	$(-9.41 \pm 12.13)\cdot10^{-8}$	$(1.01 \pm 1.17)\cdot10^{-7}$	0.17	0.113
		Bathypelagic	$(-3.81 \pm 2.45)\cdot10^{-8}$	$(6.06 \pm 2.36)\cdot10^{-8}$	0.53	0.007

Supplementary methods

Inorganic nutrients

Inorganic nutrients (included in the OMP analysis) were sampled from Niskin bottles with polyethylene tubes and stored at −20°C until analysis in the laboratory. The analysis was performed with a QuAAtro 39-SEAL Analytical AutoAnalyzer following Armstrong et al. (1967).

Data interpolation

Interpolations of discrete data were performed with DIVA (Troupin et al. 2012) in Matlab (R2017a). As samples were distributed along different depth scales in epipelagic/upper-mesopelagic waters relative to meso-/bathypelagic waters, the interpolation was done separately for depths 5-400 m ("upper layer") and 300-3500 m ("lower layer"), allowing to fine tune the interpolation appropriately for each depth scale. For the interpolation of the upper layer, the interpolation grid was [5:1:100 105:5:200 210:10:400], with horizontal (LX) and vertical (LY) *Length scales* being 4 and 50, respectively, and the *signal to noise ratio* (SN) 16. For the interpolation of the lower layer the grid was [300:10:1000 1050:50:3500], LX = 4, LY = 500 and SN = 16. Both grids were combined into a single one by a weighted mean of interpolated values in the common depth range (300-400 m): for 300 m, the upper grid was weighted 1 and the lower 0; for 350 m they were equally weighted 0.5; for 400 m 0 and 1, respectively; etc.

References

Agustí, S., J. I. González-Gordillo, D. Vaqué, M. Estrada, M. I. Cerezo, G. Salazar, J. M. Gasol, and C. M. Duarte. 2015. Ubiquitous healthy diatoms in the deep sea confirm deep carbon injection by the biological pump. Nat. Commun. **6**: 7608. doi:10.1038/ncomms8608

Álvarez-Salgado, X. A., M. Nieto-Cid, M. Álvarez, F. F. Pérez, P. Morin, and H. Mercier. 2013. New insights on the mineralization of dissolved organic matter in central, intermediate, and deep water masses of the northeast North Atlantic. Limnol. Oceanogr. **58**: 681–696. doi:10.4319/lo.2013.58.2.0681

Álvarez, M., and X. A. Álvarez-Salgado. 2009. Chemical tracer transport in the eastern boundary current system of the North Atlantic. Ciencias Mar. **35**: 123–139.

Álvarez, M., S. Brea, H. Mercier, and X. A. Álvarez-Salgado. 2014. Mineralization of biogenic materials in the water masses of the South Atlantic Ocean. I: Assessment and results of an optimum multiparameter analysis. Prog. Oceanogr. **123**: 1–23. doi:10.1016/j.pocean.2013.12.007

Ambar, I., and M. R. Howe. 1979. Observations of the Mediterranean outflow—I mixing in the Mediterranean outflow. Deep Sea Res. Part A. Oceanogr. Res. Pap. **26**: 535–554. doi:10.1016/0198-0149(79)90095-5

Arístegui, J., J. M. Gasol, C. M. Duarte, and G. J. Herndl. 2009. Microbial oceanography of the dark ocean's pelagic realm. Limnol. Oceanogr. **54**: 1501–1529. doi:10.4319/lo.2009.54.5.1501

Armstrong, F. A. J., C. R. Stearns, and J. D. H. Strickland. 1967. The measurement of upwelling and subsequent biological process by means of the Technicon Autoanalyzer® and associated equipment. Deep. Res. Oceanogr. Abstr. **14**: 381–389. doi:10.1016/0011-7471(67)90082-4

Baltar, F., J. Arístegui, J. M. Gasol, and G. J. Herndl. 2012. Microbial functioning and community structure variability in the mesopelagic and epipelagic waters of the subtropical northeast Atlantic Ocean. Appl. Environ. Microbiol. **78**: 3309–3316. doi:10.1128/AEM.07962-11

Baltar, F., J. Arístegui, J. M. Gasol, I. Lekunberri, and G. J. Herndl. 2010a. Mesoscale eddies: Hotspots of prokaryotic activity and differential community structure in the ocean. ISME J. **4**: 975–988. doi:10.1038/ismej.2010.33

Baltar, F., J. Arístegui, J. M. Gasol, E. Sintes, H. M. Van Aken, and G. J. Herndl. 2010b. High dissolved extracellular enzymatic activity in the deep central Atlantic ocean. Aquat. Microb. Ecol. **11**: 1998–2014. doi:10.3354/ame01377

Baltar, F., J. Arístegui, E. Sintes, J. M. Gasol, T. Reinthaler, and G. J. Herndl. 2010c. Significance of non-sinking particulate organic carbon and dark CO 2 fixation to heterotrophic carbon demand in the mesopelagic northeast Atlantic. Geophys. Res. Lett. **37**: L09602. doi:10.1029/2010GL043105

Bar-On, Y. M., R. Phillips, and R. Milo. 2018. The biomass distribution on Earth. Proc. Natl. Acad. Sci. **115**: 6506 LP – 6511. doi:10.1073/pnas.1711842115

Boeuf, D., B. R. Edwards, J. M. Eppley, and others. 2019. Biological composition and microbial dynamics of sinking particulate organic matter at abyssal depths in the oligotrophic open ocean. Proc. Natl. Acad. Sci. **116**: 11824–11832. doi:10.1073/pnas.1903080116

Bouvier, T., P. A. Del Giorgio, and J. M. Gasol. 2007. A comparative study of the cytometric characteristics of High and Low nucleic-acid bacterioplankton cells from different aquatic ecosystems. Environ. Microbiol. **9**: 2050–2066. doi:10.1111/j.1462-2920.2007.01321.x

Boyd, P. W., H. Claustre, M. Levy, D. A. Siegel, and T. Weber. 2019. Multi-faceted particle pumps drive carbon sequestration in the ocean. Nature **568**: 327–335. doi:10.1038/s41586-019-1098-2

Brandt, P., V. Hormann, B. Bourlès, J. Fischer, F. A. Schott, L. Stramma, and M. Dengler. 2008. Oxygen tongues and zonal currents in the equatorial Atlantic. J. Geophys. Res. Ocean. **113**. doi:10.1029/2007JC004435

Broecker, W. S. 1974. "NO", a conservative water-mass tracer. Earth Planet. Sci. Lett. **23**: 100–107. doi:10.1016/0012-821X(74)90036-3

Broecker, W. S., T. Takahashi, and T. Takahashi. 1985. Sources and flow patterns of deep-ocean waters as deduced from potential temperature, salinity, and initial phosphate concentration. J. Geophys. Res. Ocean. **90**: 6925–6939. doi:10.1029/JC090iC04p06925

Calvo-Díaz, A., and X. A. G. Morán. 2006. Seasonal dynamics of picoplankton in shelf waters of the southern Bay of Biscay. Aquat. Microb. Ecol. **42**: 159–174. doi:10.3354/ame042159

Carlson, C. A., P. A. del Giorgio, and G. J. Herndl. 2007. Microbes and the Dissipation of Energy and Respiration: From Cells to Ecosystems. Oceanography **20**: 89–100.

Carr, M. E., and E. J. Kearns. 2003. Production regimes in four Eastern Boundary Current systems. Deep-Sea Res. Part II Top. Stud. Oceanogr. **50**: 3199–3221. doi:10.1016/j.dsr2.2003.07.015

Castro, C. G., F. F. Pérez, S. E. Holley, and A. F. Ríos. 1998. Chemical characterisation and modelling of water masses in the Northeast Atlantic. Prog. Oceanogr. **41**: 249–279. doi:10.1016/S0079-6611(98)00021-4

Catalá, T. S., I. Reche, A. Fuentes-Lema, and others. 2015. Turnover time of fluorescent dissolved organic matter in the dark global ocean. Nat. Commun. **6:5986**. doi:10.1038/ncomms6986

Coble, P. G. 1996. Characterization of marine and terrestrial DOM in seawater using excitation-emission matrix spectroscopy. Mar. Chem. **51**: 325–346. doi:10.1016/0304-4203(95)00062-3

De Corte, D., E. Sintes, C. Winter, T. Yokokawa, T. Reinthaler, and G. J. Herndl. 2010. Links between viral and prokaryotic communities throughout the water column in the (sub)tropical Atlantic Ocean. ISME J. **4**: 1431–1442. doi:10.1038/ismej.2010.65

Falcioni, T., S. Papa, and J. M. Gasol. 2008. Evaluating the flow-cytometric nucleic acid double-staining protocol in realistic situations of planktonic bacterial death. Appl. Environ. Microbiol. **74**: 1767–79. doi:10.1128/AEM.01668-07

La Ferla, R., G. Maimone, M. Azzaro, F. Conversano, C. Brunet, A. S. Cabral, and R. Paranhos. 2012. Vertical distribution of the prokaryotic cell size in the Mediterranean Sea. Helgol. Mar. Res. **66**: 635–650. doi:10.1007/s10152-012-0297-0

La Ferla, R., G. Maimone, A. Lo Giudice, F. Azzaro, A. Cosenza, and M. Azzaro. 2015. Cell size and other phenotypic traits of prokaryotic cells in pelagic areas of the Ross Sea (Antarctica). Hydrobiologia **761**: 181–194. doi:10.1007/s10750-015-2426-7

Fischer, G., S. Neuer, S. Ramondenc, and others. 2020. Long-Term Changes of Particle Flux in the Canary Basin Between 1991 and 2009 and Comparison to Sediment Trap Records Off Mauritania. Front. Earth Sci. **8**: 280. doi:10.3389/feart.2020.00280

Fischer, G., C. Reuter, G. Karakas, N. Nowald, and G. Wefer. 2009. Offshore advection of particles within the Cape Blanc filament, Mauritania: Results from observational and modelling studies. Prog. Oceanogr. **83**: 322–330. doi:10.1016/j.pocean.2009.07.023

Friedrichs, M. A. M., M. S. McCartney, and M. M. Hall. 1994. Hemispheric asymmetry of deep water

transport modes in the western Atlantic. J. Geophys. Res. Ocean. **99**: 25165–25179. doi:10.1029/94JC02087

Gasol, J. M., L. Alonso-Sáez, D. Vaqué, F. Baltar, M. L. Calleja, C. M. Duarte, and J. Arístegui. 2009. Mesopelagic prokaryotic bulk and single-cell heterotrophic activity and community composition in the NW Africa-Canary Islands coastal-transition zone. Prog. Oceanogr. **83**: 189–196. doi:10.1016/j.pocean.2009.07.014

Georgi, D. T. 1981. On the relationship between the large-scale property variations and fine structure in the Circumpolar Deep Water. J. Geophys. Res. **86**: 6556–6566. doi:10.1029/JC086iC07p06556

Giering, S. L. C., and C. Evans. 2022. Overestimation of prokaryotic production by leucine incorporation—and how to avoid it. Limnol. Oceanogr. **67**: 726–738. doi:10.1002/lno.12032

del Giorgio, P. A., and J. J. Cole. 1998. Bacterial growth efficiency in natural aquatic systems. Annu. Rev. Ecol. Syst. **29**: 503–541. doi:10.1146/annurev.ecolsys.29.1.503

del Giorgio, P. A., and J. M. Gasol. 2008. Physiological Structure and Single-Cell Activity in Marine Bacterioplankton, p. 243–298. *In* D.L. Kirchman [ed.], Microbial Ecology of the Oceans. John Wiley & Sons.

Guidi, L., L. Stemmann, G. A. Jackson, F. Ibanez, H. Claustre, L. Legendre, M. Picheral, and G. Gorskya. 2009. Effects of phytoplankton community on production, size, and export of large aggregates: A world-ocean analysis. Limnol. Oceanogr. **54**: 1951–1963. doi:10.4319/lo.2009.54.6.1951

Hansell, D. A., and H. W. Ducklow. 2003. Bacterioplankton distribution and production in the bathypelagic ocean: Directly coupled to particulate organic carbon export?,. Limnol. Oceanogr. **48**: 150–156. doi:10.4319/lo.2003.48.1.0150

Harvey, J. 1982. θ-S relationships and water masses in the eastern North Atlantic. Deep Sea Res. A **29**: 1021–1033. doi:10.1016/0198-0149(82)90025-5

Herndl, G. J., and T. Reinthaler. 2013. Microbial control of the dark end of the biological pump. Nat. Geosci. **6**: 718–724. doi:10.1038/ngeo1921

Kirchman, D., E. K'nees, and R. Hodson. 1985. Leucine incorporation and its potential as a measure of protein synthesis by bacteria in natural aquatic systems. Appl. Environ. Microbiol. **49**: 599–607. doi:10.1128/AEM.67.4.1775-1782.2001

Lasternas, S., and S. Agustí. 2014. The percentage of living bacterial cells related to organic carbon release from senescent oceanic phytoplankton. Biogeosciences **11**: 6377–6387. doi:10.5194/bg-11-6377-2014

Lønborg, C., and X. A. Álvarez-Salgado. 2014. Tracing dissolved organic matter cycling in the eastern boundary of the temperate North Atlantic using absorption and fluorescence spectroscopy. Deep Sea Res. Part I Oceanogr. Res. Pap. **85**: 35–46. doi:10.1016/j.dsr.2013.11.002

McCartney, M. S. 1982. The subtropical recirculation of mode waters. J. Mar. Res. **40**, **Supple**: 427–464.

Mémery, L., M. Arhan, X. A. Alvarez-Salgado, M.-J. Messias, H. Mercier, C. G. Castro, and A. F. Rios. 2000. The water masses along the western boundary of the south and equatorial Atlantic. Prog. Oceanogr. **47**: 69–98. doi:10.1016/S0079-6611(00)00032-X

Mestre, M., C. Ruiz-González, R. Logares, C. M. Duarte, J. M. Gasol, and M. M. Sala. 2018. Sinking particles promote vertical connectivity in the ocean microbiome. Proc. Natl. Acad. Sci. U. S. A.

115: E6799–E6807. doi:10.1073/pnas.1802470115

Montgomery, R. B. 1958. Water characteristics of Atlantic Ocean and of world ocean. Deep Sea Res. **5**: 134–148. doi:10.1016/0146-6313(58)90004-2

Moran, M. A. 2015. The global ocean microbiome. Science, **350**: aac8455. doi:10.1126/science.aac8455

Morán, X. A. G., L. Alonso-Sáez, E. Nogueira, and others. 2015. More, smaller bacteria in response to ocean's warming? Proc. R. Soc. B Biol. Sci. **282**: 20150371. doi:10.1098/rspb.2015.0371

Norland, S. 1993. The relationship between biomass and volume of bacteria, p. 303–307. *In* P.F. Kemp, B.F. Sherr, E.B. Sherr, and J.J. Cole [eds.], Handboook of methods in aquatic microbial ecology. Lewis Publishers.

Orta-Ponce, C. P., T. Rodríguez-Ramos, M. Nieto-Cid, E. Teira, E. Guerrero-Feijóo, A. Bode, and M. M. Varela. 2021. Empirical leucine-to-carbon conversion factors in north-eastern Atlantic waters (50–2000 m) shaped by bacterial community composition and optical signature of DOM. Sci. Rep. **11**: 24370. doi:10.1038/s41598-021-03790-y

Park, C. B., and D. S. Clark. 2002. Rupture of the cell envelope by decompression of the deep-sea methanogen Methanococcus jannaschii. Appl. Environ. Microbiol. **68**: 1458–1463. doi:10.1128/AEM.68.3.1458-1463.2002

Pérez, F. F., L. Mintrop, O. Llinás, and others. 2001. Mixing analysis of nutrients, oxygen and inorganic carbon in the Canary Islands region. J. Mar. Syst. **28**: 183–201. doi:10.1016/S0924-7963(01)00003-3

Piola, A. R., and A. L. Gordon. 1989. Intermediate waters in the southwest South Atlantic. Deep Sea Res. Part A. Oceanogr. Res. Pap. **36**: 1–16. doi:10.1016/0198-0149(89)90015-0

Pollard, R. T., and S. Pu. 1985. Structure and circulation of the Upper Atlantic Ocean northeast of the Azores. Prog. Oceanogr. **14**: 443–462. doi:10.1016/0079-6611(85)90022-9

Quéric, N.-V., T. Soltwedel, and W. E. Arntz. 2004. Application of a rapid direct viable count method to deep-sea sediment bacteria. J. Microbiol. Methods **57**: 351–367. doi:10.1016/j.mimet.2004.02.005

R Core Team. 2019. R: A language and environment for statistical computing. R Foundation for Statistical Computing, Vienna, Austria. URL https://www.R-project.org/.

Ríos, A. F., F. F. Pérez, and F. Fraga. 1992. Water masses in the upper and middle North Atlantic Ocean east of the Azores. Deep Sea Res. Part A. Oceanogr. Res. Pap. **39**: 645–658. doi:10.1016/0198-0149(92)90093-9

Ruiz-González, C., M. Mestre, M. Estrada, and others. 2020. Major imprint of surface plankton on deep ocean prokaryotic structure and activity. Mol. Ecol. **29**: 1820–1838. doi:10.1111/mec.15454

Santana-Falcón, Y., E. Mason, and J. Arístegui. 2020. Offshore transport of organic carbon by upwelling filaments in the Canary Current System. Prog. Oceanogr. **186**: 102322. doi:10.1016/j.pocean.2020.102322

Sebastián, M., and J. M. Gasol. 2019. Visualization is crucial for understanding microbial processes in the ocean. Philos. Trans. R. Soc. B Biol. Sci. **374**: 20190083. doi:10.1098/rstb.2019.0083

Servais, P., E. O. Casamayor, C. Courties, P. Catala, N. Parthuisot, and P. Lebaron. 2003. Activity and diversity of bacterial cells with high and low nucleic acid content. Aquat. Microb. Ecol. **33**: 41–51. doi:10.3354/ame033041

Siedler, G., A. Kuhl, and W. Zenk. 1987. The Madeira Mode Water. J. Phys. Oceanogr. **17**: 1561–1570. doi:10.1175/1520-0485(1987)017<1561:TMMW>2.0.CO;2

Smith, D., and F. Azam. 1992. A simple, economical method for measuring bacterial protein synthesis rates in seawater using. Mar. Microb. food webs **6**: 107–114.

Smith, L. K., A. H. Ruhl, L. C. Huffard, M. Messié, and M. Kahru. 2018. Episodic organic carbon fluxes from surface ocean to abyssal depths during long-term monitoring in NE Pacific. Proc. Natl. Acad. Sci. **115**: 12235–12240. doi:10.1073/pnas.1814559115

Speer, K. G., and M. S. McCartney. 1992. Bottom Water Circulation in the Western North Atlantic. J. Phys. Oceanogr. **22**: 83–92. doi:10.1175/1520-0485(1992)022<0083:BWCITW>2.0.CO;2

Steinberg, D. K., B. A. S. Van Mooy, K. O. Buesseler, P. W. Boyd, T. Kobari, and D. M. Karl. 2008. Bacterial vs. zooplankton control of sinking particle flux in the ocean's twilight zone. Limnol. Oceanogr. **53**: 1327–1338. doi:10.4319/lo.2008.53.4.1327

Stramma, L., and M. England. 1999. On the water masses and mean circulation of the South Atlantic Ocean. J. Geophys. Res. Ocean. **104**: 20863–20883. doi:10.1029/1999JC900139

Stramma, L., and F. Schott. 1999. The mean flow field of the tropical Atlantic Ocean. Deep-Sea Res. Part II Top. Stud. Oceanogr. **46**: 279–303. doi:10.1016/S0967-0645(98)00109-X

Talley, L. D. 1996. Antarctic intermediate water in the South Atlantic, p. 219–238. *In* G. Wefer, W.H. Berger, G. Siedler, and D.J. Webb [eds.], The South Atlantic. Present and Past Circulation. Springer-Verlag.

Troupin, C., A. Barth, D. Sirjacobs, and others. 2012. Generation of analysis and consistent error fields using the Data Interpolating Variational Analysis (DIVA). Ocean Model. **52–53**: 90–101. doi:10.1016/j.ocemod.2012.05.002

Tsuchiya, M. 1986. Thermostads and circulation in the upper layer of the Atlantic Ocean. Prog. Oceanogr. **16**: 235–267. doi:10.1016/0079-6611(86)90040-6

Turner, J. T. 2015. Zooplankton fecal pellets, marine snow, phytodetritus and the ocean's biological pump. Prog. Oceanogr. **130**: 205–248. doi:10.1016/j.pocean.2014.08.005

Varela, M. M., H. M. Van Aken, E. Sintes, and G. J. Herndl. 2008. Latitudinal trends of Crenarchaeota and Bacteria in the meso- and bathypelagic water masses of the Eastern North Atlantic. Environ. Microbiol. **10**: 110–124. doi:10.1111/j.1462-2920.2007.01437.x

Verdugo, P. 2012. Marine Microgels. Ann. Rev. Mar. Sci. **4**: 375–400. doi:10.1146/annurev-marine-120709-142759

Van Wambeke, F., P. Catala, M. Pujo-Pay, and P. Lebaron. 2011. Vertical and longitudinal gradients in HNA-LNA cell abundances and cytometric characteristics in the Mediterranean Sea. Biogeosciences **8**: 1853–1863. doi:10.5194/bg-8-1853-2011

Whitman, W. B., D. C. Coleman, and W. J. Wiebe. 1998. Prokaryotes: The unseen majority. Proc. Natl. Acad. Sci. **95**: 6578 LP – 6583. doi:10.1073/pnas.95.12.6578

Worthington, L. V. 1976. On the North Atlantic circulation, Johns Hopkins University Press.

Wüst, G. 1935. Schichtung und Zirkulation des Atlantischen Ozeans, Die Stratosphäre. Wissenschaftliche Ergebnisse der Deutschen Atlantischen Expedition auf dem Forschungsund Vermessungsschiff "Meteor" 1925–1927. 6, 180pp., English translation edited by W.J. Emery, The stratosphere of the Atlantic Ocean. Scientific Results of the German Atlantic Expedition of the Research Vessel 'Meteor' 1925–27. Amerind Publishing Co., 1978.

Yokokawa, T., Y. Yang, C. Motegi, and T. Nagata. 2013. Large-scale geographical variation in prokaryotic abundance and production in meso- and bathypelagic zones of the central Pacific and Southern Ocean. Limnol. Oceanogr. **58**: 61–73. doi:10.4319/lo.2013.58.1.0061

Zenk, W. 1975. On the Mediterranean outflow west of Gibraltar. Meteor. Forsch.-Ergebnisse A **16**: 23–24.

Ziervogel, K., C. Dike, V. Asper, and others. 2016. Enhanced particle fluxes and heterotrophic bacterial activities in Gulf of Mexico bottom waters following storm-induced sediment resuspension. Deep Sea Res. Part II Top. Stud. Oceanogr. **129**: 77–88. doi:10.1016/j.dsr2.2015.06.017

Chapter 4

Prokaryotes and DOM in the water masses of the Atlantic

Deep ocean prokaryotes and fluorescent dissolved organic matter reflect the history of the water masses across the Atlantic Ocean

Markel Gómez-Letona, Javier Arístegui, Nauzet Hernández-Hernández, Xosé Antón Álvarez-Salgado, Marta Álvarez, Erick Delgadillo, María Pérez-Lorenzo, Eva Teira, Santiago Hernández-León, Marta Sebastián

Progress in Oceanography, 2022. doi: 10.1016/j.pocean.2022.102819

Organic matter is known to influence community composition and metabolism of marine prokaryotes. However, few studies have addressed this linkage in the deep ocean. We studied the relationship between fluorescent dissolved organic matter and prokaryotic community composition in meso- and bathypelagic water masses along a surface productivity gradient crossing the subtropical and tropical Atlantic Ocean. Four fluorescence components were identified, three humic-like and one protein-like. The distributions of the humic-like components were significantly explained by water mass mixing, apparent oxygen utilisation (AOU) and epipelagic productivity proxies in varying degrees, while the protein-like component was explained only by water mass mixing and epipelagic productivity. The diversity and taxonomic composition of the prokaryotic community differed between water masses: the Nitrosopumilales order dominated in water masses with high AOU and humic-like fluorescence (notably, the SubPolar Mode Water), and tended to co-occur with Marine Group II archaea, the SAR324 clade and Thiomicrospirales, while bathypelagic water masses displayed greater abundances of members of Marinimicrobia, SAR202 and SAR324. Water mass mixing regression models suggested that the distribution of some taxa (e.g., Marinimicrobia, SAR202) was dominated by mixing and selection within the water masses during ageing, while others (chiefly, Alteromonadales) were mostly influenced by local processes. Our results suggest a link between the composition of the prokaryotic community, oxygen utilisation and the signalof fluorescent dissolved organic matter, and has implications for our understanding of the processes that shape the carbon cycling and the prokaryotic communities in the deep ocean.

Introduction

Prokaryotic communities (bacteria and archaea) play a major role in the cycling of organic matter in marine ecosystems (Moran et al. 2016). They interact with the continuum of organic matter –from particulate to dissolved organic matter (DOM)– through assimilation, excretion and remineralisation of organic compounds. This interaction sets the stage for their influence on the biogeochemical cycles of carbon and other elements (Falkowski et al. 2008; Offre et al. 2013), the ocean-atmosphere exchange fluxes of CO_2 (Kwon et al. 2009) and the sequestration of organic carbon (Lechtenfeld et al. 2015).

The myriad of prokaryotes that take part in these processes in the global ocean are influenced by a variety of factors, such as temperature (Laufkötter et al. 2017), nutrient availability (Wohlers-Zöllner et al. 2011), oxygen concentration (Beman and Carolan 2013) and interactions with other organisms (Seymour et al. 2017). Nonetheless, DOM concentration and composition have been shown to play a major role in how and to which extent prokaryotes interact with organic matter (Gómez-Consarnau et al. 2012).

In recent years, there has been significant progress towards understanding how microbial activity influences the distribution and processes that shape the DOM pool in the deep ocean, and vice versa (Moran et al. 2016). The composition of DOM has been posed to be one factor determining its bioavailability (Dittmar et al. 2021): from labile, easily degradable molecules –such as amino acids and sugars– to refractory ones that can last for decades to millennia in the deep ocean (Hansell 2013). Fluorescence spectroscopy of DOM has proven to be a valuable tool to differentiate between the protein-like, and refractory, humic-like, fractions of the DOM pool (Murphy et al. 2008; Stedmon and Bro 2008). Furthermore, recent ultra-high resolution analytical techniques, such as Fourier-transform ion cyclotron resonance mass spectrometry (FT-ICR-MS), have shown that DOM is extremely diverse in composition, with the number of molecular formulae being in the order of 10^5 (Zark et al. 2017).

Chemical characteristics of DOM however are not the sole factor influencing its reactivity, i.e., how readily it is utilised by microbes (Carlson and Hansell 2015): environmental conditions (e.g., concentration of organic compounds and availability of nutrients),the metabolic capabilities of the consumers and ecological interactions also seem to influence the ability of microbes to degrade DOM (Baltar et al. 2021; Dittmar et al. 2021). The prokaryotic community hosts a vast array of metabolisms

(Sunagawa et al. 2015) that enables the use of organic matter with varying chemical characteristics, both directly (Bergauer et al. 2018) or indirectly via extracellular enzymatic activity (Arnosti 2011). This yields distinctive imprints in the optical characteristics of DOM (Catalá et al. 2015a). Microbial remineralisation and deep ocean circulation (responsible for DOM transport from subduction zones and around the global ocean, during which microbes act upon DOM, transforming it) are hence the main drivers of DOM distribution patterns in the dark ocean (Hansell et al. 2009; Catalá et al. 2015b).

Some recent studies have shown that the quality of DOM, rather than its quantity, shape the composition and abundance of the prokaryotic community in deep ocean layers (Guerrero-Feijóo et al. 2017; Ruiz-González et al. 2020). In the deep water masses off a coastal system characterized by seasonal upwelling pulses, Guerrero-Feijóo et al. (2017) found that archaeal taxa were linked to fluorescence properties of DOM while bacteria were related to its average molecular weight. Furthermore, Ruiz-González et al. (2020) analysed samples collected in 8 locations from distinct biogeographic provinces within the Pacific, Indian and Atlantic oceans during the Malaspina 2010 circumnavigation expedition and found a link between amino-acid-like FDOM of both surface and bathypelagic (~4000 m) waters, and the activity of bathypelagic prokaryotes. This link was suggested to arise from vertical connectivity through sinking particles, as these would potentially release bioavailable FDOM and fuel prokaryotic activity.

To further elucidate the links between DOM and deep ocean prokaryotic communities, we combined a thorough characterisation of the optical properties of the DOM pool with high-throughput sequencing of the 16S rRNA gene in central, intermediate and deep water masses along a surface productivity gradient in the tropical and subtropical Atlantic Ocean. We hypothesised that water masses could harbour different FDOM pools and prokaryotic communities based on their initial properties in their respective source regions, their ageing history as they circulate through the world ocean, the mixing between different water masses and the remineralisation processes occurring within the study region. On the one hand, the present study crossing distinct oceanographic environments along a productivity gradient bridges the gap between previous local studies (e.g., Guerrero-Feijóo et al. 2017) or a global ocean surveys with low spatial resolution (Ruiz-González et al. 2020). On the other hand, the characterisation of water masses by means of an optimum multiparameter analysis adds relevant information to interpret the link between the origin and fate of DOM, and microbial organisms in the deep ocean.

Thus, the present work provides an opportunity to expand our knowledge on how the distributions of DOM and prokaryotic communities in the mesopelagic (200-1000 m) and bathypelagic (1000-4000 m) ocean are mediated by water mass mixing and biogeochemical processes.

Materials and methods

Sample collection

Samples for this study were collected during the MAFIA cruise (*Migrants and Active Flux In the Atlantic ocean*, April 2015) on board the BIO Hespérides. Seawater samples for biogeochemical analyses were collected at 13 stations in the subtropical and tropical Atlantic (Fig. 1) using a General Oceanics oceanographic rosette equipped with 24L PVC Niskin bottles alongside a Seabird 911-plus CTD, a Seapoint Chlorophyll Fluorometer and a Seabird-43 Dissolved Oxygen Sensor. The chlorophyll *a* (Chl *a*) values provided by the fluorometer were based on the factory calibration. Oxygen sensor measurements were calibrated with samples potentiometrically titrated with the Winkler method following the procedure described in Moreno-Ostos (2012). Oxygen solubility was computed using the equation of Benson and Krause (1984). AOU ($\mu mol \cdot Kg^{-1}$) was calculated by subtracting measured oxygen concentration from the oxygen solubility values at saturation, with respect to the atmosphere.

FDOM samples

Seawater samples (18 depths per station) for the analysis of fluorescent dissolved organic matter (FDOM) were collected directly from the Niskin bottles into 250 mL glass flasks that had previously been cleaned with solutions of bleach (10%) and HCl (5%), and rinsed with abundant ultrapure water. Samples were left in the dark to allow them reach room temperature prior to their analysis.

Fluorescence measurements

Fluorescence measurements were performed with a Perkin-Elmer LS55 spectrofluorometer, using excitation (Ex) and emission (Em) slit widths of 10 nm. The excitation range was between 250 and 450 nm and the emission range between 270 and 670 nm. The measurements were collected as synchronic excitation-emission

matrices (EEM). A total of 21 synchronic scans were recorded. The first scan started at Ex 250 nm and Em 270 nm (= Ex + 20 nm) and followed with increments of 0.5 nm in both Ex and Em wavelengths up to Ex 450 nm and Em 470 nm. The last scan started at Ex 250 nm and Em 470 nm (= Exc + 220 nm) and followed with increments of 0.5 nm in both Ex and Em wavelengths up to Ex 450 nm and Em 670 nm. Blanks were measured using freshly produced ultrapure water following the same procedure.

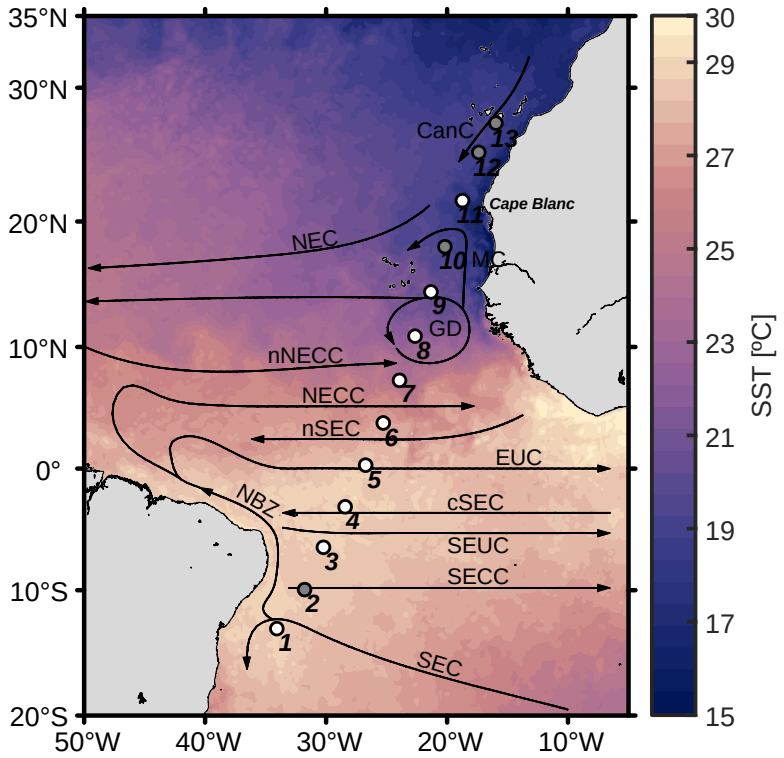

Figure 1. Sampling stations during the MAFIA cruise. Stations in which samples for 16S amplicon sequencing were collected are shown in white. The underlying colormap represents the reprocessed Global Ocean OSTIA Sea Surface Temperature (SST) from the CMEMS (product code: SST-GLO-SST-L4-REP-OBSERVATIONS-010-011) for 15/04/2015. Major ocean currents in the study region (based on Stramma and Schott, 1999 and Brandt et al. 2008) are also displayed: CanC, Canary Current; NEC, North Equatorial Current; MC, Mauritanian Current; GD, Guinea Dome; nNECC, northern North Equatorial Counter Current; NECC, North Equatorial Counter Current; nSEC, northern South Equatorial Current; EUC, Equatorial Under Current; NBZ, North Brazil Current; cSEC, central South Equatorial Current; SEUC, South Equatorial Under Current; SECC, South Equatorial Counter Current; SEC, South Equatorial Current.

Raw measurements were processed using the DOMFluor toolbox (v. 1.7; Stedmon and Bro, 2008) for Matlab (R2017a). First, blank measurements were subtracted from seawater EEMs. Second, EEMs were normalised to the Raman area (RA), which was estimated applying the trapezoidal rule of integration on the emission scan at the 350 nm excitation wavelength in the blank measurements. Recording EEMs in synchronic mode avoids sampling first and second order Rayleigh scatter bands. Inner filter correction was not applied because during the entire cruise the absorption coefficient at 250 nm ($a_{CDOM}(250)$; see Supplementary methods for details) displayed mean values of 0.99 ± 0.25 m^{-1} (max. = 1.95 m^{-1}; n = 250) and this correction is deemed necessary only above 10 m^{-1} (Stedmon and Bro 2008).

Parallel factor analysis of fluorescence data

The processed EEMs (see Fig. S1 for examples) were analysed applying a Parallel Factor analysis (PARAFAC) (Stedmon and Bro 2008) using the DOMFluor toolbox. The PARAFAC model was constructed based on 222 samples (outliers were removed) and it was validated using split-half validation and random initialisation. The resulting model was made up of four components (Fig. S2). For each one, the fluorescence maximum (F_{max}) was recorded in each of the samples.

The optical characteristics of the four components, named according to their fluorescence emission maxima, are summarised in Table S1, along with similar fluorophores found in the literature. The identification of previously described fluorophores was performed using the OpenFluor database (openfluor.lablicate.com, Murphy et al. 2014), based on the combined Tucker Congruence Coefficient of the excitation and emission spectra ($TCC_{ex\text{-}em}$). For components $C_{462\text{-}490}$, C_{406} and C_{366}, 6, 7 and 12 matches with high congruence ($TCC_{ex\text{-}em} > 0.95$) were found, respectively. $C_{462\text{-}490}$ had an excitation peak at 278 nm, with a secondary one at 370 nm, and a relatively wide emission maxima at 462 nm - 490 nm. This component was found to be related to general humic-like dissolved organic matter. Analogous fluorophores have been described to be positively correlated to AOU in the deep ocean (Catalá et al. 2015b), and were previously found in the study area (Aparicio et al. 2015). C_{454} had an excitation maximum below 250 nm and the emission maximum at 454 nm. No matches with high congruence were found for this component, probably because it was not fully resolved by the PARAFAC modelling and had a slight contribution from $C_{462\text{-}490}$ (Fig. S2). However, among the matches with lower $TCC_{ex\text{-}em}$, C_{454} was found to be similar to fluorophores described as humic/fulvic-like, related to the typical Coble's (1996) peak A (Stedmon and Markager 2005; Lapierre and Del

Giorgio 2014). C_{406} had excitation and emission maxima at 328 nm and 406 nm, respectively. Similar signals have also been related to humic-like substances, usually of specifically marine origin (Stedmon et al. 2003; Catalá et al. 2015b). Like $C_{462\text{-}490}$, C_{406} has also been linked to AOU and had been previously found in the study area (De La Fuente et al. 2014; Catalá et al. 2015b). Finally, C_{366} was different to the previous components: the excitation peak was located at 286 nm (with a secondary one below 250 nm), while the emission peak was at 366 nm, lower than $C_{462\text{-}490}$ and C_{406}. This protein-like component has been found to be related to material associated with phytoplankton production and has been shown to be partially bioavailable for microbial consumption (Stedmon et al. 2003; Lønborg et al. 2010; Kida et al. 2019).

DNA sampling, extraction and sequencing

Seawater samples for DNA were collected at stations 1– 9 and 11 from selected meso- and bathypelagic depths: 300 m, 700 m, 1500 m, 2500 m and 3500 m (3200 m for station 5) and kept at 4°C in the dark (2h at most) until further processing. Samples were prefiltered with a 20 μm mesh and subsequently filtered through 0.22 μm Sterivex filters (Millipore, SVGP01050) using a peristaltic pump. Upon filtration, filters were sealed with parafilm, flash-frozen with liquid nitrogen and stored at -80°C.

DNA from biomass retained in the 0.22 μm Sterivex filters was extracted using the PowerWater DNA isolation kit (MoBio Laboratories Inc., CA, USA) according to the manufacturer's instructions. DNA concentration was fluorometrically quantified with a Qubit 3.0 instrument and Qubit dsDNA HS (high sensitivity) Assay Kits (Invitrogen). Prokaryote community composition was assessed by sequencing the V4 and V5 regions of the 16S rRNA gene (16S rDNA) by using the universal primers "515F" and "926R" (Parada et al. 2016). Amplified regions were sequenced with the Illumina MiSeq platform (paired-end reads; 2 × 250 bp) by Fasteris SA (Geneva, Switzerland).

16S amplicon sequence analysis

Bioinformatic analyses were performed at the Marine Bioinformatics platform (Marbits, marbits.icm.csic.es) of the Institut de Ciències del Mar (ICM-CSIC, Barcelona). Primers were removed using *cutadapt* (Martin 2011). All subsequent analyses were performed in R (3.6; R Core Team, 2019). The *DADA2* package (Callahan et al. 2016) was used to process the amplicon sequence data (*trunclen* =

(210, 205), *maxEE* = (2, 4), *minOverlap* = 15). *DADA2* models errors in the Illumina-sequenced amplicon reads to infer exact amplicon sequence variants (ASV) down to one nucleotide difference. Taxonomic assignation of ASVs was carried out using the '*IDTaxa*' function (Murali et al. 2018) from the *DECIPHER* package, with SILVA v. 138 as the training set. Identification of contaminant sequences was performed using the *decontam* package (Davis et al. 2018) applying the frequency method (*threshold* = 0.1). This analysis suggested that sequences of ASVs classified within the orders *Burkholderiales* and *Propionibacteriales* (*Cutibacterium* genus) were contaminants, although not all of them were identified as such. Nonetheless, all sequences assigned to these orders were removed, as they are known reagent/laboratory contaminants (Salter et al. 2014). In the end, samples with at least 1000 reads were preserved for downstream analyses (mean 56028, min. 1092, max. 115430).

Statistical analyses

All statistical analyses were carried out in R (R Core Team 2019). Non-metric multidimensional scaling (NMDS; *vegan* package, Oksanen et al. 2019) was performed to visualize the similarity in prokaryotic community composition among samples. Prior to the analysis, the ASV count table was normalised by centred log-ratio (CLR) transformation (*compositions* package, van den Boogaart et al. 2020) and Euclidean distances were estimated (*vegan* package, Oksanen et al. 2019) based on this normalised table.

Diversity of the prokaryotic community in the different water masses was studied by estimating classical diversity indicators: species richness, the Pielou evenness index (*microbiome* package, Lahti and Shetty, 2019), Faith's phylogenetic diversity index (*picante* package, Kembel et al. 2010) and the Shannon index (*vegan* package, Oksanen et al. 2019). To compute these estimates, amplicon samples with over 30000 counts (n = 29) were rarefied with permutations using the *EcolUtils* R package (version 0.1, Salazar, 2020).

Multiparameter Water Mass Analysis

The contribution of each water mass to each sample was objectively quantified applying an optimum multiparameter analysis in Matlab (R2017a). Briefly, based on previous hydrographic studies in the area (e.g. Álvarez et al. 2014; Catalá et al. 2015b), twelve source water types (SWT) were identified in the collected water

samples (Fig. 2a, Table S2): Salinity Maximum Water (SMW), Madeira Mode Water (MMW), Equatorial Water (EQ_{13}), Eastern North Atlantic Central Water of 15°C ($ENACW_{15}$) and 12°C ($ENACW_{12}$), Subpolar Mode Water (SPMW), Mediterranean Water (MW), Antarctic Intermediate Water of 5°C ($AAIW_5$) and 3.1°C ($AAIW_{3.1}$), Circumpolar Deep Water (CDW) and North Atlantic Deep Water of 4.6°C ($NADW_{4.6}$) and 2°C ($NADW_2$). The contribution of each SWT to each sample is

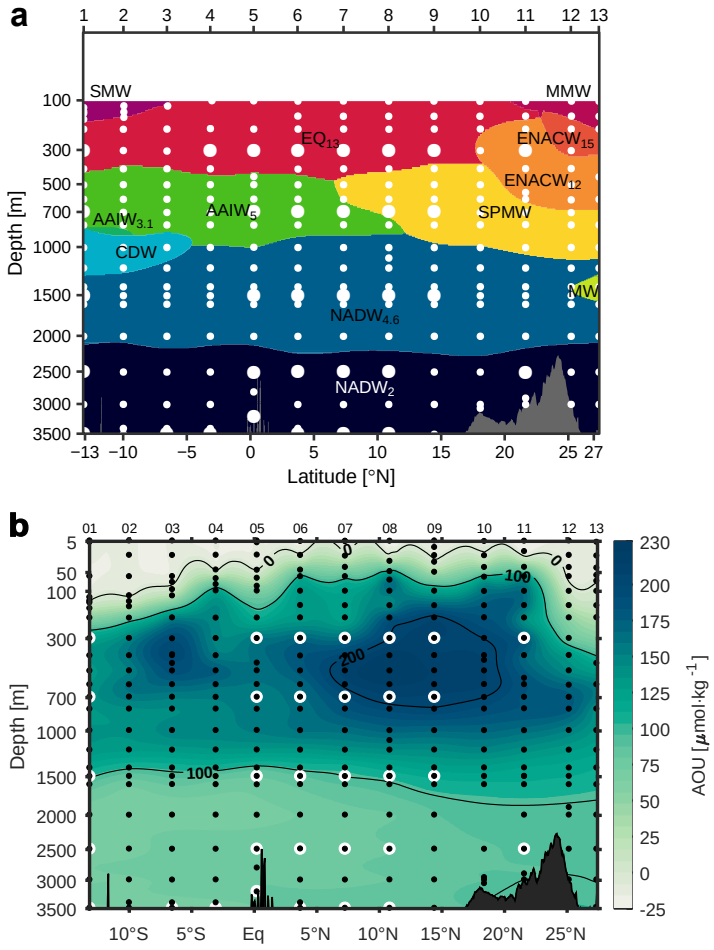

Figure 2. Distribution of the water masses and Apparent Oxygen Utilisation (AOU) in the study section. (a) Approximate area in which each water mass has its highest contribution is shown. (b) AOU estimates. Small dots represent samples of the physical and geochemical variables included in the optimum multiparameter analysis and big white circles the locations of amplicon samples. Note that the vertical scale is square root-transformed to allow for a better visualisation of the results. Numbers on top correspond to stations in Fig. 1. Data interpolation was performed with Data Interpolating Variational Analysis (DIVA; Troupin et al. 2012) in Matlab (R2017a).

quantified by solving a set of four conservative linear mixing equations defined by potential temperature (θ), salinity (S), silicate (SiO_4H_4) and the conservative NO tracer (= O_2 + R_N·NO_3 with R_N = 9.3; Álvarez et al. 2014; Broecker, 1974), plus a fifth equation that constrained the sum of the SWT contributions to 1. These equations were normalised and weighted according to how conservative each variable is, using weights 10, 5, 1, 2 and 100 for potential temperature, salinity, SiO_4H_4, NO and volume, respectively (Álvarez et al. 2014). Therefore, the mixing of a maximum of five of these SWT can be solved simultaneously. Given that we identified 12 SWT, they were grouped into the following mixing clusters, based on oceanographic criteria of water density and geographic proximity: $AAIW_5$-$AAIW_{3.1}$-CDW-$NADW_2$-$NADW_{4.6}$, $AAIW_5$-$NADW_{4.6}$-EQ_{13}, EQ_{13}-SMW, $NADW_2$-$NADW_{4.6}$-MW, $NADW_{4.6}$-MW-SPMW-$ENACW_{12}$, $NADW_{4.6}$-$AAIW_5$-SPMW-$ENACW_{12}$, $ENACW_{12}$-$ENACW_{15}$, $ENACW_{15}$-MMW, $AAIW_5$-$NADW_{4.6}$-SPMW-EQ_{13}, EQ_{13}-$ENACW_{12}$-SPMW and EQ_{13}-$ENACW_{12}$-$ENACW_{15}$-MMW (Fig. 2a). The initial values of the SWTs were based on previous hydrographic studies (Table S3). Based on the contribution (as %) of SWTs to each sample, archetype values were estimated for each SWT as weighed means of physical and biogeochemical variables, diversity indices, and CLR-transformed abundances of taxonomic orders that contained dominant ASVs (representing >0.5% of reads at least in a sample) (Álvarez-Salgado et al. 2013; Catalá et al. 2015b). Note that mixed layer samples (here < 100 m) are excluded from the optimum multiparameter analysis because temperature, salinity, SiO_4H_4 and NO do not behave conservatively in this layer.

To assess the degree of variance of FDOM that was explained by conservative water mass mixing and non-conservative biogeochemical processes, multiple linear least squares regressions were performed between FDOM components and water mass proportions alone (mixing models), which account both for the initial values in the source regions plus the large-scale mineralisation processes occurring from the source to the study region. Note that closer to their source regions the proportion of each water type is the highest. This proportion declines as the water type moves away from its source region due to mixing with other water types. At the same time, ageing of the water type occurs in parallel to mixing. Thus, mixing models also retain the large-scale mineralisation processes (Álvarez-Salgado et al. 2013). Individual biogeochemical variables were also included in the regressions (mixing + biogeochemistry models), capturing local biogeochemical processes not considered in the mixing models (Álvarez-Salgado et al. 2013). Among the biogeochemical variables we included the integrated values in the epipelagic layer (as first 200 m) of Chl *a* (Chl a_{int}), the protein-like C_{366} ($C_{366\text{-int}}$) and the chromophoric DOM (CDOM) absorption

coefficient at 254 nm ($a_{CDOM}(254)_{int}$, see Supplementary Methods for absorption data processing). Integrated values of these variables were estimated by multiplying the discrete measurements by the distance, in meters, between samples. The integrated values of each station were assigned to all samples from that station when estimating the multiple linear regressions. These integrated estimates were included as proxies of epipelagic productivity, as they agreed with satellite-derived net primary production estimates (Fig. S3). They provide insights into potential vertical transport of organic matter, as highly productive areas are known to support high vertical export rates of particles (Fischer et al. 2020), while DOM accumulated in the surface ocean can be eventually transported to the ocean's interior (Baetge et al. 2020). Furthermore, positive relationships have been found between surface and bathypelagic levels of protein-like FDOM, and also between bathypelagic protein-like FDOM and prokaryotic activity (Ruiz-González et al. 2020), suggesting that surface waters with higher amount of protein-like FDOM lead to higher protein-like FDOM export. The mixing and mixing + biogeochemistry models were also applied to the CLR-transformed abundances of dominant ASVs.

Results

FDOM distribution

The humic-like FDOM components ($C_{462\text{-}490}$, C_{454}, C_{406}) and the protein-like C_{366} component presented remarkably contrasting distributions (Fig. 3). Humic-like components overall had higher fluorescence values below 200 m, although there were latitudinal changes both in the photic and dark layers. $C_{462\text{-}490}$ (Fig. 3a) displayed higher levels north of 5°N, with maximum values (> 0.013 RU) at stations 9 and 10 below 300 m, maintaining high values down to the deepest samples. In surface waters $C_{462\text{-}490}$ fluorescence increased from station 1 (~0.001 RU) to station 11 (0.013 RU), off Cape Blanc. Archetype values of $C_{462\text{-}490}$ were higher in water masses located deeper (Table 1): 0.0050 ± 0.0007 RU for the SMW vs 0.0138 ± 0.0003 for the $NADW_2$. Nonetheless, meridional differences were also observed as $AAIW_5$ (core at 0.22 ± 1.86 °N) and SPMW (17.32 ± 1.39 °N), while occupying the same portion of the water column (core at ~700 m), presented markedly different archetype values: 0.0115 ± 0.0003 and 0.0133 ± 0.0003 RU, respectively (Table 1).

C_{454} (Fig. 3b) displayed the highest fluorescence values among all four components, but with similar patterns to $C_{462\text{-}490}$: surface waters showed increased fluorescence from station 1 to 11, and maximum values (> 0.027 RU) were found in stations 9

and 10 at depths below 300 m. C_{454} archetype values were highest in the SPMW (0.0261 ± 0.0005 RU; the MW estimate was slightly higher but had a large error, Table 1). C_{454} decreased slightly with depth ($NADW_{4.6}$, 0.0216 ± 0.0008 RU) and notably towards the south ($AAIW_5$, 0.0176 ± 0.0012 RU; SMW, 0.0087 ± 0.0014). There was a marked change in the values of C_{454} throughout the water column close to the equator, from station 5 (< 0.019 RU) to station 6 (> 0.019 RU). Interestingly, the region between stations 5 and 7 presented a strong SST gradient (Fig. 1), with

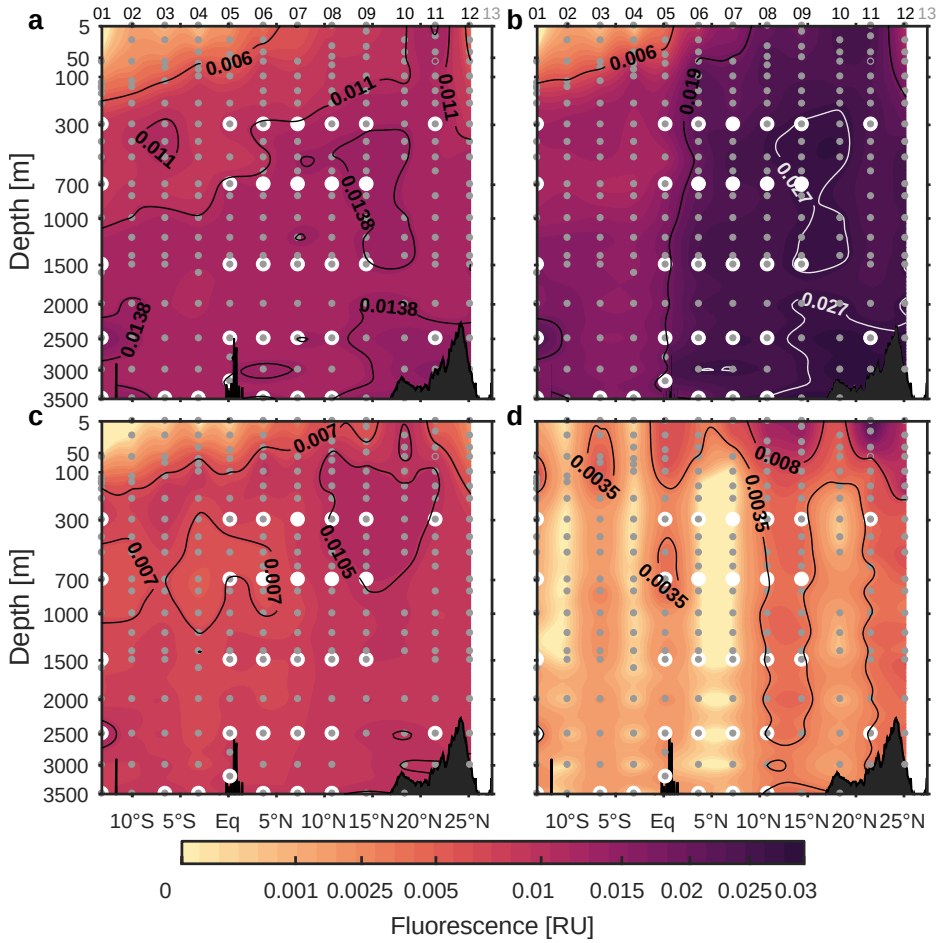

Figure 3. Distribution of the FDOM components along the cruise section: $C_{462\text{-}490}$ (a), C_{454} (b), C_{406} (c) and C_{366} (d). Grey dots represent FDOM samples and white circles indicate samples for which 16S amplicon sequencing was also performed. Fluorescence is represented in Raman Units (RU). Note that both the vertical and colour scales are square root-transformed to allow for a better visualisation of the results. Data interpolation was performed with Data Interpolating Variational Analysis (DIVA; Troupin et al. 2012) in Matlab (R2017a).

higher temperatures south of the Equator (station 5), leading to increased stratification of the surface layer (Fig. S4).

Component C_{406} (Fig. 3c) was also widespread in deep waters and presented an increase at stations 8-10, with maximum values of >0.0105 RU between ~150-800 m depth, shallower than the $C_{462\text{-}490}$ and C_{454} maxima. This maximum tended to follow AOU patterns (although not entirely): peaks of AOU exceeding 200 $\mu mol \cdot Kg^{-1}$ were found in stations 8-10 between depths of ~200-800 m (Fig. 2b), where oxygen concentrations were as low as ~50 $\mu mol \cdot Kg^{-1}$ (Fig. S5). Higher fluorescence values at shallower depths were reflected in increased archetype C_{406} values particularly of central and intermediate waters in the tropical North Atlantic. The $ENACW_{12}$ presented the highest C_{406} estimates among water masses (0.0103 ± 0.0004 RU; Table 1), followed by the SPMW (0.0100 ± 0.0003 RU). Again, this contrasted with the archetype values of $AAIW_5$, which were markedly lower (0.0075 ± 0.0003). SMW (0.0063 ± 0.0008) and bathypelagic water masses also displayed low archetype values (Table 1).

The protein-like component C_{366} (Fig. 3d) presented a patchy distribution, with high values in surface waters, particularly at stations 8, 9 and 11 (0.025 RU, off Cape Blanc). Deep water masses had lower C_{366} fluorescence but, overall, stations with greater surface C_{366} values also presented higher C_{366} values in deep waters. Archetype values of C_{366} were higher in central and to a lesser extent intermediate water masses, but standard errors were larger than for the other components (Table 1).

Effects of conservative water mass mixing and biogeochemical processes on FDOM

Multiple linear regressions between the measured variables and the water mass proportions ('mixing models') captured two sources of variability: the effects of 1) conservative water mass mixing, which also retains the effects of temperature and depth on the test variables, and 2) the mineralisation processes that occur from the water mass formation area to the study region (Álvarez-Salgado et al. 2013). We found that depending on the FDOM component, differing degrees of their variability were explained by mixing models (Table 2): $C_{462\text{-}490}$ was explained in 80%, C_{454} in 56%, C_{406} in 57% and C_{366} only in 42%. Including AOU in the models rendered significant results for components $C_{462\text{-}490}$, C_{454}, and C_{406}: the explained variance increased to 87% (+7%), 67% (+11%) and 66% (+9%), respectively (Table 3), while C_{366} was not significantly affected. The positive regression coefficients of AOU

Table 1. Water mass characteristics in the study region. Contribution of each water mass to the total sampled volume (as %), along the archetype values of potential temperature (θ), salinity, oxygen concentration (O_2), apparent oxygen utilisation (AOU) and FDOM components. Values are displayed as archetype ± standard error. Water mass acronyms are: Salinity Maximum Water (SMW), Madeira Mode Water (MMW), Equatorial Water (EQ_{13}), Eastern North Atlantic Central Water of 15°C ($ENACW_{15}$) and 12°C ($ENACW_{12}$), Subpolar Mode Water (SPMW), Mediterranean Water (MW), Antarctic Intermediate Water of 5°C ($AAIW_5$) and 3.1°C ($AAIW_{3.1}$), Circumpolar Deep Water (CDW) and North Atlantic Deep Water of 4.6°C ($NADW_{4.6}$) and 2°C ($NADW_2$).

Water mass	Volume [%]	Depth [m]	Latitude [°N]	θ [°C]	Salinity	O_2 [μmol·Kg^{-1}]	AOU [μmol·Kg^{-1}]	$C_{462\text{-}490}$[a] [RU]	C_{454}[a] [RU]	C_{406}[a] [RU]	C_{366}[a] [RU]
SMW	2.88	134 ± 11	-9.68 ± 1.80	21.03 ± 1.11	36.56 ± 0.18	193.0 ± 8.0	26.2 ± 12.7	5.0 ± 0.7	8.7 ± 1.4	6.3 ± 0.8	3.8 ± 1.2
MMW	1.95	130 ± 17	22.13 ± 2.67	16.22 ± 0.63	36.28 ± 0.20	160.7 ± 28.0	79.0 ± 30.9	9.9 ± 1.1	21.5 ± 1.6	8.8 ± 1.4	7.0 ± 2.2
EQ_{13}	15.71	252 ± 23	3.13 ± 1.66	12.70 ± 0.61	35.39 ± 0.09	118.8 ± 6.4	141.3 ± 8.6	10.1 ± 0.4	18.6 ± 1.1	8.9 ± 0.3	2.2 ± 0.4
$ENACW_{15}$	2.09	186 ± 34	25.40 ± 1.07	16.20 ± 0.60	36.40 ± 0.13	188.9 ± 17.1	50.7 ± 19.6	8.8 ± 0.8	20.0 ± 1.2	7.4 ± 0.9	8.3 ± 2.2
$ENACW_{12}$	4.68	413 ± 53	22. 40 ± 1.26	11.72 ± 0.51	35.61 ± 0.08	110.5 ± 10.0	153.5 ± 10.5	12.1 ± 0.4	24.9 ± 0.7	10.3 ± 0.4	4.2 ± 0.7
SPMW	8.34	696 ± 56	17.32 ± 1.39	8.20 ± 0.38	35.09 ± 0.04	101.5 ± 7.9	184.5 ± 6.8	13.3 ± 0.2	26.1 ± 0.5	10.0 ± 0.3	3.1 ± 0.5
MW	0.76	1632 ± 386	25.28 ± 1.68	5.17 ± 1.11	35.17 ± 0.09	199.7 ± 16.2	106.9 ± 9.3	13.4 ± 1.4	26.6 ± 2.4	9.6 ± 0.7	4.3 ± 0.8
$AAIW_5$	12.83	713 ± 47	0.22 ± 1.86	6.27 ± 0.33	34.70 ± 0.04	137.8 ± 6.2	162.0 ± 4.7	11.5 ± 0.3	17.6 ± 1.2	7.5 ± 0.3	1.6 ± 0.4
$AAIW_{3.1}$	0.30	1052 ± 315	-9.26 ± 6.56	4.05 ± 0.29	34.60 ± 0.23	188.6 ± 21.4	127.4 ± 21.8	11.2 ± 1.2	15.0 ± 4.9	7.1 ± 1.0	0.5 ± 1.1
CDW	5.89	1917 ± 232	3.92 ± 3.47	3.65 ± 0.25	34.87 ± 0.05	213.1 ± 8.1	105.4 ± 6.6	13.0 ± 0.5	20.9 ± 1.9	8.5 ± 0.4	1.9 ± 0.5
$NADW_{4.6}$	30.00	1485 ± 75	5.99 ± 1.46	4.57 ± 0.17	34.92 ± 0.02	196.2 ± 4.7	115.4 ± 3.7	12.8 ± 0.2	21.6 ± 0.8	8.5 ± 0.2	2.0 ± 0.3
$NADW_2$	14.57	2754 ± 98	4.66 ± 2.12	2.73 ± 0.09	34.94 ± 0.01	240.9 ± 1.9	84.7 ± 1.6	13.8 ± 0.3	22.8 ± 1.1	9.2 ± 0.2	2.0 ± 0.3

[a] $\times 10^{-3}$

suggest a link between prokaryotic oxygen consumption in the water mass since it was formed and the generation of humic-like fluorescence. Including $C_{366\text{-int}}$ and $a_{CDOM}(254)_{int}$ as explanatory variables of FDOM components yielded significant results (but not for Chl a_{int}). $C_{366\text{-int}}$ increased the explained variance in 1, 2, 10 and 16% for $C_{462\text{-}490}$, C_{454}, C_{406} and C_{366}, respectively, while $a_{CDOM}(254)_{int}$ did it in 4, 15, 14 and 3% (Table 3). These improvements in the explained variance were accompanied by a reduction in the standard error of the residuals.

Table 2. Results of the mixing models of FDOM components and apparent oxygen utilisation (AOU). r^2 is the coefficient of determination, representing the fraction of variance accounted for water mass mixing; SE_{res} the standard error of the residuals; n the number of samples included in the regression; p the p-value of the model.

Parameter	Unit	r^2	SE_{res}	n	p
$C_{462\text{-}490}$[a]	RU	0.80	1.09	178	<0.0001
C_{454}[a]	RU	0.56	4.13	178	<0.0001
C_{406}[a]	RU	0.57	1.09	178	<0.0001
C_{366}[a]	RU	0.42	1.81	178	<0.0001
AOU	μmol·kg^{-1}	0.86	18.47	234	<0.0001

[a] $\times 10^{-3}$

AOU itself was explained in 86% by the mixing model (Table 2), with significant improvements when adding prokaryotic abundance (+2%), $C_{366\text{-int}}$ (+3%), Chl a_{int} (+3%) and $a_{CDOM}(254)_{int}$ (+5%) (Table 3). Likewise, Chl a_{int} and $a_{CDOM}(254)_{int}$ significantly contributed to explain the variance of prokaryotic abundance in the dark ocean (r^2 = 0.94 (+2%) and 0.93 (+1%), respectively; not shown). Taken together, these results suggest that, while water mass mixing and history, and AOU were the main drivers of humic-like fluorescence variability, there was also a significant link between epipelagic productivity, the production and vertical transport of organic matter (including protein-like DOM), and the generation of humic-like FDOM in the dark ocean.

Prokaryotic community composition in dark waters of the Atlantic Ocean

Prokaryotic community composition was somehow uniform at the phylum level except for three samples which were clearly different from the rest (Fig. 4a): st3-3500m, st4-3500m and st9-700m. Excluding these outlier samples, dark ocean

Table 3. Results of the multiple linear regressions combining biochemical variables with the mixing models. *Parameter 1* corresponds to the dependent variable of the regression and *Parameter 2* to the predictor biochemical variable added to the mixing regression model. *Unit 1* and *Unit 2* are their units, respectively. *Coefficient* is the regression coefficient of *Parameter 2*; r^2 the coefficient of determination, representing the fraction of variance accounted for the model; SE_{res} the standard error of the residuals; *n* the number of samples included in the regression; p_{coef} the p-value of the coefficient of *Parameter 2*. AOU stands for apparent oxygen utilisation. *ns* = not significant (p >0.05).

Parameter 1	Parameter 2	Unit 1	Unit 2	Coefficient[a]	r^2	SE_{res}[a]	*n*	p_{coef}
$C_{462\text{-}490}$	AOU	RU	$\mu mol \cdot kg^{-1}$	0.04 ± 0.00	0.87	0.87	178	<0.0001
C_{454}	AOU	RU	$\mu mol \cdot kg^{-1}$	0.12 ± 0.02	0.67	3.58	178	<0.0001
C_{406}	AOU	RU	$\mu mol \cdot kg^{-1}$	0.03 ± 0.00	0.66	0.97	178	<0.0001
C_{366}	AOU	RU	$\mu mol \cdot kg^{-1}$	0.01 ± 0.01	0.42	1.81	178	ns
$C_{462\text{-}490}$	$C_{366\text{-}int}$	RU	RU	0.38 ± 0.18	0.81	1.08	178	0.0345
C_{454}	$C_{366\text{-}int}$	RU	RU	2.34 ± 0.67	0.58	4	178	0.0006
C_{406}	$C_{366\text{-}int}$	RU	RU	1.12 ± 0.16	0.67	0.96	178	<0.0001
C_{366}	$C_{366\text{-}int}$	RU	RU	3.04 ± 0.19	0.78	1.13	178	<0.0001
$C_{462\text{-}490}$	$a_{CDOM}(254)_{int}$	RU	m^{-1}	0.02 ± 0.00	0.84	0.97	178	<0.0001
C_{454}	$a_{CDOM}(254)_{int}$	RU	m^{-1}	0.10 ± 0.01	0.71	3.32	178	<0.0001
C_{406}	$a_{CDOM}(254)_{int}$	RU	m^{-1}	0.03 ± 0.00	0.71	0.89	178	<0.0001
C_{366}	$a_{CDOM}(254)_{int}$	RU	m^{-1}	0.02 ± 0.01	0.45	1.76	178	0.0022
AOU	Prok. Abun.	$\mu mol \cdot kg^{-1}$	$cell \cdot mL^{-1}$	0.29 ± 0.04	0.88	16635.91	219	<0.0001
AOU	$C_{366\text{-}int}$	$\mu mol \cdot kg^{-1}$	RU	4.92 ± 2.39	0.89	16.13	221	0.0405
AOU	Chl a_{int}	$\mu mol \cdot kg^{-1}$	mg Chl $a \cdot m^{-2}$	0.10 ± 0.04	0.89	16.04	221	0.0115
AOU	$a_{CDOM}(254)_{int}$	$\mu mol \cdot kg^{-1}$	m^{-1}	0.30 ± 0.04	0.91	14.59	221	<0.0001

a $\times 10^{-3}$, if 'Parameter 1' is an FDOM component, or if 'Parameter 1' is AOU and 'Parameter 2' is prokaryotic abundance.

communities were usually dominated in abundance by Crenarchaeota (formerly Thaumarchaeota, comprising 22.5% of reads on average, but ranging between 2.2 – 42.4%), followed by the SAR324 clade (12.6%; 6.3 – 20.6%), Thermoplasmatota (10.8%; 2.3 – 28.1%), Marinimicrobia (10.0%; 4.5 – 15.1%), the proteobacteria classes Gammaproteobacteria (9.5%; 5.4 – 16.3%) and Alphaproteobacteria (6.3%; 3.7 – 14%), and Chloroflexi (5.0%; 1.0 – 15.8%), respectively. The rest of the taxa made up 12.2% of reads on average, while the mean abundance of unidentified sequences was 7.9%. The outlier samples had heterogenous community compositions. They presented unusually high abundances of taxa that otherwise were infrequent, especially members of *Actinobacteria* and *Firmicutes*. Nevertheless, Alpha- and

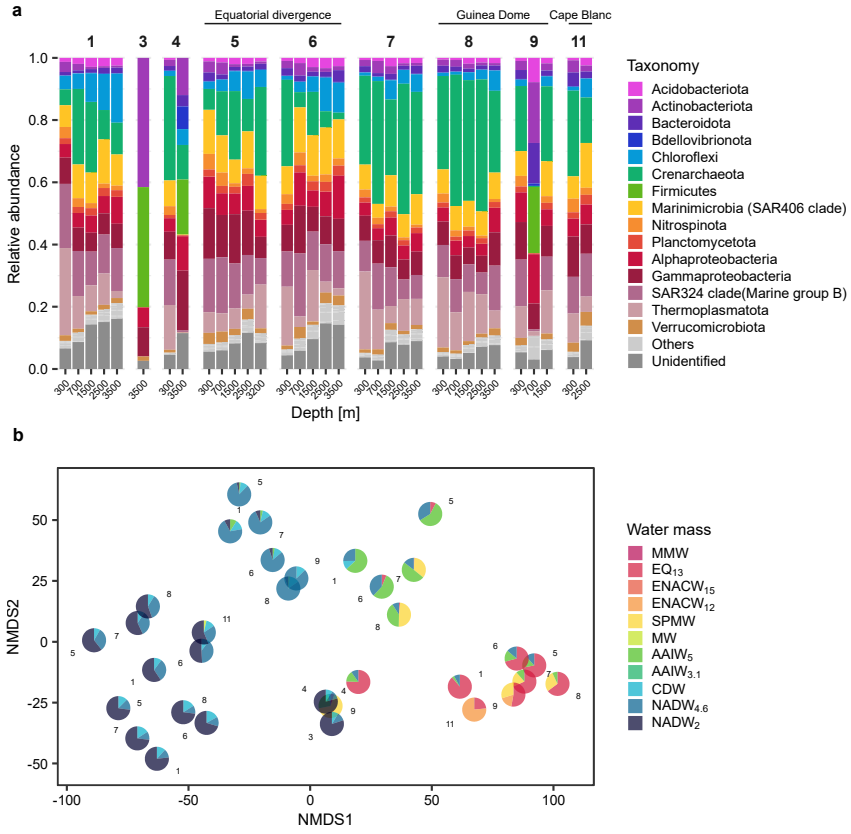

Figure 4. Prokaryotic community composition. (a) Relative abundances of prokaryotic phyla (or class for Proteobacteria) along the cruise section. Numbers on top of bars represent the stations. (b) Distribution of prokaryotic communities in the NMDS space according to their similarities in taxonomic composition. Each pie chart corresponds to a sample, where colours represent the contribution of the different water masses. See the text for water mass abbreviations. Numbers beside pie charts correspond to stations.

Gammaproteobacteria, and Bacteroidota (in st. 9) were also present in high relative abundances (see Supplementary results, and Fig. S6 and S7 for a more detailed description).

NMDS ordination of the samples (Fig. 4b) based on their prokaryotic community structure showed that this was clearly associated with the water mass composition, as samples with similar water mass contributions were overall more similar to each other than to those with different water mass proportions.

Changes in prokaryotic community diversity and composition across water masses

Archetype diversity indices were estimated for water masses that presented a sizeable contribution in the amplicon samples: EQ_{13}, $ENACW_{12}$, SPMW, $AAIW_5$, CDW, $NADW_{4.6}$ and $NADW_2$. In conjunction, these 7 water masses represented 99.87% of the water volume in the amplicon samples (min. $ENACW_{12}$ = 3.12%, max. $NADW_{4.6}$ = 30.14%; Fig. S8). Other water masses were left out as very low contributions would potentially bias archetype estimates. Species (here ASVs) richness (Fig. 5a) was lowest in SPMW (2920 ± 214 ASVs), and highest in bathypelagic water masses (3485-3554). The Pielou index (Fig. 5b), a measure of evenness, was lowest also in the SPMW (0.754 ± 0.026), followed by $AAIW_5$ (0.771 ± 0.016), and highest in $ENACW_{12}$ (0.807 ± 0.004). Similarly, the Shannon alpha diversity index (Fig. 5c) presented minimum values in the SPMW (6.019 ± 0.265) and highest values in $ENACW_{12}$ (6.459 ± 0.091) and $NADW_2$ (6.475 ± 0.116). The phylogenetic diversity to species richness ratio (Fig. 5d) gives an estimate of the phylogenetic relatedness of the ASVs that form the community: low ratios mean that the richness is due to phylogenetically close taxa (microdiversity), and vice versa. This ratio was lowest in EQ_{13} (0.0393 ± 0.0004), relatively stable in the mesopelagic (SPMW, 0.0404 ± 0.0011), and highest in the deep $NADW_2$ (0.0440 ± 0.0009). These results suggest that important differences in prokaryotic community diversity exist between water masses. SPMW, the water mass with the highest archetype AOU value (Table 1), tended to harbour a less diverse and less even prokaryotic community, as opposed to bathypelagic water masses. $ENACW_{12}$, while showing richness and phylogenetic diversity/richness estimates similar to those of SPMW, harboured a more even and diverse community.

An in-depth look into the taxonomic composition of the community in each of the water masses revealed further differences between them. The archetype CLR-transformed abundances of the dominant orders (Fig. 6) showed that

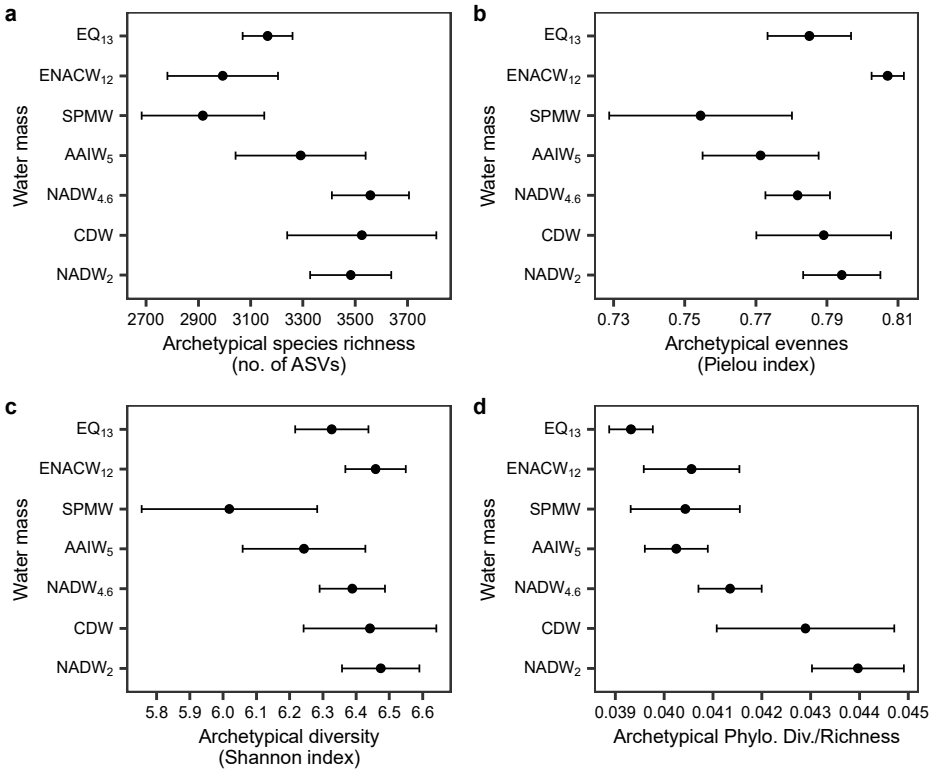

Figure 5. Prokaryotic community diversity indices. Archetype values of (a) species richness (as no. of amplicon sequence variants, ASVs), (b) Pielou evenness index, (c) Shannon index and (d) Faith's Phylogenetic Diversity index / ASV richness ratio. Error bars represent the standard error of the estimates.

Nitrosopumilales, within the Crenarchaetoa phylum, displayed clearly superior abundances in the SPMW and were the dominant ASVs in this water mass (Fig. S9 and Supplementary results). Nonetheless, there were within-order differences in the abundance patterns of the Nitrosopumilales. A close inspection of the archetype abundances of the dominant Nitrosopumilales ASVs showed two groups with contrasting distributions: one with peak abundances in the SPMW (including most of the ASVs with the highest abundances, thus, dominating the order-level trend) and a second group that presented maximum abundance values in bathypelagic waters (Fig. S10). Fitting mixing models to CLR-transformed abundances of dominant ASVs showed that the variability explained by the mixing models markedly differed within the Nitrosopumilales order (Fig. S11): overall, ASVs associated with the SPMW presented lower r^2 (< 0.6), while those with highest archetype abundances in bathypelagic water masses were better explained by mixing (r^2 > 0.7). Mixing

models account for the mixing between the different water masses, but also for the history of these water masses, i.e., all the remineralization processes that have occurred from the formation area of the water mass to the study region (Álvarez-Salgado et al. 2013). Considering the turnover rates of prokaryotes in the deep North Atlantic (24-55 days, Reinthaler et al. 2013) relative to the age of the studied water masses (few years to over a hundred years, Khatiwala et al. 2012; Catalá et al. 2015a), the ASVs that are highly explained by the mixing models would have experienced a selection over time in those water masses, leading them to sustain the abundances they display. Including biogeochemical variables in the regressions did not always yield significant regression coefficients, but multiple ASVs were positively associated with C_{454} and, to a lesser extent, AOU (Fig. S12).

The SAR324 clade, Marine Group II (maximum in the SPMW, but also in EQ_{13}), SAR11 clade (Alphaproteobacteria), Microtrichales (Acidobacteria),

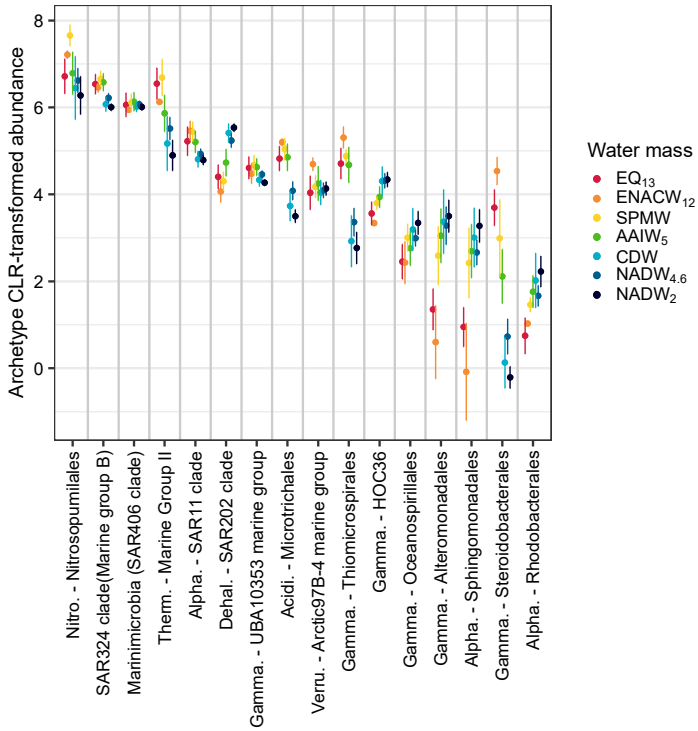

Figure 6. Taxonomic characterisation of the water masses. CLR-transformed archetype abundances in water masses of orders (phyla, for SAR324 clade and Marinimicrobia) that contain dominant amplicon sequence variants (>0.5% in at least one sample). Bars represent standard errors of archetype abundances. When available, the abbreviated class designation is shown to the left of order label.

Thiomicrospirales and Steroidobacterales (Gammaproteobacteria) were more abundant in mesopelagic water masses, while the SAR202 clade (Chloroflexi), HOC36 (Gammaproteobacteria), Oceanospirillales (Gammaproteobacteria), Alteromonadales (Gammaproteobacteria), Sphingomonadales (Alphaproteobacteria) and Rhodobacterales (Alphaproteobacteria) presented higher archetype abundances in bathypelagic water masses (Fig. 6, Fig. S10). Thiomicrospirales, Alteromonadales, Sphingomonadales and Steroidobacterales displayed the largest differences between water masses. On the contrary, Marinimicrobia, UBA10353 marine group (Gammaproteobacteria) and the Arctic97B-4 marine group (Verrucomicrobiota) were equally abundant in the different water masses. Marinimicrobia presented differences at the ASV level (Fig. S10), with one group of ASVs enriched in mesopelagic waters and another group in bathypelagic water masses. Mixing models showed greatest explanatory capacity for Marinimicrobia, Marine Group II, SAR202 and HOC36 with r^2 exceeding 0.8 - 0.9, while Alteromonadales only reached r^2 of 0.35 - 0.55 (Fig. S11). Among biogeochemical variables, humic-like fluorescence components, AOU and $a_{CDOM}(254)_{int}$ helped explain the distributions of these prokaryotic taxa. SAR202 bacteria showed significant negative coefficients for C_{454}, AOU and $a_{CDOM}(254)_{int}$ (Fig. S12), in agreement with their greater abundances in bathypelagic water masses and, to a lesser extent, in $AAIW_5$ (Fig. 6). Alteromonadales ASVs also displayed negative coefficients for C_{454} and, to a lesser extent, $C_{462\text{-}490}$ and C_{406}. On the contrary, a considerable part of the Marine Group II and HOC36 ASVs presented positive significant coefficients for C_{454} and $a_{CDOM}(254)_{int}$ (Fig. S12).

Discussion

FDOM characteristics and distribution in water masses

Detailed descriptions of FDOM distributions in the deep tropical Atlantic are scarce. Catalá et al. (2015b) reported values for components similar to $C_{462\text{-}490}$ and C_{406} within the Equatorial Atlantic Central Water and North Atlantic Deep Water that agree with our findings both qualitatively, with an overall increase in fluorescence from intermediate to deep waters (Fig. 3 and Table 1), and quantitatively, as their fluorescence values fall within the range of those found here. The humic-like components generally displayed higher values below the epipelagic layer, probably due to photobleaching in surface waters (Catalá et al. 2016), while also showing a northward increase in fluorescence in the entire water column, specially marked for component C_{454} (Fig. 3). This change in fluorescence was coupled with an increase in

AOU, but not entirely: $NADW_{4.6}$ and $NADW_2$ presented high $C_{462\text{-}490}$ and C_{454} fluorescence relative to their AOU (Table 1, Fig. S13), suggesting a contribution by terrestrial FDOM introduced in the source region of NADW (Benner et al. 2005; Jørgensen et al. 2011; Catalá et al. 2015b). High values of C_{406} were measured within the Oxygen Minimum Zone (OMZ) of the eastern tropical Atlantic (10-18°N, Fig. 2b and S5). This oceanographic feature is generated by the combination of remineralisation by prokaryotes of abundant sinking organic matter from the highly productive surface waters between the Guinea Dome and Cape Blanc (influenced by the Northwest African upwelling zone, Fig. 1 and Fig. S14; Carr and Kearns, 2003) and reduced ventilation by currents (Stramma et al. 2008). Minimum O_2 concentrations in the OMZ were ~50 μmol·Kg^{-1}, which agree with values reported in the literature that ascribe the eastern tropical Atlantic OMZ as an hypoxic zone (Karstensen et al. 2008; Stramma et al. 2008). The fluorescence-AOU coupling (Fig. S13) suggests that the increase in fluorescence was related to microbial transformation of organic matter, producing humic-like DOM, which has been documented in the literature (Jørgensen et al. 2014). The direct C_{406}-AOU relationship displayed variability (Fig. S13), suggesting that multiple factors, including potential consumption by prokaryotes, might influence its distribution. The transformation of vertically transported organic matter might have enhanced the humic-like FDOM signal, as stations 8, 9, 11 and12 showed high levels of the protein-like C_{366} throughout the water column. Moreover, stations 8-11 also presented widespread, high humic-like fluorescence in the bathypelagic layer which, in addition to the NADW influence, could reflect a considerable remineralisation below 1000 m as a consequence of high export rates in these productive stations. OMZs are known to reduce the remineralisation rates of sinking particles, allowing them to reach greater depths than they otherwise would in environments with greater O_2 concentrations (Rasse and Dall'Olmo 2019).

As expected from their spatial distributions, humic-like FDOM components ($C_{462\text{-}490}$, C_{454}, C_{406}) were found to be significantly related to AOU (Table 3, Fig. S13), agreeing with previous findings that described fluorophores similar to $C_{462\text{-}490}$ and C_{406} displaying positive correlations with AOU in the deep ocean (De La Fuente et al. 2014; Catalá et al. 2015b). The higher explanatory power of $C_{462\text{-}490}$ by water mass mixing, and slightly lower by AOU relative to C_{454} and C_{406} (Tables 2 and 3), suggests that the characteristics of compounds comprising this fluorophore hindered biologically mediated degradation processes to a greater degree. Contrary to humic-like components, the protein-like C_{366} was the least explained by the mixing model and showed no improvement when including AOU, suggesting totally different

dynamics. The explanatory capacity of $C_{366\text{-int}}$ (C_{366} values integrated over the epipelagic layer) was significant for all FDOM components but highest for C_{366}, further supporting the view that deep ocean protein-like DOM is linked to the downward flux of protein-like material through sinking particles (Ruiz-González et al. 2020). Another factor that could potentially contribute to the protein-like FDOM signal in the dark ocean (especially in the mesopelagic layer) is the excretion of protein-like DOM by zooplankton and micronecton (Urban-Rich et al. 2006; Morán et al. 2022). High biomasses of these organisms were found in stations 8, 9 and 11 (Hernández-León et al. 2019), where the C_{366} signal was strong (Fig. 3d).

Together, these observations would suggest that the increased humic-like fluorescence is partially a consequence of the vertical export of organic matter and subsequent remineralization, which is supported by the fact that several proxies of epipelagic productivity (here as $C_{366\text{-int}}$, $a_{CDOM}(254)_{int}$ proxies) significantly contributed to the explained variance of FDOM components, AOU and prokaryotic abundance (Table 3). This links the surface conditions to the microbial reworking of organic matter in the water masses of the dark tropical and subtropical Atlantic. These results support the view that, while water mass mixing and history play an important role, there is a strong vertical connection between the processes occurring in the water column, as it has been recently suggested (Mestre et al. 2018; Ruiz-González et al. 2020).

Water mass-specific differences in prokaryotic community composition

While the overall composition of the prokaryotic communities followed water mass composition (Fig. 4), this pattern might have been partly influenced by the vertical distribution of communities (DeLong et al. 2006), since bathypelagic water masses occupied much of the section in their depth ranges (Fig. 2a). Nonetheless, differences were identified between water masses both in terms of overall diversity (Fig. 5) and specific taxonomic composition of the prokaryotic communities (Fig. 6 and S10), in agreement with previous studies showing that water masses harbour distinct prokaryotic communities (Agogué et al. 2011; Salazar et al. 2016). Among water masses, the SPMW, directly influenced by the OMZ of the Eastern North Atlantic, presented the less diverse and even community (dominated by several abundant taxa). Decreases in diversity of the prokaryotic community have been observed in OMZs elsewhere (Bertagnolli and Stewart 2018; Beman et al. 2020) and point to a narrower range of prokaryotes able to thrive in low oxygen conditions, although contrasting results have been reported (Stevens and Ulloa 2008). The community in deep water

masses was in general more diverse and had higher evenness (Fig. 5b), which agrees with previous reports from the deep North Atlantic (Agogué et al. 2011; Frank et al. 2016). This was paired with high phylogenetic diversity/ASV richness ratios (Fig. 5d), indicating that the diversity was due to phylogenetically distant ASVs, which suggests that the prokaryotic communities present in bathypelagic water masses could potentially display a wider range of metabolic capabilities.

Specific orders of prokaryotes showed different distributions across waters masses (Fig. 6), with three main patterns emerging: orders that were 1) more abundant in one or multiple central/intermediate water masses (predominantly, Nitrosopumilales and Marine Group II), 2) more abundant in deep water masses (SAR202 clade, Alteromonadales), and 3) equally abundant across water masses (Marinimicrobia). This association of prokaryotic taxa with specific water masses has been previously reported (Agogué et al. 2011). Nonetheless, within-order variability was observed in multiple instances (Fig. S10) as ASVs belonging to the same order showed differing patterns, suggesting distinct associations with environmental conditions even for closely related prokaryotes.

Nitrosopumilales presented a notable enrichment in the SPMW (Fig. 6 and S10). The fact that ASVs belonging to this order thrived in waters associated to high humic-like FDOM and AOU values suggests that an effective metabolism under suboxic conditions allow this group to prevail in environments where predominantly recalcitrant DOM and low O_2 concentrations hinder activity of heterotrophic organisms. Nitrosopumilales have an efficient autotrophic metabolism using energy derived from the oxidation of very low concentrations of ammonia via a modified version of the hydroxypropionate/hydroxybutyrate (HP/HB) cycle (Könneke et al. 2014), and are also known to utilise cyanate and urea as sources of energy and nitrogen (Kitzinger et al. 2019). It has been recently shown that they can produce small amounts of O_2 that would aid their ammonia-oxidising metabolism (and potentially to other microbes) in low oxygen waters (Kraft et al. 2022). The dominance of this archaeal order in the SPMW agrees with previous reports of organisms closely related to Nitrosopumilales dominating nitrifying processes in suboxic waters (Labrenz et al. 2010; Stewart et al. 2012). Nonetheless, the presence of another group of Nitrosopumilales ASVs with abundance peaks in the bathypelagic (Fig. S10) suggests a functional partitioning within this order adapted to specific conditions within the water column.

ASVs classified as Marine Group II (Thermoplasmatota) were among the most abundant orders in the different water masses and displayed co-occurrence patterns

with Nitrosopumilales (Fig. S10). Members of Marine Group II are deemed to play an important role in the cycling of organic matter, as it has been observed that they possess genes for the degradation of high molecular weight compounds (such as proteins, polysaccharides and lipids) and the intermembrane transport of organic molecules (Tully 2019). Marine Group II ASVs were most abundant in the SPMW (although EQ_{13} presented similar archetype abundance, Fig. 6), where there was a strong signal of FDOM and AOU (Fig. 2b and 3, Table 1) and higher productivity in surface waters (Fig. S14). This is in agreement with the observation in the Iberian upwelling zone of Marine Group II archaea in high abundances in low oxygen conditions, in correlation with humic-like FDOM (Guerrero-Feijóo et al. 2017). Moreover, this order has been reported as an important contributor to both the uptake of glucose and the degradation of complex organic matter in the bathypelagic Mediterranean (Boutrif et al. 2011). Thus, in contrast to Nitrosopumilales, Marine Group II archaea inhabiting the dark ocean seem to have a prevalent heterotrophic life-style (Deschamps et al. 2014). The presence of organisms of this order in low-oxygen conditions has been previously observed (Belmar et al. 2011) and might be favoured by their ability to conduct nitrate respiration (Rinke et al. 2019).

An important number of ASVs classified as members of the SAR324 clade were associated with mesopelagic water masses while others seemed to favour bathypelagic environments (Fig. S10). The widespread presence and high abundances of ASVs belonging to this phylum indicates that they are well adapted to the varying conditions in the dark ocean, including suboxic waters (Pajares et al. 2020), as suggested by their autotrophic and extremely versatile metabolism (Swan et al. 2011; Sheik et al. 2014).

SAR202 showed higher archetype abundances in bathypelagic water masses, increasing from 300 m to 3500 m (Fig. 6 and S10) agreeing with previous reports from the Atlantic (Varela et al. 2008). Members of SAR202 are considered to be heterotrophic, free-living bacterioplankton (Mehrshad et al. 2018), and genomic studies have suggested their ability to utilise recalcitrant DOM (Landry et al. 2017; Saw et al. 2020). For instance, Landry et al. (2017) highlighted the number of genes predicted to encode a variety of monooxygenases and dehydrogenases, which they deemed likely to participate in the activation of alicyclic and long-chain molecules for their degradation. Thus, the ability of SAR202 to utilise diverse recalcitrant compounds would potentially explain their high contribution to communities in deep water masses.

Differences were observed in the explanatory capacity of the mixing models on the abundances of dominant taxa (Fig. S11). For instance, ASVs belonging to Marinimicrobia, which was abundant across water masses (Fig. 6 and S10) and known to inhabit a variety of oceanic environments (Hawley et al. 2017), were highly explained by the mixing models, as did SAR202 ASVs. Thus, their distribution seemed to be largely determined by a combination of water mass mixing and the selection they had experienced in the different water masses since their formation. On the contrary, some orders were weakly explained by the mixing models (Fig. S11), suggesting that local biogeochemical processes, such as the vertical connection associated with surface productivity (Frank et al. 2016; Mestre et al. 2018) or other undetermined processes, were more important for their distribution. Alteromonadales was an example of such taxa (Fig. S11), as they are known copiotrophs and opportunists that are usually found associated with particles, quickly reacting to organic matter inputs in 'boom-and-bust' dynamics (Mestre et al. 2018; Reintjes et al. 2020). Nonetheless, while negative relations were observed with humic-like FDOM (Fig. S12), no significant relationship was found between Alteromonadales and protein-like FDOM (Fig. S12). Thus, a definitive explanation about the factors involved in controlling their distribution in accordance with their known copiotrophy cannot be inferred from our results.

Conclusions

In this study we jointly characterised the FDOM pool and the prokaryotic community compositions across water masses of the tropical and subtropical Atlantic Ocean. We found that the most humic, aromatic and complex fraction of FDOM ($C_{462\text{-}490}$) was more influenced by mixing and the history of the water masses, while the protein-like component (C_{366}) was the most subjected to intra-regional, non-conservative biogeochemical processes (likely due to vertical transport of sinking organic matter related to surface productivity gradients). Other humic components (C_{454}, C_{406}) laid in between those extremes. AOU was observed to significantly explain the variance of the humic components, linking them to microbial activity. The composition of the prokaryotic community was found to be associated with these processes: diversity decreased with increasing values of AOU, with minimum values in the SPMW, the water mass most influenced by the Eastern North Atlantic OMZ. Likewise, specific taxa displayed differing abundances between water masses: Nitrosopumilales were more abundant in the SPMW, dominating low-oxygen waters, and Marine Group II archaea, SAR324 clade and Thiomicrospirales tended

to co-occur with them in this water mass. On the contrary, members of the SAR202 clade were more abundant in bathypelagic water masses, while Marinimicrobia were distributed across the water column. Mixing models explained in varying degrees the abundance patterns of different taxa, suggesting that the distribution of some of them (e.g., Marinimicrobia, SAR202) was dominated by mixing and selection within the water masses since their formation, while others (e.g., Alteromonadales) were not. Thus, while water masses showed differences in their DOM characteristics and prokaryotic communities depending on their initial properties, ageing history and mixing, a fraction of the DOM signal and prokaryotic community was deemed to be controlled (in varying degrees) by local processes (such as vertical inputs of organic matter, as suggested by the relationships displayed with the epipelagic productivity proxies). Our observations are relevant to the understanding of how microbial-DOM interactions, including long-term changes within water masses and the vertical connectivity along surface productivity gradients, affect the compositions of both the DOM pool and the prokaryotic community in the dark ocean. Distinct prokaryotic taxonomic groups would display different metabolisms favouring the consumption and transformation of certain types of DOM, affecting the long-term (i.e., centennial scales) storage of C in the deep ocean. Future studies including the characterization of the organic matter with non-targeted ultra-high resolution analytical techniques such as FT-ICR-MS are necessary to provide detailed insights into the role of distinct prokaryotic communities in the degradation and/or generation of specific compound classes.

Supplementary material

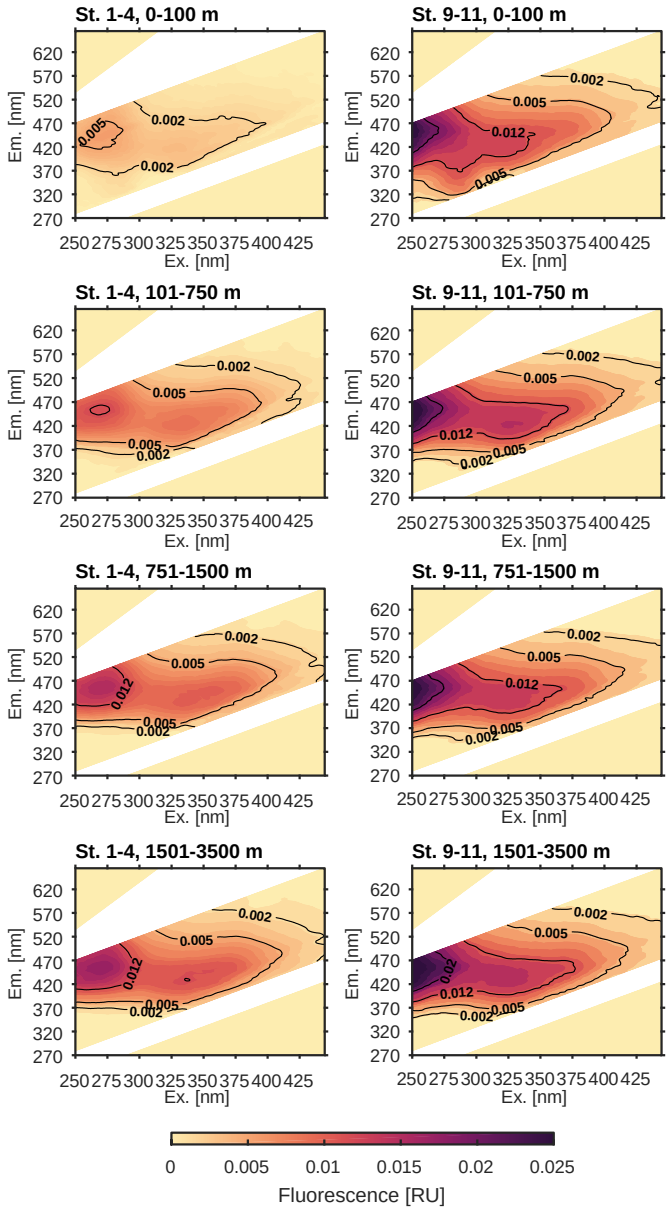

Figure S1. Average excitation-emission matrices of FDOM samples from stations 1-4 (left column) and 9-11 (right column), and depths (from top to bottom) 0-100 m, 101-750 m, 751-1500 m and 1501-3500 m. EEMs were processed using the DOMFluor toolbox (v. 1.7; Stedmon and Bro, 2008) toolbox for Matlab (R2017a), see Methods for details.

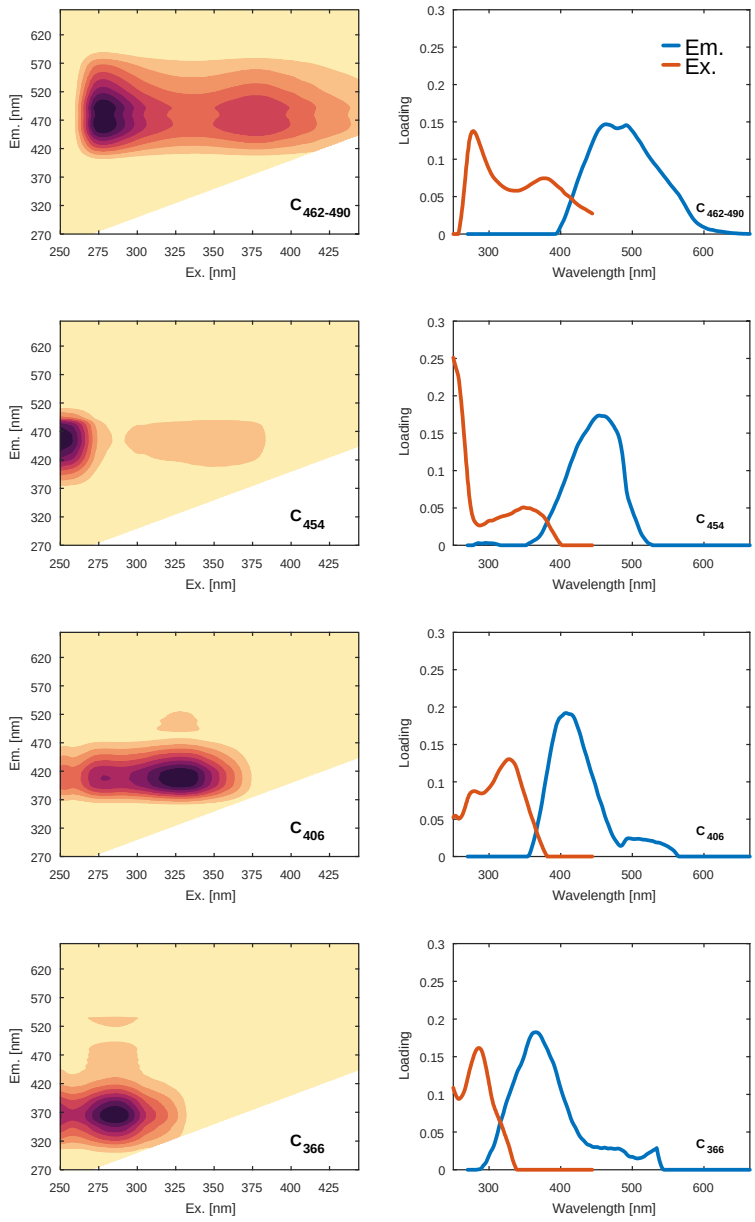

Figure S2. FDOM components derived from the PARAFAC analysis (see Methods for details). In the left column, excitation-emission matrices (EEMs) of each component; in the right column, excitation (red) and emission (blue) spectra. The processed EEMs were analysed using the DOMFluor toolbox (v. 1.7; Stedmon and Bro, 2008) toolbox for Matlab (R2017a).

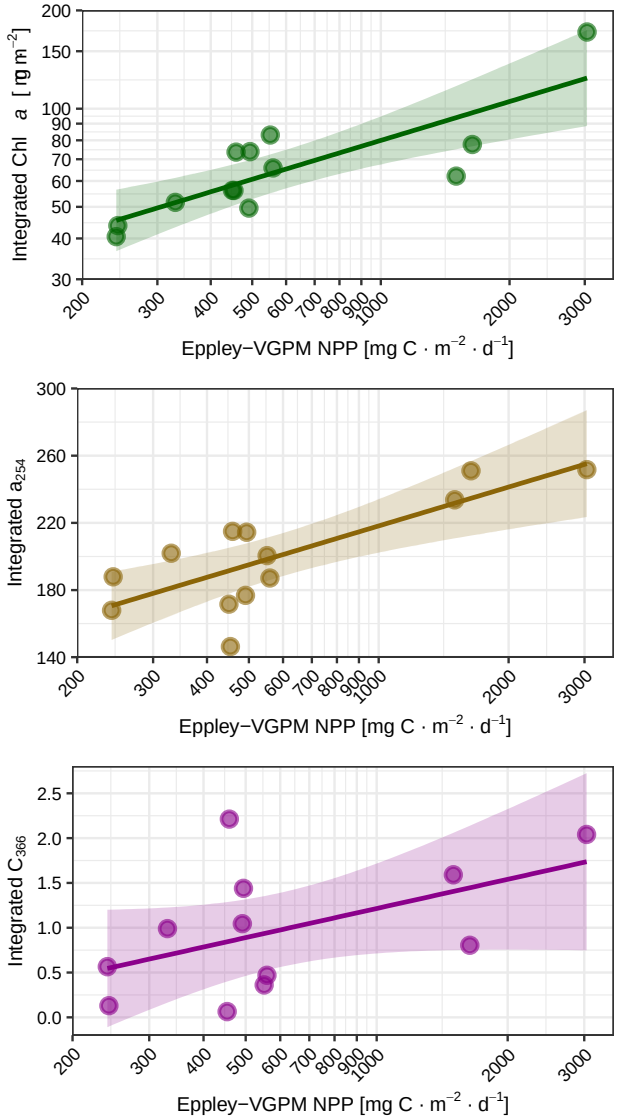

Figure S3. Relationships between satellite-derived NPP (Eppley-VGPM model, MODIS dataset, April 2015; sites.science.oregonstate.edu/ocean.productivity) and integrated values of Chl *a*, $a_{CDOM}(254)$ and C_{366} over the upper 200 m.

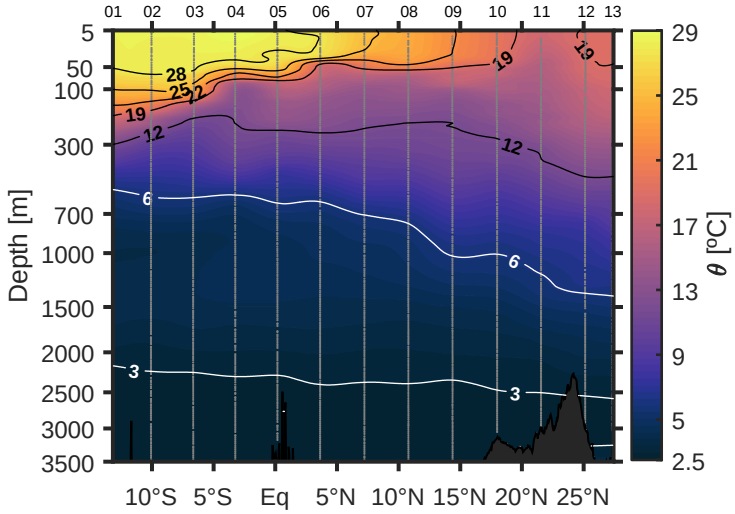

Figure S4. Potential temperature (θ) along the cruise section. Data interpolation was performed with DIVA in Matlab (R2017a).

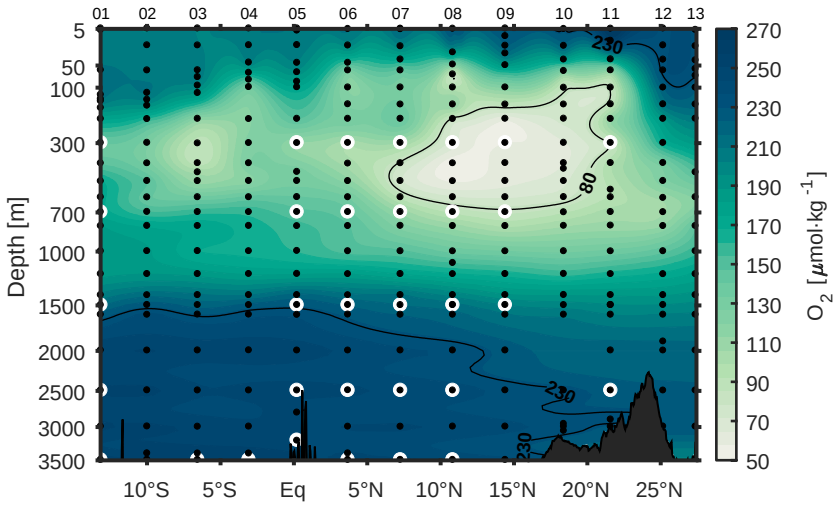

Figure S5. Latitudinal distribution of dissolved oxygen concentration. Black points represent bottle samples included in the OMP and white circles the locations of amplicon samples. Note that the vertical scale is square root-transformed to allow for a better visualisation of the results. Numbers on top correspond to stations in Fig. 1. Data interpolation was performed with DIVA in Matlab (R2017a).

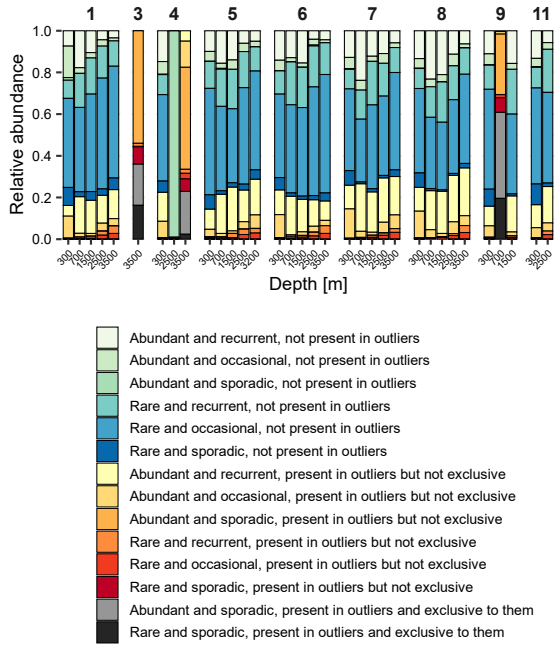

Figure S6. Amplicon sequence variant (ASV) classification by abundance and appearance frequency. ASVs that represented >1% of the community in at least one sample were defined abundant. The rest were considered rare. As to appearance frequency, ASVs present in >75% of samples were considered recurrent, those present in <75% and >25% of samples were considered occasional and those present only in <25% of samples were considered sporadic. Furthermore, ASVs were also classified according to their relation to outlier samples: ASVs exclusive to outlier samples, ASVs present both in outlier and regular samples, and ASVs absent in outlier samples.

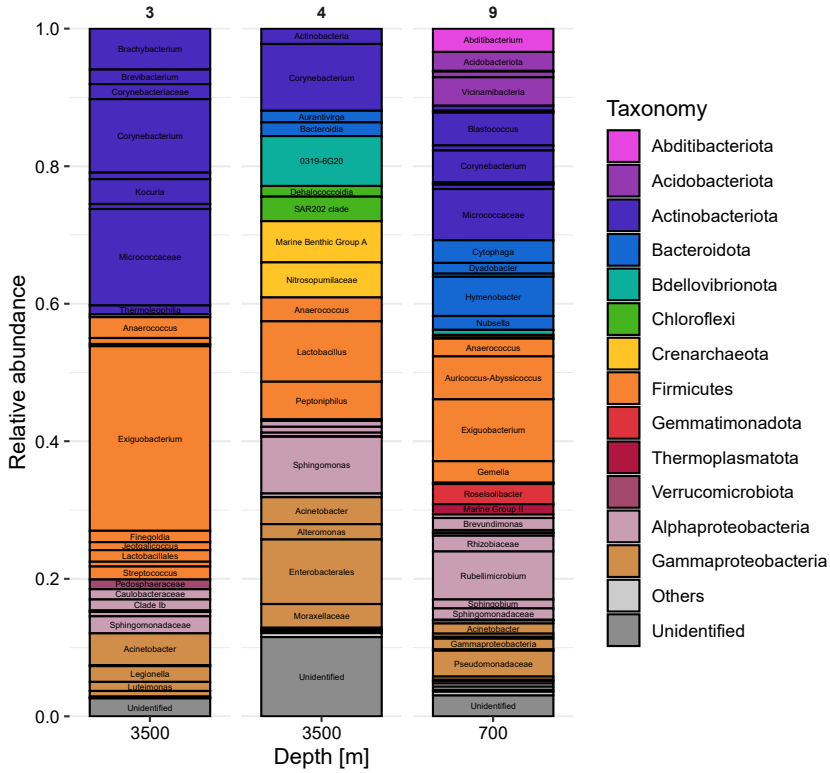

Figure S7. Detailed taxonomic classification, down to the genus level where possible, of the amplicon sequence variants (ASVs) in the outlying samples (st3-3500m, st4-3500m, st9-700m).

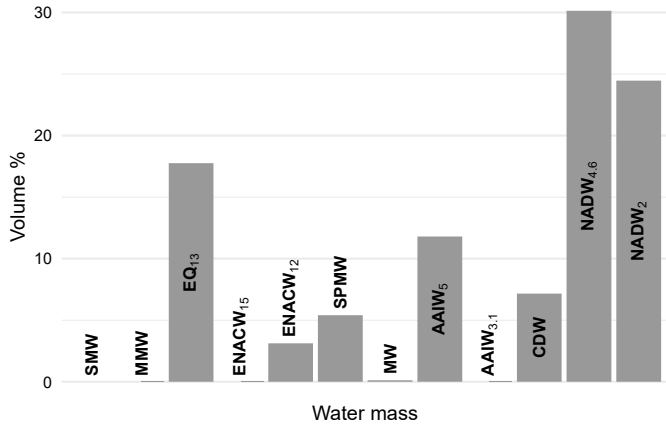

Figure S8. Accumulated contribution, as % of the total volume sampled, of the water masses in the amplicon samples.

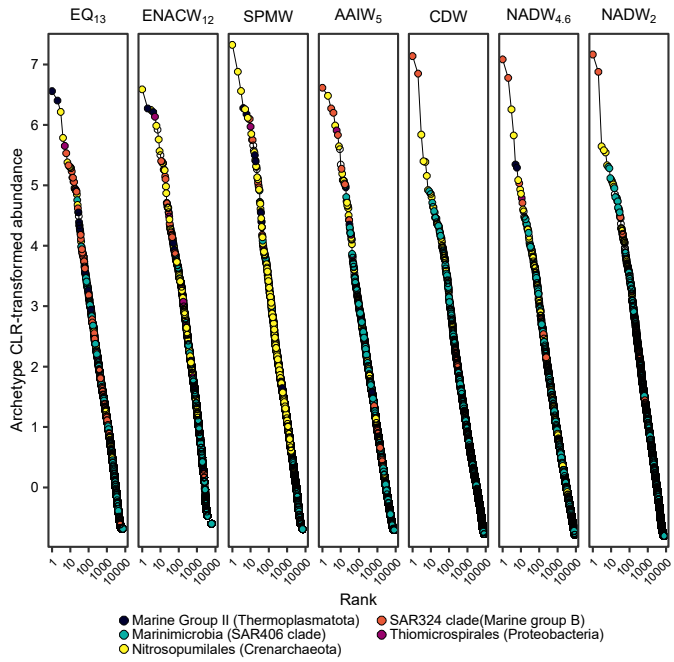

Figure S9. Taxonomic characterisation of the water masses. Rank abundance curves of amplicon sequence variants (ASVs), per water mass. Only the orders of the most abundant ASVs are colour-coded for simplicity.

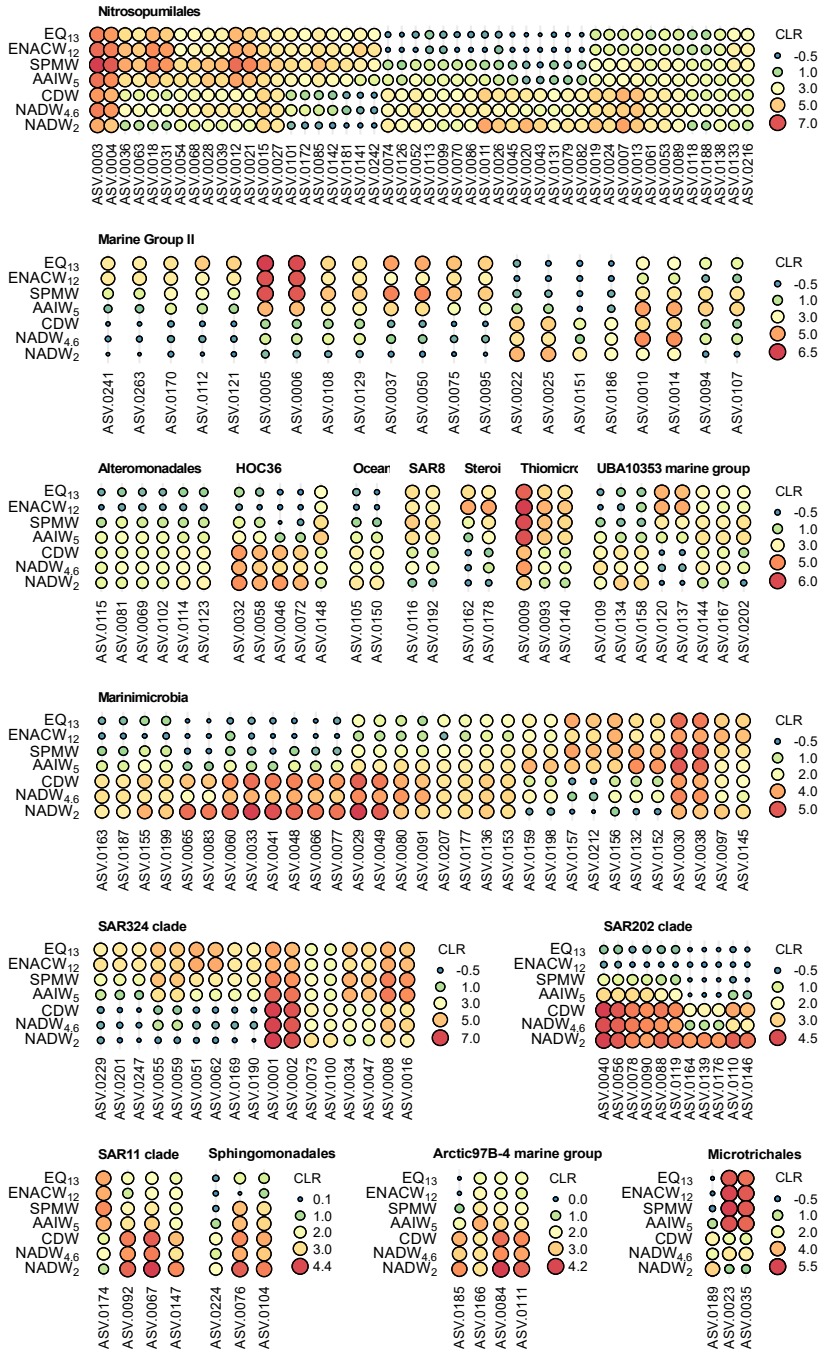

Figure S10. Archetype CLR-transformed abundances of amplicon sequence variants (ASVs) belonging to the orders/phyla shown in Fig. 6 that are present among the top-200 most abundant ones. ASVs are ordered by hierarchical clustering to group those with similar results in order to aid visualisation.

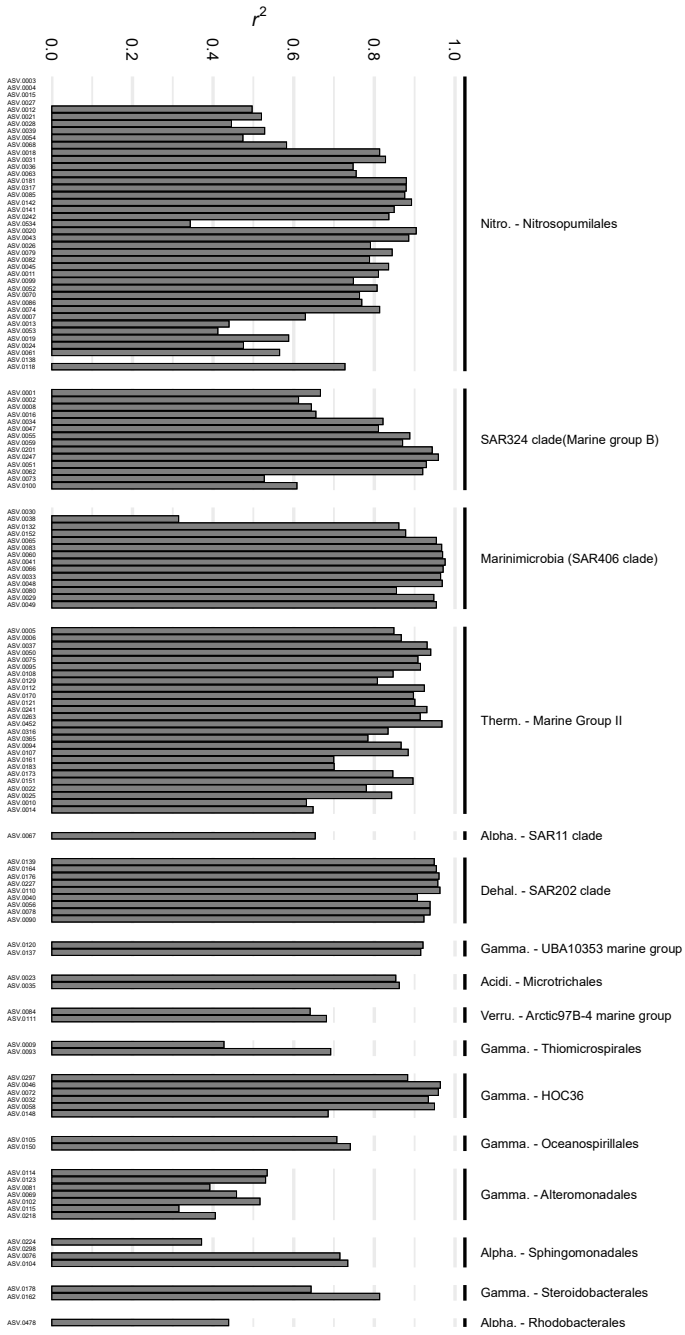

Figure S11. Results from the mixing regression models for dominant amplicon sequence variants (ASVs) (>0.5% in a sample). The explanatory capacity of the mixing models for each ASV is represented by the coefficient of determination (r^2). ASVs are grouped by order (phylum, for SAR324 clade and Marinimicrobia). When available, the abbreviated class designation is shown to the left of order label.

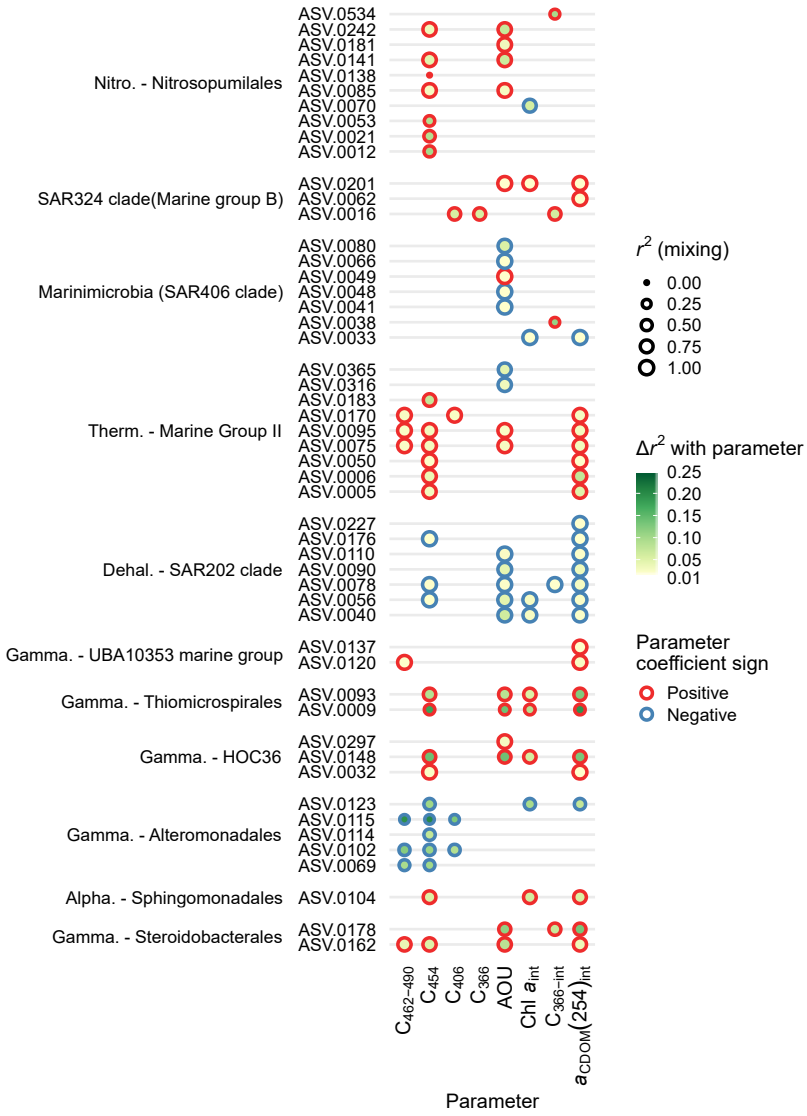

Figure S12. Results from the mixing + biogeochemistry regression models for dominant amplicon sequence variants (ASVs) (>0.5% in at least a sample). Only ASVs with significant results are shown. Circle size represents the coefficient of determination (r^2) of the mixing model, circle fill colour represents the r^2 improvement when including each of the biogeochemical parameters into the models, and circle border colour represents the sign of the regression coefficient of each biogeochemical parameter. ASVs are grouped by order (phylum, for SAR324 clade and Marinimicrobia). When available, the abbreviated class designation is shown to the left of order label.

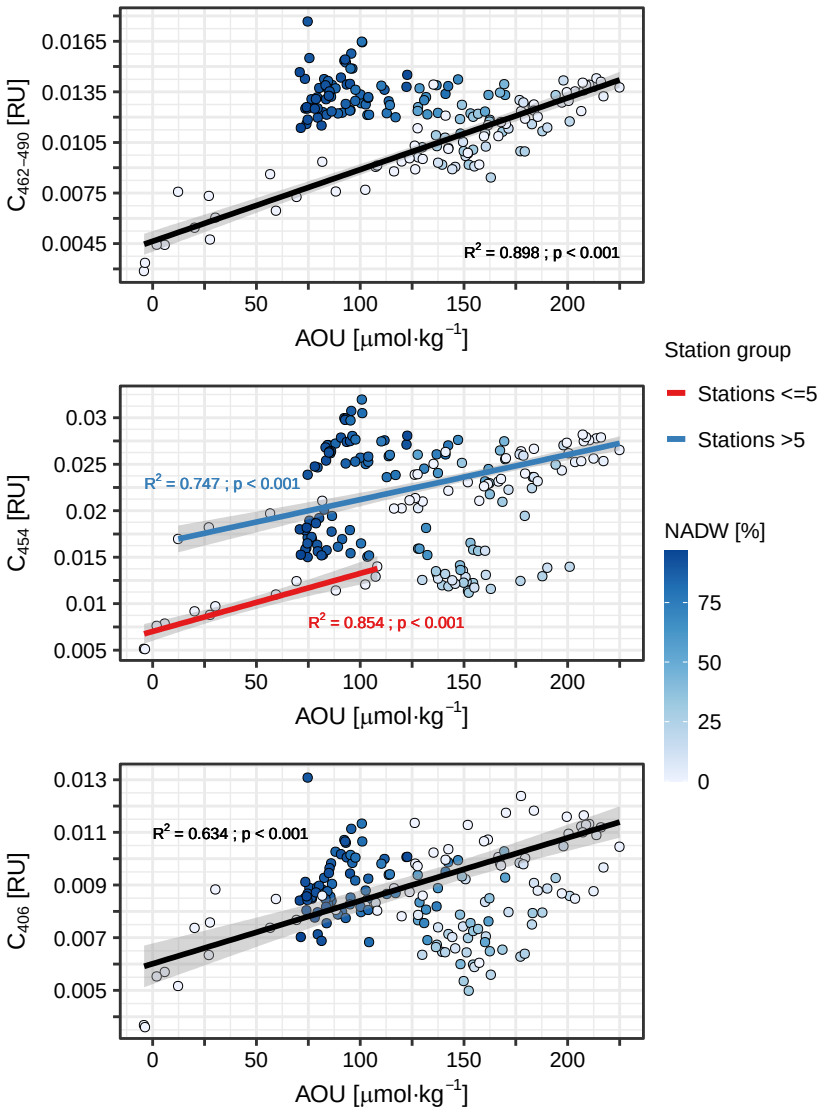

Figure S13. Influence of NADW in humic-like FDOM signals, and relationship between humic-like FDOM and AOU. Linear regressions were performed only including samples with NADW ($NADW_{4.6}$ + $NADW_2$) contributions of <5%. Colormap represents the contribution of NADW (as %) in each sample. For C_{454}, regressions were divided in two station groups (1-5 and 6-12).

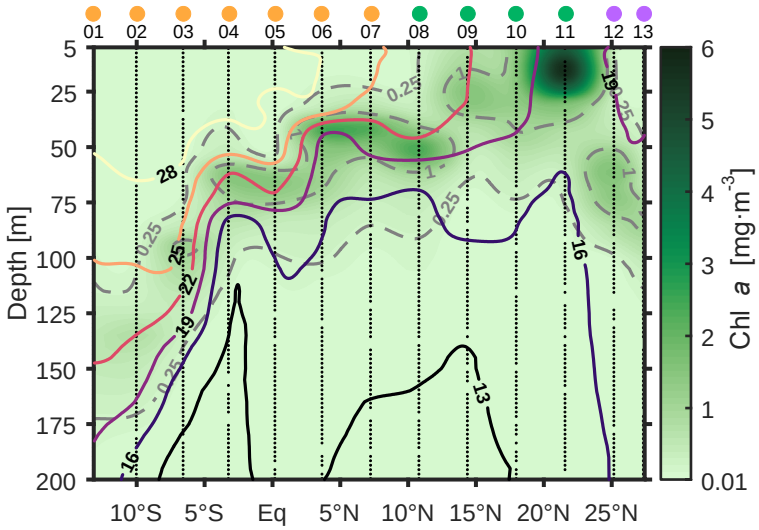

Figure S14. Fluorescence-based Chl *a* estimates derived from the CTD fluorometer within the first 200 m.

Supplementary methods

Chromophoric dissolved organic matter

Seawater samples for the analysis of chromophoric dissolved organic matter (CDOM) were collected following the same procedure as for FDOM samples (see Materials and methods section).

Absorption spectra were determined using an Ocean Optics USB2000+UV-VIS-ES Spectrometer alongside a World Precision Instruments liquid waveguide capillary cell (LWCC) with a path length of 0.9982 m. Absorbance was recorded between 200 and 750 nm both for seawater samples and blanks (performed with freshly produced ultrapure water). Raw data was processed by subtracting the blanks to the seawater measurements (blank correction), followed by the subtraction of the average absorbance between 600 and 700 nm to the whole spectrum (dispersion correction).

The absorbance ($A_{CDOM}(\lambda)$) spectra were transformed into absorption coefficient ($a_{CDOM}(\lambda)$) spectra following the definition of the Napierian absorption coefficient:

$$a_{CDOM}(\lambda) = 2.303 \cdot \frac{A_{CDOM}(\lambda)}{L}$$

Where, for each wavelength λ, the absorption coefficient $a_{CDOM}(\lambda)$ is given by the absorbance at wavelength λ (A_λ), the path length of the cuvette (L, in meters) and 2.303, the factor that converts from decadic to natural logarithms.

The absorption coefficient at 250 nm ($a_{CDOM}(250)$) was used during the preprocessing of the excitation-emission matrices of the fluorescence data. The absorption coefficient at 254 nm ($a_{CDOM}(254)$) was used as a proxy for dissolved organic carbon concentration (Catalá et al., 2018; Lønborg and Álvarez-Salgado, 2014).

Prokaryotic cell abundance

Seawater samples for measuring the abundance of prokaryotes were collected in all stations at 22 depths, from surface to 3500 m (or bottom, where it was above this depth). Samples were collected into cryovials and fixed with paraformaldehyde at 1%, left at 4°C in the dark for 15' and subsequently stored at -80°C. After 24h they were analysed in a FACSCalibur (Becton-Dickinson) flow cytometer, by staining 1.2 mL of sample with 4 μL of SybrGreen I (Molecular Probes) diluted in DMSO (1:10). Fluorescent beads (Polysciences) were added for internal calibration ($10^5 \cdot mL^{-1}$).

Inorganic nutrients

Inorganic nutrients were sampled from Niskin bottles with polyethylene tubes and stored at −20°C until analysis in the laboratory. The analysis was performed with a QuAAtro 39-SEAL Analytical AutoAnalyzer following Armstrong et al. (1967).

Supplementary results

Atypical prokaryotic communities

Three samples presented prokaryotic community compositions which starkly differed from the bulk of samples (Fig. 4 in the main text): samples st3-3500m, st4-3500m and st9-700m displayed rare amplicon sequence variants (ASVs) with unusually high relative abundances. Most of the ASVs present in these samples were also detected in others (Fig. S9), but a number of them (92, 1.05% of total ASVs) were only found in the outliers. The taxonomic classification of the ASVs (Fig. S7) showed important contributions by Actinobacteria (Corynebacterium, Micrococcaceae) and Firmicutes (Exiguobacterium, Anaerococcus, Lactobacillus), followed by Alphaproteobacteria (Sphingomonadales), Gammaproteobacteria (Acinetobacter) and Bacteroidota. Specially interesting is the case of st4-3500m, where these rare prokaryotic community compositions were coupled with maxima of prokaryotic cell abundance (not shown). This may be indicative of a local bloom of these rare prokaryotes. For the other two samples, however, there were no major changes in organic matter or cytometric properties.

Abundance rank curves

Abundance rank curves provided details on the differences in the taxonomy of the prokaryotic communities present in the distinct water masses. The top ASVs consistently belonged to the SAR324 clade, Nitrosopumilales (Crenarchaeota) and Marine Group II (Thermoplasmatota) (Fig. S9). However, clear changes were observed between water masses: in EQ_{13} and $ENACW_{12}$, Marine Group II was prominently found within the top taxa, alongside Nitrosopumilales and, to a lesser extent, Thiomicrospirales (Gammaproteobacteria) and SAR324. SPMW displayed a similar arrange of ASVs, but three Nitrosopumilales ASVs stood out above the rest. In $AAIW_5$ and, specially, CWD, $NADW_{4.6}$ and $NADW_2$, SAR324 ASVs were the most abundant ones and Marinimicrobia ASVs tended to occupy higher ranks. Differences between water masses were further evidenced by the dominance of the

top ASVs, which can be assessed by the steepness of the rank curve (Fig. S9). EQ13, $ENACW_{12}$ and $AAIW_5$ contrasted with the bathypelagic water masses, as the former showed a gentle slope, with the top ASVs presenting relatively similar archetype abundances without marked drops. On the contrary, the CDW, $NADW_{4.6}$ and $NADW_2$ presented abrupt decreases in archetype abundances within the top 10 ASVs, especially between the first two (SAR324) and the following ones. A marked decrease was also observed for the first three ASVs in the SPMW, all classified as Nitrosopumilales. The SPMW was the only water mass dominated to such an extent by Nitrosopumilales ASVs.

Supplementary tables

Table S1. Characteristics of the FDOM components derived from the PARAFAC analysis, along with analogous fluorophores previously described in the literature. FDOM fluorophores from the literature were identified making use of the OpenFluor database (Murphy et al., 2014), applying threshold values of the Tucker Congruence Coefficients (TCC) of 0.95 for both excitation and emission spectra, yielding a minimum $TCC_{ex\text{-}em}$ value of 0.9025 (except for C_{454}). Wavelengths between parentheses represent secondary maxima.

This study			Previously identified					
Comp.	Excitation max [nm]	Emission max [nm]	Study	Comp. name	Excitation max [nm]	Emission max [nm]	$TCC_{ex\text{-}em}$	Description
$C_{462\text{-}490}$	278 (370)	462 - 490	Catalá et al. (2015b)	C1	275 (370)	480	0.9891	Humic-like, positively correlated to apparent oxygen utilisation.
			Chen et al. (2018)	$C_{<260(365)/476}$	< 265 (365)	476	0.9665	
			Aparicio et al. (2015)	FIC2	275	468	NA	Coble's (1996) peak A-C
C_{454}	< 250	454	Stedmon & Markager (2005)	C4	< 250 (360)	440	0.8879	UV humic-like / Fulvic acid fluorophore group.
			Stedmon et al. (2003)	C1	< 240	436	NA	Coble's (1996) Peak A.
			Lapierre & Del Giorgio (2014)	C3	275 (345)	436	0.9184	

Continued

Table S1. Continued. Characteristics of the FDOM components derived from the PARAFAC analysis.

Comp.	Excitation max [nm]	Emission max [nm]	Study	Comp. name	Excitation max [nm]	Emission max [nm]	$TCC_{ex\text{-}em}$	Description
C_{406}	328	406	Catalá et al. (2015b)	C2	320	400	0.9720	Marine humic-like, positively correlated to apparent oxygen utilisation. Coble's (1996) Peak M.
			Stedmon et al. (2003)	C4	325 (250)	416	0.9724	
			Aparicio et al. (2015)	FIC1	325	423	NA	
C_{366}	286 (< 250)	366	Stedmon et al. (2003)	C5	280 (< 240)	368	0.9782	Labile, protein-like material generated as a result of biological production in the water column. It is close to Coble's (1996) peak T
			Coble (1996)	Peak T	275	340	NA	
			Kida et al. (2019)	C_{360}	290	362	0.9805	

Table S2. Water types intercepted during the MAFIA cruise, brief description of source point where they belong to, characteristics, and some references with more details about their origin and circulation.

Name	Source	Characteristics	SWT	References
Salinity Maximum Water	Tropical area (12–22°S)	Warmest (27°C) mode water in the SAO, formed by evaporation, transported westward to America with SEC	SMW	Worthington (1976), Stramma and England (1999), Mémery et al. (2000)
Equatorial Atlantic Central Water (13°C)	Eastern South Atlantic, near Namibia	Formed by mixing of low salinity water outcropped further south with overlying high salinity water. Transported by the South Equatorial current to the Equator and along the Brazilian coast by the North Brazil current.	EQ_{13}	Tsuchiya (1986)
Madeira Mode Water	Madeira Mode Water	Mode water formed near the Madeira Island	MMW	Siedler et al. (1987)
Eastern North Atlantic Central water	Eastern North Atlantic Subtropical gyre	Mode waters defining the upper (15°C) and lower (12°C) limits of the subtropical ENACW formed between the area of the Azores and Portugal currents.	$ENACW_{15}$ $ENACW_{12}$	Harvey (1982), Pollard and Pu (1985), Ríos et al. (1992), Álvarez-Salgado et al. (2013)
Mediterranean Water	Gulf of Cadiz	Formed in the Gulf of Cadiz by entrainment of Eastern North Atlantic Central water on the high-salinity outflow from the Mediterranean Sea, spreads at 800–1300 m, S > 36 and θ ~ 11–12 °C.	MW	Zenk (1975), Ambar and Howe (1979), Castro et al. (1998), Álvarez-Salgado et al. (2013)
Antarctic Intermediate Water	Pacific Ocean north of the Sub-Antarctic Front & Malvinas-Brazil Confluence.	Formed north of the Subantarctic Front (SAF) and east of the Drake Passage by ventilation of the Subantarctic Mode Water (SAMW) formed in the Southeast Pacific.	$AAIW_{5.0}$ $AAIW_{3.1}$	McCartney (1982), Piola and Gordon (1989), Talley (1996)
Circumpolar Deep Water	Antarctic Circumpolar Current	Also named Common Water, formed by mixing in the Antarctic Circumpolar current of mid-depth Indian, Pacific and Atlantic deep water with WSDW and NADW.	CDW	Montgomery (1958), Georgi (1981), Broecker et al. (1985)
North Atlantic Deep Water	North Atlantic Ocean	Carried into the South Atlantic by the Deep Western Boundary Current (DWBC). Characterized by salinity maximum and silicate minimum (4.6°C); and θ–S discontinuity and oxygen maximum (2.0 °C). Defined at their entry in the South Atlantic Ocean off South America.	$NADW_{4.6}$ $NADW_{2.0}$	Wüst (1935), Speer and McCartney (1992), Friedrichs et al. (1994)

Table S3. Thermohaline and chemical characteristics (average value ± uncertainty) of the water types (WT) introduced in the OMP analysis of the water masses intercepted during the MAFIA cruise. Water mass acronyms stand for: Salinity Maximum Water (SMW), Madeira Mode Water (MMW), Equatorial Water (EQ_{13}), Eastern North Atlantic Central Water of 15°C ($ENACW_{15}$) and 12°C ($ENACW_{12}$), Subpolar Mode Water (SPMW), Mediterranean Water (MW), Antarctic Intermediate Water of 5°C ($AAIW_5$) and 3.1°C ($AAIW_{3.1}$), Circumpolar Deep Water (CDW) and North Atlantic Deep Water of 4.6°C ($NADW_{4.6}$) and 2°C ($NADW_2$).

WT	θ_i (°C)	S_i	SiO_4H_{4i} (μmol kg^{-1})	NO_i (μmol kg^{-1})
SMW [a]	27.0 ± 0.1	37.50 ± 0.01	1.1 ± 0.5	206 ± 3
MMW [b]	20.0 ± 0.5	37.00 ± 0.04	0.4 ± 0.3	225 ± 10
EQ_{13} [a]	13.0 ± 0.1	35.20 ± 0.01	5.3 ± 0.7	315 ± 3
$ENACW_{15}$ [b]	15.3 ± 0.4	36.10 ± 0.02	2.2 ± 1.7	264 ± 8
$ENACW_{12}$ [c]	12.2 ± 0.4	35.66 ± 0.02	4.9 ± 0.2	322 ± 8
SPMW [c]	8.2 ± 0.4	35.23 ± 0.01	14.5 ± 0.4	386 ± 7
MW [c]	11.8 ± 0.1	36.50 ± 0.01	7.2 ± 0.7	304 ± 9
$AAIW_5$ [a]	5.00 ± 0.08	34.14 ± 0.01	7.0 ± 0.7	482 ± 3
$AAIW_{3.1}$ [a]	3.10 ± 0.08	34.12 ± 0.01	16.4 ± 0.7	558 ± 3
CDW [a]	1.60 ± 0.03	34.720 ± 0.003	110.6 ± 0.9	497 ± 1
$NADW_{4.6}$ [a]	4.6 ± 0.1	35.020 ± 0.005	7.3 ± 0.5	426 ± 2
$NADW_2$ [a]	2.02 ± 0.03	34.910 ± 0.003	28.2 ± 0.9	446 ± 1

[a] Álvarez et al. (2014)

[b] Álvarez and Álvarez-Salgado (2009); Lønborg and Álvarez-Salgado (2014)

[c] Pérez et al. (2001); Álvarez and Álvarez-Salgado (2009)

References

Agogué, H., D. Lamy, P. R. Neal, M. L. Sogin, and G. J. Herndl. 2011. Water mass-specificity of bacterial communities in the North Atlantic revealed by massively parallel sequencing. Mol. Ecol. **20**: 258–274. doi:10.1111/j.1365-294X.2010.04932.x

Álvarez-Salgado, X. A., M. Nieto-Cid, M. Álvarez, F. F. Pérez, P. Morin, and H. Mercier. 2013. New insights on the mineralization of dissolved organic matter in central, intermediate, and deep water masses of the northeast North Atlantic. Limnol. Oceanogr. **58**: 681–696. doi:10.4319/lo.2013.58.2.0681

Álvarez, M., and X. A. Álvarez-Salgado. 2009. Chemical tracer transport in the eastern boundary current system of the North Atlantic. Ciencias Mar. **35**: 123–139.

Álvarez, M., S. Brea, H. Mercier, and X. A. Álvarez-Salgado. 2014. Mineralization of biogenic materials in the water masses of the South Atlantic Ocean. I: Assessment and results of an optimum multiparameter analysis. Prog. Oceanogr. **123**: 1–23. doi:10.1016/j.pocean.2013.12.007

Ambar, I., and M. R. Howe. 1979. Observations of the Mediterranean outflow—I mixing in the Mediterranean outflow. Deep Sea Res. Part A. Oceanogr. Res. Pap. 26: 535–554. doi:10.1016/0198-0149(79)90095-5

Aparicio, F. L., M. Nieto-Cid, E. Borrull, and others. 2015. Microbially-mediated fluorescent organic matter transformations in the deep ocean. Do the chemical precursors matter? Front. Mar. Sci. **2**: 106. doi:10.3389/fmars.2015.00106

Armstrong, F. A. J., C. R. Stearns, and J. D. H. Strickland. 1967. The measurement of upwelling and subsequent biological process by means of the Technicon Autoanalyzer® and associated equipment. Deep. Res. Oceanogr. Abstr. **14**: 381–389. doi:10.1016/0011-7471(67)90082-4

Arnosti, C. 2011. Microbial Extracellular Enzymes and the Marine Carbon Cycle. Ann. Rev. Mar. Sci. **3**: 401–425. doi:10.1146/annurev-marine-120709-142731

Baetge, N., J. R. Graff, M. J. Behrenfeld, and C. A. Carlson. 2020. Net Community Production, Dissolved Organic Carbon Accumulation, and Vertical Export in the Western North Atlantic. Front. Mar. Sci. **7**: 227. doi:10.3389/fmars.2020.00227

Baltar, F., X. A. Alvarez-Salgado, J. Arístegui, R. Benner, D. A. Hansell, G. J. Herndl, and C. Lønborg. 2021. What Is Refractory Organic Matter in the Ocean? Front. Mar. Sci. **8**: 642637. doi:10.3389/fmars.2021.642637

Belmar, L., V. Molina, and O. Ulloa. 2011. Abundance and phylogenetic identity of archaeoplankton in the permanent oxygen minimum zone of the eastern tropical South Pacific. FEMS Microbiol. Ecol. **78**: 314–326. doi:10.1111/j.1574-6941.2011.01159.x

Beman, J. M., and M. T. Carolan. 2013. Deoxygenation alters bacterial diversity and community composition in the ocean's largest oxygen minimum zone. Nat. Commun. **4**: 2705. doi:10.1038/ncomms3705

Beman, J. M., S. M. Vargas, S. Vazquez, J. Mac Wilson, A. Yu, A. Cairo, and E. Perez-Coronel. 2020. Biogeochemistry and hydrography shape microbial community assembly and activity in the eastern tropical North Pacific Ocean oxygen minimum zone. Environ. Microbiol. doi:10.1111/1462-2920.15215

Benner, R., P. Louchouarn, and R. M. W. Amon. 2005. Terrigenous dissolved organic matter in the Arctic Ocean and its transport to surface and deep waters of the North Atlantic. Global

Biogeochem. Cycles **19**. doi:10.1029/2004GB002398

Benson, B. B., and D. Krause. 1984. The concentration and isotopic fractionation of oxygen dissolved in freshwater and seawater in equilibrium with the atmosphere. Limnol. Oceanogr. **29**: 620–632. doi:10.4319/lo.1984.29.3.0620

Bergauer, K., A. Fernandez-Guerra, J. A. L. Garcia, R. R. Sprenger, R. Stepanauskas, M. G. Pachiadaki, O. N. Jensen, and G. J. Herndl. 2018. Organic matter processing by microbial communities throughout the Atlantic water column as revealed by metaproteomics. Proc. Natl. Acad. Sci. U. S. A. **115**: E400–E408. doi:10.1073/pnas.1708779115

Bertagnolli, A. D., and F. J. Stewart. 2018. Microbial niches in marine oxygen minimum zones. Nat. Rev. Microbiol. **16**: 723–729. doi:10.1038/s41579-018-0087-z

van den Boogaart, K. G., R. Tolosana-Delgado, and M. Bren. 2020. compositions: Compositional Data Analysis. R package version 1.40-5. https://CRAN.R-project.org/package=compositions.

Boutrif, M., M. Garel, M. T. Cottrell, and C. Tamburini. 2011. Assimilation of marine extracellular polymeric substances by deep-sea prokaryotes in the NW Mediterranean Sea. Environ. Microbiol. Rep. **3**: 705–709. doi:10.1111/j.1758-2229.2011.00285.x

Brandt, P., V. Hormann, B. Bourlès, J. Fischer, F. A. Schott, L. Stramma, and M. Dengler. 2008. Oxygen tongues and zonal currents in the equatorial Atlantic. J. Geophys. Res. Ocean. **113**. doi:10.1029/2007JC004435

Broecker, W. S. 1974. "NO", a conservative water-mass tracer. Earth Planet. Sci. Lett. **23**: 100–107. doi:10.1016/0012-821X(74)90036-3

Broecker, W. S., T. Takahashi, and T. Takahashi. 1985. Sources and flow patterns of deep-ocean waters as deduced from potential temperature, salinity, and initial phosphate concentration. J. Geophys. Res. Ocean. **90**: 6925–6939. doi:10.1029/JC090iC04p06925

Callahan, B. J., P. J. McMurdie, M. J. Rosen, A. W. Han, A. J. A. Johnson, and S. P. Holmes. 2016. DADA2: High-resolution sample inference from Illumina amplicon data. Nat. Methods **13**: 581–583. doi:10.1038/nmeth.3869

Carlson, C. A., and D. A. Hansell. 2015. DOM Sources, Sinks, Reactivity, and Budgets, p. 65–126. *In* D.A. Hansell and C.A. Carlson [eds.], Biogeochemistry of Marine Dissolved Organic Matter: Second Edition. Academic Press.

Carr, M. E., and E. J. Kearns. 2003. Production regimes in four Eastern Boundary Current systems. Deep-Sea Res. Part II Top. Stud. Oceanogr. **50**: 3199–3221. doi:10.1016/j.dsr2.2003.07.015

Castro, C. G., F. F. Pérez, S. E. Holley, and A. F. Ríos. 1998. Chemical characterisation and modelling of water masses in the Northeast Atlantic. Prog. Oceanogr. **41**: 249–279. doi:10.1016/S0079-6611(98)00021-4

Catalá, T. S., X. A. Álvarez-Salgado, J. Otero, and others. 2016. Drivers of fluorescent dissolved organic matter in the global epipelagic ocean. Limnol. Oceanogr. **61**: 1101–1119. doi:10.1002/lno.10281

Catalá, T. S., A. M. Martínez-Pérez, M. Nieto-Cid, and others. 2018. Dissolved Organic Matter (DOM) in the open Mediterranean Sea. I. Basin–wide distribution and drivers of chromophoric DOM. Prog. Oceanogr. **165**: 35–51. doi:10.1016/j.pocean.2018.05.002

Catalá, T. S., I. Reche, M. Álvarez, and others. 2015a. Water mass age and aging driving chromophoric dissolved organic matter in the dark global ocean. Global Biogeochem. Cycles **29**: 917–934. doi:10.1002/2014GB005048

Catalá, T. S., I. Reche, A. Fuentes-Lema, and others. 2015b. Turnover time of fluorescent dissolved organic matter in the dark global ocean. Nat. Commun. **6:5986**. doi:10.1038/ncomms6986

Chen, M., J. Jung, Y. K. Lee, and J. Hur. 2018. Surface accumulation of low molecular weight dissolved organic matter in surface waters and horizontal off-shelf spreading of nutrients and humic-like fluorescence in the Chukchi Sea of the Arctic Ocean. Sci. Total Environ. **639**: 624–632. doi:10.1016/j.scitotenv.2018.05.205

Coble, P. G. 1996. Characterization of marine and terrestrial DOM in seawater using excitation-emission matrix spectroscopy. Mar. Chem. **51**: 325–346. doi:10.1016/0304-4203(95)00062-3

Davis, N. M., Di. M. Proctor, S. P. Holmes, D. A. Relman, and B. J. Callahan. 2018. Simple statistical identification and removal of contaminant sequences in marker-gene and metagenomics data. Microbiome **6**: 226. doi:10.1186/s40168-018-0605-2

De La Fuente, P., C. Marrasé, A. Canepa, X. Antón Álvarez-Salgado, M. Gasser, N. M. Fajar, C. Romera-Castillo, and J. L. Pelegrí. 2014. Does a general relationship exist between fluorescent dissolved organic matter and microbial respiration?-The case of the dark equatorial Atlantic Ocean. Deep-Sea Res. Part I Oceanogr. Res. Pap. **89**: 44–55. doi:10.1016/j.dsr.2014.03.007

DeLong, E. F., C. M. Preston, T. Mincer, and others. 2006. Community genomics among stratified microbial assemblages in the ocean's interior. Science (80-.). **311**: 496–503. doi:10.1126/science.1120250

Deschamps, P., Y. Zivanovic, D. Moreira, F. Rodriguez-Valera, and P. Lopez-García. 2014. Pangenome evidence for extensive interdomain horizontal transfer affecting lineage coreandshell genes inuncultured planktonic thaumarchaeota and euryarchaeota. Genome Biol. Evol. **6**: 1549–1563. doi:10.1093/gbe/evu127

Dittmar, T., S. T. Lennartz, H. Buck-Wiese, D. A. Hansell, C. Santinelli, C. Vanni, B. Blasius, and J.-H. Hehemann. 2021. Enigmatic persistence of dissolved organic matter in the ocean. Nat. Rev. Earth Environ. **2**: 570–583. doi:10.1038/s43017-021-00183-7

Falkowski, P. G., T. Fenchel, and E. F. Delong. 2008. The microbial engines that drive earth's biogeochemical cycles. Science (80-.). **320**: 1034–1039. doi:10.1126/science.1153213

Fischer, G., S. Neuer, S. Ramondenc, and others. 2020. Long-Term Changes of Particle Flux in the Canary Basin Between 1991 and 2009 and Comparison to Sediment Trap Records Off Mauritania. Front. Earth Sci. **8**: 280. doi:10.3389/feart.2020.00280

Frank, A. H., J. A. L. Garcia, G. J. Herndl, and T. Reinthaler. 2016. Connectivity between surface and deep waters determines prokaryotic diversity in the North Atlantic Deep Water. Environ. Microbiol. **18**: 2052–2063. doi:10.1111/1462-2920.13237

Friedrichs, M. A. M., M. S. McCartney, and M. M. Hall. 1994. Hemispheric asymmetry of deep water transport modes in the western Atlantic. J. Geophys. Res. Ocean. **99**: 25165–25179. doi:10.1029/94JC02087

Georgi, D. T. 1981. On the relationship between the large-scale property variations and fine structure in the Circumpolar Deep Water. J. Geophys. Res. **86**: 6556–6566. doi:10.1029/JC086iC07p06556

Gómez-Consarnau, L., M. V. Lindh, J. M. Gasol, and J. Pinhassi. 2012. Structuring of bacterioplankton communities by specific dissolved organic carbon compounds. Environ. Microbiol. **14**: 2361–2378. doi:10.1111/j.1462-2920.2012.02804.x

Guerrero-Feijóo, E., M. Nieto-Cid, E. Sintes, V. Dobal-Amador, V. Hernando-Morales, M. Álvarez, V. Balagué, and M. M. Varela. 2017. Optical properties of dissolved organic matter relate to

different depth-specific patterns of archaeal and bacterial community structure in the North Atlantic Ocean. FEMS Mcrobiology Ecol. **93**: fiw224. doi:10.1093/femsec/fiw224

Hansell, D. A. 2013. Recalcitrant dissolved organic carbon fractions. Ann. Rev. Mar. Sci. **5**: 421–445. doi:10.1146/annurev-marine-120710-100757

Hansell, D. A., C. A. Carlson, D. J. Repeta, and R. Schlitzer. 2009. Dissolved organic matter in the ocean: A controversy stimulates new insights. Oceanography **22**: 202–211.

Harvey, J. 1982. θ-S relationships and water masses in the eastern North Atlantic. Deep Sea Res. A 29: 1021–1033. doi:10.1016/0198-0149(82)90025-5

Hawley, A. K., M. K. Nobu, J. J. Wright, and others. 2017. Diverse Marinimicrobia bacteria may mediate coupled biogeochemical cycles along eco-thermodynamic gradients. Nat. Commun. **8**: 1507. doi:10.1038/s41467-017-01376-9

Hernández-León, S., M. P. Olivar, M. L. Fernández de Puelles, A. Bode, A. Castellón, C. López-Pérez, V. M. Tuset, and J. I. González-Gordillo. 2019. Zooplankton and Micronekton Active Flux Across the Tropical and Subtropical Atlantic Ocean . Front. Mar. Sci. **6**: 535.

Jørgensen, L., C. A. Stedmon, M. A. Granskog, and M. Middelboe. 2014. Tracing the long-term microbial production of recalcitrant fluorescent dissolved organic matter in seawater. Geophys. Res. Lett. **41**: 2481–2488. doi:10.1002/2014GL059428

Jørgensen, L., C. A. Stedmon, T. Kragh, S. Markager, M. Middelboe, and M. Søndergaard. 2011. Global trends in the fluorescence characteristics and distribution of marine dissolved organic matter. Mar. Chem. **126**: 139–148. doi:10.1016/j.marchem.2011.05.002

Karstensen, J., L. Stramma, and M. Visbeck. 2008. Oxygen minimum zones in the eastern tropical Atlantic and Pacific oceans. Prog. Oceanogr. **77**: 331–350. doi:10.1016/j.pocean.2007.05.009

Kembel, S. W., P. D. Cowan, M. R. Helmus, W. K. Cornwell, H. Morlon, D. D. Ackerly, S. P. Blomberg, and C. O. Webb. 2010. Picante: R tools for integrating phylogenies and ecology. Bioinformatics **26**: 1463–1464. doi:10.1093/bioinformatics/btq166

Khatiwala, S., F. Primeau, and M. Holzer. 2012. Ventilation of the deep ocean constrained with tracer observations and implications for radiocarbon estimates of ideal mean age. Earth Planet. Sci. Lett. **325–326**: 116–125. doi:10.1016/j.epsl.2012.01.038

Kida, M., T. Kojima, Y. Tanabe, K. Hayashi, S. Kudoh, N. Maie, and N. Fujitake. 2019. Origin, distributions, and environmental significance of ubiquitous humic-like fluorophores in Antarctic lakes and streams. Water Res. **163**: 114901. doi:10.1016/j.watres.2019.114901

Kitzinger, K., C. C. Padilla, H. K. Marchant, and others. 2019. Cyanate and urea are substrates for nitrification by Thaumarchaeota in the marine environment. Nat. Microbiol. **4**: 234–243. doi:10.1038/s41564-018-0316-2

Könneke, M., D. M. Schubert, P. C. Brown, and others. 2014. Ammonia-oxidizing archaea use the most energy-efficient aerobic pathway for CO2 fixation. Proc. Natl. Acad. Sci. U. S. A. **111**: 8239–8244. doi:10.1073/pnas.1402028111

Kraft, B., N. Jehmlich, M. Larsen, L. A. Bristow, M. Könneke, B. Thamdrup, and D. E. Canfield. 2022. Oxygen and nitrogen production by an ammonia-oxidizing archaeon. Science (80-.). **375**: 97–100. doi:10.1126/science.abe6733

Kwon, E. Y., F. Primeau, and J. L. Sarmiento. 2009. The impact of remineralization depth on the air-sea carbon balance. Nat. Geosci. **2**: 630–635. doi:10.1038/ngeo612

Labrenz, M., E. Sintes, F. Toetzke, A. Zumsteg, G. J. Herndl, M. Seidler, and K. Jürgens. 2010. Relevance of a crenarchaeotal subcluster related to Candidatus Nitrosopumilus maritimus to ammonia oxidation in the suboxic zone of the central Baltic Sea. ISME J. **4**: 1496–1508. doi:10.1038/ismej.2010.78

Lahti, L., and S. Shetty. 2019. microbiome R package, version 1.8.0 http://microbiome.github.io.

Landry, Z., B. K. Swa, G. J. Herndl, R. Stepanauskas, and S. J. Giovannoni. 2017. SAR202 genomes from the dark ocean predict pathways for the oxidation of recalcitrant dissolved organic matter. MBio **8**: e00413-17. doi:10.1128/mBio.00413-17

Lapierre, J. F., and P. A. Del Giorgio. 2014. Partial coupling and differential regulation of biologically and photochemically labile dissolved organic carbon across boreal aquatic networks. Biogeosciences **11**: 5969–5985. doi:10.5194/bg-11-5969-2014

Laufkötter, C., J. G. John, C. A. Stock, and J. P. Dunne. 2017. Temperature and oxygen dependence of the remineralization of organic matter. Global Biogeochem. Cycles **31**: 1038–1050. doi:10.1002/2017GB005643

Lechtenfeld, O. J., N. Hertkorn, Y. Shen, M. Witt, and R. Benner. 2015. Marine sequestration of carbon in bacterial metabolites. Nat. Commun. **6**: 6711. doi:10.1038/ncomms7711

Lønborg, C., and X. A. Álvarez-Salgado. 2014. Tracing dissolved organic matter cycling in the eastern boundary of the temperate North Atlantic using absorption and fluorescence spectroscopy. Deep Sea Res. Part I Oceanogr. Res. Pap. **85**: 35–46. doi:10.1016/j.dsr.2013.11.002

Lønborg, C., X. A. Álvarez-Salgado, K. Davidson, S. Martínez-García, and E. Teira. 2010. Assessing the microbial bioavailability and degradation rate constants of dissolved organic matter by fluorescence spectroscopy in the coastal upwelling system of the Ría de Vigo. Mar. Chem. **119**: 121–129. doi:10.1016/j.marchem.2010.02.001

Martin, M. 2011. Cutadapt removes adapter sequences from high-throughput sequencing reads. EMBnet.journal. doi:10.14806/ej.17.1.200

McCartney, M. S. 1982. The subtropical recirculation of mode waters. J. Mar. Res. **40**, Supple: 427–464.

Mehrshad, M., F. Rodriguez-Valera, M. A. Amoozegar, P. López-García, and R. Ghai. 2018. The enigmatic SAR202 cluster up close: Shedding light on a globally distributed dark ocean lineage involved in sulfur cycling. ISME J. **12**: 655–668. doi:10.1038/s41396-017-0009-5

Mémery, L., M. Arhan, X. A. Alvarez-Salgado, M.-J. Messias, H. Mercier, C. G. Castro, and A. F. Rios. 2000. The water masses along the western boundary of the south and equatorial Atlantic. Prog. Oceanogr. **47**: 69–98. doi:10.1016/S0079-6611(00)00032-X

Mestre, M., C. Ruiz-González, R. Logares, C. M. Duarte, J. M. Gasol, and M. M. Sala. 2018. Sinking particles promote vertical connectivity in the ocean microbiome. Proc. Natl. Acad. Sci. U. S. A. **115**: E6799–E6807. doi:10.1073/pnas.1802470115

Montgomery, R. B. 1958. Water characteristics of Atlantic Ocean and of world ocean. Deep Sea Res. **5**: 134–148. doi:10.1016/0146-6313(58)90004-2

Moran, M. A., E. B. Kujawinski, A. Stubbins, and others. 2016. Deciphering ocean carbon in a changing world. Proc. Natl. Acad. Sci. U. S. A. **113**: 3143–3151. doi:10.1073/pnas.1514645113

Morán, X. A. G., F. C. García, A. Røstad, L. Silva, N. Al-Otaibi, X. Irigoien, and M. L. Calleja. 2022. Diel dynamics of dissolved organic matter and heterotrophic prokaryotes reveal enhanced growth

at the ocean's mesopelagic fish layer during daytime. Sci. Total Environ. **804**: 150098. doi:10.1016/j.scitotenv.2021.150098

Moreno-Ostos, E. 2012. Expedición de circunnavegación Malaspina 2010: cambio global y exploración de la biodiversidad del océano. Libro blanco de métodos y técnicas de trabajo oceanográfico, Consejo Superior de Investigaciones Científicas.

Murali, A., A. Bhargava, and E. S. Wright. 2018. IDTAXA: A novel approach for accurate taxonomic classification of microbiome sequences. Microbiome **6**: 140. doi:10.1186/s40168-018-0521-5

Murphy, K. R., C. A. Stedmon, T. D. Waite, and G. M. Ruiz. 2008. Distinguishing between terrestrial and autochthonous organic matter sources in marine environments using fluorescence spectroscopy. Mar. Chem. **108**: 40–58. doi:10.1016/j.marchem.2007.10.003

Murphy, K. R., C. A. Stedmon, P. Wenig, and R. Bro. 2014. OpenFluor- An online spectral library of auto-fluorescence by organic compounds in the environment. Anal. Methods **6**: 658–661. doi:10.1039/c3ay41935e

Offre, P., A. Spang, and C. Schleper. 2013. Archaea in Biogeochemical Cycles. Annu. Rev. Microbiol. **67**: 437–457. doi:10.1146/annurev-micro-092412-155614

Oksanen, J., F. G. Blanchet, M. Friendly, and others. 2019. vegan: Community Ecology Package. R package version 2.5-6. https://CRAN.R-project.org/package=vegan.

Pajares, S., F. Varona-Cordero, and D. U. Hernández-Becerril. 2020. Spatial Distribution Patterns of Bacterioplankton in the Oxygen Minimum Zone of the Tropical Mexican Pacific. Microb. Ecol. **80**: 519–536. doi:10.1007/s00248-020-01508-7

Parada, A. E., D. M. Needham, and J. A. Fuhrman. 2016. Every base matters: Assessing small subunit rRNA primers for marine microbiomes with mock communities, time series and global field samples. Environ. Microbiol. **18**: 1403–1414. doi:10.1111/1462-2920.13023

Pérez, F. F., L. Mintrop, O. Llinás, and others. 2001. Mixing analysis of nutrients, oxygen and inorganic carbon in the Canary Islands region. J. Mar. Syst. **28**: 183–201. doi:10.1016/S0924-7963(01)00003-3

Piola, A. R., and A. L. Gordon. 1989. Intermediate waters in the southwest South Atlantic. Deep Sea Res. Part A. Oceanogr. Res. Pap. **36**: 1–16. doi:10.1016/0198-0149(89)90015-0

Pollard, R. T., and S. Pu. 1985. Structure and circulation of the Upper Atlantic Ocean northeast of the Azores. Prog. Oceanogr. **14**: 443–462. doi:10.1016/0079-6611(85)90022-9

R Core Team. 2019. R: A language and environment for statistical computing. R Foundation for Statistical Computing, Vienna, Austria. URL https://www.R-project.org/.

Rasse, R., and G. Dall'Olmo. 2019. Do Oceanic Hypoxic Regions Act as Barriers for Sinking Particles? A Case Study in the Eastern Tropical North Atlantic. Global Biogeochem. Cycles **33**: 1611–1630. doi:10.1029/2019GB006305

Reinthaler, T., X. A. Álvarez Salgado, M. Álvarez, H. M. van Aken, and G. J. Herndl. 2013. Impact of water mass mixing on the biogeochemistry and microbiology of the Northeast Atlantic Deep Water. Global Biogeochem. Cycles **27**: 1151–1162. doi:10.1002/2013GB004634

Reintjes, G., B. M. Fuchs, R. Amann, and C. Arnosti. 2020. Extensive Microbial Processing of Polysaccharides in the South Pacific Gyre via Selfish Uptake and Extracellular Hydrolysis. Front. Microbiol. **11**: 583158. doi:10.3389/fmicb.2020.583158

Rinke, C., F. Rubino, L. F. Messer, and others. 2019. A phylogenomic and ecological analysis of the

globally abundant Marine Group II archaea (Ca. Poseidoniales ord. nov.). ISME J. **13**: 663–675. doi:10.1038/s41396-018-0282-y

Ríos, A. F., F. F. Pérez, and F. Fraga. 1992. Water masses in the upper and middle North Atlantic Ocean east of the Azores. Deep Sea Res. Part A. Oceanogr. Res. Pap. **39**: 645–658. doi:10.1016/0198-0149(92)90093-9

Ruiz-González, C., M. Mestre, M. Estrada, and others. 2020. Major imprint of surface plankton on deep ocean prokaryotic structure and activity. Mol. Ecol. **29**: 1820–1838. doi:10.1111/mec.15454

Salazar, G. 2020. EcolUtils: Utilities for community ecology analysis. R package version 0.1. https://github.com/GuillemSalazar/EcolUtils.

Salazar, G., F. M. Cornejo-Castillo, V. Benítez-Barrios, E. Fraile-Nuez, X. A. Álvarez-Salgado, C. M. Duarte, J. M. Gasol, and S. G. Acinas. 2016. Global diversity and biogeography of deep-sea pelagic prokaryotes. ISME J. **10**: 596–608. doi:10.1038/ismej.2015.137

Salter, S. J., M. J. Cox, E. M. Turek, and others. 2014. Reagent and laboratory contamination can critically impact sequence-based microbiome analyses. BMC Biol. **12**: 87. doi:10.1186/s12915-014-0087-z

Saw, J. H. W., T. Nunoura, M. Hirai, and others. 2020. Pangenomics analysis reveals diversification of enzyme families and niche specialization in globally abundant SAR202 bacteria. MBio **11**: e02975-19. doi:10.1128/mBio.02975-19

Seymour, J. R., S. A. Amin, J. B. Raina, and R. Stocker. 2017. Zooming in on the phycosphere: The ecological interface for phytoplankton-bacteria relationships. Nat. Microbiol. **2**. doi:10.1038/nmicrobiol.2017.65

Sheik, C. S., S. Jain, and G. J. Dick. 2014. Metabolic flexibility of enigmatic SAR324 revealed through metagenomics and metatranscriptomics. Environ. Microbiol. **16**: 304–317. doi:10.1111/1462-2920.12165

Siedler, G., A. Kuhl, and W. Zenk. 1987. The Madeira Mode Water. J. Phys. Oceanogr. **17**: 1561–1570. doi:10.1175/1520-0485(1987)017<1561:TMMW>2.0.CO;2

Speer, K. G., and M. S. McCartney. 1992. Bottom Water Circulation in the Western North Atlantic. J. Phys. Oceanogr. **22**: 83–92. doi:10.1175/1520-0485(1992)022<0083:BWCITW>2.0.CO;2

Stedmon, C. A., and R. Bro. 2008. Characterizing dissolved organic matter fluorescence with parallel factor analysis: A tutorial. Limnol. Oceanogr. Methods **6**: 572–579. doi:10.4319/lom.2008.6.572

Stedmon, C. A., and S. Markager. 2005. Resolving the variability in dissolved organic matter fluorescence in a temperate estuary and its catchment using PARAFAC analysis. Limnol. Oceanogr. **50**: 686–697. doi:10.4319/lo.2005.50.2.0686

Stedmon, C. A., S. Markager, and R. Bro. 2003. Tracing dissolved organic matter in aquatic environments using a new approach to fluorescence spectroscopy. Mar. Chem. **82**: 239–254. doi:10.1016/S0304-4203(03)00072-0

Stevens, H., and O. Ulloa. 2008. Bacterial diversity in the oxygen minimum zone of the eastern tropical South Pacific. Environ. Microbiol. **10**: 1244–1259. doi:10.1111/j.1462-2920.2007.01539.x

Stewart, F. J., O. Ulloa, and E. F. Delong. 2012. Microbial metatranscriptomics in a permanent marine oxygen minimum zone. Environ. Microbiol. **14**: 23–40. doi:10.1111/j.1462-2920.2010.02400.x

Stramma, L., P. Brandt, J. Schafstall, F. Schott, J. Fischer, and A. Körtzinger. 2008. Oxygen minimum zone in the North Atlantic south and east of the Cape Verde Islands. J. Geophys. Res. Ocean.

113: C04014. doi:10.1029/2007JC004369

Stramma, L., and M. England. 1999. On the water masses and mean circulation of the South Atlantic Ocean. J. Geophys. Res. Ocean. **104**: 20863–20883. doi:10.1029/1999JC900139

Stramma, L., and F. Schott. 1999. The mean flow field of the tropical Atlantic Ocean. Deep-Sea Res. Part II Top. Stud. Oceanogr. **46**: 279–303. doi:10.1016/S0967-0645(98)00109-X

Sunagawa, S., L. P. Coelho, S. Chaffron, and others. 2015. Structure and function of the global ocean microbiome. Science (80-.). **348**: 1261359. doi:10.1126/science.1261359

Swan, B. K., M. Martinez-Garcia, C. M. Preston, and others. 2011. Potential for Chemolithoautotrophy Among Ubiquitous Bacteria Lineages in the Dark Ocean. Science (80-.). **333**: 1296–1300. doi:10.1126/science.1203690

Talley, L. D. 1996. Antarctic intermediate water in the South Atlantic, p. 219–238. In G. Wefer, W.H. Berger, G. Siedler, and D.J. Webb [eds.], The South Atlantic. Present and Past Circulation. Springer-Verlag.

Troupin, C., A. Barth, D. Sirjacobs, and others. 2012. Generation of analysis and consistent error fields using the Data Interpolating Variational Analysis (DIVA). Ocean Model. **52–53**: 90–101. doi:10.1016/j.ocemod.2012.05.002

Tsuchiya, M. 1986. Thermostads and circulation in the upper layer of the Atlantic Ocean. Prog. Oceanogr. **16**: 235–267. doi:10.1016/0079-6611(86)90040-6

Tully, B. J. 2019. Metabolic diversity within the globally abundant Marine Group II Euryarchaea offers insight into ecological patterns. Nat. Commun. **10:271**. doi:10.1038/s41467-018-07840-4

Urban-Rich, J., J. T. McCarty, D. Fernández, and J. L. Acuña. 2006. Larvaceans and copepods excrete fluorescent dissolved organic matter (FDOM). J. Exp. Mar. Bio. Ecol. **332**: 96–105. doi:10.1016/j.jembe.2005.11.023

Varela, M. M., H. M. Van Aken, and G. J. Herndl. 2008. Abundance and activity of Chloroflexi-type SAR202 bacterioplankton in the meso- and bathypelagic waters of the (sub)tropical Atlantic. Environ. Microbiol. **10**: 1903–1911. doi:10.1111/j.1462-2920.2008.01627.x

Wohlers-Zöllner, J., P. Breithaupt, K. Walther, K. Jürgens, and U. Riebesella. 2011. Temperature and nutrient stoichiometry interactively modulate organic matter cycling in a pelagic algal-bacterial community. Limnol. Oceanogr. **56**: 599–610. doi:10.4319/lo.2011.56.2.0599

Worthington, L. V. 1976. On the North Atlantic circulation, Johns Hopkins University Press.

Wüst, G. 1935. Schichtung und Zirkulation des Atlantischen Ozeans, Die Stratosphäre. Wissenschaftliche Ergebnisse der Deutschen Atlantischen Expedition auf dem Forschungsund Vermessungsschiff "Meteor" 1925–1927. 6, 180pp., English translation edited by W.J. Emery, The stratosphere of the Atlantic Ocean. Scientific Results of the German Atlantic Expedition of the Research Vessel 'Meteor' 1925–27. Amerind Publishing Co., 1978.

Zark, M., J. Christoffers, and T. Dittmar. 2017. Molecular properties of deep-sea dissolved organic matter are predictable by the central limit theorem: Evidence from tandem FT-ICR-MS. Mar. Chem. **191**: 9–15. doi:10.1016/j.marchem.2017.02.005

Zenk, W. 1975. On the Mediterranean outflow west of Gibraltar. Meteor. Forsch.-Ergebnisse A **16**: 23–24.

Discussion

Synthesis and general discussion

This thesis has investigated how upwelling of nutrient-rich waters influences prokaryotic communities and the DOM pool they interact with. The combination of mesocosm experiments (**Chapters 1 and 2**) and synoptic field samplings (**Chapters 3 and 4**) provided the means to i) test hypotheses on how the phytoplankton blooms caused by upwelling events affect DOM and prokaryotic communities, and ii) observe the implications upwelling-related productivity enhancements at sea. This has been achieved combining biogeochemical measurements (determination of DOM concentrations, its optical properties, and oxygen utilisation; **Chapters 1 and 4**) with microbiological analyses (determination of standing stocks, physiological status, activity, and diversity of prokaryotes; **Chapters 2, 3 and 4**), which has provided a composite picture of i) organic matter cycling by prokaryotes during the initial (days) and medium-term stages (weeks) of upwelling under different scenarios, and ii) how upwelling-associated productivity is related to deep water microbial ecology and biogeochemistry, thus exploring the relevance of the oceanographical context to understand dark ocean microbiology.

Prokaryotic communities under upwelling

Phytoplankton blooms have been studied for several decades (Sverdrup 1953). These massive proliferations of photoautotrophs occur when their biomass loss (through respiration, mortality, sinking, etc.) is exceeded by growth. The amount of CO_2 fixed into organic compounds during these events, along with all associated processes, make them relevant components of the carbon cycle in the ocean (Loucaides et al. 2012; Tréguer et al. 2018; Irion et al. 2021). Prokaryotes are recognised as key players in the cycling of the organic matter produced in blooms and have accordingly been studied (Buchan et al. 2014). Nonetheless, research has focused to a great extent on blooms induced by the addition of individual nutrients (e.g., Allers et al. 2007; Hoikkala et al. 2016; Tada et al. 2012) and seasonal blooms, chiefly in the North Atlantic (e.g., Baetge et al. 2020; Francis et al. 2021; Teeling et al. 2016, 2012), and less in blooms generated in upwelling systems (e.g., Needham and Fuhrman, 2016; Pontiller et al. 2022). In the latter case, communities have been usually studied in the field or experimentally under a limited set of conditions, making it difficult to directly contrast the response of prokaryotes under varied upwelling settings. Precisely to provide the means for such a direct comparison, **Chapters 1 and 2** have been dedicated to simultaneously study the dynamics of DOM and prokaryotes under

different upwelling scenarios, combining a range of intensities with two distinct upwelling modes: a single pulse of upwelled waters (*singular* treatment) has been compared to conditions of recurring upwelling (*recurring* treatment).

The simulation of the two distinct upwelling modes yielded contrasting phytoplankton bloom dynamics, best exemplified by the most intense treatments of each mode. Even though both featured diatoms as the dominant phytoplanktonic group, the singular treatments yielded large, short-lived blooms, while the recurring ones sustained relatively smaller blooms for weeks. Nutrient and Chl *a* concentrations were in the range of those observed in natural upwelling conditions and thus our experiment represented a realistic setting (Chavez and Messié 2009). Despite the markedly different bloom outcomes, changes in the DOM pool were ultimately similar for both upwelling modes (Fig. 1): DOC accumulation, increased relative C content of DOM, and accumulation of humic-like FDOM. Notably, only the CDOM quantity and molecular weight differed between upwelling modes. Albeit favoured by the necessarily enclosed nature of the experimental setting, the large DOC accumulations leave no doubt that DOM was profusely released during the blooms. The exact reason behind its persistence, however, remains elusive. Optical properties and prokaryotic activity showed that DOM transformation was happening and thus there was at least a certain balance between DOM production

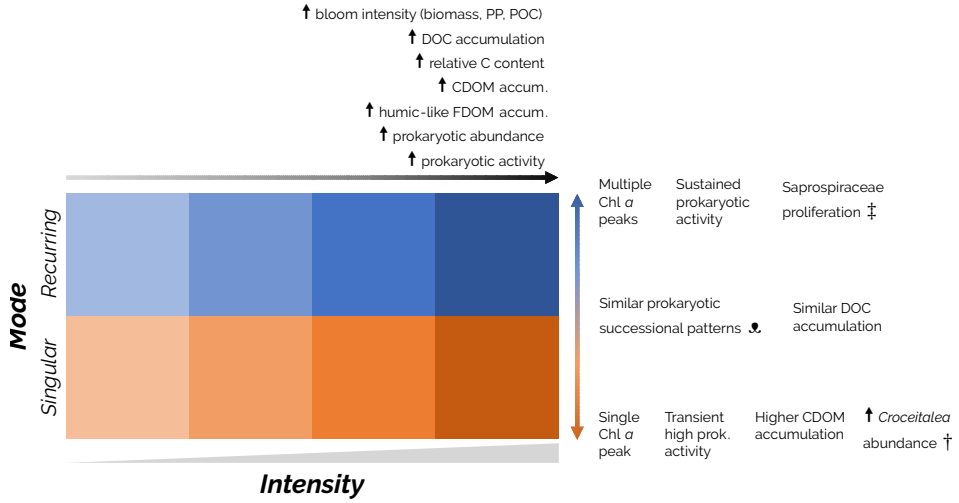

Figure 1. Outcome of the different simulated upwelling scenarios. Graphical outline of the main results presented in **Chapters 1 and 2**. The X axis denotes upwelling intensity (increasing to the right) and the Y axis the upwelling mode (blue = recurring; orange = singular). Notes: ‡ Only in the extreme recurring treatment; ♣ In both size fractions (free-living and particle-attached); † *Croceitalea* abundance increased with the intensity of singular treatments.

and consumption, particularly in the recurring upwelling where primary production was more sustained. However, fertilisation experiments have shown that there tends to be net consumption of DOC after a few weeks (Fry et al. 1996; Meon and Kirchman 2001). The sustained blooms in recurring treatments could help explain the absence of DOC decrease, but in the singular ones no signal of reduction was visible 4-5 weeks after bloom development. Results from **Chapter 1** suggest that this persistence could arise from a combination of factors: 1) preferential consumption of N- and P-containing compounds (see changes in relative C content), accumulating others that are less easily consumed, and 2) molecular diversification of DOM by microbial transformation, decreasing bulk consumption rates by decreasing individual concentrations and, hence, lowering consumption rates of individual molecules (Zark et al. 2017; Hach et al. 2020; Dittmar et al. 2021). Moreover, viral infection of phytoplankton has been shown to affect prokaryotic dynamics and DOM production during blooms and could at least partly help explain recycling of DOM through the viral shunt (Vincent et al. 2021; Hevroni et al. 2022; Kuhlisch et al. 2022). Likewise, DOM release through excretion and sloppy feeding by zooplankton could have also contributed to the observed accumulation (Saba et al. 2011; Steinberg and Landry 2017).

As one of the main driving agents of DOM cycling, prokaryotes are studied in parallel in **Chapter 2** applying varied approaches that included flow cytometry, single cell activity measurements and taxonomic determination through the sequencing of the 16S rRNA gene. Prokaryotic communities were nearly completely dominated by bacteria, which following upwelling and the onset of diatom blooms presented dramatic abundance increases (positively related to upwelling intensity; Fig. 1). Although usually bacterial abundances are sustained for some time after the bloom decay and the release of DOM (Buchan et al. 2014), we observed marked declines that were subsequently followed by two other synchronous oscillations in all treatments. Community composition was clearly distinct between size fractions (free-living vs particle-attached), but equally displayed similar succession patterns across treatments.

There is evidence of repeating prokaryotic succession patterns in annual cycles (Fuhrman et al. 2006; Auladell et al. 2019), natural seasonal blooms (Teeling et al. 2016) and particle colonisation experiments (Datta et al. 2016). Repeating annual patterns of a major fraction of prokaryotic taxa have been suggested as evidence of low functional redundancy, as otherwise functionally similar taxa would substitute each other, diminishing their reoccurrence (Fuhrman et al. 2006; Galand et al. 2018).

Such patterns are, in principle, predictably controlled by environmental conditions. Under phytoplankton blooms, the DOM released by primary producers—chiefly, structurally distinct polysaccharides—has been deemed one of the main drivers behind reproducible prokaryotic successions, seemingly presenting little variability across phytoplankton species (Teeling et al. 2016). During the different upwelling scenarios that we simulated, DOM characteristics followed similar trends (**Chapter 1**), likely contributing to the observed reproducible successions despite differences in organic matter concentrations. Other factors such as trophic interactions (Gralka et al. 2020), viral lysis (Riemann et al. 2000; Szabo et al. 2022) or predation (Allers et al. 2007) also probably played important roles, although no measurements to corroborate this were available. Thus, our results show that phytoplankton blooms under varying upwelling scenarios tend to induce predictable alterations in the form of specific prokaryotic successions (**Chapter 2**), similarly to the repeating patterns observed over seasonal cycles (Teeling et al. 2016). This was the case regardless of prokaryotic lifestyle (free-living vs particle-attached), something remarkable considering the complexity of the particle colonisation process. Given the myriad of microbial interactions that occur during the colonisation, successions could drift apart from each other due to contingent variations. Instead, factors like dispersal limitation and interactions favouring secondary colonisers seem to strongly drive succession of prokaryotes in particles (Datta et al. 2016), resulting in repeating patterns. In any case, it is noteworthy that, despite successional patterns being consistent among treatments, there were some taxonomic differences among them. These may arise from changes in environmental conditions (e.g., the Saprospiraceae proliferation was coupled with the coccolithophorid bloom) or due to some degree of functional redundancy among closely related taxa (**Chapter 2**).

Cell viability remained high throughout the successions, evidencing that most of the community was structurally healthy. Successional patterns were, however, coupled with differences in the activity of prokaryotes both across and within communities. Particle-attached prokaryotes were highly active (Fig. 8b of **Chapter 2**, Fig. 2a), as colonisers were fuelled by the large amounts of POC that were generated (**Chapter 1**; Grossart et al. 2007). Activity differences were also present among free-living prokaryotes (Fig. 2b). Variability in cell-specific metabolism is known among prokaryotes, differing in orders of magnitude between taxa (Munson-McGee et al. 2022). Oligotrophs, like the numerically dominant SAR11 clade, display low metabolic rates (Alonso and Pernthaler 2006; Alonso-Sáez and Gasol 2007), whereas the less abundant Rhodobacterales and Alteromonadales tend to contribute disproportionately to prokaryotic metabolism (Munson-McGee et al. 2022; Pontiller

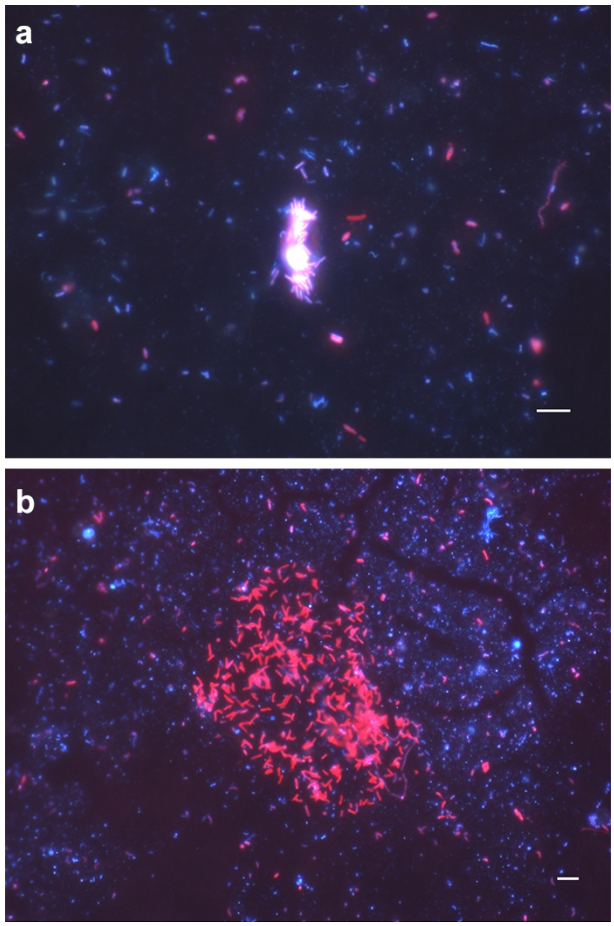

Figure 2. Cell-specific activity differences within prokaryotic communities. Pictures show the combined signal of 4′,6-diamidino-2-phenylindole (DAPI; all cells, blue) and Alexa594 (BONCAT, protein-synthesising cells, red) in two different samples from **Chapter 2**: extreme singular treatment a) on day 13 (100x), and b) on day 25 (63x). Both scale bars (lower right) are 5 μm.

et al. 2022). Besides the intrinsic heterogeneity in metabolic rates among marine prokaryotes, they may also exhibit temporal variability, like Flavobacteriales increasing their respiration rates during and after phytoplankton blooms (Munson-McGee et al. 2022). In our experiment, temporal changes in the translationally active fraction of the community were evident, especially in the singular treatments, where after the activity peak during the collapse of the bloom, the percentage of active cells steadily decreased (**Chapter 2**). These activity variations evidence changes from favourable to unfavourable conditions for prokaryotes (e.g. in the composition of available DOM or inorganic nutrient concentration), as observed during culture

experiments (Leizeaga et al. 2017). In summary, the taxonomic and temporal differences in metabolism highlight the importance of linking activity to identity if we are to properly understand the roles of prokaryotes in carbon cycling under upwelling conditions, in particular, and in the biosphere, in general.

Lastly, time scales must be taken into consideration to properly understand the results from **Chapters 1 and 2**. Experiments have shown that organic matter accumulations following diatom blooms can take anywhere from weeks to months to be consumed and recycled (Fry et al. 1996; Meon and Kirchman 2001). The simulated upwelling experiment presented here lasted approximately 6 weeks and thus falls in the lower end of the adequate time frame to address the DOM cycling, indicating that an extended period would be needed to properly track the full evolution of the DOM pool and concomitant prokaryotic community changes (both in terms of composition and activity). On top of that, phytoplankton blooms in natural conditions tend to develop slower than experimental ones (Buchan et al. 2014), although not always (Pontiller et al. 2022), and, thus, this ought to be considered too when transferring the information gained from simulated-upwelling experiments to the natural environment.

Indirect influence of upwelling on deep ocean biogeochemistry

Recent years have seen increasing recognition of the importance of the vertical connectivity of microbial communities in the ocean (Herndl et al. 2023). Sinking particles transport organic matter and attached prokaryotes from surface waters into the ocean interior, influencing the community composition and activity of prokaryotes in deep waters by providing carbon and energy sources, and introducing cells from overlaying waters (Mestre et al. 2018). This vertical connection is driven by the productivity levels of surface waters (Ruiz-González et al. 2020), albeit the phytoplankton composition can also influence vertical export of carbon and prokaryotes (Fadeev et al. 2021). Building on these findings, in **Chapters 3 and 4** we explored to which extent, if at all, the high productivity and organic matter concentration associated with upwelling affect prokaryotes in meso- and bathypelagic waters. Abundance, volume and viability of cells were all highly correlated to surface productivity (**Chapter 3**), suggesting a strong influence of vertical connectivity not only on standing stocks, as has been previously shown (Arístegui et al. 2009), but on the physiological status of deep ocean prokaryotes (Fig. 3). Activity, as measured by leucine incorporation, lacked any relationship or, in the case of viable cell specific rates in the bathypelagic, was negatively correlated to surface productivity.

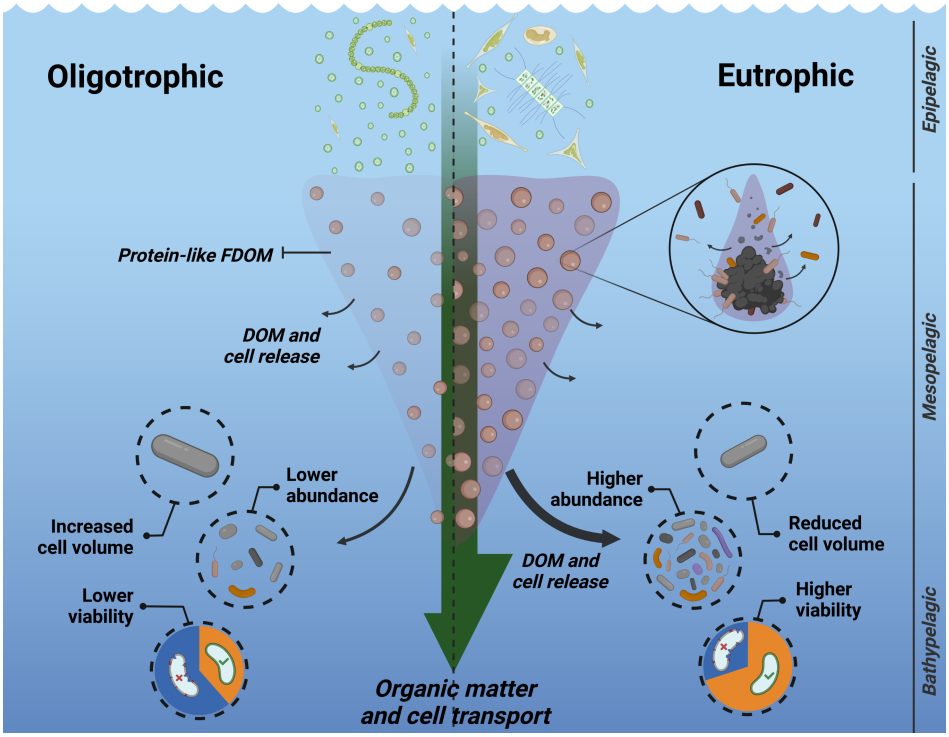

Figure 3. Effect of vertical connectivity on dark ocean prokaryotic communities. Sinking particles act as vectors transporting not only organic matter, but also attached prokaryotic cells. Thus, they act as sources of carbon and energy, and seed epipelagic communities into deep waters. This effect is larger under highly productive waters, where more intense particle fluxes occur (including the release of protein-like FDOM, **Chapter 4**), and thus results in higher abundances and viabilities, and smaller cells sizes (more similar to epipelagic waters) (**Chapter 3**). Created with BioRender.com.

Differences in the response of prokaryotes to resource availability possibly contributed to the observed trends, as cells under reduced vertical inputs of organic matter could have been more stimulated by the added leucine during incubations. Additionally, comparatively higher rates were observed coincident with larger cell sizes, which likely have higher cell-maintenance costs. Methodological limitations (does leucine uptake always reflect production?) could also help explain the negative correlation with surface productivity. Metabolic resource allocation (growth vs maintenance) varies between environments with distinct energy and substrate availability (Carlson et al. 2007; Giering and Evans 2022), and under oligotrophic waters, with less resources, prokaryotic metabolism is possibly more directed towards maintenance. This is in line with leucine-to-carbon conversion factors being smaller

with depth and in oligotrophic waters (Orta-Ponce et al. 2021). The reduced conversion factors suggest that increasing fractions of leucine tend to be respired for maintenance, rather than channelled to biomass accumulation.

Taxonomic composition of communities also displayed an imprint of vertical connectivity, although, superimposed to it, patterns linked to vertical gradients in environmental conditions and water mass specificity were evident (**Chapter 4**). As with standing stocks, physiological status and activity (**Chapter 3**), vertical gradients in temperature, pressure, and inorganic and organic nutrients are known to control community composition of free-living communities (Herndl et al. 2023). Simultaneously, water masses present variability in specific biogeochemical conditions and, as density boundaries, can act limiting dispersal, hence resulting in taxonomic composition differences between them (Agogué et al. 2011). Notably, this dispersal limitation effect has been observed to affect also prokaryotes attached to the smallest size fractions of particles (0.8-20 μm) (Salazar et al. 2016), which is explained by the fact that these are predominantly suspended, non-sinking particles (Herndl et al. 2023). Here we had no means to discern drivers of free-living and particle-attached communities as samples were not size fractionated. Thus, the results shown in **Chapter 4** necessarily reflect collective patterns of all prokaryotes regardless of lifestyle. Still, aided by the optimum multiparameter analysis (which provided the contribution of water masses in each sample), we tried to disentangle which taxa were most influenced by water mass distribution and which by local nonconservative biogeochemical processes, including vertical connectivity (Frank et al. 2016). Some taxa, like the free-living specialist SAR202 clade (Mehrshad et al. 2018), were mostly explained by water mass distribution (probably partly influenced by their vertical zonation), while the variability of others, e.g., members of the Alteromonadales order, was poorly described by water masses. Even if the latter group did not display clear relationships with our surface productivity proxies, the fact that they are copiotrophs known to be among the most prominent consumers of labile DOM (Pedler et al. 2014; Reintjes et al. 2020) suggests that vertical inputs of organic matter could be involved in their abundance patterns. Protein-like FDOM signals indeed point that downward transport of surface organic matter is a common feature of the study area (Fig. 3; **Chapter 4**), an observation that reinforces the results from **Chapter 3**. This process of vertical organic matter transport also markedly drove microbial transformation of DOM in the water masses, as indicated by the intense humic-like FDOM signal associated with O_2 consumption (**Chapter 4**; Catalá et al. 2015).

Given the section location and its distance to the coast, the observed link to surface productivity is at least partially mediated by horizontal advection of highly productive waters, evidencing the importance of mesoscale processes in vertical connectivity. All of the Northwest African upwelling system, but specially the Cape Blanc area, displays notable offshore export of upwelled waters with high organic matter concentrations (Santana-Falcón et al. 2016, 2020; Lovecchio et al. 2017). Such mesoscale surface circulation can move waters hundreds of kilometres offshore (Meunier et al. 2012; Castellanos et al. 2013), advecting to the open ocean not only DOM, but also particles (Fischer et al. 2009). Thus, waters from upwelling areas can reach points far from their origin, simultaneously extending the influence of upwelling on vertical connectivity, as evidenced by the results from **Chapters 3 and 4**. Considering the regional oceanography is hence shown to be fundamental to understand microbial and biogeochemical processes which might otherwise seem disconnected. This is not limited to horizontal advection processes, and other examples abound: mesoscale and submesoscale physics can contribute to primary production variability (Mahadevan 2016); eddies, a common feature of the global ocean including upwelling systems (Pegliasco et al. 2015), can transport particles offshore as well (Amos et al. 2019), and have been shown to harbour prokaryotic communities with enhanced activity and distinct composition (Baltar et al. 2010); and fronts act as oceanic watersheds dividing zones with distinct vertical carbon export (Valiente et al. 2022) and prokaryotic communities, an effect that may reach down to the deep ocean (Baltar and Arístegui 2017).

Perspectives on prokaryotes and dissolved organic matter cycling

The analysis of the optical properties of DOM is a valuable tool to track its microbial transformation in the ocean. From experiments (Lønborg et al. 2010; Romera-Castillo et al. 2010; Jørgensen et al. 2014; Loginova et al. 2015) to regional and global surveys (Lønborg and Álvarez-Salgado 2014; Catalá et al. 2015, 2016b; a, 2018; Yamashita et al. 2017; Martínez–Pérez et al. 2019), specific optical signatures have been identified in relation to prokaryotic activity proxies and changes in the organic matter pool. For instance, humic-like FDOM and spectral slopes of CDOM are correlated to microbial oxygen consumption during water mass ageing, meaning they act as footprints of DOM transformation by prokaryotes (Catalá et al. 2015, 2016b). We have taken advantage of such approaches due to their proven utility and relative ease of application (**Chapters 1 and 4**). However, the information they provide is necessarily limited as they 1) represent only a fraction of the DOM pool and 2) do

not give information about composition. Other techniques such as the Fourier Transform Ion Cyclotron Resonance Mass Spectra (FT-ICR-MS) and high-field nuclear magnetic resonance spectroscopy (NMR) offer the possibility of determining the molecular formulae and functional groups present in seawater. These approaches have been applied to DOM characterisation both in experiments (Lechtenfeld et al. 2015; Osterholz et al. 2015; Zark et al. 2017) and natural oceanic environments (Martínez-Pérez et al. 2017; Seidel et al. 2022; LaBrie et al. 2022), but despite being profoundly informative they are not easily accessible. Thus, the universalisation of such techniques remains a much-needed step in the path towards a complete understanding of marine DOM cycling. Going forward, the systematic identification and quantification of molecular structures remain the ultimate challenge, although the extreme complexity of DOM makes this a difficult task. A molecular perspective will be important to discern the reasons behind the observed persistence of DOM, as discussed in the **Introduction,** and **Chapters 1 and 4**: whether it is primarily emergent, inherent or a combination of both (Dittmar et al. 2021).

Coupled with a more detailed characterisation of DOM, the study of community-wide genes (metagenomics) and their expressions levels (metatranscriptomics) will provide knowledge about the metabolic capabilities of prokaryotes and *in situ* processes. Such approaches act as complements of taxonomic identification (as in **Chapters 2 and 4**), which does not provide information about the ongoing metabolic processes, relying instead on previous functional knowledge to infer interpretations. Indeed, the combination of taxonomy and transcriptomics has been successfully applied to better understand the short-term dynamics of prokaryotes during an upwelling-induced phytoplankton bloom (Pontiller et al. 2022). Longer time-series or oceanographic studies like the ones presented here would benefit from such approaches. Relatedly, it has become ever more valuable to study both bulk (**Chapters 2 and 3**) and cell-specific metabolism (**Chapter 2**). Assessment of bulk metabolic rates is fundamental to estimate biogeochemical elemental cycling by planktonic communities. Nonetheless, we usually rely on indirect measurements and require some sort of conversion to estimate rates in units of the element of interest (e.g., carbon), introducing uncertainties that need to be addressed (**Chapter 3**; Giering and Evans, 2022). Single cell methods in turn provide information about which fraction of the community is driving the community-wide rates (Ferrera et al. 2011; Munson-McGee et al. 2022) and enable linking them with taxonomic identity, a task for which visualisation is still—and should remain—crucial (Sebastián and Gasol 2019). The joint application of community-wide and single cell approaches ought to be continued in future studies.

Prokaryotes do not carry out their metabolism isolated from each other (and from other microbes). Interactions between prokaryotes and other planktonic microorganisms (other prokaryotes, phytoplankton, zooplankton, and viruses) are fundamental to marine microbial ecosystems and, like many other factors, influence elemental cycling in the ocean (Moran 2015; Worden et al. 2015). One of the best-known prokaryote-prokaryote interactions is termed *quorum sensing*, a mechanism mediated by organic molecules that act as signals through which prokaryotes coordinate gene expression and cooperate. Quorum sensing is most effective beyond a certain threshold of cell density and, thus, bears major importance among particle colonisers, where it is known to regulate exopolysaccharide and exohydrolase production, key for attachment, biofilm formation and POM degradation (Hmelo 2017). Prokaryotes are also found associated with larger eukaryotic cells, either attached to them or in close proximity, attracted by the DOM-rich microenvironment they produce, the phycosphere (Seymour et al. 2017). While prokaryotes readily utilise the DOM pool released by phytoplankton (Kieft et al. 2021; Eigemann et al. 2022), complex relationships involving specific compounds have also been documented, like provision of organosulfur molecules and infochemical exchanges (Seymour et al. 2017), which can be vital for both interacting partners. The nature of the interactions in which they engage is varied—from mutualism to antagonism—and these can ultimately also affect other components of the microbial trophic webs, e.g., bacteria protecting phytoplanktonic cells from viral mortality (Pollara et al. 2021). In contrast to surface-attached prokaryotes, encounter rates of free-living cells are comparatively lower, and thus direct interactions are less frequent and not as essential. However, indirect interactions within free-living communities have been argued to be crucial. For instance, prokaryotes with reduced genomes that have lost the ability to synthesise certain metabolites (such as the ubiquitous, free-living SAR11 clade and *Prochlorococcus*) rely on other prokaryotes that are able to produce them (Morris et al. 2012; Mas et al. 2016). Mutual interdependences, like the ones involving the synthesis and auxotrophy of the different B vitamins (Gómez-Consarnau et al. 2018), also contribute to create complex webs of relationships among free-living prokaryotes.

Bacterivory by protists exerts important top-down control over prokaryotes. Predation of prokaryotes is carried out by both heterotrophic and mixotrophic protists (Jürgens and Massana 2008; Stoecker et al. 2017), and happens across the global ocean, from surface waters (Teira et al. 2019) to deep water masses (Rocke et al. 2015). Overall, prokaryotic production tends to be in balance with (or be higher than) biomass loss through predation (Jürgens and Massana 2008), albeit under

certain circumstances—including phytoplankton blooms—predation can strongly reduce prokaryotic standing stocks (Pernthaler 2005; Baltar et al. 2016). Predators can have an impact on the structure of the community, as they have been observed to exert selective pressure over certain prokaryotic groups. For instance, they seem to prey more on active bacteria (Sintes and del Giorgio 2014) and can also display size-selective grazing (Prokopchuk et al. 2022). Evidence on selective predation based on taxonomy is elusive, and it has been reported to be absent during experimental phytoplankton blooms (Baltar et al. 2016). For their part, prokaryotes have developed strategies to avoid or diminish predation. Motility (Matz and Jürgens 2005), changes in cell surface properties (Dadon-Pilosof et al. 2017) and protection through production of specific compounds (Teng et al. 2021) have all been observed as defence mechanisms. Along predators, viruses represent a second pathway of top-down control over prokaryotes (Breitbart et al. 2018). Their interactions involve the infection of prokaryotic cells and can alter the biomass levels of the community (Riemann et al. 2000; Vaqué et al. 2017). During infection, viruses are able to change the metabolism of the hosts and modify the composition of the DOM they release during lysis (Ankrah et al. 2014). The overall reduced range of hosts that a virus is able to infect (several strains or a few closely related genera) (Martiny et al. 2014) can produce changes in the diversity and composition of prokaryotic communities, although viruses with relatively wide host ranges are being discovered (Breitbart et al. 2018). Hence, viruses have important roles influencing the involvement of prokaryotes in biogeochemical cycles, both directly and indirectly—e.g., viral infections during coccolithophorid blooms have been observed to potentially divert DOM recycling from prokaryotes to heterotrophic eukaryotes (Vincent et al. 2021).

All aforementioned microbial dependencies and interactions—uni-, bi- or multidirectional, both intra- and inter-domain—regulate the standing stocks and metabolism of prokaryotes, create co-occurrence patterns of different taxa and influence their involvement in biogeochemical processes. While this thesis has not investigated microbial interactions, their study is a promising avenue to improve our understanding of microbiology and organic matter cycling in upwelling environments.

References

Agogué, H., D. Lamy, P. R. Neal, M. L. Sogin, and G. J. Herndl. 2011. Water mass-specificity of bacterial communities in the North Atlantic revealed by massively parallel sequencing. Mol. Ecol. **20**: 258–274. doi:10.1111/j.1365-294X.2010.04932.x

Allers, E., L. Gómez-Consarnau, J. Pinhassi, J. M. Gasol, K. Šimek, and J. Pernthaler. 2007. Response of Alteromonadaceae and Rhodobacteriaceae to glucose and phosphorus manipulation in marine mesocosms. Environ. Microbiol. **9**: 2417–2429. doi:10.1111/j.1462-2920.2007.01360.x

Alonso-Sáez, L., and J. M. Gasol. 2007. Seasonal Variations in the Contributions of Different Bacterial Groups to the Uptake of Low-Molecular-Weight Compounds in Northwestern Mediterranean Coastal Waters. Appl. Environ. Microbiol. **73**: 3528–3535. doi:10.1128/AEM.02627-06

Alonso, C., and J. Pernthaler. 2006. Roseobacter and SAR11 dominate microbial glucose uptake in coastal North Sea waters. Environ. Microbiol. **8**: 2022–2030. doi:10.1111/j.1462-2920.2006.01082.x

Amos, C. M., R. M. Castelao, and P. M. Medeiros. 2019. Offshore transport of particulate organic carbon in the California Current System by mesoscale eddies. Nat. Commun. **10**: 4940. doi:10.1038/s41467-019-12783-5

Ankrah, N. Y. D., A. L. May, J. L. Middleton, and others. 2014. Phage infection of an environmentally relevant marine bacterium alters host metabolism and lysate composition. ISME J. **8**: 1089–1100. doi:10.1038/ismej.2013.216

Arístegui, J., J. M. Gasol, C. M. Duarte, and G. J. Herndl. 2009. Microbial oceanography of the dark ocean's pelagic realm. Limnol. Oceanogr. **54**: 1501–1529. doi:10.4319/lo.2009.54.5.1501

Auladell, A., P. Sánchez, O. Sánchez, J. M. Gasol, and I. Ferrera. 2019. Long-term seasonal and interannual variability of marine aerobic anoxygenic photoheterotrophic bacteria. ISME J. **13**: 1975–1987. doi:10.1038/s41396-019-0401-4

Baetge, N., J. R. Graff, M. J. Behrenfeld, and C. A. Carlson. 2020. Net Community Production, Dissolved Organic Carbon Accumulation, and Vertical Export in the Western North Atlantic. Front. Mar. Sci. **7**: 227. doi:10.3389/fmars.2020.00227

Baltar, F., and J. Arístegui. 2017. Fronts at the Surface Ocean Can Shape Distinct Regions of Microbial Activity and Community Assemblages Down to the Bathypelagic Zone: The Azores Front as a Case Study. Front. Mar. Sci. **4**: 252. doi:10.3389/fmars.2017.00252

Baltar, F., J. Arístegui, J. M. Gasol, I. Lekunberri, and G. J. Herndl. 2010. Mesoscale eddies: Hotspots of prokaryotic activity and differential community structure in the ocean. ISME J. **4**: 975–988. doi:10.1038/ismej.2010.33

Baltar, F., J. Palovaara, F. Unrein, and others. 2016. Marine bacterial community structure resilience to changes in protist predation under phytoplankton bloom conditions. ISME J. **10**: 568–581. doi:10.1038/ismej.2015.135

Breitbart, M., C. Bonnain, K. Malki, and N. A. Sawaya. 2018. Phage puppet masters of the marine microbial realm. Nat. Microbiol. **3**: 754–766. doi:10.1038/s41564-018-0166-y

Buchan, A., G. R. LeCleir, C. A. Gulvik, and J. M. González. 2014. Master recyclers: features and functions of bacteria associated with phytoplankton blooms. Nat. Rev. Microbiol. **12**: 686–698. doi:10.1038/nrmicro3326

Carlson, C. A., P. A. del Giorgio, and G. J. Herndl. 2007. Microbes and the Dissipation of Energy and Respiration: From Cells to Ecosystems. Oceanography **20**: 89–100.

Castellanos, P., J. L. Pelegrí, and A. Benazzouz. 2013. Wind-driven surface circulation in the Cape Blanc region. Cont. Shelf Res. **60**: 87–103. doi:10.1016/j.csr.2013.02.003

Catalá, T. S., X. A. Álvarez-Salgado, J. Otero, and others. 2016a. Drivers of fluorescent dissolved organic matter in the global epipelagic ocean. Limnol. Oceanogr. **61**: 1101–1119. doi:10.1002/lno.10281

Catalá, T. S., A. M. Martínez-Pérez, M. Nieto-Cid, and others. 2018. Dissolved Organic Matter (DOM) in the open Mediterranean Sea. I. Basin–wide distribution and drivers of chromophoric DOM. Prog. Oceanogr. **165**: 35–51. doi:10.1016/j.pocean.2018.05.002

Catalá, T. S., I. Reche, A. Fuentes-Lema, and others. 2015. Turnover time of fluorescent dissolved organic matter in the dark global ocean. Nat. Commun. **6:5986**. doi:10.1038/ncomms6986

Catalá, T. S., I. Reche, C. L. Ramón, À. López-Sanz, M. Álvarez, E. Calvo, and X. A. Álvarez-Salgado. 2016b. Chromophoric signatures of microbial by-products in the dark ocean. Geophys. Res. Lett. **43**: 7639–7648. doi:10.1002/2016GL069878

Chavez, F. P., and M. Messié. 2009. A comparison of Eastern Boundary Upwelling Ecosystems. Prog. Oceanogr. **83**: 80–96. doi:10.1016/j.pocean.2009.07.032

Dadon-Pilosof, A., K. R. Conley, Y. Jacobi, and others. 2017. Surface properties of SAR11 bacteria facilitate grazing avoidance. Nat. Microbiol. **2**: 1608–1615. doi:10.1038/s41564-017-0030-5

Datta, M. S., E. Sliwerska, J. Gore, M. F. Polz, and O. X. Cordero. 2016. Microbial interactions lead to rapid micro-scale successions on model marine particles. Nat. Commun. **7**: 11965. doi:10.1038/ncomms11965

Dittmar, T., S. T. Lennartz, H. Buck-Wiese, D. A. Hansell, C. Santinelli, C. Vanni, B. Blasius, and J.-H. Hehemann. 2021. Enigmatic persistence of dissolved organic matter in the ocean. Nat. Rev. Earth Environ. **2**: 570–583. doi:10.1038/s43017-021-00183-7

Eigemann, F., E. Rahav, H.-P. Grossart, D. Aharonovich, D. Sher, A. Vogts, and M. Voss. 2022. Phytoplankton exudates provide full nutrition to a subset of accompanying heterotrophic bacteria via carbon, nitrogen and phosphorus allocation. Environ. Microbiol. **24**: 2467–2483. doi:10.1111/1462-2920.15933

Fadeev, E., A. Rogge, S. Ramondenc, and others. 2021. Sea ice presence is linked to higher carbon export and vertical microbial connectivity in the Eurasian Arctic Ocean. Commun. Biol. **4**: 1255. doi:10.1038/s42003-021-02776-w

Ferrera, I., M. J. Gasol, M. Sebastián, E. Hojerová, and M. Koblížek. 2011. Comparison of Growth Rates of Aerobic Anoxygenic Phototrophic Bacteria and Other Bacterioplankton Groups in Coastal Mediterranean Waters. Appl. Environ. Microbiol. **77**: 7451–7458. doi:10.1128/AEM.00208-11

Fischer, G., C. Reuter, G. Karakas, N. Nowald, and G. Wefer. 2009. Offshore advection of particles within the Cape Blanc filament, Mauritania: Results from observational and modelling studies. Prog. Oceanogr. **83**: 322–330. doi:10.1016/j.pocean.2009.07.023

Francis, T. Ben, D. Bartosik, T. Sura, and others. 2021. Changing expression patterns of TonB-dependent transporters suggest shifts in polysaccharide consumption over the course of a spring phytoplankton bloom. ISME J. **15**: 2336–2350. doi:10.1038/s41396-021-00928-8

Frank, A. H., J. A. L. Garcia, G. J. Herndl, and T. Reinthaler. 2016. Connectivity between surface and

deep waters determines prokaryotic diversity in the North Atlantic Deep Water. Environ. Microbiol. **18**: 2052–2063. doi:10.1111/1462-2920.13237

Fry, B., C. S. Hopkinson Jr., A. Nolin, B. Norrman, and U. L. Zweifel. 1996. Long-term decomposition of DOC from experimental diatom blooms. Limnol. Oceanogr. **41**: 1344–1347. doi:10.4319/lo.1996.41.6.1344

Fuhrman, J. A., I. Hewson, M. S. Schwalbach, J. A. Steele, M. V Brown, and S. Naeem. 2006. Annually reoccurring bacterial communities are predictable from ocean conditions. Proc. Natl. Acad. Sci. **103**: 13104–13109. doi:10.1073/pnas.0602399103

Galand, P. E., O. Pereira, C. Hochart, J. C. Auguet, and D. Debroas. 2018. A strong link between marine microbial community composition and function challenges the idea of functional redundancy. ISME J. **12**: 2470–2478. doi:10.1038/s41396-018-0158-1

Giering, S. L. C., and C. Evans. 2022. Overestimation of prokaryotic production by leucine incorporation—and how to avoid it. Limnol. Oceanogr. **67**: 726–738. doi:10.1002/lno.12032

Gómez-Consarnau, L., R. Sachdeva, S. M. Gifford, L. S. Cutter, J. A. Fuhrman, S. A. Sañudo-Wilhelmy, and M. A. Moran. 2018. Mosaic patterns of B-vitamin synthesis and utilization in a natural marine microbial community. Environ. Microbiol. **20**: 2809–2823. doi:10.1111/1462-2920.14133

Gralka, M., R. Szabo, R. Stocker, and O. X. Cordero. 2020. Trophic Interactions and the Drivers of Microbial Community Assembly. Curr. Biol. **30**: R1176–R1188. doi:10.1016/j.cub.2020.08.007

Grossart, H.-P., K. W. Tang, T. Kiørboe, and H. Ploug. 2007. Comparison of cell-specific activity between free-living and attached bacteria using isolates and natural assemblages. FEMS Microbiol. Lett. **266**: 194–200. doi:10.1111/j.1574-6968.2006.00520.x

Hach, P. F., H. K. Marchant, A. Krupke, and others. 2020. Rapid microbial diversification of dissolved organic matter in oceanic surface waters leads to carbon sequestration. Sci. Rep. **10**: 13025. doi:10.1038/s41598-020-69930-y

Herndl, G. J., B. Bayer, F. Baltar, and T. Reinthaler. 2023. Prokaryotic Life in the Deep Ocean's Water Column. Ann. Rev. Mar. Sci. **15**. doi:10.1146/annurev-marine-032122-115655

Hevroni, G., F. Vincent, C. Ku, U. Sheyn, and A. Vardi. 2022. Daily turnover of active giant virus infection during algal blooms revealed by single-cell transcriptomics. bioRxiv 2022.10.15.512338. doi:10.1101/2022.10.15.512338

Hmelo, L. R. 2017. Quorum Sensing in Marine Microbial Environments. Ann. Rev. Mar. Sci. **9**: 257–281. doi:10.1146/annurev-marine-010816-060656

Hoikkala, L., H. Tammert, R. Lignell, E. Eronen-Rasimus, K. Spilling, and V. Kisand. 2016. Autochthonous dissolved organic matter drives bacterial community composition during a bloom of filamentous cyanobacteria. Front. Mar. Sci. **3**: 111. doi:10.3389/fmars.2016.00111

Irion, S., U. Christaki, H. Berthelot, S. L'Helguen, and L. Jardillier. 2021. Small phytoplankton contribute greatly to CO2-fixation after the diatom bloom in the Southern Ocean. ISME J. **15**: 2509–2522. doi:10.1038/s41396-021-00915-z

Jørgensen, L., C. A. Stedmon, M. A. Granskog, and M. Middelboe. 2014. Tracing the long-term microbial production of recalcitrant fluorescent dissolved organic matter in seawater. Geophys. Res. Lett. **41**: 2481–2488. doi:10.1002/2014GL059428

Jürgens, K., and R. Massana. 2008. Protistan Grazing on Marine Bacterioplankton, p. 383–441. *In* Microbial Ecology of the Oceans.

Kieft, B., Z. Li, S. Bryson, R. L. Hettich, C. Pan, X. Mayali, and R. S. Mueller. 2021. Phytoplankton exudates and lysates support distinct microbial consortia with specialized metabolic and ecophysiological traits. Proc. Natl. Acad. Sci. **118**: e2101178118. doi:10.1073/pnas.2101178118

Kuhlisch, C., G. Schleyer, N. Shahaf, F. Vincent, D. Schatz, and A. Vardi. 2022. Viral infection of algal blooms leaves a unique metabolic footprint on the dissolved organic matter in the ocean. Sci. Adv. **7**: eabf4680. doi:10.1126/sciadv.abf4680

LaBrie, R., B. Péquin, N. Fortin St-Gelais, and others. 2022. Deep ocean microbial communities produce more stable dissolved organic matter through the succession of rare prokaryotes. Sci. Adv. **8**: eabn0035. doi:10.1126/sciadv.abn0035

Lechtenfeld, O. J., N. Hertkorn, Y. Shen, M. Witt, and R. Benner. 2015. Marine sequestration of carbon in bacterial metabolites. Nat. Commun. **6**: 6711. doi:10.1038/ncomms7711

Leizeaga, A., M. Estrany, I. Forn, and M. Sebastián. 2017. Using click-chemistry for visualizing in situ changes of translational activity in planktonic marine bacteria. Front. Microbiol. **8**: 2360. doi:10.3389/fmicb.2017.02360

Loginova, A. N., C. Borchard, J. Meyer, H. Hauss, R. Kiko, and A. Engel. 2015. Effects of nitrate and phosphate supply on chromophoric and fluorescent dissolved organic matter in the Eastern Tropical North Atlantic: a mesocosm study. Biogeosciences **12**: 6897–6914. doi:10.5194/bg-12-6897-2015

Lønborg, C., and X. A. Álvarez-Salgado. 2014. Tracing dissolved organic matter cycling in the eastern boundary of the temperate North Atlantic using absorption and fluorescence spectroscopy. Deep Sea Res. Part I Oceanogr. Res. Pap. **85**: 35–46. doi:10.1016/j.dsr.2013.11.002

Lønborg, C., X. A. Álvarez-Salgado, K. Davidson, S. Martínez-García, and E. Teira. 2010. Assessing the microbial bioavailability and degradation rate constants of dissolved organic matter by fluorescence spectroscopy in the coastal upwelling system of the Ría de Vigo. Mar. Chem. **119**: 121–129. doi:10.1016/j.marchem.2010.02.001

Loucaides, S., T. Tyrrell, E. P. Achterberg, and others. 2012. Biological and physical forcing of carbonate chemistry in an upwelling filament off northwest Africa: Results from a Lagrangian study. Global Biogeochem. Cycles **26**. doi:10.1029/2011GB004216

Lovecchio, E., N. Gruber, M. Münnich, and Z. Lachkar. 2017. On the long-range offshore transport of organic carbon from the Canary Upwelling System to the open North Atlantic. Biogeosciences **14**: 3337–3369. doi:10.5194/bg-14-3337-2017

Mahadevan, A. 2016. The Impact of Submesoscale Physics on Primary Productivity of Plankton. Ann. Rev. Mar. Sci. **8**: 161–184. doi:10.1146/annurev-marine-010814-015912

Martínez-Pérez, A. M., H. Osterholz, M. Nieto-Cid, M. Álvarez, T. Dittmar, and X. A. Álvarez-Salgado. 2017. Molecular composition of dissolved organic matter in the Mediterranean Sea. Limnol. Oceanogr. **62**: 2699–2712. doi:10.1002/lno.10600

Martínez–Pérez, A. M., T. S. Catalá, M. Nieto–Cid, and others. 2019. Dissolved organic matter (DOM) in the open Mediterranean Sea. II: Basin–wide distribution and drivers of fluorescent DOM. Prog. Oceanogr. **170**: 93–106. doi:10.1016/j.pocean.2018.10.019

Martiny, J. B. H., L. Riemann, M. F. Marston, and M. Middelboe. 2014. Antagonistic Coevolution of Marine Planktonic Viruses and Their Hosts. Ann. Rev. Mar. Sci. **6**: 393–414.

doi:10.1146/annurev-marine-010213-135108

Mas, A., S. Jamshidi, Y. Lagadeuc, D. Eveillard, and P. Vandenkoornhuyse. 2016. Beyond the Black Queen Hypothesis. ISME J. doi:10.1038/ismej.2016.22

Matz, C., and K. Jürgens. 2005. High Motility Reduces Grazing Mortality of Planktonic Bacteria. Appl. Environ. Microbiol. **71**: 921–929. doi:10.1128/AEM.71.2.921-929.2005

Mehrshad, M., F. Rodriguez-Valera, M. A. Amoozegar, P. López-García, and R. Ghai. 2018. The enigmatic SAR202 cluster up close: Shedding light on a globally distributed dark ocean lineage involved in sulfur cycling. ISME J. **12**: 655–668. doi:10.1038/s41396-017-0009-5

Meon, B., and D. L. Kirchman. 2001. Dynamics and molecular composition of dissolved organic material during experimental phytoplankton blooms. Mar. Chem. **75**: 185–199. doi:10.1016/S0304-4203(01)00036-6

Mestre, M., C. Ruiz-González, R. Logares, C. M. Duarte, J. M. Gasol, and M. M. Sala. 2018. Sinking particles promote vertical connectivity in the ocean microbiome. Proc. Natl. Acad. Sci. U. S. A. **115**: E6799–E6807. doi:10.1073/pnas.1802470115

Meunier, T., E. D. Barton, B. Barreiro, and R. Torres. 2012. Upwelling filaments off Cap Blanc: Interaction of the NW African upwelling current and the Cape Verde frontal zone eddy field? J. Geophys. Res. Ocean. **117**: C08031. doi:10.1029/2012JC007905

Moran, M. A. 2015. The global ocean microbiome. Science, **350**: aac8455. doi:10.1126/science.aac8455

Morris, J. J., R. E. Lenski, and E. R. Zinser. 2012. The black queen hypothesis: Evolution of dependencies through adaptive gene loss. MBio. doi:10.1128/mBio.00036-12

Munson-McGee, J. H., M. R. Lindsay, E. Sintes, and others. 2022. Decoupling of respiration rates and abundance in marine prokaryoplankton. Nature. doi:10.1038/s41586-022-05505-3

Needham, D. M., and J. A. Fuhrman. 2016. Pronounced daily succession of phytoplankton, archaea and bacteria following a spring bloom. Nat. Microbiol. **1**: 16005. doi:10.1038/nmicrobiol.2016.5

Orta-Ponce, C. P., T. Rodríguez-Ramos, M. Nieto-Cid, E. Teira, E. Guerrero-Feijóo, A. Bode, and M. M. Varela. 2021. Empirical leucine-to-carbon conversion factors in north-eastern Atlantic waters (50–2000 m) shaped by bacterial community composition and optical signature of DOM. Sci. Rep. **11**: 24370. doi:10.1038/s41598-021-03790-y

Osterholz, H., J. Niggemann, H.-A. Giebel, M. Simon, and T. Dittmar. 2015. Inefficient microbial production of refractory dissolved organic matter in the ocean. Nat. Commun. **6**: 7422. doi:10.1038/ncomms8422

Pedler, B. E., L. I. Aluwihare, and F. Azam. 2014. Single bacterial strain capable of significant contribution to carbon cycling in the surface ocean. Proc. Natl. Acad. Sci. **111**: 7202–7207. doi:10.1073/pnas.1401887111

Pegliasco, C., A. Chaigneau, and R. Morrow. 2015. Main eddy vertical structures observed in the four major Eastern Boundary Upwelling Systems. J. Geophys. Res. Ocean. **120**: 6008–6033. doi:10.1002/2015JC010950

Pernthaler, J. 2005. Predation on prokaryotes in the water column and its ecological implications. Nat. Rev. Microbiol. **3**: 537–546. doi:10.1038/nrmicro1180

Pollara, S. B., J. W. Becker, B. L. Nunn, and others. 2021. Bacterial Quorum-Sensing Signal Arrests Phytoplankton Cell Division and Impacts Virus-Induced Mortality. mSphere **6**.

doi:10.1128/mSphere.00009-21

Pontiller, B., S. Martínez-García, V. Joglar, and others. 2022. Rapid bacterioplankton transcription cascades regulate organic matter utilization during phytoplankton bloom progression in a coastal upwelling system. ISME J. **16**: 2360–2372. doi:10.1038/s41396-022-01273-0

Prokopchuk, G., T. Korytář, V. Juricová, J. Majstorović, A. Horák, K. Šimek, and J. Lukeš. 2022. Trophic flexibility of marine diplonemids - switching from osmotrophy to bacterivory. ISME J. **16**: 1409–1419. doi:10.1038/s41396-022-01192-0

Reintjes, G., B. M. Fuchs, R. Amann, and C. Arnosti. 2020. Extensive Microbial Processing of Polysaccharides in the South Pacific Gyre via Selfish Uptake and Extracellular Hydrolysis. Front. Microbiol. **11**: 583158. doi:10.3389/fmicb.2020.583158

Riemann, L., G. F. Steward, and F. Azam. 2000. Dynamics of bacterial community composition and activity during a mesocosm diatom bloom. Appl. Environ. Microbiol. **66**: 578–587. doi:10.1128/AEM.66.2.578-587.2000

Rocke, E., M. G. Pachiadaki, A. Cobban, E. B. Kujawinski, and V. P. Edgcomb. 2015. Protist Community Grazing on Prokaryotic Prey in Deep Ocean Water Masses. PLoS One **10**: e0124505.

Romera-Castillo, C., H. Sarmento, X. A. Álvarez-Salgado, J. M. Gasol, and C. Marraséa. 2010. Production of chromophoric dissolved organic matter by marine phytoplankton. Limnol. Oceanogr. **55**: 446–454. doi:10.4319/lo.2010.55.1.0446

Ruiz-González, C., M. Mestre, M. Estrada, and others. 2020. Major imprint of surface plankton on deep ocean prokaryotic structure and activity. Mol. Ecol. **29**: 1820–1838. doi:10.1111/mec.15454

Saba, G. K., D. K. Steinberg, and D. A. Bronk. 2011. The relative importance of sloppy feeding, excretion, and fecal pellet leaching in the release of dissolved carbon and nitrogen by Acartia tonsa copepods. J. Exp. Mar. Bio. Ecol. **404**: 47–56. doi:10.1016/j.jembe.2011.04.013

Salazar, G., F. M. Cornejo-Castillo, V. Benítez-Barrios, E. Fraile-Nuez, X. A. Álvarez-Salgado, C. M. Duarte, J. M. Gasol, and S. G. Acinas. 2016. Global diversity and biogeography of deep-sea pelagic prokaryotes. ISME J. **10**: 596–608. doi:10.1038/ismej.2015.137

Santana-Falcón, Y., M. Benavides, P. Sangrà, E. Mason, E. D. Barton, A. Orbi, and J. Arístegui. 2016. Coastal–offshore exchange of organic matter across the Cape Ghir filament (NW Africa) during moderate upwelling. J. Mar. Syst. **154**: 233–242. doi:10.1016/j.jmarsys.2015.10.008

Santana-Falcón, Y., E. Mason, and J. Arístegui. 2020. Offshore transport of organic carbon by upwelling filaments in the Canary Current System. Prog. Oceanogr. **186**: 102322. doi:10.1016/j.pocean.2020.102322

Sebastián, M., and J. M. Gasol. 2019. Visualization is crucial for understanding microbial processes in the ocean. Philos. Trans. R. Soc. B Biol. Sci. **374**: 20190083. doi:10.1098/rstb.2019.0083

Seidel, M., S. P. B. Vemulapalli, D. Mathieu, and T. Dittmar. 2022. Marine Dissolved Organic Matter Shares Thousands of Molecular Formulae Yet Differs Structurally across Major Water Masses. Environ. Sci. Technol. **56**: 3758–3769. doi:10.1021/acs.est.1c04566

Seymour, J. R., S. A. Amin, J. B. Raina, and R. Stocker. 2017. Zooming in on the phycosphere: The ecological interface for phytoplankton-bacteria relationships. Nat. Microbiol. **2**. doi:10.1038/nmicrobiol.2017.65

Sintes, E., and P. A. del Giorgio. 2014. Feedbacks between protistan single-cell activity and bacterial

physiological structure reinforce the predator/prey link in microbial foodwebs. Front. Microbiol. **5**: 453. doi:10.3389/fmicb.2014.00453

Steinberg, D. K., and M. R. Landry. 2017. Zooplankton and the Ocean Carbon Cycle. Ann. Rev. Mar. Sci. **9**: 413–444. doi:10.1146/annurev-marine-010814-015924

Stoecker, D. K., P. J. Hansen, D. A. Caron, and A. Mitra. 2017. Mixotrophy in the Marine Plankton. Ann. Rev. Mar. Sci. **9**: 311–335. doi:10.1146/annurev-marine-010816-060617

Sverdrup, H. U. 1953. On Conditions for the Vernal Blooming of Phytoplankton. ICES J. Mar. Sci. **18**: 287–295. doi:10.1093/icesjms/18.3.287

Szabo, R. E., S. Pontrelli, J. Grilli, J. A. Schwartzman, S. Pollak, U. Sauer, and O. X. Cordero. 2022. Historical contingencies and phage induction diversify bacterioplankton communities at the microscale. Proc. Natl. Acad. Sci. **119**: e2117748119. doi:10.1073/pnas.2117748119

Tada, Y., A. Taniguchi, Y. Sato-Takabe, and K. Hamasaki. 2012. Growth and succession patterns of major phylogenetic groups of marine bacteria during a mesocosm diatom bloom. J. Oceanogr. **68**: 509–519. doi:10.1007/s10872-012-0114-z

Teeling, H., B. M. Fuchs, D. Becher, and others. 2012. Substrate-Controlled Succession of Marine Bacterioplankton Populations Induced by a Phytoplankton Bloom. Science, **336**: 608–611. doi:10.1126/science.1218344

Teeling, H., B. M. Fuchs, C. M. Bennke, and others. 2016. Recurring patterns in bacterioplankton dynamics during coastal spring algae blooms A.A. Brakhage [ed.]. Elife **5**: e11888. doi:10.7554/eLife.11888

Teira, E., R. Logares, A. Gutiérrez-Barral, I. Ferrera, M. M. Varela, X. A. G. Morán, and J. M. Gasol. 2019. Impact of grazing, resource availability and light on prokaryotic growth and diversity in the oligotrophic surface global ocean. Environ. Microbiol. **21**: 1482–1496. doi:10.1111/1462-2920.14581

Teng, Z.-J., P. Wang, X.-L. Chen, and others. 2021. Acrylate protects a marine bacterium from grazing by a ciliate predator. Nat. Microbiol. **6**: 1351–1356. doi:10.1038/s41564-021-00981-1

Tréguer, P., C. Bowler, B. Moriceau, and others. 2018. Influence of diatom diversity on the ocean biological carbon pump. Nat. Geosci. **11**: 27–37. doi:10.1038/s41561-017-0028-x

Valiente, S., B. Fernández-Castro, R. Campanero, and others. 2022. Dissolved and suspended organic matter dynamics in the Cape Verde Frontal Zone (NW Africa). Prog. Oceanogr. **201**: 102727. doi:10.1016/j.pocean.2021.102727

Vaqué, D., J. A. Boras, F. Torrent-Llagostera, and others. 2017. Viruses and Protists Induced-mortality of Prokaryotes around the Antarctic Peninsula during the Austral Summer. Front. Microbiol. **8**: 241. doi:10.3389/fmicb.2017.00241

Vincent, F., M. Gralka, G. Schleyer, and others. 2021. Viral infection switches the balance between bacterial and eukaryotic recyclers of organic matter during algal blooms. bioRxiv 2021.10.25.465659. doi:10.1101/2021.10.25.465659

Worden, A. Z., M. J. Follows, S. J. Giovannoni, S. Wilken, A. E. Zimmerman, and P. J. Keeling. 2015. Rethinking the marine carbon cycle: Factoring in the multifarious lifestyles of microbes. Science (80-.). **347**: 1257594. doi:10.1126/science.1257594

Yamashita, Y., F. Hashihama, H. Saito, H. Fukuda, and H. Ogawa. 2017. Factors controlling the geographical distribution of fluorescent dissolved organic matter in the surface waters of the

Pacific Ocean. Limnol. Oceanogr. **62**: 2360–2374. doi:10.1002/lno.10570

Zark, M., N. K. Broda, T. Hornick, H.-P. Grossart, U. Riebesell, and T. Dittmar. 2017. Ocean Acidification Experiments in Large-Scale Mesocosms Reveal Similar Dynamics of Dissolved Organic Matter Production and Biotransformation. Front. Mar. Sci. **4**: 271. doi:10.3389/fmars.2017.00271

Conclusions

The conclusions of this thesis are:

i. Primary production enhancements derived from upwelling of nutrient-rich waters resulted in increases in the concentration of dissolved organic matter, and changes in its stoichiometry and optical characteristics. These alterations were proportional to the concentrations of nutrients that were introduced. Despite differences in the induced phytoplankton blooms, single upwelling pulses (with large, but short-lived blooms) and recurring upwelling (with more sustained blooms) resulted in similar outcomes for the concentration, stoichiometry, and optical properties of dissolved organic matter.

ii. Prokaryotes actively transformed the dissolved organic matter produced during the phytoplankton blooms. Despite activity differences between upwelling modes (short-lived peak vs lower sustained levels), dissolved organic carbon did not decrease in any scenario during the duration of the experiment. The balance between the production and consumption of dissolved organic matter was probably induced, at least in part, by the production of a persistent pool of organic molecules, as suggested by the optical properties of the dissolved organic matter.

iii. During the phytoplankton blooms and the subsequent organic matter transformation, prokaryotes showed marked oscillations in abundances and viabilities. The prokaryotic communities displayed notably reproducible successional patterns across upwelling intensities, modes, and size fractions (free-living vs particle-attached). Members of the Flavobacteriales, Rhodobacterales and Enterobacterales orders, copiotrophs known to thrive during phytoplankton blooms, had major presence. While differences existed in the taxa that populated the distinct size fractions and, to a lesser extent, upwelling modes, the reproducible patterns suggest that consistent functional successions occur under varying upwelling scenarios.

iv. The productivity enhancement by upwelling positively influenced the standing stocks and viability of prokaryotes in meso- and bathypelagic waters. The observed vertical connectivity probably arises from the introduction of resources and energy to deep layers by particles, as well as the downward transport of epipelagic cells that colonise them. This is relevant as the viable fraction of the community will be the one with potential to drive organic matter cycling.

v. Humic-like fluorescent dissolved organic matter in meso- and bathypelagic waters was mostly driven by water mass mixing and ageing history. Its association with remineralisation processes included a local influence, as inferred from the relationships between humic-like fluorescence, apparent oxygen utilisation and surface productivity. On the contrary, the distribution of the protein-like fluorescence was dominated by local biogeochemical processes, mostly linked to surface productivity, suggesting a vertical input through sinking particles. Thus, upwelling influenced 1) the input of bioavailable dissolved organic matter into deep layers and 2) through this carbon input, the remineralisation processes in the water masses (as indicated by the imprint of humic-like fluorescence).

vi. The composition of the prokaryotic community in the water masses was linked to the combined effect of local processes, and water mass mixing and history. Community level diversity displayed differences between water masses, and the abundance patterns of specific taxa were explained in varying degrees by the initial properties, ageing and mixing of water masses. The level of explanatory capacity by these factors was overall related to prokaryotic lifestyle. Some taxa known to do well under low carbon availability, like the SAR202 clade, were associated with the deepest water masses. Others, more reactive to changing environmental conditions (e.g., *Alteromonas*), were not explained by the mixing models, and were likely more subject to local processes, although no clear biogeochemical relationships were found. Notably, Nitrosopumilales presented contrasting patterns among its members, suggesting different metabolic strategies within the same order.

vii. In summary, upwelling has far-reaching effects not only on the prokaryotic community dynamics and carbon cycling in the surface waters affected by it (**i–iii**), but its influence propagates down in the water column reaching the bathypelagic realm of the ocean (**iv–vi**). Together, the results presented in this thesis highlight the importance of considering the spatiotemporal coupling of microbial, biogeochemical, and physical processes in upwelling systems. They also emphasise the need of understanding the wider oceanographical context in marine microbiology.

Resumen

Introducción

Los procariotas y la materia orgánica disuelta en los océanos

Se estima que la materia orgánica disuelta (MOD) en ambientes marinos representa cerca de 660 Pg C (1 Pg = 10^{15} g), siendo el mayor reservorio de carbono reducido de los océanos y uno de los mayores de la Tierra (Hansell et al. 2009). Su distribución espacial, sin embargo, no es homogénea ni horizontal ni verticalmente. Las concentraciones de carbono orgánico disuelto (COD) en aguas superficiales varían entre 70-80 μmol · kg^{-1} en latitudes bajas (30°S–30°N), donde el agua está más estratificada, y 40-50 μmol · kg^{-1} en el océano Antártico (Fig. 1a de la introducción). Por el contrario, las aguas profundas muestran concentraciones más bajas que varían a lo largo de la circulación termohalina, desde los 50 μm · kg^{-1} en el Atlántico Norte a los 34 μm · kg^{-1} en el Pacífico Norte (Fig. 1b de la introducción). Esta distribución de la MOD a lo largo y ancho del océano global está controlada en gran medida por los microorganismos unicelulares que lo habitan, los cuales controlan los ciclos biogeoquímicos de los elementos. Entre ellos, los procariotas—un grupo muy diverso taxonómica y funcionalmente que incluye a bacterias y arqueas—juegan un papel de gran importancia dado que producen y consumen MOD, remineralizando una fracción de ella y haciéndola retornar a sus constituyentes inorgánicos.

La materia orgánica disuelta en la red microbiana de la vida

En el océano existen una gran multitud de procesos biológicos que contribuyen a la transferencia de carbono orgánico entre diferentes compartimentos durante el ciclo de este elemento (Fig. 2 de la introducción). La fuente principal de materia orgánica en entornos oceánicos es la producción primaria por parte de los fotoautótrofos unicelulares conocidos como fitoplancton que, a través de la fotosíntesis, fijan CO_2 y lo convierten en carbono orgánico a un ritmo de 100 Pg C · $año^{-1}$ (alrededor de la mitad se pierde por respiración), una cifra de magnitud similar a la de los productores primarios terrestres (Chavez et al. 2011). Aunque la práctica mayoría de la producción primaria se da en forma particulada por la producción de biomasa del fitoplancton, ésta es canalizada a la fracción disuelta a través de una serie de procesos. Cuando su crecimiento se ve limitado—por ejemplo, por la disponibilidad de nutrientes—el fitoplancton libera al ambiente moléculas orgánicas como forma para balancear los requerimientos celulares de carbono y la asimilación fotosintética (Thornton 2014). La pérdida pasiva a través de la membrana celular también contribuye a la liberación de MOD por parte del fitoplancton. Los procariotas son

además capaces de solubilizar las partículas orgánicas que colonizan y, por su parte, el zooplancton, a través de la depredación (pérdidas durante la ingesta de fracciones de las células de fitoplancton o procariotas), egestión (contenidos fecales) y excreción, también libera materia orgánica al medio (Jürgens and Massana 2008; Saba et al. 2011; Steinberg and Landry 2017). Los virus, durante el proceso de infección de las células de los organismos planctónicos, contribuyen igualmente a canalizar la materia orgánica particulada a la MOD (Breitbart et al. 2018).

El bucle microbiano

Toda esta MOD generada es empleada por los procariotas como fuente de carbono y energía (Azam and Malfatti 2007). Consumen O_2 y remineralizan la materia orgánica, generando biomasa que reintroduce así carbono en las redes tróficas marinas, quedando disponible para niveles tróficos superiores a través de la depredación de procariotas por parte de los organismos zooplanctónicos (Stoecker et al. 2017). Esta ruta recibe el nombre de *bucle microbiano* (Azam et al. 1983; Fenchel 2008). La actividad de los procariotas es, por tanto, crucial en el ciclo de la materia orgánica en el océano.

Mientras que la producción primaria y el ciclo de la MOD ocurren de forma desproporcionada en la capa epipelágica de los océanos (0-200 m), los procariotas habitan y son activos en toda la columna de agua. De hecho, los procariotas que se encuentran en las capas mesopelágica (200-1000 m) y batipelágica (1000-4000 m) representan cerca del 75% y 50% de la biomasa y la producción de los procariotas marinos, respectivamente (Arístegui et al. 2009). El carbono es introducido en las capas profundas del océano principalmente por medio del hundimiento de materia orgánica desde la capa superficial. Se estima que este flujo es de unos 5-10 Pg C · año^{-1} (Henson et al. 2011; Siegel et al. 2014; Nowicki et al. 2022). Esta exportación vertical se da por medio de una serie de procesos conocidos colectivamente como la *bomba de carbono biológica* (Boyd et al. 2019). Dichos procesos pueden agruparse en tres rutas principales: el flujo gravitacional, el flujo de mezcla y el flujo de la migración activa (Le Moigne 2019). El flujo gravitacional se refiere al hundimiento de partículas orgánicas (pellets fecales, agregados de exopolímeros, células muertas, etc.) (Turner 2015; Mari et al. 2017) y se ha estimado que, junto al flujo de mezcla, es el de mayor relevancia a nivel global (Stukel et al. 2022).

La habilidad de los procariotas para transformar, consumir y remineralizar la MOD es, sin embargo, relativamente limitada, resultando en su acumulación de forma

variable en diferentes ambientes oceánicos. Existen dos principales hipótesis para explicar esta persistencia (Fig. 3 de la introducción). Históricamente, la explicación preponderante era que los compuestos orgánicos que forman el MOD tienen niveles variables de labilidad—es decir, la facilidad con la que son degradados por los procariotas—dependiendo de su estructura química (Dittmar et al. 2021). Algunas de ellas serían difíciles de degradar y, por tanto, se acumularían. Por el contrario, una hipótesis más reciente postula que toda la MOD es transformada continuamente y que la resistencia a la degradación es sólo un propiedad emergente de las interacciones ecológicas entre microorganismos y moléculas (Mentges et al. 2019). La estabilización ocurriría a través del equilibrio entre las tasas de consumo y las concentraciones de las moléculas individuales: a medida que un tipo de molécula concreta (parte de una red compleja de MOD) es consumida y su concentración disminuye, se reducen también sus tasas de consumo por parte de los procariotas, resultando en un equilibrio a largo plazo. Esta tendencia al equilibrio, sin embargo, se vería alterada por eventos externos (proliferaciones de fitoplancton, partículas que se hunden), dando lugar a una red de interacciones en cambio perpetuo.

Rastreando la transformación de la materia orgánica disuelta

La MOD, formada posiblemente por millones de compuestos individuales, es una de las mezclas más complejas y diversas de la naturaleza (Zark et al. 2017; Dittmar et al. 2021). Las técnicas espectroscópicas ofrecen un manera relativamente simple de obtener información sobre la composición general de la MOD y se ha demostrado que son herramientas útiles para trazar los procesos que la transforman (Nelson and Siegel 2013). Existen dos subconjuntos anidados de MOD en base a las propiedades ópticas que exhiben (Fig. 4 de la introducción). La MOD cromofórica (MODC) es la fracción de la MOD que absorbe radiación solar de las bandas ultravioleta y visible (Fig. 5 de la introducción). Es omnipresente es los ambientes marinos y representa el factor más importante en el control de la penetración de la luz en el agua de mar (Nelson and Siegel 2013). La transformación microbiana de la MOD modifica la cantidad y las características espectrales de la MODC durante el envejecimiento de las masas de agua, un proceso de relevancia para los ciclos biogeoquímicos globales (Catalá et al. 2015, 2018).

Parte de la MODC es excitada por la radiación ultravioleta que absorbe y en consecuencia emite fluorescencia. Esta parte de la MOD recibe el nombre de MOD fluorescente (MODF). Determinar los diferentes componentes de la fluorescencia emitida por la MODF en un ambiente oceánico sirve para obtener información

general sobre su composición (Stedmon et al. 2003). Usualmente suelen identificarse componentes que se agrupan en dos categorías principales: la fluorescencia de características húmicas y la de características proteicas (o de aminoácidos) (Fig. 6 de la introducción). La de características proteicas suele asociarse a la producción primaria y tiende a ser consumida por los procariotas (Coble et al. 1998; Lønborg et al. 2010). La producción de MODF de características húmicas por el contrario se asocia a la transformación microbiana de la MOD (Jørgensen et al. 2011; Martínez–Pérez et al. 2019). Juntas, la MODC y MODF proveen una valiosa información para ayudar a rastrear la transformación microbiana de la MOD en el océano.

Diversidad procariota

El océano es habitado por un número de procariotas del orden de ~10^{29} (Whitman et al., 1998). Esta extraordinaria cantidad de microorganismos conforma un conjunto extremadamente diverso en términos de taxonomía, capacidades metabólicas y actividad (Acinas et al., 2021; Louca et al., 2016; Munson-McGee et al., 2022; Sunagawa et al., 2015). Pese a que el papel de las bacterias en ambientes marinos comenzó a reconocerse en la década de 1970, siendo realmente apreciado en la de 1980 (Azam et al., 1983; Fenchel, 2008), se desconocía incluso que las arqueas habitasen en el océano hasta la década de 1990. Originalmente consideradas organismos extremófilos, hoy en día se sabe que las arqueas pueblan, junto con las bacteria, todos los ambientes oceánicos, cumpliendo funciones fundamentales en los ciclos biogeoquímicos (Santoro et al., 2019).

Gracias a su gran diversidad, los procariotas muestran una extensa variedad de estrategias ecológicas. Por ejemplo, las aguas oligotróficas están dominadas por taxones altamente eficientes en condiciones de baja disponibilidad de nutrientes. De entre los especialistas oligotróficos destacan las bacterias SAR11 (también conocidas como *Pelagibacterales*), que dominan en términos numéricos las comunidades de las regiones oceánicas con bajas concentraciones de nutrientes(Giovannoni 2017). En claro contraste con ellas, los taxones copiótrofos triunfan en ambientes con altas concentraciones de materia orgánica típicos de aguas altamente productivas donde hay proliferaciones masivas de fitoplancton o los microambientes ricos en nutrientes que forman las partículas orgánicas (Buchan et al. 2014). Los procariotas copiótrofos incluyen a órdenes como Flavobacteriales, Rhodobacterales y Enterobacterales (*Alteromonas*, *Vibrio*) (Teeling et al. 2016; Pontiller et al. 2022).

Pese a que con la profundidad disminuyen las abundancias y actividades de los procariotas (Arístegui et al. 2009), cambiando su composición y capacidades metabólicas (DeLong et al. 2006; Herndl et al. 2023), las comunidades que habitan las diferentes partes de la columna de agua no están aisladas. El flujo gravitacional de partículas actúa como vector conectando comunidades espacialmente distantes. Esto se debe a que, además de proveer materia orgánica a las comunidades profundas—influenciando sus abundancias y, de forma variable, su actividad (Hansell and Ducklow 2003; Yokokawa et al. 2013)—, las partículas también transportan a los procariotas que las colonizan, generando una conectividad vertical que une comunidades superficiales y profundas (Mestre et al. 2018; Ruiz-González et al. 2020).

Sistemas de afloramiento: focos de productividad primaria

De forma general, un afloramiento se define como el transporte hacia la superficie de un volumen de agua sostenido en el tiempo (al menos varios días) y a lo largo de una distancia suficientemente larga (al menos unos 100 m) (Kämpf and Chapman 2016). En el océano, el proceso más importante—en términos de relevancia global—que genera afloramiento es el gobernado por el viento en los límites orientales de los océanos, donde se da lugar a sistemas de afloramiento altamente productivos. Este tipo de afloramiento es producido por el efecto combinado de la fricción del viento en el límite océano-atmósfera y el efecto de Coriolis (creado por la rotación de la Tierra) (Kämpf and Chapman 2016). Cuando el viento sopla paralelo a la costa, el resultado de esta combinación es el transporte de las aguas superficiales desde costa hacia mar abierto, para ser éstas sustituidas por aguas subsuperficiales ricas en nutrientes (Fig. 7 de la introducción). Ello genera ecosistemas con una alta productividad primaria (Carr and Kearns 2003).

En consecuencia, los sistemas de afloramiento son de gran relevancia biogeoquímica. El fitoplancton fija grandes cantidades de CO_2 (Loucaides et al. 2012) y la materia orgánica producida es transportada tanto horizontalmente por medio de procesos de mesoescala (Santana-Falcón et al. 2016; Amos et al. 2019), como verticalmente a través del hundimiento de partículas (Hebbeln et al. 2000; Fischer et al. 2020). Dicha materia orgánica es consumida y remineralizada por los procariotas, tanto la que se encuentra en superficie como aquélla exportada a capas profundas. Es por ello que el bucle microbiano juega un papel fundamental en la biogeoquímica de los entornos de afloramiento, siendo importante profundizar nuestro conocimiento sobre los procariotas y la materia orgánica en estos sistemas.

Objetivos

El objetivo general de la tesis es estudiar la relación entre la distribución y las dinámicas de la materia orgánica y las comunidades procariotas en ambientes de afloramiento en contraste con zonas oligotróficas. Dada la importante influencia que tiene el afloramiento de aguas profundas en los procesos biogeoquímicos marinos, entre nuestras metas se encuentra abordar no sólo sus efectos sobre su entorno inmediato, sino explorar también si su influencia se propaga a lo largo de la columna de agua, alcanzando a las comunidades procariotas del océano profundo. Para ello, planteamos tres interrogantes principales:

1. ¿Cómo influye el afloramiento de aguas profundas ricas en nutrientes la dinámica de la materia orgánica disuelta de las aguas superficiales?

2. ¿Qué cambios se observan en las comunidades procariotas superficiales tras las proliferaciones masivas de fitoplancton inducidas por episodios de afloramiento, y cómo se relacionan éstos con la materia orgánica disuelta?

3. ¿Influye el aumento de productividad superficial generado por episodios de afloramiento a las comunidades de procariotas y la materia orgánica disuelta más allá de la capa epipelágica?

Hemos tratado de dar respuesta a estas preguntas a lo largo de cuatro capítulos, combinando enfoques experimentales con el análisis de muestreos de campo a gran escala. La primera pregunta se trata en el **Capítulo 1**, en el cual se describen los cambios observados en la materia orgánica disuelta durante un experimento de simulación de afloramiento de aguas profundas llevado a cabo en las aguas oligotróficas de las Islas Canarias, en el Atlántico subtropical nororiental. Simulando diferentes combinaciones de intensidad y modo de afloramiento (un único pulso de afloramiento frente a afloramiento sostenido), evaluamos cómo se ven alteradas las concentraciones y las características de la materia orgánica disuelta bajo diversas condiciones de afloramiento. Por su parte, el **Capítulo 2** se centra en la segunda pregunta, estudiando cómo se comportan las comunidades procariotas bajo el mismo abanico de condiciones de afloramiento estudiado en el capítulo anterior. En él se analizan las sucesiones de procariotas que ocurren en el seno de las comunidades y su relación con los cambios observados en la materia orgánica.

Los otros dos capítulos acometen la tercera y última pregunta, examinando la conectividad vertical de las comunidades procariotas en aguas bajo la influencia de un sistema de afloramiento. Dado que la conectividad vertical está mediada por el flujo

de materia orgánica en la columna de agua, es esperable que las aguas superficiales con productividad más alta—tales como los sistemas de afloramiento—ejerzan una influencia mayor en los procariotas que habitan debajo de ellas que las aguas superficiales oligotróficas. Para abordar esta hipótesis, analizamos muestras recogidas durante una campaña oceanográfica que cruzó el océano Atlántico tropical y subtropical a lo largo de una gradiente de productividad superficial, desde Brasil a las Islas Canarias, incluyendo un área bajo la influencia del sistema de afloramiento del África Noroccidental. En el **Capítulo 3**, estudiamos la biomasa, las tasas metabólicas y el estado fisiológico de los procariotas en toda la columna de agua, analizando qué relación guardan estas variables con la productividad superficial. Por último, el **Capítulo 4** se centra exclusivamente en la zona afótica del océano, donde investigamos la composición taxonómica de las comunidades procariotas junto con las propiedades ópticas de la materia orgánica disuelta en las masas de agua del océano Atlántico, ya que éstas masas de agua se consideran islas geográficas con condiciones ambientales distintas que pueden dar lugar a comunidades distintas de procariotas. En el capítulo analizamos la contribución a la variabilidad en la MOD y la distribución de procariotas de dos factores contrapuestos: procesos biogeoquímicos locales (que incluyen la conectividad vertical), y la mezcla y envejecimiento de las masas de aguas a lo largo de su circulación a gran escala.

Síntesis de resultados y conclusiones

Capítulo 1 – *La importancia de la materia orgánica disuelta en el secuestro de carbono en experimentos de afloramiento artificial*

En el contexto del cambio climático, el afloramiento artificial de aguas profundas ha sido planteado como un posible método para incrementar la bomba biológica de carbono en regiones oceánicas oligotróficas y así aumentar el secuestro de carbono. Para investigar el potencial de esta propuesta, dentro del proyecto OceanArtUp se realizó un experimento de simulación de afloramiento de aguas profundas en la isla de Gran Canaria en otoño de 2018. En el **Capítulo 1** examinamos el efecto de diferentes intensidades y modos de afloramiento (un único pulso frente a pulsos recurrentes, resultando en 8 combinaciones distintas) sobre las dinámicas de la MOD. Para ello introdujimos aguas profundas ricas en nutrientes a mesocosmos de gran escala (44 m^3) ubicados en las aguas oligotróficas subtropicales del Atlántico nororiental. Este afloramiento artificial produjo proliferaciones masivas de fitoplancton en ambos modos, pero con desarrollos opuestos: el pulso único de afloramiento provocó

grandes proliferaciones con un único pico, que decayó rápidamente al agotarse los nutrientes, mientras que los pulsos recurrentes generaron proliferaciones menores pero sostenidas en el tiempo. En paralelo, se dieron marcados aumentos en las concentraciones de MOD, así como cambios en sus características. La magnitud de los cambios estuvo positivamente relacionada con la intensidad del afloramiento: los tratamientos de mayor intensidad resultaron en mayores acumulaciones de COD (+70 μM respecto a niveles ambientales en el caso de los tratamientos más intensos), un contenido relativo de carbono más elevado, y cambios más pronunciados en las propiedades ópticas de la MOD (mayores niveles de MODC y MODF de características húmicas). Por su parte, también se observaron ciertas diferencias entre los dos modos de afloramiento: el pulso singular resultó en cantidades superiores de MODC, con índices que sugieren un mayor peso molecular promedio. Las alteraciones observadas en las propiedades ópticas de la MOD han sido asociadas a su transformación por parte de la comunidad de procariotas. A pesar de ello, durante la duración del experimento (aproximadamente 6 semanas), no se observaron claras disminuciones en las acumulaciones de materia orgánica. Esta persistencia podría deberse a la combinación de diversos factores, entre los que se incluyen 1) la diversificación molecular fruto de la trasformación por parte de los procariotas que reduce las tasas de degradación, 2) limitación por nutrientes, y 3) inadecuación de las capacidades metabólicas de los procariotas. En conjunto, los resultados presentados en el **Capítulo 1** evidencian que, a pesar de las diferencias entre los modos de afloramiento y sus correspondientes proliferaciones masivas de fitoplancton, éstos generaron efectos similares en cuanto a la concentración, estequiometría y propiedades ópticas de la MOD producida. Todo ello, y en especial la persistencia observada, son de relevancia a la hora de estudiar el destino (secuestro frente a remineralización) del carbono orgánico asociado al afloramiento de aguas profundas.

Capítulo 2 – *Los patrones de sucesión de los procariotas son consistentes bajo condiciones variables de afloramiento simulado*

Los procariotas heterotróficos controlan en buena medida el procesamiento de la MOD en los océanos y se ha observado que siguen sucesiones mediadas por los sustratos orgánicos durante el desarrollo de las floraciones masivas de fitoplancton. Sin embargo, nuestra compresión de las sucesiones de procariotas durante eventos de afloramiento de intensidad y duración temporal variables es más limitada. Es por ello por lo que, en paralelo al estudio de la MOD presentado en el **Capítulo 1**, analizamos los cambios en la biomasa, actividad y composición taxonómica de las

comunidades procariotas bajo las mismas condiciones de afloramiento (intensidad y modo). Las abundancias celulares de los procariotas guardaron una relación positiva con la intensidad de afloramiento y presentaron tres picos principales en todos los tratamientos experimentales, pese a las marcadamente diferentes dinámicas que mostraron las proliferaciones masivas de fitoplancton. Los patrones de sucesión en la composición de las comunidades procariotas identificados mediante un análisis de *clustering* fueron sorprendentemente similares independientemente de la intensidad y modo de afloramiento, observándose 4 o 5 grupos de procariotas que proliferaron de forma secuencial. Los resultados fueron similares para las dos fracciones de tamaño analizadas, la de vida libre y la asociada a partículas. A pesar de la similitud en los patrones de sucesión, los taxones dominantes dentro de cada grupo difirieron entre las dos fracciones de tamaño y, en menor medida, entre modos de afloramiento. Durante la acumulación de MOD asociada a las proliferaciones masivas de fitoplancton, miembros de órdenes tales como Flavobacteriales, Rhodobacterales y Enterobacterales estuvieron presentes en todos los tratamientos, procariotas que son reconocidos copiótrofos. De forma reseñable, hubo marcadas diferencias en el nivel de actividad de los procariotas entre los modos de afloramiento: en el afloramiento de un único pulso, la actividad creció hasta alcanzar su pico tras el colapso de la proliferación masiva de fitoplancton para después reducirse a niveles cercanos a cero, mientras que en el afloramiento recurrente no se alcanzó un pico tan alto pero la actividad fue más sostenida en el tiempo. Los resultados del **Capítulo 2** muestran por tanto que, a pesar de las diferencias en las proliferaciones de fitoplancton, las dinámicas de sucesión de procariotas son marcadamente reproducibles bajo condiciones variables de intensidad y modo durante la simulación de eventos de afloramiento de aguas profundas.

Capítulo 3 – *Los gradientes de productividad superficial gobiernan los cambios en la viabilidad de los procariotas del océano profundo a lo largo del Atlántico tropical y subtropical*

Más allá del efecto directo que ejercen los eventos de afloramiento sobre las comunidades de procariotas en la superficie oceánica, en la segunda mitad de esta tesis se ha estudiado la influencia indirecta que el afloramiento puede llegar a tener en las comunidades de las capas profundas del océano. Para ello, analizamos la biomasa, el estado fisiológico (como viabilidad, una medida del estado de la membrana celular) y la actividad de los procariotas en perfiles verticales (0–3500 m) a lo largo de una sección oceanográfica en el Atlántico tropical y subtropical. Dado que la sección

atravesó un gradiente de productividad—desde Brasil a las Islas Canarias, pasando por la zona bajo la influencia del sistema de afloramiento del África Noroccidental—ésto nos posibilitó evaluar si existía una relación entre los niveles de productividad superficial y las variables medidas en las aguas epi- (0–200 m), meso- (200–1000 m) y batipelágicas (1000–3500 m). Los resultados obtenidos muestran que las variables citométricas estaban relacionadas con la productividad superficial: existía una mayor abundancia y viabilidad celular, y menor tamaño, bajo aguas superficiales de productividad más alta. Esta relación fue significativa incluso en aguas batipelágicas. La actividad, medida como incorporación de leucina, no mostró ninguna relación, o incluso fue negativa en el caso de las tasas específicas por célula viable en el batipelágico. Este resultado puede deberse a cambios en la asignación de recursos y energía a procesos de mantenimiento frente a crecimiento en ambientes desfavorables y necesidades celulares dependientes del tamaño celular. La conectividad vertical evidenciada por las variables citométricas vendría dada por la introducción de compuestos orgánicos por las partículas que se hunden desde la capa superficial, así como por la introducción a través de ellas de células epipelágicas que las colonizan. El **Capítulo 3** se suma a hallazgos recientes que subrayan la importancia de la conectividad vertical para las comunidades procariotas del océano profundo y muestra por primera vez una marcada influencia de las condiciones superficiales en la viabilidad de los procariotas de aguas profundas. Dado que son las células viables, es decir, sanas, aquéllas que llevan a cabo los procesos metabólicos dentro de la comunidad, estos resultados son relevantes a la hora de estudiar los ciclos biogeoquímicos en el océano profundo.

Capítulo 4 – *Los procariotas y la materia orgánica disuelta fluorescente del océano profundo reflejan la historia de las masas de agua del océano Atlántico*

Si bien las dinámicas asociadas a las comunidades procariotas y la MOD han sido estudiadas de forma extensa en diversos ambientes del océano superficial, el conocimiento de lo que se da en aguas profundas es más limitado. Para poder ampliar nuestros conocimientos sobre ello, analizamos la composición de las comunidades procariotas y la MODF en las masas de agua a lo largo de la misma sección estudiada en el **Capítulo 3**. Dado que, tal y como se menciona en la introducción, las masas de agua pueden actuar como islas geográficas con propiedades biogeoquímicas distintas a las aguas circundantes, este capítulo tiene como fin tratar de discernir el efecto de estas masas de agua de la influencia de la productividad superficial. Un análisis de factores paralelos para el estudio de la composición de la MODF identificó cuatro

componentes: tres de características húmicas (típicamente asociados a la transformación y remineralización de la materia orgánica por parte de los procariotas) y uno de características proteicas (que tiende a ser consumido con facilidad por los procariotas). A través un análisis multiparamétrico de las masas de agua se determinó que las distribuciones de los componentes húmicos estaban gobernadas de forma significativa por la mezcla de las masas de agua, la utilización aparente de oxígeno y la productividad superficial. Esto indica que los componentes húmicos estaban relacionados con el proceso de mezcla y de envejecimiento de las masas de agua a gran escala, pero también por procesos de remineralización a escala local ligados al transporte vertical de materia orgánica en áreas de alta productividad bajo la influencia del afloramiento. La distribución del componente proteico por su parte estaba explicada en menor medida por la mezcla de masas de agua y más dominada por la productividad superficial, sugiriendo una marcada influencia del transporte vertical por las partículas que se hunden. Así, evidenciamos que el afloramiento influencia 1) la introducción de MOD biodisponible a las capas profundas del océano, y 2) la remineralización de la MOD en las masas de agua. A su vez, la composición de las comunidades de procariotas también mostró estar controlada tanto por la mezcla y la historia de las masas de agua a gran escala como por factores intrarregionales. Por lo general existió una relación entre el grado en el que estos factores explicaban la distribución de los diferentes taxones y el estilo de vida de cada uno de ellos. Por ejemplo, la distribución de grupos como SAR202—que se desarrollan bien en ambientes con fuentes limitadas de carbono—estaban dominados por la mezcla e historia de las masas de agua, estando asociados a las más profundas (Agua Profunda del Atlántico Norte). Por el contrario, procariotas como *Alteromonas*, conocidas por reaccionar a cambios ambientales (por ejemplo, la introducción de carbono lábil), estaban más controladas por factores intrarregionales. Sin embargo, dado que no pudimos identificar ningún vínculo claro con variables biogeoquímicas específicas, los procesos concretos que controlan su distribución son una incógnita. De forma notable, se observaron grupos donde había tendencias opuestas: Nitrosopumilales mostró dos subgrupos de taxones con patrones de variabilidad opuestos en relación a la mezcla y la historia de las masas de agua, uno asociados a masas profundas (Agua Profunda del Atlántico Norte) y otro intermedias (Agua Modal Subpolar), sugiriendo estrategias metabólicas diferentes dentro de un mismo orden.

Conclusión final

El afloramiento de aguas profundas tiene efectos de gran relevancia no sólo en las dinámicas de las comunidades procariotas y el ciclo del carbono en las aguas superficiales afectadas directamente por él (**Capítulos 1** y **2**), sino que su influencia se propaga hacia abajo en la columna de agua y alcanza incluso la capa batipelágica del océano (**Capítulos 3** y **4**). Ello ocurre tanto en áreas donde se dan procesos de afloramiento como en aquéllas adyacentes que se encuentran bajo su influencia por medio de la advección horizontal de aguas altamente productivas. En conjunto, los resultados de esta tesis resaltan la importancia de tener en consideración las escalas espaciotemporales existentes en los procesos microbianos, biogeoquímicos y físicos en los sistemas de afloramiento. Asimismo, dejan claro que es necesario estudiar el contexto oceanográfico general para poder ahondar en nuestra compresión de la microbiología marina.

Referencias

Amos, C. M., R. M. Castelao, and P. M. Medeiros. 2019. Offshore transport of particulate organic carbon in the California Current System by mesoscale eddies. Nat. Commun. **10**: 4940. doi:10.1038/s41467-019-12783-5

Arístegui, J., J. M. Gasol, C. M. Duarte, and G. J. Herndl. 2009. Microbial oceanography of the dark ocean's pelagic realm. Limnol. Oceanogr. **54**: 1501–1529. doi:10.4319/lo.2009.54.5.1501

Azam, F., T. Fenchel, J. Field, J. Gray, L. Meyer-Reil, and F. Thingstad. 1983. The Ecological Role of Water-Column Microbes in the Sea. Mar. Ecol. Prog. Ser. **10**: 257–263. doi:10.3354/meps010257

Azam, F., and F. Malfatti. 2007. Microbial structuring of marine ecosystems. Nat. Rev. Microbiol. **5**: 782–791. doi:10.1038/nrmicro1747

Boyd, P. W., H. Claustre, M. Levy, D. A. Siegel, and T. Weber. 2019. Multi-faceted particle pumps drive carbon sequestration in the ocean. Nature **568**: 327–335. doi:10.1038/s41586-019-1098-2

Breitbart, M., C. Bonnain, K. Malki, and N. A. Sawaya. 2018. Phage puppet masters of the marine microbial realm. Nat. Microbiol. **3**: 754–766. doi:10.1038/s41564-018-0166-y

Buchan, A., G. R. LeCleir, C. A. Gulvik, and J. M. González. 2014. Master recyclers: features and functions of bacteria associated with phytoplankton blooms. Nat. Rev. Microbiol. **12**: 686–698. doi:10.1038/nrmicro3326

Carr, M. E., and E. J. Kearns. 2003. Production regimes in four Eastern Boundary Current systems. Deep-Sea Res. Part II Top. Stud. Oceanogr. **50**: 3199–3221. doi:10.1016/j.dsr2.2003.07.015

Catalá, T. S., A. M. Martínez-Pérez, M. Nieto-Cid, and others. 2018. Dissolved Organic Matter (DOM) in the open Mediterranean Sea. I. Basin–wide distribution and drivers of chromophoric DOM.

Prog. Oceanogr. **165**: 35–51. doi:10.1016/j.pocean.2018.05.002

Catalá, T. S., I. Reche, M. Álvarez, and others. 2015. Water mass age and aging driving chromophoric dissolved organic matter in the dark global ocean. Global Biogeochem. Cycles **29**: 917–934. doi:10.1002/2014GB005048

Chavez, F. P., M. Messié, and J. T. Pennington. 2011. Marine Primary Production in Relation to Climate Variability and Change. Ann. Rev. Mar. Sci. **3**: 227–260. doi:10.1146/annurev.marine.010908.163917

Coble, P. G., C. E. Del Castillo, and B. Avril. 1998. Distribution and optical properties of CDOM in the Arabian Sea during the 1995 Southwest Monsoon. Deep Sea Res. Part II Top. Stud. Oceanogr. **45**: 2195–2223. doi:10.1016/S0967-0645(98)00068-X

DeLong, E. F., C. M. Preston, T. Mincer, and others. 2006. Community genomics among stratified microbial assemblages in the ocean's interior. Science (80-.). **311**: 496–503. doi:10.1126/science.1120250

Dittmar, T., S. T. Lennartz, H. Buck-Wiese, D. A. Hansell, C. Santinelli, C. Vanni, B. Blasius, and J.-H. Hehemann. 2021. Enigmatic persistence of dissolved organic matter in the ocean. Nat. Rev. Earth Environ. **2**: 570–583. doi:10.1038/s43017-021-00183-7

Dittmar, T., and A. Stubbins. 2014. 12.6 - Dissolved Organic Matter in Aquatic Systems, p. 125–156. *In* H.D. Holland and K.K.B.T.-T. on G. (Second E. Turekian [eds.], Treatise on Geochemistry. Elsevier.

Fenchel, T. 2008. The microbial loop – 25 years later. J. Exp. Mar. Bio. Ecol. **366**: 99–103. doi:10.1016/j.jembe.2008.07.013

Fischer, G., S. Neuer, S. Ramondenc, and others. 2020. Long-Term Changes of Particle Flux in the Canary Basin Between 1991 and 2009 and Comparison to Sediment Trap Records Off Mauritania. Front. Earth Sci. **8**: 280. doi:10.3389/feart.2020.00280

Giovannoni, S. J. 2017. SAR11 Bacteria: The Most Abundant Plankton in the Oceans. Ann. Rev. Mar. Sci. **9**: 231–255. doi:10.1146/annurev-marine-010814-015934

Hansell, D. A., C. A. Carlson, D. J. Repeta, and R. Schlitzer. 2009. Dissolved organic matter in the ocean: A controversy stimulates new insights. Oceanography **22**: 202–211.

Hansell, D. A., and H. W. Ducklow. 2003. Bacterioplankton distribution and production in the bathypelagic ocean: Directly coupled to particulate organic carbon export?,. Limnol. Oceanogr. **48**: 150–156. doi:10.4319/lo.2003.48.1.0150

Hebbeln, D., M. Marchant, and G. Wefer. 2000. Seasonal variations of the particle flux in the Peru-Chile current at 30 °S under "normal" and El Nino conditions. Deep-Sea Res. Part II Top. Stud. Oceanogr. **47**: 2101–2128. doi:10.1016/S0967-0645(00)00018-7

Henson, S. A., R. Sanders, E. Madsen, P. J. Morris, F. Le Moigne, and G. D. Quartly. 2011. A reduced estimate of the strength of the ocean's biological carbon pump. Geophys. Res. Lett. **38**. doi:10.1029/2011GL046735

Herndl, G. J., B. Bayer, F. Baltar, and T. Reinthaler. 2023. Prokaryotic Life in the Deep Ocean's Water Column. Ann. Rev. Mar. Sci. **15**. doi:10.1146/annurev-marine-032122-115655

Jørgensen, L., C. A. Stedmon, T. Kragh, S. Markager, M. Middelboe, and M. Søndergaard. 2011. Global trends in the fluorescence characteristics and distribution of marine dissolved organic matter. Mar. Chem. **126**: 139–148. doi:10.1016/j.marchem.2011.05.002

Jürgens, K., and R. Massana. 2008. Protistan Grazing on Marine Bacterioplankton, p. 383–441. *In* Microbial Ecology of the Oceans.

Kämpf, J., and P. Chapman. 2016. Upwelling Systems of the World, 1st ed. Springer Cham.

Lønborg, C., X. A. Álvarez-Salgado, K. Davidson, S. Martínez-García, and E. Teira. 2010. Assessing the microbial bioavailability and degradation rate constants of dissolved organic matter by fluorescence spectroscopy in the coastal upwelling system of the Ría de Vigo. Mar. Chem. **119**: 121–129. doi:10.1016/j.marchem.2010.02.001

Loucaides, S., T. Tyrrell, E. P. Achterberg, and others. 2012. Biological and physical forcing of carbonate chemistry in an upwelling filament off northwest Africa: Results from a Lagrangian study. Global Biogeochem. Cycles **26**. doi:10.1029/2011GB004216

Mari, X., U. Passow, C. Migon, A. B. Burd, and L. Legendre. 2017. Transparent exopolymer particles: Effects on carbon cycling in the ocean. Prog. Oceanogr. **151**: 13–37. doi:10.1016/j.pocean.2016.11.002

Martínez–Pérez, A. M., T. S. Catalá, M. Nieto–Cid, and others. 2019. Dissolved organic matter (DOM) in the open Mediterranean Sea. II: Basin–wide distribution and drivers of fluorescent DOM. Prog. Oceanogr. **170**: 93–106. doi:10.1016/j.pocean.2018.10.019

Mentges, A., C. Feenders, C. Deutsch, B. Blasius, and T. Dittmar. 2019. Long-term stability of marine dissolved organic carbon emerges from a neutral network of compounds and microbes. Sci. Rep. **9**: 17780. doi:10.1038/s41598-019-54290-z

Mestre, M., C. Ruiz-González, R. Logares, C. M. Duarte, J. M. Gasol, and M. M. Sala. 2018. Sinking particles promote vertical connectivity in the ocean microbiome. Proc. Natl. Acad. Sci. U. S. A. **115**: E6799–E6807. doi:10.1073/pnas.1802470115

Le Moigne, F. A. C. 2019. Pathways of Organic Carbon Downward Transport by the Oceanic Biological Carbon Pump. Front. Mar. Sci. **6**: 634. doi:10.3389/fmars.2019.00634

Nelson, N. B., and D. A. Siegel. 2013. The Global Distribution and Dynamics of Chromophoric Dissolved Organic Matter. Ann. Rev. Mar. Sci. **5**: 447–476. doi:10.1146/annurev-marine-120710-100751

Nowicki, M., T. DeVries, and D. A. Siegel. 2022. Quantifying the Carbon Export and Sequestration Pathways of the Ocean's Biological Carbon Pump. Global Biogeochem. Cycles **36**: e2021GB007083. doi:10.1029/2021GB007083

Pontiller, B., S. Martínez-García, V. Joglar, and others. 2022. Rapid bacterioplankton transcription cascades regulate organic matter utilization during phytoplankton bloom progression in a coastal upwelling system. ISME J. **16**: 2360–2372. doi:10.1038/s41396-022-01273-0

Ruiz-González, C., M. Mestre, M. Estrada, and others. 2020. Major imprint of surface plankton on deep ocean prokaryotic structure and activity. Mol. Ecol. **29**: 1820–1838. doi:10.1111/mec.15454

Saba, G. K., D. K. Steinberg, and D. A. Bronk. 2011. The relative importance of sloppy feeding, excretion, and fecal pellet leaching in the release of dissolved carbon and nitrogen by Acartia tonsa copepods. J. Exp. Mar. Bio. Ecol. **404**: 47–56. doi:10.1016/j.jembe.2011.04.013

Santana-Falcón, Y., M. Benavides, P. Sangrà, E. Mason, E. D. Barton, A. Orbi, and J. Arístegui. 2016. Coastal–offshore exchange of organic matter across the Cape Ghir filament (NW Africa) during moderate upwelling. J. Mar. Syst. **154**: 233–242. doi:10.1016/j.jmarsys.2015.10.008

Siegel, D. A., K. O. Buesseler, S. C. Doney, S. F. Sailley, M. J. Behrenfeld, and P. W. Boyd. 2014. Global

assessment of ocean carbon export by combining satellite observations and food-web models. Global Biogeochem. Cycles **28**: 181–196. doi:10.1002/2013GB004743

Stedmon, C. A., S. Markager, and R. Bro. 2003. Tracing dissolved organic matter in aquatic environments using a new approach to fluorescence spectroscopy. Mar. Chem. **82**: 239–254. doi:10.1016/S0304-4203(03)00072-0

Steinberg, D. K., and M. R. Landry. 2017. Zooplankton and the Ocean Carbon Cycle. Ann. Rev. Mar. Sci. **9**: 413–444. doi:10.1146/annurev-marine-010814-015924

Stoecker, D. K., P. J. Hansen, D. A. Caron, and A. Mitra. 2017. Mixotrophy in the Marine Plankton. Ann. Rev. Mar. Sci. **9**: 311–335. doi:10.1146/annurev-marine-010816-060617

Stukel, M. R., M. Décima, and M. R. Landry. 2022. Quantifying biological carbon pump pathways with a data-constrained mechanistic model ensemble approach. Biogeosciences **19**: 3595–3624. doi:10.5194/bg-19-3595-2022

Teeling, H., B. M. Fuchs, C. M. Bennke, and others. 2016. Recurring patterns in bacterioplankton dynamics during coastal spring algae blooms A.A. Brakhage [ed.]. Elife **5**: e11888. doi:10.7554/eLife.11888

Thornton, D. C. O. 2014. Dissolved organic matter (DOM) release by phytoplankton in the contemporary and future ocean. Eur. J. Phycol. **49**: 20–46. doi:10.1080/09670262.2013.875596

Turner, J. T. 2015. Zooplankton fecal pellets, marine snow, phytodetritus and the ocean's biological pump. Prog. Oceanogr. **130**: 205–248. doi:10.1016/j.pocean.2014.08.005

Yokokawa, T., Y. Yang, C. Motegi, and T. Nagata. 2013. Large-scale geographical variation in prokaryotic abundance and production in meso- and bathypelagic zones of the central Pacific and Southern Ocean. Limnol. Oceanogr. **58**: 61–73. doi:10.4319/lo.2013.58.1.0061

Zark, M., J. Christoffers, and T. Dittmar. 2017. Molecular properties of deep-sea dissolved organic matter are predictable by the central limit theorem: Evidence from tandem FT-ICR-MS. Mar. Chem. **191**: 9–15. doi:10.1016/j.marchem.2017.02.005

Data availability

The datasets produced during this thesis can be found online in public repositories. Details on where to find each of them are listed below:

Chapter 1

The dataset from Chapter 1 is deposited in the PANGAEA repository (pangaea.de) under accession number 946776 (Gómez-Letona et al. 2022g).

Chapter 2

The datasets from Chapter 2 have not been published yet.

Chapter 3

The datasets from Chapter 3 are deposited in the PANGAEA repository under accession numbers 943414 (discrete data) and 943416 (integrated values) (Gómez-Letona et al. 2022d; e; f).

Chapter 4

The datasets from Chapter 4 are deposited in two separate repositories. The full biogeochemical dataset and the partial biogeochemical dataset (samples below the mixed layer; includes OMP results) are deposited in the PANGAEA repository under accession numbers 942940 and 942934, respectively (Gómez-Letona et al. 2022a; b; c). The 16S rRNA gene sequencing raw dataset is deposited in the European Nucleotide Archive (ENA) at EMBL-EBI (ebi.ac.uk/ena) under accession number PRJEB44713.

The list of detailed references is available in the next page.

References

Gómez-Letona, M., J. Arístegui, N. Hernández-Hernández, and others. 2022a. Biogeochemical variables and optimum multiparameter analysis results from the tropical and subtropical Atlantic of the MAFIA cruise in 2015. PANGAEA. doi:10.1594/PANGAEA.942934

Gómez-Letona, M., J. Arístegui, N. Hernández-Hernández, and others. 2022b. Biogeochemical variables including mixed layer samples from the tropical and subtropical Atlantic of the MAFIA cruise in 2015. PANGAEA. doi:10.1594/PANGAEA.942940

Gómez-Letona, M., J. Arístegui, N. Hernández-Hernández, and others. 2022c. Fluorescent dissolved organic matter and water mass distribution in the tropical and subtropical Atlantic in 2015. PANGAEA. doi:10.1594/PANGAEA.942941

Gómez-Letona, M., J. Arístegui, N. Hernández-Hernández, M. Pérez-Lorenzo, X. A. Alvarez-Salgado, E. Teira, and M. Sebastian. 2022d. Abundance, cell volume, biomass, viability and leucine incorporation rates of prokaryotes from the MAFIA cruise to the tropical and subtropical Atlantic in 2015. PANGAEA. doi:10.1594/PANGAEA.943417

Gómez-Letona, M., J. Arístegui, N. Hernández-Hernández, M. Pérez-Lorenzo, X. A. Alvarez-Salgado, E. Teira, and M. Sebastian. 2022e. Abundance, cell volume, biomass, viability and leucine incorporation rates of prokaryotes in the tropical and subtropical Atlantic. PANGAEA. doi:10.1594/PANGAEA.943414

Gómez-Letona, M., J. Arístegui, N. Hernández-Hernández, M. Pérez-Lorenzo, X. A. Alvarez-Salgado, E. Teira, and M. Sebastian. 2022f. Integrated abundance, cell volume, viability and leucine incorporation rates of prokaryotes in the epipelagic, mesopelagic and bathypelagic layers of the tropical and subtropical Atlantic. PANGAEA. doi:10.1594/PANGAEA.943416

Gómez-Letona, M., M. Baumann, A. González, and others. 2022g. KOSMOS 2018 Gran Canaria mesocosm study: dissolved organic matter. PANGAEA. doi:10.1594/PANGAEA.946776